Rare Earth Element and Neodymium Isotope Tracing of Element Input and Past Ocean Circulation: Study From North and South Pacific Seawater and Sediments

Von der Fakultät V für Mathematik und Naturwissenschaften
der Carl von Ossietzky Universität Oldenburg
zur Erlangung des Grades und Titels eines

Doktors der Naturwissenschaften
(Dr. rer. nat.)

angenommene Dissertation

von **Herrn Henning Fröllje**
geboren am 01.07.1984 in Oldenburg

Erstgutachterin: Dr. Katharina Pahnke
Zweitgutachter: Prof. Dr. Thorsten Dittmar

Tag der Disputation: 09.08.2016

Abstract

Ocean circulation and cycling of trace elements within the oceanic water column is of great significance for modern and past climates. The global overturning circulation is responsible for the distribution of water masses, heat and particulate and dissolved compounds, while biological and chemical processes, such as primary productivity or particle scavenging, control the cycling of nutrients and trace elements in the ocean, and ultimately influence the ocean-atmosphere exchange of carbon. Rare earth elements (REE) and neodymium (Nd) isotopes are widely used as tracers for lithogenic element fluxes and modern and past ocean circulation and water mass mixing. The use of Nd isotopes in paleoceanographic investigations is based on the precise knowledge of processes involved in REE cycling and of the modern oceanic Nd isotope distribution. The Pacific is the largest of the world oceans, but it is highly underrepresented in present-day and past seawater Nd isotope and REE investigations compared to the Atlantic Ocean. In this study, Nd isotopes and REEs are analysed in North Pacific seawater (chapter 2) and sediment samples from the South Pacific (chapters 3-5) to contribute to a better understanding of sources and cycling of REEs and Nd isotopes in present-day seawater and to investigate past water mass mixing and circulation changes during the last glacial termination and throughout the last glacial-interglacial cycle. Neodymium isotopes in seawater and sedimentary archives (fossil fish teeth and debris, foraminifera, ferromanganese oxides, lithogenic particles) were analysed using multi-collector inductively coupled plasma mass spectrometry (MC-ICP-MS), and REE concentrations were analysed using isotope dilution ICP-MS.

Results from combined analysis of REEs, and Nd and radium isotopes from North Pacific seawater (coastal seawaters of the Hawaiian Island of Oahu and seawater from the offshore Hawaii Ocean Time-series Station ALOHA) show a clear influence of the Hawaiian Islands on coastal waters and the open ocean at Station ALOHA (chapter 2). These results indicate that contributions from volcanic islands (e.g., Hawaii) cannot be disregarded when investigating element budgets in the North Pacific. It is further shown that seasonal variability of Asian dust input most likely has significant influence on the Nd isotope signature of central North Pacific surface waters. New results from measurements of colloidal and truly dissolved REE concentrations indicate for the first time the absence of colloidal-bound REEs in open ocean waters at different depths. Further, a complete water column profile from Station ALOHA allows tracing of North Pacific water masses based on Nd isotopes. This study presents an adjustment of the Nd isotope signature and Nd concentration of North Pacific Deep Water (NPDW), which is considered the radiogenic endmember in the global overturning circulation, and therefore of particular importance for paleoceanographic studies. Moreover, REE patterns demonstrate that vertical processes overprint the REE concentrations in deep and bottom waters, precluding their use to trace water masses in the deep Pacific.

Sedimentary Nd isotopes from the last 30,000 years demonstrate the variability in water mass structure in the South Pacific and the evolution of water mass mixing in Circumpolar Deep Water (CDW) during the last glacial-interglacial transition (chapter 3). Combined results from five sediment cores show an expansion of glacial bottom water and its isolation from CDW during the Last Glacial Maximum (LGM) based on differences in the Nd isotope signatures in cores below and above ~4000 m. Admixture of bottom water into CDW during the early deglaciation is suggested based on the early deglacial decrease of Nd isotope signatures in CDW-bathed cores before the re-strengthening of North Atlantic Deep Water (NADW) advection. This is related to Southern Hemisphere climate and only later during the deglaciation did the incorporation of NADW contribute to the changes in the Nd isotope signature of CDW. The absence of such early deglacial Nd isotope changes in the northernmost core were attributed to the isolation of this core from bottom waters by South Pacific bathymetry with potential contribution from shifts in the Southern Ocean’s frontal system and potential influence of increased deglacial NPDW convection. Overall the results highlight the important role of glacial deep stratification in sustaining a deep glacial carbon reservoir in the Southern Ocean and the importance of Southern Hemisphere climate to the breakdown of deep stratification and the release of sequestered CO_2 through upwelling.

A 140,000 year long Nd isotope record from the Southeast Pacific covering the last glacial-interglacial cycle demonstrates comparable deep water mass mixing in the South Pacific during the last two glacial maxima, but higher NADW contributions during the glacial Marine Isotope Stage (MIS) 4 (chapter 4). Likewise, the penultimate interglacial (MIS 5) was characterised by similar amounts of NADW and NPDW in CDW as the Holocene and the modern Southeast Pacific. Comparison of the last two glacial terminations thus shows high consistency and suggests similar mechanisms that controlled the deglacial change in water mass structure in the deep South Pacific, including a Southern Ocean contribution to early deglacial Nd isotope shifts. The results show weaker absolute glacial-interglacial Nd isotope changes compared to the South Atlantic due to the lack of direct NADW and slightly higher NPDW influence in the Southeast Pacific. Further, the Nd isotope record confirms the glacial-interglacial variability in NADW and NPDW mixture in CDW obtained previously from carbon isotope records. However, it also demonstrates a decoupling of Nd and carbon isotope signals in glacial climates, which implies that carbon isotope records show clear contributions from

Southern Ocean productivity changes and cannot be interpreted to be entirely governed by water mass mixing processes in the South Pacific.

In a methodological approach, the application of sedimentary ferromanganese oxides as archive of seawater Nd isotope signatures was tested for the South Pacific (chapter 5). The results show the impracticality of leaching protocols to reconstruct ambient bottom water Nd isotope signatures in this area. A set of modifications of the method in terms of acid strength, used sediment size fraction, and omission of initial decarbonation could not reliably reproduce Nd isotope signatures of fossil fish teeth. The results suggest a critical role of the decarbonation step for the success of the leaching procedure and imply that leaching protocols need to be tested on a core-to-core basis before interpreting the results in a paleoceanographic context. This study provides a base for more detailed and systematic studies of the applicability of leaching procedures in the South Pacific.

Kurzfassung

Die Ozeanzirkulation und der Kreislauf von Spurenelementen in der ozeanischen Wassersäule sind von großer Bedeutung für heutiges Klima und das Klima der Vergangenheit. Die globale Umwälzzirkulation ist verantwortlich für die Verteilung von Wassermassen, Wärme und partikulärer und gelöster Stoffe, während biologische und chemische Prozesse wie Primärproduktion oder „Partikel-Scavenging“ den Kreislauf von Nährstoffen und Spurenelementen im Ozean kontrollieren, und damit letztlich den Austausch von Kohlenstoff zwischen Ozean und Atmosphäre beeinflussen. Seltene Erdelemente (REE) und Neodym (Nd) Isotope werden häufig als Tracer für Elementflüsse und heutige und frühere Ozeanzirkulation und Wassermassenmischung genutzt. Die Nutzung von Nd-Isotopen in paläoozeanographischen Untersuchungen basiert auf der präzisen Kenntnis des Kreislaufs der REE und der heutigen ozeanischen Verteilung von Nd Isotopen. Der Pazifik ist der größte der Weltozeane, verglichen mit dem Atlantik jedoch deutlich unterrepräsentiert in Untersuchungen zu REE und Nd-Isotopen in heutigem und früherem Meerwasser. In dieser Studie werden Nd-Isotope und REE in Nordpazifischem Meerwasser (Kapitel 2) sowie in Sedimentproben aus dem Südpazifik analysiert (Kapitel 3-5), um zu einem besseren Verständnis der Quellen und des Kreislaufs der REE und Nd Isotope in heutigem Meerwasser beizutragen und um Wassermassenmischungen und Zirkulationsänderungen während der letzten glazialen Termination und des letzten glazial-interglazial Zyklus' zu untersuchen. Neodym-Isotope im Meerwasser und in Sedimentarchiven (fossile Fischzähne und Knochen, Foraminiferen, Eisen-Mangan-Oxide, lithogene Partikel) wurden mit einem Multikollektor Massenspektrometer mit induktiv gekoppeltem Plasma (MC-ICP-MS), Konzentrationen der REE durch Isotopenverdünnung mittels ICP-MS analysiert.

Die Ergebnisse der kombinierten Analyse von REE, sowie Nd- und Radium-Isotopen aus nordpazifischem Meerwasser (Küstengewässer der Hawaiianischen Insel Oahu und Meerwasser der „Hawaii Ocean Time-series Station ALOHA“) zeigen einen deutlichen Einfluss der Hawaiianischen Inseln auf die Küstengewässer und den offenen Ozean bei Station ALOHA (Kapitel 2). Diese Ergebnisse zeigen, dass Einträge von vulkanischen Inseln (z.B. Hawaii) für die Untersuchung von Elementbudgets im Nordpazifik nicht unbeachtet bleiben können. Weiterhin wird gezeigt, dass die saisonale Variabilität von asiatischem Staubeintrag sehr wahrscheinlich signifikanten Einfluss auf die Nd Isotopie der Oberflächenwässer des zentralen Nordpazifiks hat. Ergebnisse von Messungen kolloidaler und echt-gelöster REE Konzentrationen deuten zum ersten Mal auf das Fehlen von kolloidal-gebundenen REE in verschiedenen Tiefen des offenen Ozeans hin. Weiterhin erlaubt ein Tiefenprofil über die gesamte Wassersäule von Station ALOHA die

Identifizierung von nordpazifischen Wassermassen anhand ihrer Nd Isotopie. Diese Studie präsentiert eine Anpassung der Nd Isotopensignatur von Nordpazifischem Tiefenwasser (NPDW), welches als radiogenes Endglied in der globalen Umwälzzirkulation betrachtet wird und daher von besonderer Bedeutung für paläoozeanographische Studien ist. Weiterhin zeigen REE Muster, dass vertikale Prozesse die REE Konzentrationen im Tiefen- und Bodenwasser überprägen und diese daher im tiefen Pazifik nicht als Tracer für Wassermassen genutzt werden können.

Analysen der Nd-Isotopie von Sedimenten der letzten 30.000 Jahre zeigen die Variabilität der Wassermassenstruktur im Südpazifik und die Entwicklung der Mischung von Wassermassen in zirkumpolarem Tiefenwasser (CDW) während des letzten Deglazials (Kapitel 3). Kombinierte Ergebnisse von fünf Sedimentkernen zeigen eine Ausdehnung des glazialen Bodenwassers und dessen Isolation von CDW während des letzten glazialen Maximums (LGM) basierend auf unterschiedlichen Nd-Isotopensignaturen in Kernen ober- und unterhalb von ~4000 m. Die Beimischung von Bodenwasser in CDW während des frühen Deglazials wird durch Änderung der Nd-Isotopie in von CDW umgebenden Kernen angezeigt. Dies basiert auf klimatischen Änderungen in der Südlichen Hemisphäre und erst während des späteren Deglazials trägt die Beimischung von Nordatlantischem Tiefenwasser (NADW) zu Änderungen in der Isotopensignatur von CDW bei. Die fehlende früh-deglaziale Änderung in der Nd-Isotopie im nördlichsten Kern basiert auf der Isolation dieses Kernes von glazialem Bodenwasser durch die Bathymetrie mit möglichem zusätzlichem Einfluss von Verschiebungen des Frontensystems im Südpazifik und erhöhter NPDW-Konvektion im Deglazial. Insgesamt betonen die Ergebnisse die wichtige Rolle der glazialen Tiefenstratifizierung bei der Stabilisierung des Kohlenstoffreservoirs im Tiefenwasser des Südlichen Ozeans und die Bedeutung des Klimas der Südlichen Hemisphäre für den Zusammenbruch der tiefen Stratifizierung und die Freisetzung von angesammeltem CO_2 durch Auftrieb von Tiefenwasser.

Die 140.000 Jahre umfassende Nd-Isotopenkurve aus dem Südostpazifik, die den letzten glazial-interglazialen Zyklus darstellt, zeigt eine vergleichbare Mischung von Wassermassen im Südpazifik während der letzten beiden glazialen Maxima, aber einen höheren Anteil von NADW während des Marinen Isotopenstadiums (MIS) 4 (Kapitel 4). Entsprechend enthält CDW im letzten Interglazial (MIS 5) gleiche Mengen von NADW und NPDW wie das Holozän und der heutige Südostpazifik. Die letzten beiden glazialen Terminationen weisen daher eine hohe Übereinstimmung auf, was auf einen ähnlichen Mechanismus hindeutet, der die deglaziale Änderung in der Wassermassenstruktur im tiefen Südpazifik kontrolliert und einen Beitrag des Südozeans auf die früh-deglazialen Nd

Isotopenänderungen einschließt. Außerdem zeigen die Ergebnisse eine abgeschwächte absolute glazial-interglaziale Nd Isotopenänderung verglichen mit dem Südatlantik aufgrund von geringerem NADW- und höherem NPDW-Einfluss im Südostpazifik. Weiterhin bestätigt die Nd-Isotopenkurve die glazial-interglaziale Variabilität in der Mischung von NADW und NPDW in CDW, die bereits anhand von Kohlenstoff-Isotopen vermutet wurde, jedoch zeigt sie ebenso eine Entkopplung von Nd und Kohlenstoff-Isotopen im Südozean während Glazialen. Dies impliziert, dass die Änderungen der Kohlenstoff-Isotopie von Produktivitätsänderungen im Südozean beeinflusst sind und im Südpazifik nicht ausschließlich als Wassermassenmischungsprozesse interpretiert werden können.

In einem methodischen Ansatz wurde die Verwendung von Eisenmanganoxiden als Archiv für Nd Isotopensignaturen im Südpazifik getestet (Kapitel 5). Die Ergebnisse zeigen die Unbrauchbarkeit von Extraktionsprotokollen, um die Nd-Isotopie von Bodenwasser in diesem Gebiet zu rekonstruieren. So konnte auch durch eine Reihe von Modifizierungen der Methode in Bezug auf die Säurestärke, die benutzte Korngrößenfraktion des Sediments und die Vermeidung einer Entkarbonatisierung die Isotopensignatur von fossilen Fischzähnen nicht verlässlich reproduziert werden. Die Ergebnisse zeigen eine kritische Rolle der Entkarbonatisierung für den Erfolg von Extraktionsversuchen und implizieren, dass die Protokolle für jeden Kern getestet werden sollten, bevor die Ergebnisse im paläoozeanographischen Kontext interpretiert werden. Die Studie stellt eine Basis für detailliertere und systematischere Studien dar, um die Anwendbarkeit von Extraktionsprotokollen im Südpazifik zu untersuchen.

Table of Contents

1. Introduction

1.1. Ocean circulation and climate

The ocean is one of the key players in the global climate system due to its importance in the distribution of heat and water masses within the ‘great ocean conveyor’ (Broecker, 1991) and in uptake and release of carbon (e.g., Siegenthaler and Sarmiento, 1993).

In the modern ocean, the global meridional overturning circulation (MOC) is characterised by a two-cell overturning structure with deep-water formation in the high latitude North Atlantic and the Southern Ocean and the return-flow of surface and mid-depth waters. These two cells are connected via upwelling and mixing in the Southern Ocean around Antarctica (e.g., Marshall and Speer, 2012; Talley, 2013) (Fig. 1.1).

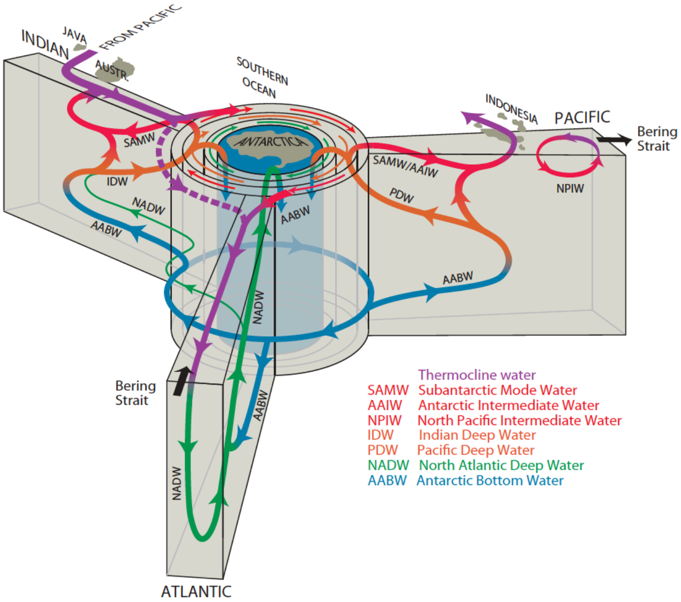

Figure 1.1: Schematic illustration of the global overturning circulation (reprinted from Talley, 2013).

North Atlantic Deep Water (NADW), which is formed in the Labrador and Nordic Seas by heat loss of surface waters, flows southward into the Southern Ocean, and gets mixed into the lower portion of Circumpolar Deep Water (CDW) (e.g., Talley et al., 2013). Circumpolar Deep Water is transported around Antarctica in the eastward flowing Antarctic Circumpolar Current (ACC) that extends over the entire water column and is estimated to transport 100-150 Sv (1 Sv = 10^6 m^3/s) (Talley et al., 2011 and references therein). In the Pacific and Indian Oceans, active deep water formation is missing, but waters distributed by the ACC circulate northward and are altered and converted into North Pacific Deep Water (NPDW) and Indian Deep Water (IDW), respectively, before returning to the Southern Ocean, where they are incorporated into the upper portion of CDW (e.g., Sloyan and Rintoul, 2001a; Kawabe and Fujio, 2010; Talley, 2013). Upwelling of upper and lower CDW (UCDW/LCDW) along isopycnals in the Southern Ocean south of the ACC contributes deep water to both, Antarctic Bottom Water (AABW) formation on the Antarctic shelves and Antarctic Intermediate and Subantarctic Mode Water (AAIW/SAMW) formation north of the ACC (e.g., Sloyan and Rintoul, 2001b; Talley, 2013). Antarctic Bottom Water is the densest water mass and is formed in the Weddell and Ross Seas and along the coastline of Antarctica through density increase induced by heat loss, sea-ice formation and brine rejection (e.g., Orsi et al., 1999; Gordon, 2001).

Antarctic ice core records suggest that climate cycles over the past 800,000 years were characterised by varying atmospheric CO_2 concentrations with lower CO_2 levels during glacial stages (Petit et al., 1999; Siegenthaler et al., 2005; Lüthi et al., 2008). For example during the last glacial termination the atmospheric CO_2 concentration increased by ~80 ppmv between ~17 and 11 ka BP (Monnin et al., 2001). This climate variability is tightly linked to past reorganisations in the global ocean (e.g., Broecker and Denton, 1989; Adkins, 2013). Especially the Southern Ocean is considered a key region for past climate since changes in stratification and upwelling intensity, sea-ice extent, buoyancy forcing, nutrient utilisation and wind systems at glacial terminations are thought to have influenced the release of CO_2 to the atmosphere from previously isolated CO_2-rich deep waters (e.g., Sigman and Boyle, 2000; Toggweiler, 2006; Anderson et al., 2009; Sigman et al., 2010; Skinner et al., 2010; Burke and Robinson, 2012; Adkins, 2013; Ferrari et al., 2014; Watson et al., 2015).

In comparison to modern conditions and potentially previous interglacials, the Last Glacial Maximum (LGM) was characterised by a different water mass geometry, i.e., a pronounced stratification and decreased mixing between deep and bottom waters (Adkins, 2013). In the North Atlantic, the production of NADW was replaced by the shallower Glacial North Atlantic Intermediate Water and the deep ocean was filled with southern-sourced waters (e.g., Curry and Oppo, 2005; Lynch-Stieglitz et al., 2007; Roberts et al., 2010; Lippold et al., 2016). In agreement with this, nutrient and circulation proxies from the South Atlantic showed less contribution of NADW to CDW and the development of a chemical divide (representing the divide between northern and southern-sourced water) at ~2500 m water depth (e.g., Charles and Fairbanks, 1992; Ninnemann and Charles, 2002; Hodell et al., 2003; Piotrowski et al., 2004; Martinez-Mendez et al., 2009; Skinner et al., 2013; Lippold et al., 2016). There is some evidence that other sectors of the Southern Ocean, such as the deep South Pacific, were also subject to reorganisations of their water mass geometry and mixing during the LGM and previous glacials (e.g., Ninnemann and Charles, 2002; McCave et al., 2008; Elderfield et al., 2012; Noble et al., 2013; Sikes et al., 2016; Molina-Kescher et al., 2016). Apart from this, there have also been suggestions that include a deepening of NPDW during the LGM (Matsumoto et al., 2002) and active deep water formation in the North Pacific during the last glacial termination (Okazaki et al., 2010; Rae et al., 2014). One major focus of this thesis is the reconstruction of glacial-interglacial variability of deep water mass mixing and circulation in the South Pacific sector of the Southern Ocean.

1.2. Study area – the Pacific Ocean

The Pacific Ocean is by far the largest ocean basin covering ~50% of the area and volume of the world ocean (Menard and Smith, 1966). It is surrounded by trenches and volcanoes that originate from the subduction of tectonic plates at its margins. The occurrence of volcanoes in this ‘ring of fire’, as well as appearance of hotspot volcanism (e.g., the Hawaiian Ridge) is expressed in positive (i.e., radiogenic) Nd isotope signatures at the Pacific margin, and of particular importance for the Nd isotope composition of Pacific waters (e.g., Jeandel et al., 2007; see also section 1.3).

One of the study areas investigated in this thesis is located in the subtropical central North Pacific midway on the Pacific plate (Fig. 1.2). The great distance to the continents precludes a significant input of lithogenic material through rivers, but the central North Pacific (and thus the Hawaiian Islands) is influenced by seasonally varying dust deposition originating from the Asian continent (e.g., Duce et al., 1980; Parrington et al., 1983). These dust plumes have been suggested to control dissolved trace element concentrations in surface waters of the open ocean North Pacific (Boyle et al., 2005; Fitzsimmons et al., 2015; Hayes et al., 2015).

The South Pacific is crossed by the Pacific-Antarctic Ridge (PAR) in the western to central part and by the East Pacific Rise (EPR) in the central to eastern part in southwest to northeast direction (e.g., Tomczak and Godfrey, 1994). This ridge system separates the Pacific plate from the Antarctic and Nazca plates and is characterised by the presence of deep channels, such as the Eltanin and Udintsev Fracture Zones, which are of importance in steering the ACC (e.g., Talley et al., 2011). The study area in the South Pacific extends from northwest of the PAR to southeast of the EPR (Fig. 1.2). The central South Pacific does not receive large amounts of lithogenic input, due to large distance to the continents and today is subject to low amounts of dust deposition (e.g., Jickells et al., 2005). However, during glacial climates dust deposition was three times higher in this area (Lamy et al., 2014) and has been suggested to contribute to the decline in atmospheric CO_2

through iron fertilisation and increased export production in the subantarctic Southern Ocean (e.g., Sigman et al., 2010; Martinez-Garcia et al., 2014).

The study areas in the North and South Pacific are interconnected through the circulation of intermediate, deep and bottom waters that originate in the high latitude North and South Pacific (Figs. 1.1, 1.2). The Pacific Ocean's major deep water mass, NPDW, originates from upwelling and mixing of southern-sourced waters (e.g., Kawabe and Fujio, 2010; Talley, 2013) and is the oldest water mass in the global ocean, characterised by high nutrient and CO_2 and low oxygen concentrations (Reid, 1997; Talley et al., 2011). Southward flow of NPDW in the upper deep layer in the East Pacific along the South American continent balances the inflow of CDW and AAIW in the bottom, deep and intermediate layers (Kawabe and Fujio, 2010).

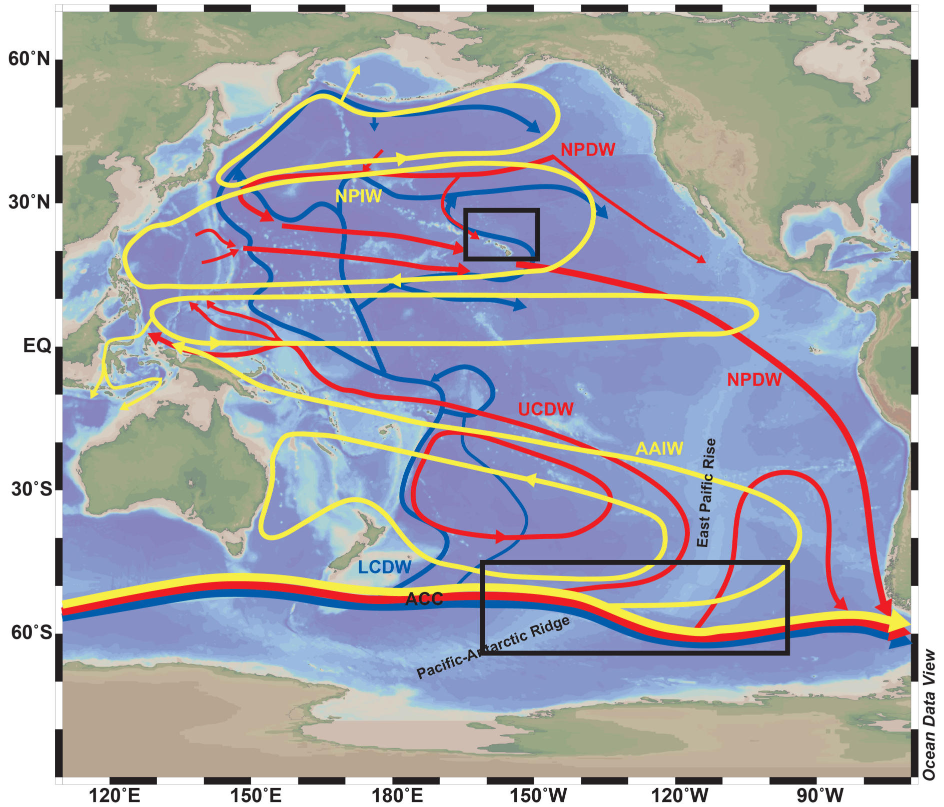

Figure 1.2: Schematic circulation in the Pacific Ocean in the intermediate layer (yellow; NPIW and AAIW), upper deep layer (red; UCDW and NPDW) and bottom layer (blue; LCDW) (circulation patterns after Kawabe and Fujio, 2010). Study areas investigated in this thesis in the central North Pacific and the South Pacific sector of the Southern Ocean are marked by black rectangles. Map was created with Ocean Data View (Schlitzer, 2014).

Figure 1.2 comprises the general schematic circulation in the Pacific and shows the study areas in the Southern Ocean (i.e., South Pacific sector of the Southern Ocean) and near the Hawaiian Islands in the subtropical central North Pacific. The basic circulation of the Pacific is briefly described in the following for the surface, intermediate, deep, and bottom layers. A more detailed description of the study areas and their hydrography is presented in chapters 2-4. Additionally, a general overview on the circulation and hydrography of both areas is illustrated in Figures 1.3 and 1.4, respectively.

Dominant features of the surface circulation are anticyclonic subtropical gyres in the North and South Pacific and a subpolar cyclonic gyre centred at 50° N (Tomczak and Godfrey, 1994; Reid, 1997). The surface circulation in the South Pacific is further characterised by the eastward flow of the ACC. In the equatorial Pacific a complex system of eastward and westward flowing surface currents and countercurrents connect the tropical East and West Pacific (e.g., Tomczak and Godfrey, 1994; Talley et al., 2011). Below the North Pacific Subtropical Gyre (NPSG), several thermocline water masses, such as North Pacific Tropical Water (NPTW), North Pacific Subtropical Mode Water (NPSTMW) and North Pacific Central Water (NPCW) characterise the subsurface depths near the Hawaiian Islands (e.g., Talley et al., 2011) (for details see chapter 2 and Fig. 1.2). The Hawaiian Ridge extends from approximately 20-30° N and acts as a natural barrier for the circulation in the North Pacific being of particular importance for the eastward flow of the Subtropical Counter Current in the NPSG (White and Walker, 1985; Karl and Lukas, 1996).

In the North Pacific, the intermediate layer is dominated by the presence of North Pacific Intermediate Water (NPIW), which is formed in the Okhotsk Sea and the Gulf of Alaska and follows the circulation of the NPSG (Talley et al., 1993; You et al., 2000; You, 2003) (Fig. 1.3A). These waters extend southward to approximately 20° N (Talley, 1993; You et al., 2000). In the equatorial region the intermediate layer is characterised by the presence of Equatorial Pacific Intermediate Water (EqPIW), a mixture of AAIW and NPDW (Bostock et al., 2010). As shown by Bostock et al. (2010) the Hawaiian Islands are located within the mixing region of NPIW and the northern fraction of EqPIW (NEqPIW) (Fig. 1.3B). Antarctic Intermediate Water is the dominant water mass in the intermediate layer of the South Pacific, being formed mainly off southern Chile from surface waters that originate from upwelled and northward transported CDW (McCartney, 1977; Talley, 1999; Sloyan and Rintoul, 2001b). Antarctic Intermediate Water flows in an anticyclonic circulation and leaves the South Pacific in its western part (Reid, 1986; Tsuchiya, 1991; Kawabe and Fujio, 2010) (Fig. 1.2).

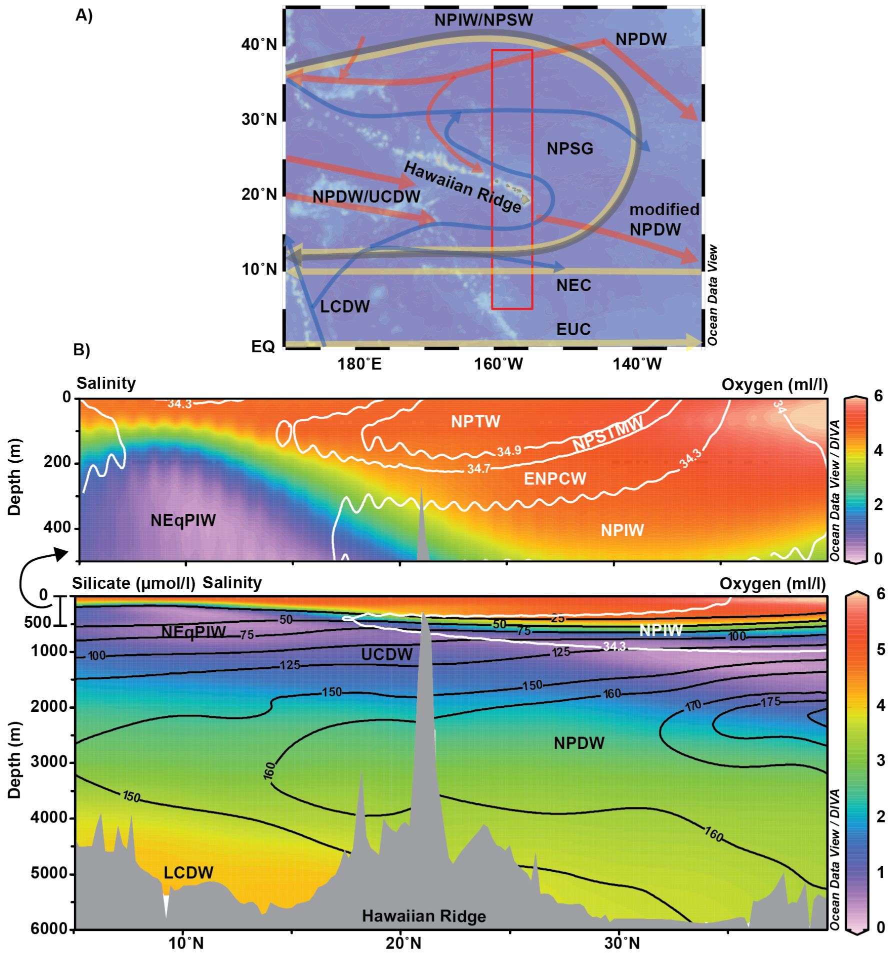

Figure 1.3: A) Schematic circulation in the central North Pacific in the surface (black), intermediate (yellow), deep (red) and bottom (blue) layers (circulation patterns after Kawabe and Fujio, 2010; Talley et al., 2011). Red rectangle: position of meridional section in B. B) Water mass structure in the central North Pacific at ~157˚ W for the upper 500 m (upper panel) and the whole water column (lower panel). Water masses identified by oxygen concentration (colour), salinity (white contours) and silicate concentration (black contours; lower panel only) (data from World Ocean Atlas 2009 (Antonov et al., 2010; Garcia et al., 2010a,b)). Upper CDW cannot be clearly identified by hydrographic properties but is present in the North Pacific at ~1000 m depth, sandwiched between NPIW and NPDW (Talley et al., 2011). For details on hydrographic properties of water masses see chapter 2. NPSW: North Pacific Surface Water, ENPCW: Eastern NPCW, NEC: North Equatorial Current, EUC: Equatorial Undercurrent. Map and section plots were created with Ocean Data View (Schlitzer, 2014).

The upper and lower deep layers are dominated by the northward flow of upper and lower CDW into the North Pacific and the return flow of NPDW to the Southern Ocean (e.g., Sloyan and Rintoul, 2001a; Kawabe and Fujio, 2010; Talley, 2013) (Fig. 1.2). Upper CDW is characterised by low oxygen concentrations imprinted from re-circulated NPDW and IDW (Callahan, 1972; Reid, 1986), whereas lower CDW is identified by high salinities that are a remnant of NADW (Reid and Lynn, 1971; Orsi et al., 1995) (Fig. 1.4B). Circumpolar Deep Water is the main water mass of the ACC, which is confined by the Subantarctic Front (SAF) in the north and by the Southern ACC front (SACCF) in the south (Orsi et al., 1995) (Figs. 1.2, 1.4A). Lower CDW is transported northward within the

Deep Western Boundary Current in the western South Pacific (Reid, 1997; Kawabe and Fujio, 2010). The main outflow of UCDW from the Southern Ocean is west of the EPR (Reid, 1997; Kawabe and Fujio, 2010) (Fig. 1.4A). Upper and Lower CDW cross the equator in the West Pacific and can be found at various locations in the North Pacific where they mix with Pacific waters and return to the Southern Ocean as modified NPDW along the South American continent (Kawabe and Fujio, 2010; Talley et al., 2011) (Fig. 1.4A).

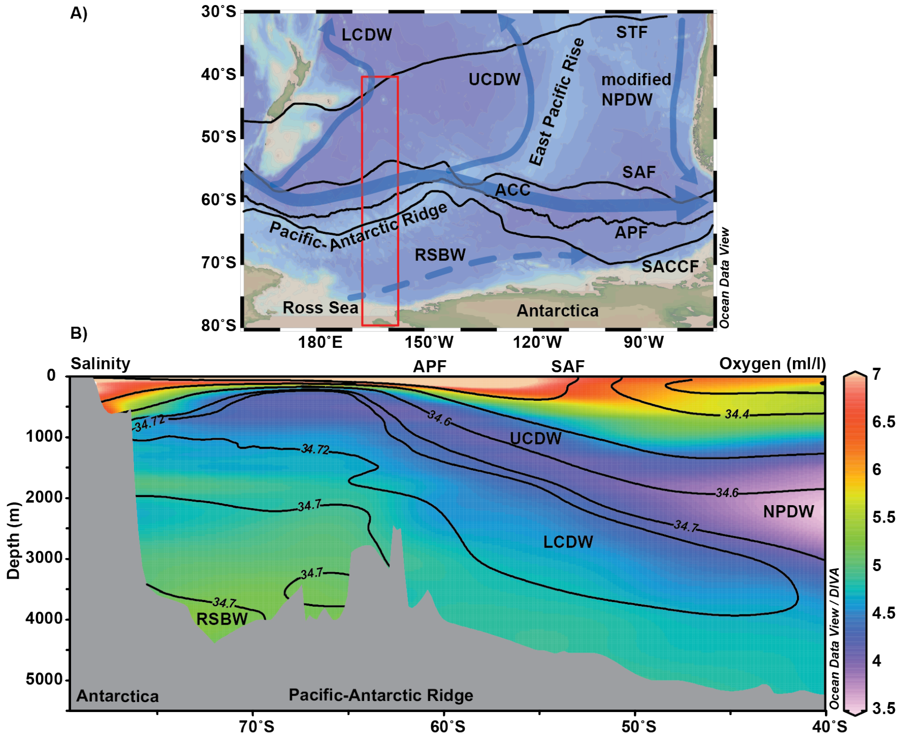

Figure 1.4: A) Schematic circulation of major water masses (after Kawabe and Fujio, 2010) and position of oceanic fronts (after Orsi et al., 1995) in the Pacific sector of the Southern Ocean. Blue arrows show eastward flow of the ACC, main outflow paths of UCDW and LCDW and southward flow of modified NPDW along the South American coast. Ross Sea Bottom Water fills the East Pacific Basin (e.g., Orsi et al., 1999) (dashed line). Red rectangle: the position of the meridional section in B. B) Water mass structure of the Southern Ocean at ~165° W. Major water masses identified by oxygen concentration (colour) and salinity (contours) (data from World Ocean Atlas 2009 (Antonov et al., 2010; Garcia et al., 2010a)). APF: Antarctic Polar Front. Map and section plot were created with Ocean Data View (Schlitzer, 2014).

Below CDW, the abyss of the Pacific sector of the Southern Ocean is dominated by the presence of Ross Sea Bottom Water (RSBW), a variety of AABW, which is formed on the Ross Sea shelf by mixing of CDW with cool and saline surface waters, and hindered from northward expansion by the Pacific-Antarctic Ridge system (Jacobs et al., 1970; Orsi et al., 1999; Orsi and Wiederwohl, 2009).

1.3. Neodymium isotopes and rare earth elements as tracers for lithogenic element input and ocean circulation

Trace elements and nutrients are delivered to the ocean by rivers, groundwater input/discharge, dust deposition and subsequent dissolution, and from hydrothermal sources and ocean margins. Yet, tracing the sources of these elements is complicated due to their participation in biogeochemical cycling within the water column. Rare earth elements (REEs) and neodymium (Nd) isotopes, however, are not subject to biological cycling and fractionation and therefore are widely used as tracers for lithogenic element input based on their distinct distribution in continental material that allows tracing their sources and input pathways (e.g., Elderfield, 1988; Nozaki, 2001; Frank, 2002; Goldstein and Hemming, 2003; Jeandel et al., 2007). Particularly, the importance of Nd isotopes for marine sciences is pointed out by its denotation as a key parameter in the international GEOTRACES program for tracing sources of elements to the ocean (Henderson et al., 2007).

Another application is the use of Nd isotopes as a tracer of modern and past ocean circulation, based on the heterogeneity of seawater Nd isotope signatures (Lacan and Jeandel, 2001; 2005a, Frank, 2002; Goldstein and Hemming, 2003; Lacan et al., 2012). Physical properties of seawater such as salinity, temperature and density as well as nutrient concentrations that are used to trace water masses in the modern ocean are not preserved in sedimentary archives. For this purpose, a set of nutrient, ventilation and circulation proxies (e.g., stable carbon and oxygen isotopes, radiocarbon activities, Cd/Ca and ^{231}Pa/^{230}Th ratios) are used in paleoceanographic studies to investigate past ocean circulation and water mass geometry (e.g., Lynch-Stieglitz et al., 2007 and references therein). The establishment of Nd isotopes as a paleo-water mass tracer provided another useful tool to study circulation changes and water mass mixing in the past ocean over millennial to glacial-interglacial timescales (e.g., Piotrowski et al., 2004; 2005; 2009; Gutjahr et al., 2008; Pahnke et al., 2008; Roberts et al., 2010; Noble et al., 2013; Böhm et al., 2015; Jonkers et al., 2015; Wei et al., 2016; Lippold et al., 2016) as well as on cenozoic timescales (e.g., Abouchami et al., 1997; Frank et al., 2002; Thomas, 2004; Scher and Martin, 2004; 2008; Osborne et al., 2014).

In the following sections the use of REEs and Nd isotopes to study processes in the modern and past ocean is described in more detail.

1.3.1. Rare earth elements

The REEs comprise the lanthanide elements from lanthanum (La) to lutetium (Lu). These are characterised by decreasing ionic radii with increasing atomic mass, the so-called lanthanide contraction, which results from progressive filling of electrons in the inner 4f shell. Other than these small differences, the REEs are a coherent group of elements that have similar chemical behaviour (Elderfield, 1988; Nozaki, 2001).

Rivers and submarine groundwater discharge (SGD) are considered important sources of particulate, colloidal and dissolved REEs to seawater (e.g., Goldstein and Jacobsen, 1988; Elderfield et al., 1990; Johannesson et al., 2011; Kim and Kim, 2011; 2014). The influence of dust is limited to particulate input and subsequent mobilisation of REEs in contact with seawater, yet, a wide range of estimates is given for the fraction of REEs extracted from atmospheric particles (Greaves et al., 1994; 1999; Tachikawa et al., 1999). Additionally, sedimentary pore fluids have been suggested to significantly influence bottom water REE concentrations (Haley and Klinkhammer, 2003; Abbott et al., 2015a). Rare earth element concentrations in the water column are mainly controlled by vertical processes of surface input, particle scavenging, and release at depth (e.g., Elderfield and Greaves, 1982; Elderfield, 1988; Bertram and Elderfield, 1993). Yet, lateral influence has also been observed in some areas (Alibo and Nozaki, 2004; Molina-Kescher et al., 2014a; Basak et al., 2015; Osborne et al., 2015; Stichel et al., 2015). Dissolved REE patterns in seawater are typically visualised by normalisation to reference lithogenic material or a reference water mass. Most commonly used references are Post-Archean Australian Sedimentary rock (PAAS; Taylor and McLennan, 1985) and North Pacific Deep Water (Alibo and Nozaki, 1999). A characteristic feature of shale-normalised REE patterns in seawater is the heavy over light REE enrichment that results from stronger complexation of heavy REEs and the preferential adsorption of light REEs onto particles (Cantrell and Byrne, 1987; Elderfield, 1988; Byrne and Kim, 1990; Sholkovitz et al., 1994). In seawater, REEs exist in the +3 oxidation state with the majority of dissolved REE species being present as carbonate complexes (Cantrell and Byrne, 1987; Elderfield, 1988; Nozaki, 2001). Exceptions are the occurrence of cerium (Ce) as Ce^{4+} and europium (Eu) as Eu^{2+}, resulting in anomalies of these REEs in normalised patterns, that is, relative enrichment or depletion compared to their neighbour elements.

Negative Ce anomalies (i.e., depletion of Ce in seawater) result from microbially controlled Ce oxidation and high particle reactivity and scavenging of Ce^{4+} in seawater (Elderfield and Greaves, 1982; de Baar et al., 1985a; Moffett, 1990). Europium anomalies, on the other hand, are not controlled by processes in seawater but result from high temperature fractionation (e.g., Bau, 1991 and references therein). In the marine environment positive Eu anomalies are observed in hydrothermal fluids (e.g., Elderfield, 1988; Mitra et al., 1994) and in areas where seawater interacts with basaltic material (Zhang et al., 2008; Grenier et al., 2013). A further positive anomaly is that of gadolinium (Gd), which is partly due to a natural 'tetrad effect' that increases the stability of Gd complexes in seawater (Masuda and Ikeuchi, 1979; de Baar et al., 1985b). Yet, the use of stable Gd-complexes as contrast agent in magnetic resonance imaging leads to high anthropogenic Gd anomalies in rivers that drain industrialised areas, and can significantly increase and overprint the naturally observed Gd anomaly in seawater (Bau and Dulski, 1996; Nozaki et al., 2000; Kulaksiz and Bau, 2007).

1.3.2. Neodymium isotopes

Neodymium is the fourth lightest element of the group of REEs with an average atomic mass of 144.24 u and has seven naturally occurring isotopes. For oceanographic and geochemical purposes, the $^{143}Nd/^{144}Nd$ ratio is of outstanding importance. The $^{143}Nd/^{144}Nd$ isotope ratio is typically expressed in the ε_{Nd} notation, which is defined as:

$$\varepsilon_{\mathrm{Nd}} = [\frac{(^{143}\mathrm{Nd}/^{144}\mathrm{Nd})_{\mathrm{sample}}}{(^{143}\mathrm{Nd}/^{144}\mathrm{Nd})_{\mathrm{CHUR}}} - 1] \cdot 10{,}000 \tag{1.1}$$

with CHUR being the Chondritic Uniform Reservoir with an isotope ratio of $^{143}Nd/^{144}Nd$ = 0.512638 (Jacobsen and Wasserburg, 1980). The use of Nd isotopes is based on the fractionation of Nd and Sm between the mantle and the continental crust. The radiogenic ^{143}Nd isotope is produced from its parent isotope ^{147}Sm by α-decay, with a half-life of 106 Gyr. Samarium is preferentially enriched in the earth's mantle, whereas Nd is enriched in the continental crust. As a result Sm/Nd ratios (and consequently $^{143}Nd/^{144}Nd$ ratios) are lower in crustal than in mantle material, which is reflected in more positive (i.e., 'radiogenic') ε_{Nd} signatures in mantle-derived material such as basaltic rocks. This fractionation is expressed in the heterogeneous composition of rocks and their weathering products (e.g., Goldstein and Hemming, 2003; Jeandel et al., 2007). The oceans Nd budget is controlled by weathering of source material and input of dissolved and particulate Nd through rivers, dust, and SGD (e.g., Goldstein et al., 1984; Frank, 2002; Goldstein and Hemming, 2003; Tachikawa et al., 2003; Johannesson and Burdige, 2007), contributions from sedimentary pore fluids (Abbott et al., 2015b), and boundary exchange at continental margins and potentially mid-ocean ridges and the seafloor (Lacan and Jeandel, 2001; 2005a; Jeandel et al., 2007; 2013; Carter et al., 2012). Hydrothermal contributions to seawater ε_{Nd} are considered negligible due to the rapid absorption and removal of REEs by particulate phases close to the source (German et al., 1990; Halliday et al., 1992; Mitra et al., 1994; Stichel et al., 2012a; Zheng et al., 2016).

The ε_{Nd} signatures of continental rocks are imprinted to surface seawater and transported to the deep ocean at deep-water formation sites, such as the North Atlantic and the circum-Antarctic region. While Nd isotopes can therefore be used to study lithogenic material input to surface water, they are considered a quasi-conservative water mass tracer in the subsurface to deep ocean due to the comparably short residence time of Nd of 300-1000 years (Tachikawa et al., 2003; Arsouze et al., 2009; Rempfer et al., 2011) compared to the oceanic mixing time of ~1500 years (Broecker and Peng, 1982). Further, due to its high atomic mass, Nd is not subject to biological or chemical fractionation processes within the water column and changes in the ε_{Nd} signature of a water mass is thus only possible through external (i.e., terrestrial or submarine) Nd input or mixing with another water mass. This allows tracing the flowpaths of water masses through the oceans (e.g., Lacan and Jeandel, 2001; 2005a; Frank, 2002; Goldstein and Hemming, 2003).

The North Atlantic is subject to input of old continental crust material with very negative ε_{Nd} signatures, that results in an average Nd isotope signature of -13.5 for NADW (Piepgras and Wasserburg, 1987; Lacan and Jeandel, 2005b). These waters flow southward to the Southern Ocean where they mix with more radiogenic NPDW that derived their ε_{Nd} signature of -3 to -5 (Piepgras and Jacobsen, 1988; Amakawa et al., 2009) from input of mantle-derived basaltic i.e.,^{143}Nd-enriched, material (Jeandel et al., 2007). In the Southern Ocean mixing of NADW and NPDW results in intermediate isotope signatures of -8 to -9 in CDW (Piepgras and Wasserburg, 1982; Stichel et al., 2012b; Carter et al., 2012; Molina-Kescher et al., 2014a; Basak et al., 2015) that additionally derives contributions from bottom waters formed around Antarctica with distinct ε_{Nd} signatures of -7 to -9, depending on their formation region (Stichel et al., 2012b; Carter et al., 2012; Rickli et al., 2014; Basak et al., 2015).

1.3.3. Neodymium isotopes in sedimentary archives

The use of Nd isotopes as a paleo water mass tracer is based on the translation of the seawater signal to sedimentary archives such as fish teeth and debris (Martin and Haley, 2000; Thomas et al., 2003; Thomas, 2004; Martin and Scher, 2004), benthic and planktonic foraminifera (Klevenz et al., 2008; Roberts et al., 2010; 2012; Kraft et al., 2013; Tachikawa et al., 2014), deep-sea corals (van de Flierdt et al., 2006; 2010; Robinson and van de Flierdt, 2009; Wilson et al., 2014), ferromanganese oxide coatings on sediment particles (e.g., Rutberg et al., 2000; Piotrowski et al., 2004; Gutjahr et al., 2008; Pahnke et al., 2008) or Fe-Mn nodules and crusts (e.g., Albarede et al., 1997; Abouchami et al., 1997; Frank et al., 2002; van de Flierdt et al., 2004). Fundamental to this concept is the assumption that these archives acquire their ε_{Nd} signature during early diagenesis while they are still in contact with ambient seawater (Staudigel et al., 1985; Palmer and Elderfield, 1986; Martin and Haley, 2000; Martin and Scher, 2004).

While the use of Nd isotope records gained from ferromanganese nodules and crusts is limited to longer timescales due to their low temporal resolution as a result of low growth rates (e.g., Frank, 2002), deep-sea coral records are so far only available from intermediate water depths (cf. van de Flierdt and Frank, 2010). Thus, the reconstruction of deep and bottom water Nd isotope signatures on millennial to glacial-interglacial timescales is mainly based on records derived from fish teeth/debris, foraminifera and Fe-Mn oxide coatings.

Fossil fish teeth and debris, that is fossilised bio-phosphates, have been shown to reliably record seawater Nd isotope signatures (e.g., Martin and Haley, 2000; Thomas et al., 2003; Martin and Scher, 2004), even when extensive chemical cleaning is omitted (Martin et al., 2010) or sampling sites are located in the vicinity of potential hydrothermal sources (Molina-Kescher et al., 2014b). Additionally, it has been shown that ε_{Nd} values in teeth and debris (i.e., bone fragments) are identical (Thomas and Via, 2007; Martin et al., 2010). Neodymium concentrations in fossilised teeth/debris are distinctly higher than those in modern phosphates (e.g., teeth of living fish) (Shaw and Wasserburg, 1985; Staudigel et al., 1985; Elderfield and Pagett, 1986; Martin and Scher, 2004), which is due to incorporation of REEs into bio-phosphates during early diagenesis when they are still in contact with bottom water (Staudigel et al., 1985; Elderfield and Pagett, 1986; Martin and Haley, 2000; Huck et al., 2016). A great advantage of fossil fish teeth and debris is their resistance against dissolution in deep sea environments and the lack of diagenetic isotope exchange with pore waters (Staudigel et al., 1985; Elderfield and Pagett, 1986; Martin and Haley, 2000; Martin and Scher, 2004; Huck et al., 2016).

Foraminifera are another reliable recorder of deep and bottom water ε_{Nd} signatures. Rare earth elements are not only incorporated into the foraminiferal calcite structure, but a large portion is also found in associated phases, such as Fe-Mn-oxide coatings or organic matter (Roberts et al., 2012; Tachikawa et al., 2013). While benthic foraminifera have been shown to record bottom water Nd signals (Klevenz et al., 2008; Kraft et al., 2013), it was debated whether sedimentary planktonic foraminifera record water column, bottom water (early diagenetic), or mixed ε_{Nd} signatures (e.g., Pomies et al., 2002; Tachikawa et al., 2014). Some studies suggested the use of chemically cleaned planktonic foraminifera to reconstruct seawater Nd isotope signatures from the calcification depth of the living species (e.g., Vance and Burton, 1999; Burton and Vance, 2000; Vance et al., 2004; Pena et al., 2013), whereas others showed that both, cleaned and chemically uncleaned planktonic foraminifera, reflect the bottom water ε_{Nd} composition (e.g., Roberts et al., 2010; 2012; Piotrowski et al., 2012; Charbonnier et al., 2012; Kraft et al., 2013; Tachikawa et al., 2013). In a recent review, Tachikawa et al. (2014) concluded that chemically cleaned and uncleaned sedimentary planktonic foraminifera have the same Nd isotope signature that reflects bottom water ε_{Nd}, whereas plankton-tow derived foraminifera record seawater Nd signatures. They further noted that pore waters do not contribute to the foraminiferal Nd isotope composition in the investigated environments, although this could not be excluded in general (Tachikawa et al., 2014).

The use of sedimentary Fe-Mn oxides as an archive for past Nd isotope signatures of bottom waters has the advantage that it is independent from the availability of bio-phosphates or foraminifera and thus can be applied to all (oxic) sedimentary environments. These oxides are present as ferromanganese coatings on authigenic and lithogenic particles and reflect bottom water ε_{Nd} signals that were incorporated during early diagenesis (e.g., Martin et al., 2010 and references therein). It has been shown in numerous studies that these leaching solutions reliably record past bottom water ε_{Nd} signatures (e.g., Rutberg et al., 2000; Piotrowski et al., 2004; Pahnke et al., 2008; Gutjahr et al., 2008). Yet, other investigations showed that Fe-Mn oxide-based Nd isotope records can be compromised by contamination from other sources, such as pre-formed riverine oxides or easily leachable components (Bayon et al., 2004; Elmore et al., 2011; Wilson et al. 2013). The use of Fe-Mn oxide leaching solutions has therefore to be tested against more robust archives, i.e., fish teeth/debris or foraminifera (e.g., Martin et al., 2010; Piotrowski et al., 2012; Kraft et al., 2013) and/or compared to the detrital fraction to monitor potential contamination (e.g., Gutjahr et al., 2007) before interpreting them in a paleoceanographic context. Additionally, adequate leaching protocols have to be developed and tested for each environment, in particular with respect to prior decarbonation of the sediment samples (Wilson et al., 2013; 2015; Molina-Kescher et al., 2014b; Wu et al., 2015).

1.4. Motivation and thesis objectives

As indicated in the previous section the Nd isotope composition and Nd concentration in seawater has been studied for a couple of decades (cf. Lacan et al., 2012) and this dataset is continuously growing through the progress of the GEOTRACES program. Yet, the spatial resolution of Nd isotope and concentration data is still low, and investigated sites are not equally distributed throughout the ocean. Particularly in the Pacific Ocean, dissolved Nd data is scarce with limited amount of complete water column profiles (cf. Lacan et al., 2012). While the Nd isotope signature of NADW is well documented (e.g., Piepgras and Wasserburg, 1987; Lacan and Jeandel, 2005b), a broader range of values is suggested for NPDW (e.g., Piepgras and Jacobsen, 1988; van de Flierdt et al., 2004; Amakawa et al., 2009). However, detailed knowledge of water mass Nd isotope signatures is of significant importance for their use as a paleo-circulation tracer. This is particularly true for NPDW, since it is considered the radiogenic endmember in the modern and past global overturning circulation. Apart from this, many open questions remain, concerning the budget and cycling of Nd (and other REEs) in the ocean. For instance, dust is considered one of the sources of REEs to the surface ocean (Tachikawa et al., 1999). Yet, the influence of atmospheric input to the oceans REE and Nd isotope budget is still debated (Nakai et al., 1993; Jones et al., 1994; Greaves et al., 1994; 1999; Tachikawa et al., 1999; van de Flierdt et al., 2004). Several studies addressed the problem of the decoupling of Nd concentrations and isotopes in seawater (the so-called Nd-paradox), as well as the missing Nd flux to the ocean that is needed to explain the oceanic ε_{Nd} composition (Tachikawa et al., 2003; Goldstein and Hemming, 2003; Johannesson and Burdige, 2007; Jones et al., 2008; Siddall et al., 2008; Rempfer et al., 2011). While some authors suggested margin sediments and deep sediment pore water fluxes as an important source of Nd (Tachikawa et al., 2003; Arsouze et al., 2009; Rempfer et al., 2011; Abbott et al., 2015a,b), others recognised the importance of SGD for the oceans Nd and REE budget (Johannesson and Burdige, 2007; Johannesson et al., 2011). The analysis of Nd isotopes and REE concentrations in central North Pacific seawater has the potential to contribute to a better understanding of REE fluxes from volcanic islands to surface and deep waters, to better characterise North Pacific water masses concerning their Nd isotope signatures, and to better understand the dust influence to the oceans REE and Nd isotope budget.

For the application as a paleo-circulation tracer it is crucial to better understand the sinks and sources of REEs and Nd isotopes in seawater and to gain better knowledge about present-day Nd isotope distribution and processes that control the cycling in the modern ocean. Paleoceanographic studies that use Nd isotopes as proxy for past ocean circulation rely on the fact that Nd isotopes are a quasi-conservative tracer of water masses (e.g., Frank, 2002; Goldstein and Hemming, 2003). Despite the above described ambiguities in the oceanic Nd cycle, it has been shown in many studies that Nd isotopes extracted from sedimentary archives reliably record past water mass circulation and mixing processes (e.g., Piotrowski et al., 2004; Pahnke et al., 2008; Roberts et al., 2010). Yet, as for the modern ocean, the Pacific, and particularly the South Pacific (or South

Pacific sector of the Southern Ocean), is underrepresented in paleoceanographic investigations using Nd isotopes compared to the Atlantic Ocean. For the South Atlantic several deep water Nd isotope records show changes in water mass mixing and circulation during the last glacial termination (Rutberg et al., 2000; Bayon et al., 2002; Piotrowski et al., 2004; 2012; Skinner et al., 2013; Wei et al., 2016: Lippold et al., 2016) and throughout the last glacial-interglacial cycle (Piotrowski et al., 2005; 2008; Jonkers et al., 2015) mainly as a result of varying fractions of northern- and southern-sourced waters at the study sites. While studies of the modern Nd isotope composition of waters from the South Pacific and the adjacent sector of the Southern Ocean have increased during the last years (Carter et al., 2012; Jeandel et al., 2013; Noble et al., 2013; Molina-Kescher et al., 2014a; Rickli et al., 2014; Basak et al., 2015), only a very limited amount of paleo Nd isotope studies are published from this area, all being located north of 50˚ S (Elderfield et al., 2012; Noble et al., 2013; Molina-Kescher et al., 2016). Similarly, there is only a limited amount of paleo-circulation studies available based on carbon and oxygen isotopes across the Pacific sector of the Southern Ocean (Matsumoto and Lynch-Stieglitz, 1999; Hodell et al., 2000; Matsumoto et al., 2001; Ninnemann and Charles, 2002; Waddell et al., 2009; Ullermann et al., 2016), since most studies from this area focus on the western South Pacific close to New Zealand and Tasmania (e.g., Hall et al., 2001; Moy et al., 2006; McCave et al., 2008; Sikes et al., 2000; 2016; Ronge et al., 2015; 2016; Skinner et al., 2015). Neodymium isotopes can contribute to a better understanding of past variability in ocean circulation, water mass mixing and water column structure in the deep South Pacific sector Southern Ocean, thereby also contributing to a better understanding of mechanisms important for glacial deep carbon sequestration and deglacial CO_2 release from upwelled deep waters. An advantage of the South Pacific over the South Atlantic sector to investigate changes in ocean circulation and water mass mixing is the missing, or very limited (Rae et al., 2014), deep water production in the high latitude North Pacific, which eliminates the effect of monitoring fluctuations in direct input of northern-sourced deep water to CDW. Thus, it provides the opportunity to monitor the evolution of Southern Ocean endmember mixing. Further, Nd isotopes provide an independent proxy to test if deep-water carbon isotope records from the South Pacific (e.g., Ninnemann and Charles, 2002; McCave et al., 2008; Ullermann et al., 2016) are entirely governed by water mass circulation and water mass geometry, or if other processes, such as air-sea gas exchange or biogeochemical cycling, contribute to the carbon isotope variability.

The main objectives of this thesis therefore include (1) contributing to a better understanding of REE cycling and budgets in Pacific seawater by investigating lithogenic REE input and Nd isotope variations in Hawaiian coastal waters and the open ocean North Pacific and (2) the application of Nd isotopes as a tracer for past water mass circulation and mixing process during the last deglaciation and throughout the last glacial-interglacial cycle in the Pacific sector of the Southern Ocean. The goals of this thesis are to:

- evaluate the influence of the Hawaiian Islands on coastal water and open ocean North Pacific Nd isotope signatures and REE concentrations, and evaluate the relative importance of local *versus* distal sources and their seasonal variability to the North Pacific surface water REE budget, thereby contributing to a better understanding of REE and Nd cycling in the water column and a better characterisation of sources of REEs and potentially other trace elements to the ocean.
- contribute to a better characterisation of the REE concentration and Nd isotope composition of North Pacific water masses, in particular that of NPDW, which is the radiogenic endmember in the global meridional overturning circulation and of particular importance in paleo-circulation studies.
- investigate the variability in water mass mixing and water mass structure in the deep South Pacific during the last glacial-interglacial transition and its relation to Southern Hemisphere climate and NADW advection by the use of Nd isotopes measured on fossil fish teeth and foraminifera from five sediment cores.
- contribute to a better understanding of the variability in deep water mass mixing in the South Pacific during the last glacial-interglacial cycle (0-140 ka) by providing a Nd isotope record that allows comparison of the last two glacials, interglacials and glacial terminations as well as an inter-basin comparison with South Atlantic and Indian Ocean deep water records.
- present new insight into the reliability of the extraction of Nd isotopes from sedimentary ferromanganese oxides in the deep South Pacific.

1.5. Outline of the thesis

This thesis is divided into six main chapters. This introductory chapter provides a short introduction to the global meridional overturning circulation in modern and glacial climates as well as a general overview of the study areas and the modern hydrography in the Pacific Ocean. Further, the concepts of using Nd isotopes and rare earth elements as tracers for lithogenic element input and ocean circulation and the paleoceanographic use of Nd isotopes extracted from sedimentary archives are explained in detail. Finally, die motivation and objectives of this thesis are outlined.

Chapter 2 focuses on the modern dissolved Nd isotope and REE composition of surface, subsurface, intermediate and deep waters in the subtropical North Pacific around the Hawaiian Island of Oahu and at Hawaii Ocean Time-series Station ALOHA (HOT-ALOHA). Neodymium isotopes and REEs in combination with Radium (Ra) isotopes (^{226}Ra and ^{228}Ra, measured by Henrietta Dulai, University of Hawaii) are used to trace Hawaiian input to the surface ocean and to monitor the seasonal influence of distal Asian dust input *versus* local contributions. This chapter aims to contribute to the better understanding of Nd and REE cycling in the modern ocean and to the characterisation of Nd and REE sources to the open North Pacific. Investigation of the complete water column at Station ALOHA contributes to the better characterisation of North Pacific water masses, in particular NPDW, one of the endmembers in the global meridional overturning circulation. Further, for the first time the association of REEs to colloidal material in the open ocean is investigated. Part of the data produced in the course of this study (GEOTRACES Process Study GPpr05; cruise KM1107) will be included in the GEOTRACES Intermediate Data Product 2017 (IDP2017).

In chapter 3, Nd isotopes measured in fossil fish teeth/debris and planktonic foraminifera are used to investigate the changes in the water column structure and water mass mixing in the South Pacific Ocean from the LGM into the Holocene. This chapter includes Nd isotope records of five sediment cores from the southwest and southeast Pacific sector of the Southern Ocean covering deep (3000-4000 m) and abyssal waters (>4000 m). The focus of this study lies on investigating the water column structure in the South Pacific during the LGM and the evolution of the deep water column throughout the last deglaciation, with particular emphasis on the influence of Southern Hemisphere climate to deep water mass mixing.

Chapter 4 deals with the glacial-interglacial variability of deep water Nd isotope signatures in the Southern Ocean within the last 140,000 years. In this chapter the Nd isotope record of one sediment core from the Southeast Pacific investigated in chapter 3 is extended into the penultimate glacial maximum of Marine Isotope Stage (MIS) 6. This record allows monitoring the variability in water mass mixing in the Southeast Pacific over the last glacial-interglacial cycle and comparison of the last two glacial maxima, interglacials and glacial-interglacial transitions. Further, the new Nd isotope record allows an inter-basin comparison to the available glacial-interglacial Nd isotope records from the Indian and Atlantic Oceans, as well as a comparison with available carbon isotope records from the same core and a nearby location.

In chapter 5, the use of sedimentary ferromanganese oxide leachates to reconstruct past seawater Nd isotope signatures is tested for the Pacific sector of the Southern Ocean by comparing Nd isotope values derived from different leaching protocols to those gained from analysis of fossil fish teeth.

Finally, chapter 6 gives an overview of the general conclusions drawn from the results of this thesis together with an outlook of open questions and potential future research.

1.6. Author's contribution

This thesis includes one chapter that has been published in *Geochimica et Cosmochimica Acta* (chapter 2) and two chapters that have been prepared for publication (chapters 3 and 4). Chapter 5 will not be published. The chapters are prepared under consideration of the journal requirements, to which they have been submitted or are intended for submission, but the style is partly adapted to the thesis style and figures and tables are numbered consecutively throughout the thesis. A complete list of references is given at the end of the thesis. In the following, a detailed overview of the authors' contributions to each chapter is presented.

Chapter 2: Hawaiian imprint on dissolved Nd and Ra isotopes and rare earth elements in the central North Pacific: local survey and seasonal variability (published):

This chapter has been published in the journal *Geochimica et Cosmochimica Acta* (2016), 189, 110-131, http://dx.doi.org/10.1016/j.gca.2016.06.001 and is authored by Henning Fröllje, Katharina Pahnke, Bernhard Schnetger, Hans-Jürgen Brumsack, Henrietta Dulai, and Jessica N. Fitzsimmons.

Seawater and groundwater samples were taken by Katharina Pahnke, Henrietta Dulai (University of Hawaii, Honolulu; cruise KM1107), Jessica Fitzsimmons, Gonzalo Carrasco, Edward Boyle, and Christopher Hayes (all MIT, Boston; remaining cruises), who also did the onboard processing of the samples (i.e., filtration and acidification). Jessica Fitzsimmons performed cross-flow filtration of samples from cruise KM1316. Sampling was coordinated by Katharina Pahnke, who also initially devised and planned the project. Radium isotope analyses were performed by Henrietta Dulai, who also interpreted the Ra isotope data and wrote the sections on Ra isotopes in the manuscript. Katharina Pahnke measured groundwater Nd isotopes. Thomas Badewien (ICBM) processed CTD data of cruise KM1107. I received pre-filtered seawater samples and did all the laboratory-based sample preparation for Nd isotope and REE analysis. A small set of samples (16 Nd isotope samples) was prepared by Sebastian Haas (MPI) during a research project under my supervision. I measured all seawater Nd isotope and REE samples and evaluated and interpreted the data. All authors contributed to the interpretation and the discussion. I wrote the manuscript with input from all co-authors.

Chapter 3: Break-up of last glacial deep stratification in the South Pacific (in preparation):

This chapter is in preparation for submission to the journal *Science*. It is a collaboration between me and Chandranath Basak (MPI/ICBM, now LDEO, New York) and written as a co-first-authored manuscript, to which the first and second authors contributed equally. The final manuscript will be authored by Chandranath Basak, Henning Fröllje, Frank Lamy, Rainer Gersonde, Verena Benz, Robert F. Anderson, and Katharina Pahnke.

Material for this study was provided by Rainer Gersonde, Frank Lamy (both AWI Bremerhaven; Polarstern cores) and Robert F. Anderson (LDEO; core E11-2). We received most samples as dry, size-fractionated samples. I re-sampled core PS75/073-2 at AWI to increase the sampling resolution. I prepared and measured all samples of cores PS75/073-2, PS75/059-2 and some samples of core PS75/056-1. Samples of cores PS75/054-1, E11-2 and the majority of the samples of core PS75/056-1 were prepared and analysed by C. Basak. Student Research Assistants Kim Arndt and Felix Mielke (both University of Oldenburg) picked some of the foraminifera and fish teeth/debris from the samples under my and C. Basak's supervision. The results were evaluated and interpreted by C. Basak and me with contributions from the co-authors. I created the age models in collaboration with C. Basak, K. Pahnke, and F. Lamy. Johannes Ullermann (AWI) measured benthic $\delta^{18}O$ of cores PS75/059-2 and PS75/056-1, and V. Benz and R. Gersonde (both AWI) provided planktonic $\delta^{18}O$ data of core PS75/073-2, which were used for age model construction. Verena Benz and Thomas Ronge (both AWI) provided preliminary age models for earlier stages of interpretation. XRF data were measured with the XRF core scanner at the AWI Bremerhaven and were provided by F. Lamy and R. Gersonde. I wrote the manuscript together with C. Basak, with input from K. Pahnke.

Chapter 4: Neodymium isotope evidence for variable glacial-interglacial deep-water mixing in the Southern Ocean over the last 140 ka (in preparation):

This chapter will be submitted to the journal *Paleoceanography* and will be authored by Henning Fröllje, Chandranath Basak, Katharina Pahnke, Frank Lamy, and Rainer Gersonde.

Material for this study was provided by R. Gersonde and F. Lamy (both AWI Bremerhaven). I received sieved, size-fractionated samples and did most of the fish teeth picking, assisted by Student Research Assistants Felix Mielke and Kim Arndt (both University of Oldenburg). I prepared and measured all samples and created the age model. Benthic $\delta^{18}O$ used for age model construction was measured by Johannes

Ullermann (AWI) and provided by J. Ullermann and F. Lamy. I evaluated the data, interpreted the results, and wrote the manuscript, with input from all co-authors.

Chapter 5 Leaching of sedimentary Fe-Mn oxides fails to produce reliable Nd isotope records in the deep South Pacific:

Material for this study was provided by the Antarctic Marine Geology Research Facility at Florida State University (Eltanin samples) and by Frank Lamy and Rainer Gersonde (both AWI Bremerhaven, Polarstern samples). I sampled the Polarstern core PS75/095-5 at AWI, did all sample preparations and performed all leaching procedures. I measured all samples for their Nd isotope composition, interpreted the data and wrote the chapter. Comments of Katharina Pahnke, Claudia Ehlert (MPI), and Chandranath Basak (LDEO) contributed to the interpretation and discussion of the results.

2. Hawaiian imprint on dissolved Nd and Ra isotopes and rare earth elements in the central North Pacific: local survey and seasonal variability

Henning Fröllje[a], Katharina Pahnke[a], Bernhard Schnetger[b], Hans-Jürgen Brumsack[b], Henrietta Dulai[c], Jessica N. Fitzsimmons[d,1]

This chapter corresponds to a full manuscript that has been published
in the journal Geochimica et Cosmochimica Acta (2016), 189, 110-131,
http://dx.doi.org/10.1016/j.gca.2016.06.001

[a] Max Planck Research Group for Marine Isotope Geochemistry, Institute for Chemistry and Biology of the Marine Environment (ICBM), University of Oldenburg, Carl-von-Ossietzky-Str. 9-11, 26129 Oldenburg, Germany.

[b] Microbiogeochemistry, Institute for Chemistry and Biology of the Marine Environment (ICBM), University of Oldenburg, Carl-von-Ossietzky-Str. 9-11, 26129 Oldenburg, Germany.

[c] Department of Geology and Geophysics, School of Ocean and Earth Science
and Technology, University of Hawaii, 1680 East-West Rd, Honolulu, HI 96822, USA.

[d] Massachusetts Institute of Technology, Department of Earth Atmospheric and Planetary Sciences, 77 Massachusetts Avenue, Cambridge, MA 02139, USA

[1] Present Address: Texas A&M University, Department of Oceanography, College Station, TX 77843, USA.

Abstract

Dissolved neodymium isotopes ($^{143}Nd/^{144}Nd$, expressed as ε_{Nd}) and rare earth elements (REE) have the potential to trace the provenance of lithogenic material as well as water masses. The central North Pacific is poorly investigated with respect to its Nd isotope signature and REE cycling, and little is known about the contributions of volcanic islands, such as Hawaii, relative to dust input from Asian deserts to the surface water REE budgets. Here we present dissolved Nd isotope and REE data along with long-lived radium isotope activities from Hawaii Ocean Time-Series Station ALOHA and coastal waters from Oahu, sampled for a GEOTRACES process study in February 2011. The data are supplemented with seasonal samples from ALOHA. Our results show a clear influence of the Hawaiian Islands on the coastal ocean and surface waters at ALOHA during February, expressed by higher surface water Ra activities, radiogenic surface ε_{Nd} (ε_{Nd} = +1.4 to -1.0), and elevated Eu anomalies (Eu/Eu* ≥ 1.3). Seasonal cycles of Asian dust deposition most likely contribute to the seasonal ε_{Nd} variability of surface waters at ALOHA, as suggested by more negative ε_{Nd} and the lack of Eu anomalies in summer. Neodymium isotopes in the intermediate and deep water column at ALOHA trace typical North Pacific water masses, such as North Pacific Intermediate Water and North Pacific Deep Water. We suggest that a radiogenic ε_{Nd} excursion in 1000-2000 m water depth, observed in various North Pacific profiles, is controlled by advection of a modified Upper Circumpolar Deep Water or North Equatorial Pacific Intermediate Water. We further present an updated average ε_{Nd} signature of -3.5 ± 0.5 for North Pacific Deep Water and show that REE patterns of deep waters at ALOHA are dominantly controlled by vertical processes.

2.1. Introduction

Rare earth element (REE) patterns and neodymium isotopes in seawater, authigenic Fe-Mn oxides, and lithogenic particles are widely used to study modern and past ocean circulation, lithogenic particle provenance, and aeolian input. Nonetheless many open questions remain, including the budget of Nd and REE with potential contributions of submarine groundwater discharge (SGD) and margin sediments (Tachikawa et al., 2003; Johannesson and Burdige, 2007), benthic flux from sediment pore fluids (Abbott et al., 2015a,b), and a missing flux of radiogenic Nd to the North Pacific (e.g., Jones et al., 2008). Moreover, the importance of dust to the Nd and REE budget is still under debate. While some studies suggest little or no influence of dust particles on the Nd isotope and REE signal in the North Pacific (Nakai et al., 1993; Jones et al., 1994; van de Flierdt et al., 2004; Hongo et al., 2006), others show clear evidence that dust deposition modifies at least the surface water signal of ε_{Nd} and REEs in this area and in the North Atlantic under the Saharan dust plume (e.g., Shimizu et al., 1994; Greaves et al., 1999; Tachikawa et al., 1999; Stichel et al., 2015).

Neodymium isotope ratios ($^{143}Nd/^{144}Nd$) are typically expressed in ε_{Nd} notation, where $\varepsilon_{Nd} = [(^{143}Nd/^{144}Nd)_{sample}/(^{143}Nd/^{144}Nd)_{CHUR} - 1]*10^4$, with $(^{143}Nd/^{144}Nd)_{CHUR} = 0.512638$ representing the Chondritic Uniform Reservoir (Jacobsen and Wasserburg, 1980). The ε_{Nd} of seawater varies locally as a result of the heterogeneity of weathered material that is delivered to the ocean in particulate, colloidal, and/or dissolved form through fluvial and aeolian input (e.g., Frank, 2002), SGD (e.g., Tachikawa et al., 2003; Johannesson and Burdige, 2007), and boundary exchange processes (Lacan and Jeandel, 2001; 2005a). Apart from lithogenic input, the quasi-conservative behaviour of ε_{Nd} in the ocean and the short residence time of 300-1000 years (Tachikawa et al., 2003; Arsouze et al., 2009; Rempfer et al., 2011) lead to characteristic ε_{Nd} signatures in different parts of the ocean, with the Pacific being generally more radiogenic ($\varepsilon_{Nd} \approx -4$; Piepgras and Jacobsen, 1988; Amakawa et al., 2009; Pahnke et al., 2012) than Atlantic, Indian, and Southern Ocean waters (cf. Lacan et al., 2012). Neodymium isotopes are therefore widely used as a tracer of modern and past ocean circulation (e.g., von Blanckenburg, 1999; Frank, 2002; Piotrowski et al., 2004; Lacan and Jeandel, 2005a; Pahnke et al., 2008).

Neodymium concentrations, on the other hand, are mainly controlled by vertical processes of surface input, particle scavenging, and release at depth, as typical for the coherent group of REEs (e.g., Elderfield and Greaves, 1982; Elderfield, 1988; Bertram and Elderfield, 1993; Tachikawa et al., 1999), but can also be influenced by lateral transport in some areas of the ocean (e.g., Basak et al., 2015; Stichel et al., 2015). Preferential adsorption of light REEs (LREE) onto particles and stronger complexation of heavy REEs (HREE) lead to fractionation that results in a heavy over light REE enrichment in seawater (Cantrell and Byrne, 1987; Elderfield, 1988; Byrne and Kim, 1990; Sholkovitz et al., 1994; Tachikawa et al., 1999), which is typically visualised by normalisation to a reference water mass or lithogenic background. Dissolved REE patterns of seawater are further characterised by a negative Ce anomaly that results from microbially controlled Ce oxidation (Elderfield and Greaves, 1982; Moffett, 1990). Normalised REE patterns and resulting anomalies, such as of Eu and Gd, as well as individual elemental ratios can be used to identify lithogenic input to the ocean, processes associated with particle scavenging and release in the water column, and redox conditions (e.g., Bertram and Elderfield, 1993; Greaves et al., 1994; Sholkovitz et al., 1999; Zhang et al., 2008; Grenier et al., 2013; Jeandel et al., 2013).

Here we present Nd and Ra isotope and REE concentration data of coastal waters of the Hawaiian Island of Oahu and from Hawaii Ocean Time-series Station ALOHA (HOT-ALOHA; ALOHA = A Long-term Oligotrophic Habitat Assessment) from the GEOTRACES process study cruise KM1107 (Process Study GPpr05) together with additional data from seasonal cruises conducted by the Center for Microbial Oceanography: Research and Education (C-MORE).

We evaluate the influence of the Hawaiian Islands on the coastal surface and subsurface waters and on the open ocean of the central North Pacific at Station ALOHA. Seasonal sampling of surface waters at ALOHA further allows for an assessment of local Hawaiian *versus* distal Asian dust influence on the dissolved REE and ε_{Nd} at this open ocean station. Boyle et al. (2005) and Fitzsimmons et al. (2015) previously argued for a prominent Asian dust impact on dissolved iron concentrations at ALOHA. Given the distinct ε_{Nd} and REE signatures of Asian dust (ε_{Nd} = -10.3; Taylor et al., 1983; Goldstein et al., 1984; Nakai et al., 1993; Liu et al., 1994) and Hawaiian basalts (average ε_{Nd} = +6.2, Tanaka et al., 2008; positive Eu anomaly, e.g., Ren et al., 2009), combined Nd isotope and REE analyses of waters from coastal sites around Oahu and Station ALOHA allow for a detailed characterisation of the Hawaiian and Asian dust impact on coastal and open ocean waters.

At selected stations and depths, long-lived radium isotope signatures were used to complement the REE information to further support the terrestrial overprinting on water masses around the island of Oahu and at Station ALOHA. Sources of long-lived radium isotopes in the ocean are bottom sediments and coastal sources that include diffusion from shelf sediments, rivers, and SGD. Radium-226 (half-life = 1600 y) occurs at relatively high activities offshore in the Pacific Ocean due to release from bottom sediments and continental sources that mix up into the open ocean where it persists due to its relatively long half-life (Broecker et al., 1967; 1970; Huh and Ku, 1998). Radium-228 (half-life = 5.8 y) decays much faster, and can only be observed near margins and bottom waters, where it provides evidence for recent terrestrial input from streams, SGD, or sediment/rocks (e.g., Moore et al., 2008; Kwon et al., 2014).

Additionally, sampling of the full water column at Station ALOHA adds significantly to the rather sparse spatial resolution of water column sites with available Nd isotope data in the central North Pacific Ocean (cf. Lacan et al., 2012) and allows investigation of the potential contribution of volcanic islands to the intermediate and deep water ε_{Nd} composition in the North Pacific.

2.1.1. Study area

The North Pacific study area comprises the coastal waters of the Hawaiian Island of Oahu and Station ALOHA (Fig. 2.1). In coastal waters, the sampling sites are located a few km off the coast with a maximum sampling depth of 350 m. A station between the northern tip of Oahu and ALOHA is located approximately 15 km off Oahu with a maximum sampling depth of ~1350 m. Station ALOHA, established in 1988 as an oligotrophic ocean time-series station, is located 100 km north (i.e., upstream) of Oahu within the North Pacific Subtropical Gyre at a location where biogeochemical influence of the Hawaiian Islands is assumed to be negligible, and has a water depth of ~4800 m (Karl and Lukas, 1996).

The Hawaiian climate is characterised by higher rainfall in winter than in summer and by spatial differences in precipitation and discharge due to high mountain ranges and the predominant easterly trade winds (Oki, 2003; Giambelluca et al., 2013). On Oahu, the eastern part of the island therefore receives higher rainfall than the western part (Giambelluca et al., 2013). Submarine groundwater discharge has been shown to be an important contributor of freshwater and nutrients to the coastal ocean of the Hawaiian Islands (see review of Moosdorf et al., 2015 and references therein). In addition, the North Pacific Ocean is subject to seasonally varying dust input from the Asian continent with peak fluxes during spring (Duce et al., 1980; Uematsu et al., 1985; Prospero et al., 1989). This seasonal cycle of dust transport also affects the deposition on the Hawaiian Islands (Parrington et al., 1983) and has been proposed to influence Fe and Th concentrations in surface waters at ALOHA (Boyle et al., 2005; Fitzsimmons et al., 2015; Hayes et al., 2015). Isotope investigations have shown that dust deposited in the central North Pacific Ocean mainly consists of Chinese Loess (Nakai et al., 1993; Jones et al., 1994; 2000; Asahara et al., 1995).

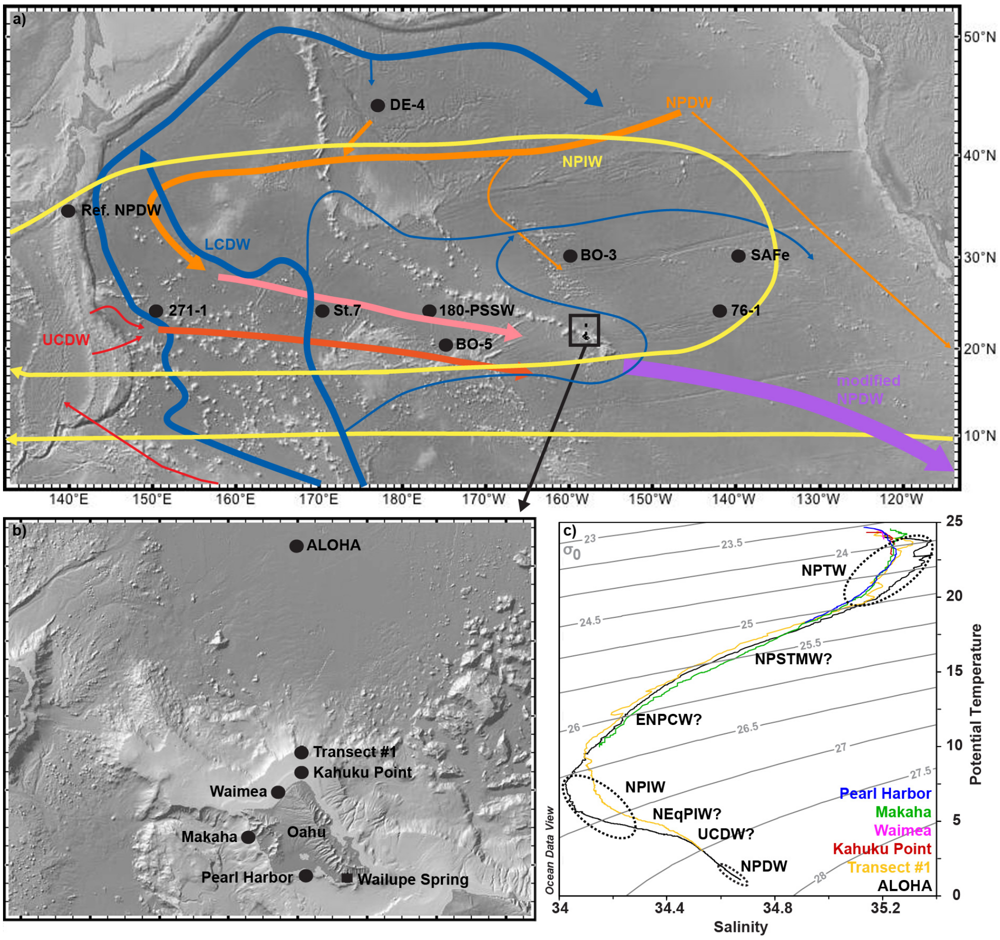

Figure 2.1: Maps showing locations of the Hawaiian Islands in the central North Pacific and sampling sites around Oahu, Hawaii. a) North Pacific general circulation scheme (after Kawabe and Fujio, 2010) with sampling sites from other studies discussed in the text. TPS24 271-1 and TPS24 76-1 (Piepgras and Jacobsen, 1988; 1992); DE-4 (Shimizu et al., 1994); 180-PSSW (Greaves et al., 1999); BO-3 and BO-5 (Amakawa et al., 2009); St. 7 (Zimmermann et al., 2009); SAFe (Pahnke et al., 2012); and a site near Japan (Alibo and Nozaki, 1999), here named Ref. NPDW. b) Map of Oahu, Hawaii with sampling stations of cruise KM1107 and at time series Station ALOHA (different cruises), and groundwater sampling site at Wailupe Spring (black square). Maps created with GeoMapApp. c) Potential temperature vs. salinity plot of KM1107 samples. Water masses that could be identified based on their hydrographic properties were NPTW, NPIW and NPDW. The presence of the remaining water masses was not explicitly established. Figure c) was created with Ocean Data View (Schlitzer, 2014).

2.2. Material and Methods

2.2.1. Sampling and REE pre-concentration

Seawater samples for Nd isotope and REE concentration analyses were taken during the GEOTRACES process study cruise KM1107 (GPpr05) on *R/V Kilo Moana* around the island of Oahu and at Station ALOHA in February 2011 (Fig. 2.1b; Tab. 2.1). Additional samples were collected during several C-MORE cruises to Station ALOHA from water depths of 0-750 m: KM1215, July 2012, C-MORE HOE-DYLAN V (Wilson and

Fitzsimmons, 2012); KM1219, August 2012, C-MORE HOE-DYLAN IX (Wilson and Tozzi, 2012); KM1309, June 2013, C-MORE HOE-PhoR I (Björkman and Fontanez, 2013) (Tab. 2.1). Furthermore, we received samples for REE concentration measurements from three water depths (15 m, 130 m, 1000 m) from cruise KM1316 conducted in September 2013 (C-MORE HOE-PhoR II, Clemente and Samo, 2013; Tab. 2.1). All seawater samples were collected in 12 L Niskin/Bullister bottles with nylon-coated stainless steel springs attached to a rosette frame equipped with a Sea-Bird CTD.

Groundwater was sampled from Wailupe Spring on Wailupe Beach at the south coast of Oahu, where groundwater is discharged in discrete springs (21˚16.54 N, 157˚45.73 W, May 2010). The samples were taken from 0.8 m and 1.4 m sediment depth using a push-point sampler. The samples were filtered through AcroPak500 cartridges (0.8/0.45 µm) and acidified to pH = 2.

For Nd isotope analyses, five litres of seawater were filtered on board of the research vessel through AcroPak500/200 cartridges (pore size of 0.8/0.45 µm and 0.8/0.2 µm, respectively) into pre-cleaned LDPE containers (cf. Pahnke et al., 2012) and acidified to a pH of ~2 with ultra-clean 6 N HCl (self-distilled or Fisher Scientific optima grade). For analyses of dissolved REE concentrations, a volume of 50-250 mL of filtered seawater was either collected directly from Niskin/Bullister bottles (cruises KM1107, KM1316) into pre-cleaned LDPE bottles and acidified to a pH of ~2 with ultra-pure 6 N HCl, or subsamples were taken from the 5 L Nd containers in the land-based laboratory (cruises KM1215, KM1219, and KM1309). On cruise KM1316, the sample from 15 m water depth was collected with a Teflon pump directly into a pre-cleaned LDPE bottle through an AcroPak1500 filter (0.2 µm).

All samples from cruise KM1316 were additionally size fractionated by cross flow filtration to provide one dissolved sample (<0.2 µm (15m) or <0.45 µm (130 m, 1000 m)), one permeate sample (soluble Nd, <10 kDa, ~0.003 µm), and one retentate sample (10 kDa to 0.2 µm or 10 kDa to 0.45 µm, plus the soluble REEs in each case). It is important to note that during cross flow filtration, the soluble-sized REEs (like the water carrier phase) both pass through the filter into the permeate and across the filter into the retentate fractions, with a balance established based on the relative permeate and retentate flow rates that is quantified as the concentration factor. Thus, the retentate fraction contains both the colloidal REE fraction retained by the filter as well as a portion of the soluble fraction (see below and Fitzsimmons and Boyle, 2014), such that the true colloidal REE concentration must be calculated from the permeate and retentate measurements and the concentration factor. Cross flow filtration was completed on board the ship using pre-filtered seawater following the method described for Fe in Fitzsimmons and Boyle (2014). Briefly, a pre-cleaned Millipore *Pellicon XL* filter was rinsed with 500 mL of 1.5 N HCl and conditioned with 350-400 mL of the pre-filtered (<0.2 or <0.45 µm) seawater. Cross flow filtration was executed at a total flow rate of ~25 mL/min to a final retentate and permeate volume of ~500 mL each. The colloidal REE fraction (c_{REE}) of the samples was calculated as ($REE_{retentate}$-$REE_{permeate}$)/CF (Buesseler et al., 1996), with CF = 2 being the concentration factor that results from the equal permeate and retentate flows of ~12.5 mL/min. The concentration factor is calculated by ($Vol._{retentate}$+$Vol._{permeate}$)/$Vol._{retentate}$ (Buesseler et al., 1996) and the recovery of each REE can be calculated by (s_{REE}+c_{REE})/d_{REE}*100%, where s_{REE} corresponds to the concentration of the REE in the permeate fraction and d_{REE} to the REE concentration in the dissolved (<0.2 or <0.45 µm) fraction.

2.2.2. Neodymium isotope analysis

For Nd isotope analyses in seawater, REEs were pre-concentrated from the samples using C_{18} SepPak® cartridges (Waters Inc.) following a method modified after Shabani et al. (1992) and Jeandel et al. (1998). The C_{18} cartridges were cleaned using 5-10 mL 0.5 N HCl and rinsed with MilliQ to bring the pH back to neutral. They were filled with 300 mg of a REE complexing agent (HDEHP, 2-ethylhexyl phosphate for synthesis, Merck), followed by another cleaning step with 2 mL 6 N HCl and rinsing with MilliQ prior to further use. After adjusting to a pH of 3.5 using distilled ammonia hydroxide solution (self-distilled from reagent grade ammonia hydroxide, 35%, Fisher Scientific), the samples were pumped through the pre-cleaned C_{18} cartridges at a pump rate of 20 mL/min. The cartridges were then rinsed with 0.01 N HCl to remove Ba and the REEs were eluted with 35 mL of 6 N HCl. Neodymium was then isolated by a two-step column procedure (Pin and Zalduegui, 1997). The first set of columns was filled with Eichrom TRU-Spec resin (100 µL, particle size 100-150 µm) and used for separation of REEs from any HDEHP that may have leaked out of the C_{18} cartridges. In the second step, columns filled with TrisKem LN-Spec resin (250 µL, particle size 50-100 µm) were used to isolate Nd from the other REEs with 0.23-0.25 N HCl as eluent. The Nd aliquot was treated with a 1:1 mixture of H_2O_2 (30%) and concentrated HNO_3, dried, and re-dissolved in 2% HNO_3 for isotope measurements. All used acids were of ultra-clean quality (self-distilled or Fisher Scientific optima grade).

Neodymium isotopes were measured on a ThermoScientific *Neptune Plus* multi-collector inductively coupled plasma mass spectrometer (MC-ICP-MS) at the University of Oldenburg. A Cetac *Aridus II* desolvating nebuliser system was used for sample introduction. We varied the sample volume and measurement time depending on the Nd concentration of the samples. Samples with ≥5 ng Nd were analysed for 4x12 cycles at a concentration of 5-10 ppb (1 mL sample solution) with previous peak centring, whereas samples with <5 ng Nd were measured for 1x36 cycles at a concentration of 4-5 ppb (500-600 µL sample solution). For these low concentration samples, peak centring was only done prior to the analysis of the Nd standard JNdi-1, which was measured generally every 2nd-3rd sample at the same concentration as the samples. All samples were corrected for mass bias with $^{146}Nd/^{144}Nd = 0.7219$ using an exponential law (O'Nions et al., 1977). We applied a secondary mass bias correction using linear correlation of $^{143}Nd/^{144}Nd$ to $^{142}Nd/^{144}Nd$ (Vance and Thirlwall, 2002). All data were normalised to the accepted JNdi-1 value of $^{143}Nd/^{144}Nd = 0.512115$ (Tanaka et al., 2000). External reproducibility, checked with multiple runs of 5-10 ppb JNdi-1 during each session, was generally better than 40 ppm (± 0.4 ε_{Nd} units, 2σ, n=8-24 per session). An independent secondary in-house standard (5-10 ppb, n=16) was measured one to two times per session and had a reproducibility of 30 ppm (± 0.3 ε_{Nd} units, 2σ) over the entire measurement period. Two of the secondary standards were measured in REE-free seawater matrix, produced from co-precipitation of trace metals with Fe hydroxide according to the method described in detail in Stichel et al. (2012b). The Nd isotope measurements of these standards with seawater matrix did not differ from the matrix-free standards. Three independently processed duplicate samples had the same ε_{Nd} within analytical uncertainty (Fig. 2.2; Tabs. 2.1, A2.1). The lab is intercalibrated for Nd isotope measurements through analysis of GEOTRACES intercalibration samples BATS and SAFe. The procedural laboratory Nd blank (n=12; comprising column chemistry (all) and elution from C_{18} cartridges (n=4)) was ≤10 pg, representing <1% of the Nd concentration of the samples. Therefore, no blank correction was applied. Groundwater samples were analysed at the University of Hawaii at Manoa using Fe co-precipitation for pre-concentration, two-step column chemistry for Nd isolation, and thermal ionisation mass spectrometry (TIMS) as described in Basak et al. (2015).

2.2.3. Rare earth element analysis

We used isotope dilution (ID) analysis for the determination of REE concentrations in the seawater samples. For this purpose, 10-80 mL aliquots of the samples, depending on REE concentrations, were mixed with a multi-element REE spike (enriched in the isotopes ^{139}La, ^{142}Ce, ^{145}Nd, ^{149}Sm, ^{153}Eu, ^{155}Gd, ^{161}Dy, ^{167}Er, ^{171}Yb, ^{175}Lu). The sample-spike mix was equilibrated for at least 24 h and pre-concentrated and purified with the commercially available *seaFAST* system (Elemental Scientific Inc.) according to a method modified from Hathorne et al. (2012). The system was operated in offline mode. Briefly, the samples were loaded together with a buffer-solution (pH = 6.2) made of ammonia hydroxide solution (ultra-quality, Carl Roth) and glacial acetic acid (supra-quality, Carl Roth) onto a column containing a REE-complexing resin (EDTriA/IDA). The column was washed with the buffer solution and MilliQ to remove the seawater matrix and REEs were eluted from the column with 500-2000 µL of 1.5 N ultra-pure HNO_3 (Fisher Scientific optima grade) depending on the used sample volume, resulting in concentration factors of 20-40.

The pre-concentrated samples were diluted with MilliQ to volumes of 0.8-1 mL for ICP-MS analysis. Rare earth element concentrations were measured on a Thermo Finnigan *Element II* sector field inductively coupled plasma mass spectrometer (ICP-MS) at the University of Oldenburg in low-resolution mode. The ICP-MS was coupled to a Cetac *Aridus II* desolvating nebuliser system that ran with argon and nitrogen gas in order to decrease oxide formation rates. Sample introduction was achieved with a 100 µL nebuliser and a Cetac *ASX-100* autosampler. Oxide formation rates were monitored for Ba and Ce before each measurement session and were lower than 0.03%. The blank of the ICP-MS measurements was checked by analysis of 2% HNO_3 every five samples and the daily-averaged blank counts were subtracted from each sample. Total procedural blanks (n=9; made from 10-80 ml 2% HNO_3) were spiked and prepared analogous to the samples.

Procedural blanks averaged <3% of the average sample concentration (except for Tb = 3.4% and Ce = 14%) and <5% of the minimum concentration of the samples (except for La = 8.2%, Ce = 31% and Tb = 7%). The average procedural blank results are given in Table A2.2. The internal error was typically <5% for all elements. The reproducibility (2σ) of the measurements between sessions was checked with multiple runs (1-2 per session) of a standard solution that contains REEs at seawater-like relative concentrations (coral standard from the Coral Sea, provided by Gideon Henderson, University of Oxford, UK) and was <7% for all elements except for Gd (7.3%) (n=6). The external reproducibility (2σ) was checked by multiple processing and analyses of the international GEOTRACES reference standards BATS (15 m, n=4; van de Flierdt et al., 2012) and SAFe (3000 m, n=9; Pahnke et al., 2012 (Nd concentration only)) and was <9% for all elements except for Ce (66 %) and Gd (10.8%). Detailed results are given in Table A2.2. The average measured REE concentrations are in good agreement with published values (deviation of <5% for all elements for BATS, van de Flierdt et al., 2012; 5.4% for SAFe (Nd), Pahnke et al., 2012). Analyses of three independently processed duplicate samples agreed within analytical uncertainty (Fig. 2.2; Tab. A2.2).

2.2.4. Radium isotope analysis

Seawater samples for radium isotope activity analyses were taken concurrently with REE samples during the GEOTRACES process study cruise KM1107 on *R/V Kilo Moana* around the island of Oahu and at ALOHA in February 2011 (Fig. 2.1b; Tab. A2.1). Furthermore, radium isotopes were also analysed in Wailupe Springs in samples collected concurrently with the Nd isotope samples as described above. The ocean sample volumes were ~100 L and the spring samples were 5 and 13 L. All samples were filtered through a MnO_2-coated acrylic fibre at flow rates below 1 L/min. The fibres were then ashed and packed into tin containers for analysis on an Ortec GEM40 coaxial gamma-spectrometer at the University of Hawaii. Radium-226 was analysed via its decay product Bi-214 at 609 keV and ^{228}Ra via ^{228}Ac at 911 keV (Dulaiova and Burnett, 2004).

2.3. Results

Detailed results are listed in Tables A2.1-A2.3 in Appendix A and on Pangaea (www.pangaea.de) under doi: 10.1594/PANGAEA.855127.

2.3.1. Hydrography

Surface and subsurface waters within the upper ~200 m at the coastal stations and at ALOHA have salinity and density properties characteristic of North Pacific Tropical Water (NPTW; salinity >34.9; σ_θ = 23-25 kg/m^3; Cannon, 1966; Suga et al., 2000) (Fig. 2.1c; Tab. 2.1). North Pacific Intermediate Water (NPIW) at ALOHA is present between ~500 m and 1200 m water depth (σ_θ = 26.6-27.4; e.g., Yasuda, 2004), while its characteristic salinity minimum (34.0-34.3; e.g., Talley, 1993; You et al., 2000; You, 2003; Yasuda, 2004) is centred at ~570 m (Fig. 2.2a). At station Transect #1, NPIW is found at ~400-1200 m water depth, with the salinity minimum centred at ~350 m, above the oxygen minimum at 750 m (Fig. 2.2b). The circulation of NPIW follows the gyre circulation and extends to about 20° N in the central North Pacific (e.g., Talley, 1993; You et al., 2000) (Fig. 2.1a). The water column between NPTW and NPIW may be either a mixture of both or is influenced by North Pacific Subtropical Mode Water (NPSTMW; σ_θ = 25.2 kg/m^3, salinity = 34.7-34.9; e.g., Suga et al., 1989; Talley et al., 2011) and/or Eastern North Pacific Central Water (ENPCW; σ_θ = 26.0 kg/m^3; Talley et al., 2011). The σ_θ = 27.0 kg/m^3 density surface that separates old (lower) and new (upper) NPIW (Yasuda, 2004), is located at ~660 m depth, thus separating samples taken at 500 m and 750 m at ALOHA. The oxygen minimum is centred at ~750 m depth (σ_θ = 27.2 kg/m^3) within the lower NPIW layer (Fig. 2.2a). Influence of North Equatorial Pacific Intermediate Water (NEqPIW) at

ALOHA, characterised by an oxygen minimum north of the equator and a higher salinity (34.5-34.6) than NPIW (Bostock et al., 2010) may also contribute to the oxygen minimum in the lower NPIW layer. Bostock et al. (2010) show that the Hawaiian Islands lie within the mixing zone of NPIW and NEqPIW.

Table 2.1: Site information, hydrographic data, and dissolved Nd isotope ratios for all seawater samples of this study. For more detailed information refer to Table A2.1.

Site information	Water depth [a] [db]	θ [a] [°C]	S [a]	σ_θ [a] [kg/m^3]	ε_{Nd}	Error [b] ±	Water mass
Pearl Harbor (KM1107-2)							
21°17.087' N; 157°57.596' W	10	24.49	35.19	23.64	0.5	0.6	NPTW
02/25/2011	29	24.28	35.21	23.72	-1.0	0.6	NPTW
Bottom Depth: 226 m	50	24.18	35.22	23.75	0.0	0.5	NPTW
MLD: 17 m	99	22.41	35.23	24.28	-1.5	0.6	NPTW
	179	18.49	34.94	25.10	-3.0	0.5	NPTW
Makaha (KM1107-4)							
21°27.93' N; 158°14.466' W	10	24.53	35.23	23.66	0.5	0.5	NPTW
02/23/2011	31	24.48	35.24	23.68	-0.6	0.5	NPTW
Bottom Depth: 367 m	49	24.30	35.27	23.75	0.5	0.5	NPTW
MLD: 62 m	100	23.56	35.24	23.96	-2.8	0.5	NPTW
	150	20.88	35.17	24.66	-1.9	0.5	NPTW
	249	15.32	34.58	25.58	-3.3	0.5	
	344	10.08	34.15	26.28	-3.1	0.4	
Waimea (KM1107-6)							
21°39.453' N; 158°5.508' W	10	24.55	35.18	23.61	1.4	0.5	NPTW
02/23/2011	29	24.10	35.20	23.77	0.1	0.5	NPTW
Bottom Depth: 72 m	50	23.91	35.21	23.82	0.9	0.5	NPTW
MLD: 21 m							
Kahuku Point (KM1107-7)							
21°45.042' N; 157°59.123' W	11	24.33	35.20	23.70	1.3	0.5	NPTW
02/23/2011	30	24.32	35.21	23.70	0.4	0.5	NPTW
Bottom Depth: 124 m	51	24.25	35.21	23.73	-5.4	0.4	NPTW
MLD: 55 m	100	23.38	35.23	24.00	-0.6	0.5	NPTW
	108	23.25	35.23	24.04	-0.5	1.5	NPTW
Transect #1 (KM1107-8)							
21°50.679' N; 157°58.973' W	11	24.41	35.18	23.66	-0.7	0.6	NPTW
02/23/2011	49	24.06	35.22	23.79	-0.9	0.6	NPTW
Bottom Depth: 1389 m	100	23.17	35.26	24.08	-1.7	0.5	NPTW
MLD: 41 m	251	15.31	34.49	25.51	-3.2	0.5	
	347	9.90	34.10	26.27	-3.3	0.6	
	496	6.94	34.14	26.75	-2.4	0.3	NPIW
	743	4.88	34.35	27.18	-2.1	0.3	NPIW
	993	4.00	34.46	27.36	-2.1	0.3	NPIW
	1188	3.54	34.50	27.43	-2.2	0.2	NPIW
	1189	3.54	34.50	27.43	-2.3	0.3	NPIW
	1345	3.13	34.53	27.50	-2.1	0.3	
ALOHA (KM1107-11)							
22°45.022' N; 157°59.995' W	9	24.20	35.21	23.74	0.8	0.4	NPTW
02/24/2011	49	24.05	35.21	23.78	0.3	0.5	NPTW
Bottom Depth: 4749 m	102	23.35	35.35	24.10	-1.4	0.5	NPTW
MLD: 66 m	248	17.03	34.76	25.32	-3.8	0.5	
	351	11.88	34.23	26.02	-3.3	0.4	
	496	7.44	34.03	26.59	-3.5	0.3	NPIW
	745	4.62	34.27	27.14	-2.6	0.3	NPIW
	746	4.62	34.27	27.14	-2.8	0.5	NPIW
	991	3.90	34.45	27.36	-2.3	0.3	NPIW
	1489	2.66	34.56	27.56	-2.4	0.3	
	1979	1.98	34.61	27.66	-2.7	0.2	NPDW
	2960	1.36	34.65	27.74	-3.0	0.4	NPDW
	3938	1.14	34.67	27.77	-3.5	0.3	NPDW
	4644	1.10	34.67	27.78	-3.9	0.3	NPDW
	4644	1.10	34.67	27.78	-3.6	0.3	NPDW

Table 2.1: continued.

Site information	Water depth [a] [db]	θ [a] [˚C]	S [a]	σ_θ [a] [kg/m^3]	ε_{Nd}	Error [b] ±	Water mass
ALOHA (KM1215/Hoe-Dylan V)							
22˚48.45' N; 158˚1.92' W	4	25.10	35.29	23.53	-0.6	0.5	NPTW
07/21/2012	24	24.74	35.30	23.65	-5.8	0.4	NPTW
Bottom Depth: 4742 m	75	23.95	35.31	23.90	-0.8	0.4	NPTW
MLD/DCM [a]: 37 m / 137 m	136	22.02	35.36	24.49	-2.3	0.4	NPTW
	175	20.37	35.22	24.83	-3.7	0.5	NPTW
	250	14.77	34.41	25.57	-3.0	0.5	
	500	6.94	34.07	26.70	-3.0	1.7	NPIW
	749	4.80	34.30	27.14	-2.4	0.3	NPIW
ALOHA (KM1219/Hoe-Dylan IX)							
22˚48.48' N; 158˚3' W	5	25.68	35.24	23.32	-1.4	0.2	NPTW
08/27/2012 and 08/28/2012	25	25.66	35.25	23.33	-0.4	0.3	NPTW
Bottom Depth: 4739 m	75	23.65	35.27	23.95	-0.9	0.6	NPTW
MLD/DCM [a]: 33 m / 132 m	126	22.23	35.35	24.42	-1.2	0.5	NPTW
	174	19.77	35.07	24.88	-2.5	0.3	NPTW
	248	15.28	34.46	25.50	-3.0	0.3	
	496	7.66	34.08	26.60	-3.3	0.3	NPIW
	744	4.79	34.26	27.12	-2.7	0.3	NPIW
ALOHA (KM1309/Hoe-Phor I)							
22˚44.986' N; 157˚59.994' W	5	25.53	34.93	23.13	-5.2	0.6	NPTW
06/01/2013 and 06/02/2013	25	25.43	34.94	23.17	-2.0	0.5	NPTW
Bottom Depth: ~4800 m	75	23.62	35.24	23.94	-1.8	0.6	NPTW
MLD/DCM [a]: 34 m / 147 m	120	22.42	35.42	24.42	-3.0	0.4	NPTW
	175	21.02	35.29	24.71	-3.9	0.5	NPTW
	250	17.51	34.76	25.21	-4.2	0.7	
	500	7.82	34.22	26.69	-2.8	0.3	NPIW
	750	4.81	34.29	27.14	-2.5	0.3	NPIW
ALOHA (KM1316/Hoe-Phor II)							
~22˚45' N; 158˚ W	15	26.89	35.52	23.15			NPTW
09/18-19-20/2013	130	21.33	35.29	24.62			NPTW
Bottom Depth: ~4800 m	1000	3.88	34.46	27.37			NPIW
MLD/DCM [a]: 57 m / 130 m							
Wailupe Spring							
21˚16.54' N; 157˚45.73' W	0.8 [c]	24.49	5.68	23.64	0.6	0.2	
05/30/2010	1.4 [c]	24.28	1.81	23.72	1.3	0.2	
		24.18		23.75			
		22.41		24.28			

MLD: Mixed layer depth; DCM: Deep chlorophyll maximum; S: Salinity. Mixed layer depth corresponds to 0.125 kg/m3 density offset from surface value (Miller, 1976). DCM not determinable during cruise KM1107.

[a] The hydrographic data (potential temperature, potential density, salinity, MLD, DCM) of cruises KM1215, KM1219, KM1309 and KM1316 used in this publication came from the Center for Microbial Oceanography: Research and Education (C-MORE), an NSF Science and Technology Center (EF-0424599); http://hahana.soest.hawaii.edu/cmoreDS/interface.html.

[b] Calculated propagated error combined from internal and external error (both 2σ), with external errors representing session-based repeated analysis of JNdi-1.

[c] Sediment depth.

North Pacific Deep Water (NPDW; salinity >34.6, σ_θ >27.6 kg/m^3; e.g., Talley, 2008; Talley et al., 2011) can only be identified at Station ALOHA, where its characteristic properties cover water depths below ~1900 m (Fig. 2.1c, Tab. 2.1), comprising the four deepest samples of cruise KM1107 (1979-4644 m water depth). The hydrography at ALOHA does not allow for a clear identification of Upper Circumpolar Deep Water (UCDW) that is centred at ~1000 m water depth in the North Pacific, sandwiched between NPIW and NPDW (Talley et al., 2011) and mixes with NPDW close to Hawaii, forming modified NPDW (Kawabe and Fujio, 2010). The typical salinity and temperature values and high oxygen concentrations of Lower CDW (LCDW) (e.g. Wijffels et al., 1996; Orsi, 1999; Talley et al., 2011) are not reached in the lowermost samples at ALOHA, suggesting the absence of LCDW and the extension of NPDW to the bottom at this location.

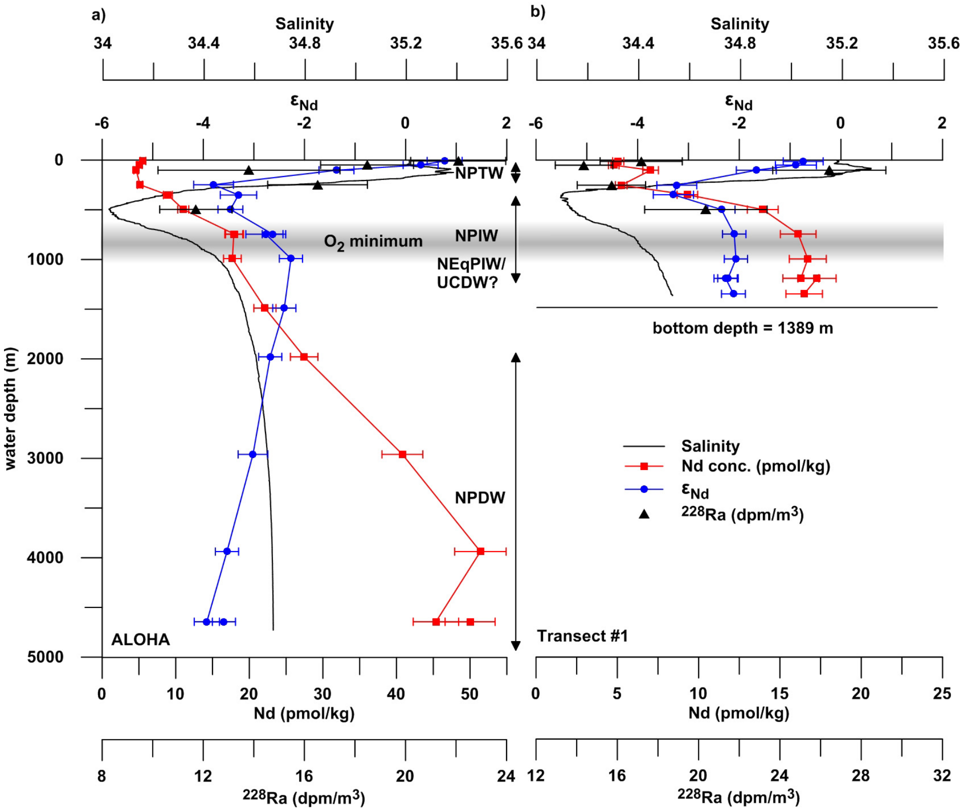

Figure 2.2: Full water column profiles of dissolved ε_{Nd}, Nd concentrations, and 228Ra activity from cruise KM1107 (February 2011) at a) Station ALOHA and b) Station Transect #1. Error bars represent propagated errors (ε_{Nd}, Ra) or external reproducibility (Nd). Salinity profiles from the same casts. Grey shaded bar marks the approximate depth of the oxygen minimum. Duplicate samples at 745 m and 4644 m water depth in a) and at 1188 m water depth in b) agree within error for both ε_{Nd} and Nd concentrations. Note different scales of the Nd concentration axes. The depth ranges of NPTW, NPIW and NPDW, which could be clearly identified based on their hydrographic properties, are illustrated by vertical arrows.

2.3.2. Dissolved neodymium isotope composition

The dissolved neodymium isotope composition at the stations around Oahu and at ALOHA ranges from -4.2 to +1.4 (Figs. 2.2, 2.3, 2.4, Tab. 2.1). Three significantly less radiogenic values ($\varepsilon_{Nd} \leq -5.2$) are considered to be subject to contamination (Tab. A2.1). The negative ε_{Nd} at 51 m water depth at Kahuku Point is not paralleled by anomalous REE concentrations or REE pattern, which indicates a contamination of the ε_{Nd} sample (Fig. 2.5d). Since REE and ε_{Nd} samples were taken separately during cruise KM1107 (see

Section 2.2), it is likely that the ε_{Nd} sample was contaminated during sampling or processing, while the REE sample was not. For the other two samples (25 m from July 2012 and 5 m from June 2013) the REE sample is a subsample from the Nd isotope sample and thus potentially both ε_{Nd} and REE aliquots are contaminated (Fig. 2.4).

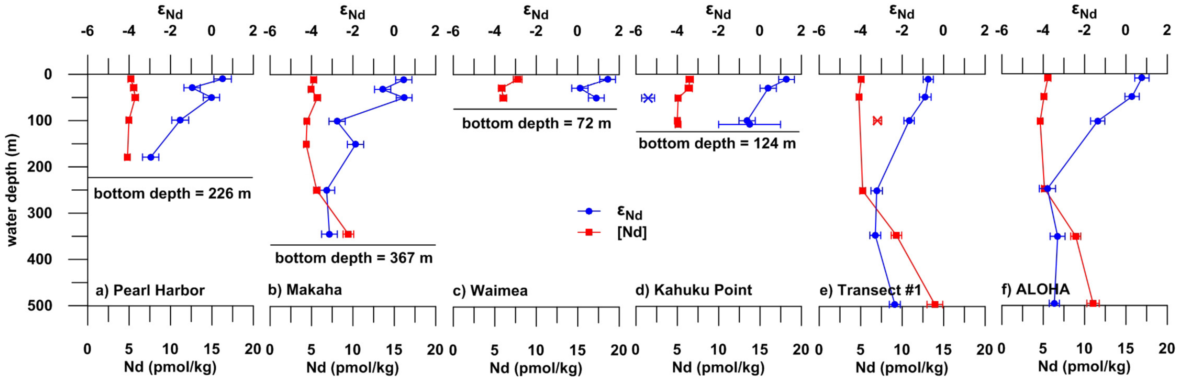

Figure 2.3: ε_{Nd} and Nd concentrations of all stations of cruise KM1107 for the upper 500 m of the water column. For full water column profiles of stations Transect #1 and ALOHA see Fig. 2.2. One data point in d) and e) is excluded from profiles due to potential contamination (blue and red crosses; for details see section 2.3.2 and 2.3.3). Errors bars for Nd concentration are generally smaller than size of the symbols.

The coastal sites have the most radiogenic ε_{Nd} of -1 to +1.4 within the upper 50 m of the water column, with the highest surface values found at stations Waimea (ε_{Nd} = +1.4) and Kahuku Point (ε_{Nd} = +1.3). All surface values decrease by 1-1.5 ε_{Nd} units towards ~30 m water depth (Fig. 2.3). At stations Makaha, Pearl Harbor, and Waimea, this is followed by a shift towards more positive values at ~50 m depth. Below 50 m, we find gradually decreasing ε_{Nd} signatures that reach -0.5 to -2.8 at 100-150 m depth and least radiogenic values of ≤-3 below 150 m depth at stations Makaha and Pearl Harbor.

Groundwater samples from Wailupe Spring (southeast coast of Oahu) have ε_{Nd} values of +0.6 at 0.8 m sediment depth and +1.3 at 1.4 m sediment depth, similar to the coastal surface waters.

Similar to the coastal sites, ε_{Nd} at station Transect #1, some 15 km off the coast of Oahu, is most radiogenic (ε_{Nd} = -0.7 to -0.9) within the upper 50 m, although these values are slightly less radiogenic than those at more coastal sites at corresponding depths (Fig. 2.2b, 2.3). At 250-350 m, ε_{Nd} decreases to ~-3.3 at Transect #1 followed by an increase to constant ε_{Nd} of about -2.2 from 500 m depth to the bottom (1345 m).

At Station ALOHA, we observe a seasonal variability of the isotope composition within the upper 250 m of the water column (Fig. 2.4, Tab. 2.1). The largest differences are found within the upper 100 m, where ε_{Nd} ranges from +0.8 in February 2011 to -2.0 in June 2013. We observe a general trend of decreasing ε_{Nd} values with depth between the surface and 250 m. Below, the signatures show increasing conformity, being indistinguishable at 500 m and 750 m depth, the depth range of NPIW. The only full water column profile from February 2011 shows a gradual ε_{Nd} decrease in deep waters starting from -2.3 at ~1000 m towards -3.8 ± 0.2 (mean and standard deviation of the replicate samples) close to the bottom (Fig. 2.2a).

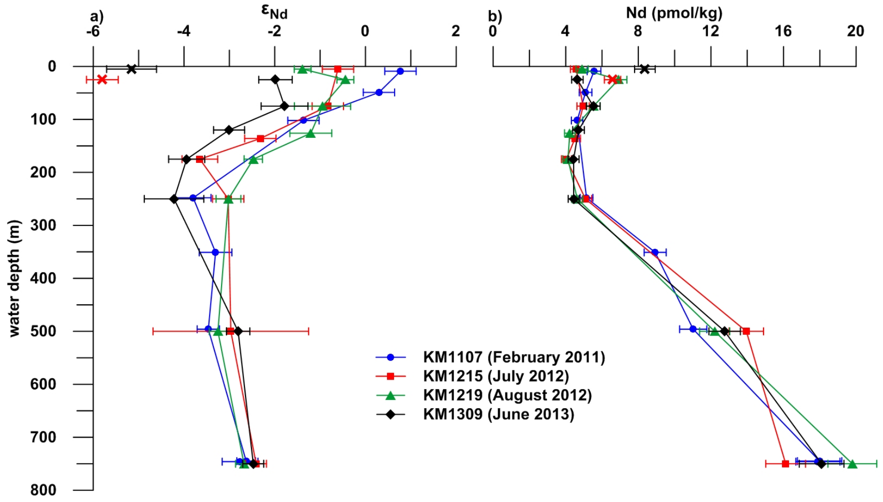

Figure 2.4: Dissolved seawater ε_{Nd} and Nd concentration profiles at Station ALOHA of four cruises during different months. a) Dissolved ε_{Nd}, b) dissolved Nd concentrations. Samples at 5 m depth of cruise KM1309 (black crosses) and 25 m depth of KM1215 (red crosses) are excluded from the profiles due to potential contamination (see section 2.3 for details).

2.3.3. Rare earth element concentrations and patterns

In the following description of the REE concentrations, we will use Nd as a representative for LREE concentrations and Er for the HREEs. Middle REEs (MREE) have an intermediate behaviour and are not described in detail. Three samples are excluded from the discussion due to potential contamination (Tab. A2.2; crosses in the figures). Contamination in two of these samples, expressed by anomalously high Nd, Pr, and Dy values (25 m from July 2012 and 5 m from June 2013), is also observed in ε_{Nd} (see section 2.3.2). In the sample from 100 m at Transect #1, the LREE subsurface maximum is only supported by one data point without corresponding ε_{Nd} change (Fig. 2.3e) and is therefore not thought to be a natural feature but the result of contamination of the REE aliquot during sampling or processing.

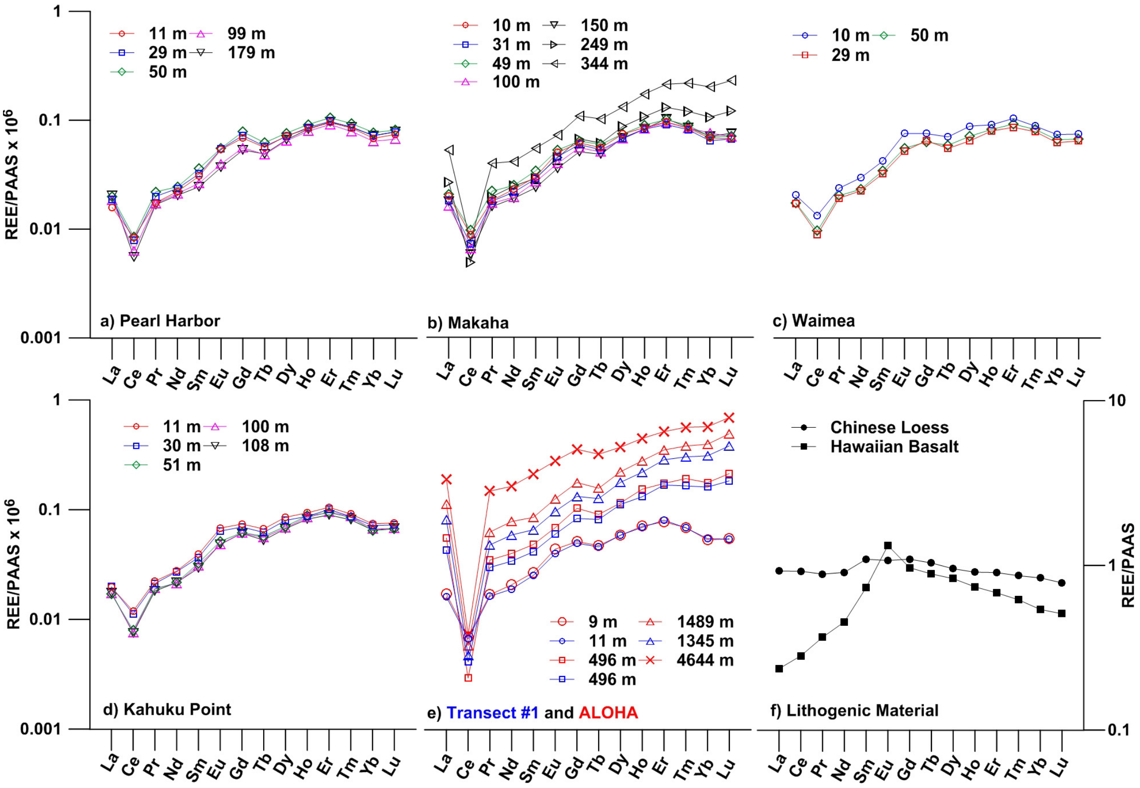

Figure 2.5: PAAS-normalised REE patterns of a)-d) coastal waters, e) selected depths of Transect #1 (blue) and ALOHA (red) from cruise KM1107, and f) typical patterns of Hawaiian Basalts (based on average REE concentrations from Ren et al., 2009) and Chinese loess (based on average REE concentrations from Taylor et al., 1983; Liu et al., 1993; Nakai et al., 1993) on a logarithmic scale. PAAS data from Taylor and McLennan (1985). Note different scale in f).

Coastal waters are characterised by elevated REE concentrations (~5-8 pmol Nd/kg; ~1.6-2.1 pmol Er/kg) in the upper 50 m compared to 100-200 m water depth, with highest surface concentrations at Waimea and Kahuku Point (>6 pmol Nd/kg; >1.8 pmol Er/kg) (Figs. 2.3, 2.6, Tab. A2.2). Subsurface (50 m) maxima are present at Pearl Harbor and Makaha (~5.7 pmol Nd/kg; ~1.6-1.8 pmol Er/kg). Coastal waters below 200 m, only sampled at station Makaha, show a rapid REE increase towards the bottom. At stations Transect #1 and ALOHA, surface REE concentrations are similar to the coastal waters at Makaha and Pearl Harbor, but clearly depleted compared to Waimea and Kahuku Point. They are rather constant within the upper 250 m of the water column and increase below that depth. At ALOHA, subsurface maxima in REE concentrations are found at 25 m in August 2012 (potential contamination in July 2012), while they are absent in June (25 m was not sampled in February) (Fig. 2.6). Surface LREE and MREE maxima are found in February (5.6 pmol Nd/kg in February *vs.* 4.6-4.9 pmol Nd/kg in July and August). Below 250 m, we observe a typical nutrient-type profile with increasing concentrations towards the bottom for all REEs except for Ce, which also increases with depth below 500 m but varies within the analytical uncertainty (Tab. A2.2).

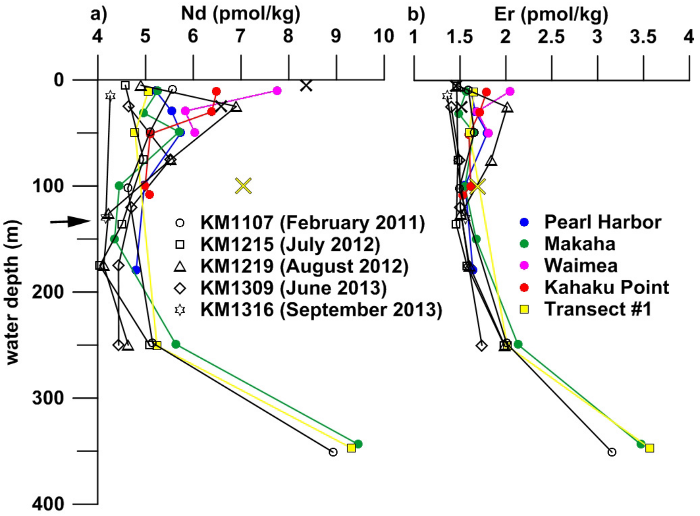

Figure 2.6: a) Nd (LREE), and b) Er (HREE) concentration profiles for the upper 400 m of the coastal stations (coloured circles) and ALOHA (open symbols). Arrow marks approximate position of the DCM obtained from summer cruises (Tab. 2.1). The crosses indicate samples that are subject to contamination (see section 2.3 and Figs. 2.3, 2.4).

Rare earth elements normalised to Post-Archean Australian Sedimentary rock (PAAS) concentrations (Taylor and McLennan, 1985) of stations ALOHA (cruise KM1107, February 2011), Transect #1, and coastal sites are shown in Fig. 2.5. REE patterns ≥500 m water depth (ALOHA and Transect #1) show a pronounced HREE over LREE enrichment typical for seawater, which is also visualised by PAAS-normalised Nd/Er ratios ($(\text{Nd/Er})_N$, in the following referred to as Nd/Er) in Fig. 2.7a. Samples from the upper 250 m of the coastal sites and the open ocean station, show a flatter PAAS-normalised pattern (higher Nd/Er) and a slight depletion of the heaviest REEs (Tm, Yb, Lu) compared to their precursor Er (Fig. 2.5). REE patterns at 250 to 350 m water depth mark a transition between surface and deep waters. The HREE over LREE enrichment is lower in surface waters above ~200 m (high Nd/Er), and also decreases (increasing Nd/Er) in the deep samples at ≥3000 m (Fig. 2.7a). The surface depletion of the heaviest REEs Tm, Yb, and Lu, visualised by PAAS-normalised Er/Lu ratios ($(\text{Er/Lu})_N$, in the following referred to as Er/Lu) and also clearly seen in the REE patterns in Fig. 2.5, is a feature of surface samples and vanishes with increasing depth (Fig. 2.7b). Similarly, MREE anomalies ($[\text{MREE/MREE*}]_N = [2*(\text{Gd+Tb+Dy})_N/(\text{La+Pr+Nd+Tm+Yb+Lu})_N]$; Martin et al., 2010) are elevated in surface waters and rapidly decrease within the upper 500 m (Fig. 2.7d; Tab. A2.2).

We observe a consistent increase of Ce anomalies with increasing depth (Tab. A2.2). However, measurements of Ce are subject to high errors, which are potentially caused by high and variable blank contributions and low initial Ce concentrations (Tab. A2.2 and section 2.2), precluding the detailed discussion of Ce data. Europium anomalies (calculated using Tb instead of Gd as $[Eu/Eu^*]_N = [3^*Eu_N/(2^*Sm_N+Tb_N)]$, to account for potential anomalies of Gd in seawater; e.g., Zhang et al., 2008) are higher in some surface and subsurface samples than at depth and show an overall range of 1.0 to 1.48, with highest anomalies at stations Waimea and Kahuku Point (>1.4) (Fig. 2.7c; Tab. A2.2). Gadolinium anomalies ($[Gd/Gd^*]_N = [Gd_N/(Sm_N^*0.33+Tb_N^*0.67)]$, Bau and Dulski, 1996) in coastal waters and at ALOHA range from 1.2 to 1.4 and are only slightly increased to >1.4 at 10-50 m depth at station Pearl Harbor (Tab. A2.2).

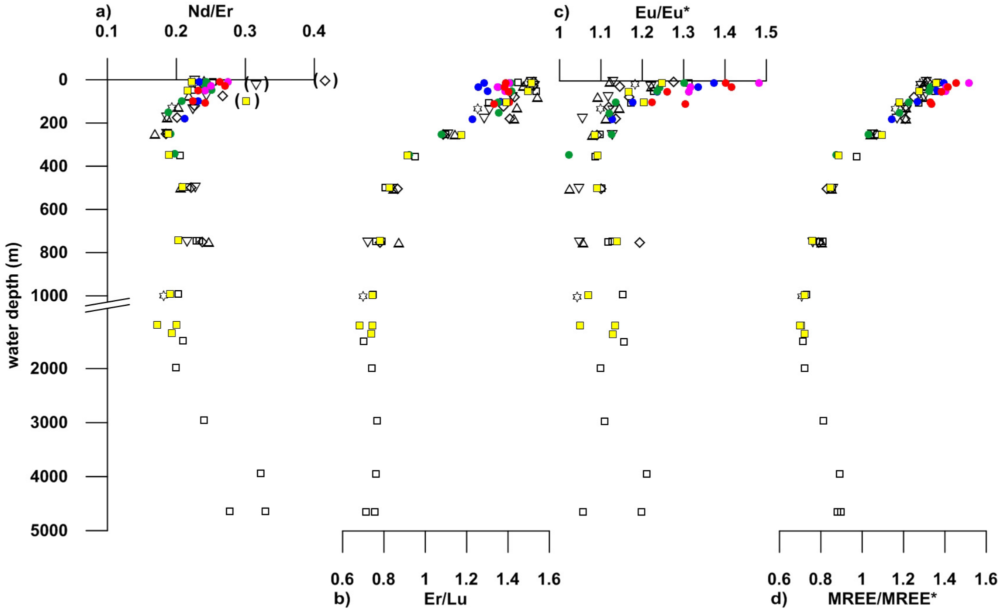

Figure 2.7: PAAS-normalised REE ratios and anomalies for all coastal sites and ALOHA profiles of this study: a) Nd/Er, b) Er/Lu, c) Eu/Eu*, and d) MREE/MREE*. Coastal sites of Pearl Harbor (blue circles), Makaha (green circles), Waimea (pink circles), Kahuku Point (red circles) and Transect #1 (yellow squares). ALOHA profiles of KM1107 (February 2011, open squares), KM1215 (July 2012, open inverted triangles), KM1219 (August 2012, open triangles), KM1309 (June 2013, open diamonds), and KM1316 (September 2013, open asterisks). Bracketed data points in a) potentially influenced by contamination (see section 2.3). Note break in y-axis at 1000 m water depth.

2.3.4. Colloidal REEs

We use the dissolved and ultra-filtrated permeate and retentate samples of cruise KM1316 (0 m, 130 m, 1000 m water depth at ALOHA) to distinguish between truly dissolved (i.e., soluble, s_{REE}) and colloidal REE fractions (c_{REE}), the sum of which make up the dissolved REE (d_{REE}) pool (e.g., Sholkovitz and Elderfield, 1988; Elderfield et al., 1990; Sholkovitz, 1992; Rousseau et al., 2015). Given the analytical uncertainty of 4-9% (except for Gd: 10.8% and Ce: 66%, 2σ SD), derived from the routine analysis of standards of the same concentration as the samples (section 2.2.3 and Tab. A2.2), the three fractions, $REE_{dissolved}$, $REE_{retentate}$ and $REE_{permeate}$, are identical (Tab. A2.3). Using a concentration factor of 2 and a calculation of c_{REE} concentrations as described above in section 2.2, then, there is no significantly measurable colloidal fraction for any of the REEs in Station ALOHA seawater, and the similar concentrations in each fraction are explained by the presence of soluble-sized REEs in each fraction. The REE recovery through the cross flow filtration system is >95% for the 0 m and 130 m samples and >88% for the 1000 m sample.

2.3.5. Radium isotopes

Due to terrestrial influences (streams, SGD, and diffusion from sediments), all samples collected had detectable ^{228}Ra (8-22 dpm/m^3). Except for stations Pearl Harbor and Makaha, all stations also had elevated ^{226}Ra (87-98 dpm/m^3) over the established 80 dpm/m^3 for offshore northwest Pacific Ocean seawater (e.g., Broecker et al., 1967). The nearshore springs were slightly depleted in ^{226}Ra (40 and 47 dpm/m^3) and enriched in ^{228}Ra (19 and 53 dpm/m^3) compared to expected offshore activities (Tab. A2.1).

Radium patterns agree very well with the REE signature in that all stations were enriched and Waimea and Kahuku Point samples had the highest surface water ^{226}Ra and ^{228}Ra. At Station ALOHA and Transect #1, the radium depth profile reached down to 500 m, and ^{226}Ra activities increased at 500 m depth at both stations as expected for a Pacific Ocean profile. ^{228}Ra was present at both stations and persisted down to 500 m, although at Station ALOHA its activity significantly decreased at depth (Fig. 2.2).

2.4. Discussion

2.4.1. Hawaiian imprint on surface and subsurface waters at the coastal sites and at ALOHA in February 2011 (KM1107)

Surface waters at the coastal sites, Transect #1, and ALOHA show REE patterns that are different from typical seawater patterns (e.g., ALOHA deep water; Fig. 2.5). All surface samples show elevated PAAS-normalised Nd/Er and Er/Lu ratios that are indicative of lithogenic input (e.g., Bertram and Elderfield, 1993; Hongo et al., 2006; Zhang et al., 2008; Jeandel et al., 2013; Pearce et al., 2013) (Fig. 2.7). Radiogenic ε_{Nd} signatures and the occurrence of positive Eu anomalies (Eu/Eu*) and MREE enrichment (MREE/MREE*) are characteristic of Hawaiian basaltic material (e.g., Tanaka et al., 2008; Ren et al., 2009) (Fig. 2.5f), suggesting that the lithogenic signature in coastal waters as well as at Transect #1 and ALOHA is derived from the Hawaiian Islands. High surface Er/Lu ratios and similar Er/Lu profiles as Nd/Er, Eu/Eu*, and MREE/MREE* (Fig. 2.7), suggest that Er/Lu also reflects lithogenic input. This confirms the assumption of Hongo et al. (2006), who suggested that high Er/Lu ratios may develop during weathering of source material similar to what has been observed for MREE enrichment in an experimental study by Hannigan and Sholkovitz (2001).

The upper 100 m of the water column at ALOHA have much more positive ε_{Nd} (ε_{Nd} = -1.4 to 0.8) than surface waters at other open ocean stations in the central North Pacific (ε_{Nd} = -5.4 to -1.8, Piepgras and Jacobsen, 1988; Amakawa et al., 2009; Zimmermann et al., 2009, Pahnke et al., 2012) and are similar to those at our coastal sites (Figs. 2.3, 2.8a). Similar surface ε_{Nd} was also observed by Vance et al. (2004) near the Hawaiian Islands and at ALOHA. Surface [Nd] (4.6-5.6 pmol/kg) is similar to published Nd concentrations from the region (Fig. 2.8b; Greaves et al., 1999; compilation in Hongo et al., 2006) and to the surface [Nd] at Pearl Harbor, Makaha, and Transect #1 (Fig. 2.3). The most radiogenic surface ε_{Nd} values at Waimea and Kahuku Point ($1.3 < \varepsilon_{Nd} < 1.4$) are accompanied by highest REE and ^{228}Ra concentrations and most positive Eu (Eu/Eu* >1.4) and MREE anomalies, providing evidence for increased input from Oahu through rivers near these sites (Figs. 2.3, 2.6, 2.7). It is consistent with the spatial heterogeneity of precipitation and surface runoff on Oahu (Oki, 2003; Giambelluca et al., 2013), as rivers originating from the Ko'olau Range drain into the coastal ocean near these sites. SGD is another important source for REEs to the coastal ocean (e.g., Johannesson and Burdige 2007; Johannesson et al., 2011; Kim and Kim, 2011; 2014) and has been shown to equal or exceed river volumetric discharge and river nutrient input on both the windward and leeward sides of Oahu (Moosdorf et al., 2015; Garrison et al., 2003; Kelly et al., 2013), suggesting that SGD is an important contributor of REE along the shoreline of Oahu.

Positive Eu anomalies of the same magnitude as observed here were reported in seawater near Papua New Guinea and the Kerguelen Plateau and attributed to a basaltic (submarine) source (Zhang et al., 2008; Grenier et al., 2013). The linear correlation of our ε_{Nd} and Eu/Eu* ($R^2 = 0.65$, excluding three outliers) supports a similar source of these signals. Samples from Wailupe Spring (southeast coast of Oahu; Fig. 2.1b) have an isotope composition of +0.6 to +1.3, similar to the coastal waters, confirming the Hawaiian source of the radiogenic signal in coastal waters and at ALOHA. Groundwater and coastal surface water ε_{Nd} signatures are less positive than the Hawaiian basaltic bedrock (average ε_{Nd} of +6.2; Tanaka et al., 2008), because of the influence of Asian dust (ε_{Nd} = -10.3; Taylor et al., 1983; Goldstein et al., 1984; Nakai et al., 1993; Liu et al., 1994) that modifies the soil ε_{Nd} signature (Kurtz et al., 2001), and the mixture with open ocean water near the coast (Fig. 2.1c). Groundwater ε_{Nd} may also be subject to seawater admixture (salinity of 1-6 in the spring samples) and modified towards less radiogenic ε_{Nd} values by the presence of calcareous reef rocks at the southeast coast of Oahu.

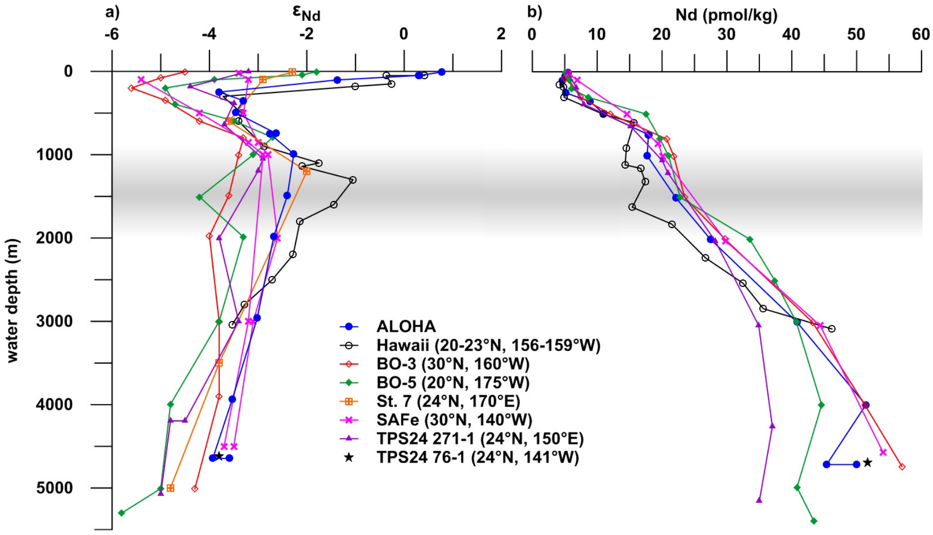

Figure 2.8: Comparison of ALOHA full water column profiles of a) ε_{Nd} and b) Nd concentrations to other North Pacific stations (for locations see Fig. 2.1a). Bottom samples of BO-3 out of depicted range. BO-3 and BO-5 from Amakawa et al. (2009), St. 7 from Zimmermann et al. (2009), Hawaii composite from Vance et al. (2004), SAFe (two profiles) from Pahnke et al. (2012), TPS24 271-1 and TPS24 76-1 from Piepgras and Jacobsen (1988). For errors bars of Station ALOHA see Fig. 2.2a. Grey shaded area marks the depth of the radiogenic ε_{Nd} excursion at ALOHA.

Normalisation of our surface water REE data to those from an open ocean North Pacific station that is thought to be unaffected by lithogenic input (177˚ E, 24˚ N, see Fig. 2.1a; Greaves et al., 1999) further visualises the clear Hawaiian imprint on coastal waters and ALOHA during February by showing a pronounced Eu anomaly and MREE enrichment (Fig. 2.9), with most pronounced signals at Waimea and Kahuku Point. These anomalies, however, are absent or attenuated at ALOHA in July and August. Middle REE enrichments have been proposed to result from input of REEs from weathered phosphate minerals through river water (Sholkovitz et al., 1999; Hannigan and Sholkovitz, 2001), dissolution of oxy-hydroxides in pore waters (Haley et al., 2004), discharge of MREE-enriched groundwater (Kim and Kim, 2011; 2014) or submarine weathering of basaltic particles (Grenier et al., 2013). The latter is consistent with the influence of Hawaiian basalts on surface waters around Oahu and at ALOHA, suggested based on positive ε_{Nd} and Eu/Eu* (Figs. 2.3, 2.7c,d). A small positive Gd anomaly (Gd/Gd* >1.4) at Pearl Harbor (Figs. 2.5a, 2.9) may be a hint for a contribution of anthropogenic Gd (Bau and Dulski, 1996) from the urban area around Honolulu, thus providing additional evidence for Hawaiian input.

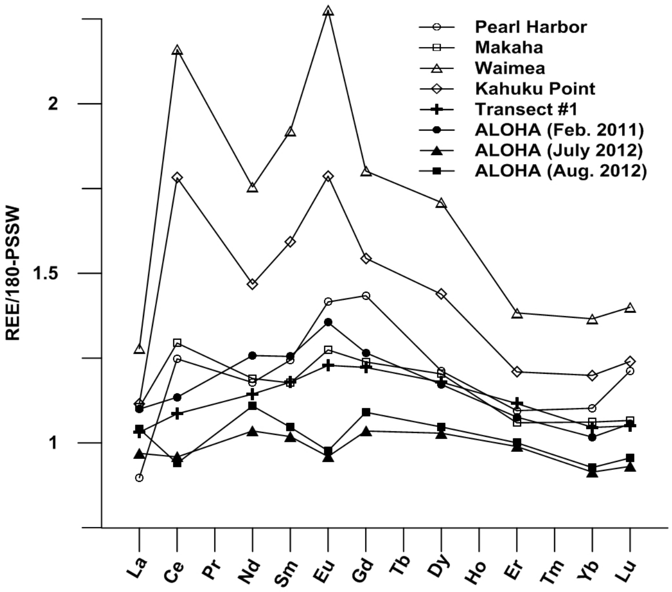

Figure 2.9: Surface waters of coastal sites and ALOHA normalised to surface seawater from the North Pacific believed to lack lithogenic influence (station 180-PSSW, ~24˚N, ~176˚E; Greaves et al., 1999). Surface sample of June 2013 excluded due to potential contamination (for details see section 2.3).

Elevated surface ^{228}Ra activities at ALOHA, indicating recent terrestrial freshwater and sediment input, further support local Hawaiian influence as far offshore as station ALOHA (Fig. 2.2a, Tab. A2.1). Radium-226 activity at ALOHA is uniform between 0-250 m and increases at 500 m at the depth of NPIW. The ^{228}Ra/^{226}Ra activity ratios therefore decrease from 0.25 at the surface to 0.09 at depth at ALOHA, indicating decreasing local Hawaiian influence and increasing contribution of NPIW with depth. At Transect #1, the ^{228}Ra profile is uniform down to 500 m, except for a small excursion to higher activity at 100 m, which coincides with a similar excursion in the [Nd] signature (Fig. 2.2b). The ^{228}Ra 0-500 m inventory at Transect #1 was 9450 dpm/m^2 and at ALOHA 7590 dpm/m^2, reflecting the proximity of Transect #1 to Oahu and dilution of water masses by mixing and decay at Station ALOHA. Nevertheless, the elevated ^{228}Ra inventory at Station ALOHA is a clear indicator of a strong terrestrial contribution. Due to the fact that Oahu is probably not the only island contributing the terrestrial signature, it is difficult to quantify the terrestrial radium contribution to Station ALOHA.

At subsurface depths (>180 m – 350 m), similar ε_{Nd} of -3.8 to -3.0 at ALOHA, Transect #1, Makaha, and Pearl Harbor (only sites covering these depths) suggests the presence of a uniform water mass (Fig. 2.3). This unradiogenic signature is identical to that at North Pacific open ocean stations from intermediate depth (Vance et al., 2004; Amakawa et al., 2009; Zimmermann et al., 2009; Pahnke et al., 2012) (Figs. 2.3, 2.8), suggesting a North Pacific-wide extent of this subsurface water mass rather than a local Nd imprint. Hydrographic properties do not allow for a characterisation of this water (NPSTMW, ENPCW, or NPIW), but the salinity decreases rapidly towards the characteristic salinity minimum of NPIW (Fig. 2.2) and the ε_{Nd} signatures are identical to those of NPIW elsewhere (e.g., Amakawa et al., 2009), suggesting that the unradiogenic ε_{Nd} at this depth represents NPIW. Rare earth element patterns rapidly lose the characteristic surface features (high Nd/Er and Er/Lu ratios, positive Eu and MREE anomalies) and evolve towards the typical seawater pattern (Figs. 2.5b, 2.7). This suggests that Hawaiian input controls both REE concentrations and ε_{Nd} of the surface waters, but that subsurface waters are unaffected by local overprints. The isotope results further show that there is no radiogenic ε_{Nd} imprint from bottom sediments on the deepest waters at each station (20-40 m above the seafloor) (Tab. 2.1). Abbott et al. (2015a,b) showed significant influence of benthic REE flux from sediment pore fluids on the bottom water ε_{Nd} signature several hundreds of metres above the seafloor and suggested that the diffusive flux of pore water REE are a major REE source to the ocean. We do not find any evidence for this flux at our study sites based on the Nd isotope signature (Fig. 2.3) and REE patterns (Fig. 2.5) at stations above the Hawaiian shelf. This suggests that pore water REE contributions to bottom waters need to be investigated on a regional basis. For the Hawaiian region it is obvious that surface processes are more important for controlling the REE budget and Nd isotope signature than sedimentary pore water fluxes.

2.4.2. The intermediate and deep water column at Station ALOHA

2.4.2.1. Intermediate waters

The most negative ε_{Nd} values (ε_{Nd} = -3.3 to -3.8) at intermediate depth at ALOHA are found at or just above the salinity minimum, which corresponds to the upper NPIW layer and is similar to the ε_{Nd} signature of NPIW in the central North Pacific and close to its formation region (Piepgras and Jacobsen, 1988; Vance et al., 2004; Amakawa et al., 2004; 2009; Pahnke et al., 2012). The waters below the salinity minimum, through the oxygen minimum of lower NPIW at ~800 m water depth, are marked by an ε_{Nd} increase towards maximum values of -2.3 to -2.8 at ~750-1500 m water depth and rather constant Nd concentrations of 17.7-22 pmol/kg (Figs. 2.2a, 2.8). Even at a depth of ~2000 m, the isotope signatures at ALOHA are still more radiogenic (ε_{Nd} = -2.7) than expected from typical NPDW (ε_{Nd} = -3.9 ± 0.7, Amakawa et al., 2009, calculated from 26 data points from 1500-4000 m depth from Amakawa et al., 2009, Piepgras and Jacobsen, 1988, and Amakawa et al., 2004). Based on the presence of a similar feature at other sites in the North Pacific (Piepgras and Jacobsen, 1988; Zimmermann et al., 2009; Pahnke et al., 2012; Figs. 2.1a, 2.8a), we suggest that it may represent the presence of modified NEqPIW or UCDW. However, previous studies suggested input from the nearby Loihi seamount (18.55° N, 156.15° W) to explain high Fe concentrations at 1000-15000 m water depth at ALOHA (Boyle et al., 2005; Fitzsimmons et al., 2015) and we will therefore discuss this and the possibility of margin and hydrothermal exchange first.

Loihi basalts have a very radiogenic isotope signature of ε_{Nd} = +6.0 (cf. compilation in Tanaka et al., 2008) and may therefore influence the isotope signature as suggested for seawater from above the East Pacific Rise which was suggested to be subject to ridge exchange processes (Jeandel et al., 2013). However, Stichel et al. (2012a) showed the very limited (if any) influence of hydrothermal fluids on dissolved ε_{Nd} within the hydrothermal plume at the Mid Atlantic Ridge (TAG hydrothermal vent). This is in line with other studies that do not consider hydrothermal activity to change seawater ε_{Nd} (e.g., German et al., 1990; Halliday et al., 1992). Additionally, Basak et al. (2015) observed influence of the East Pacific Rise on seawater ε_{Nd} only at one station directly above the ridge and suggested boundary exchange processes for this, while the remaining sites showed pure seawater signatures, pointing towards very limited spatial extent of hydrothermal or ridge exchange processes. We would further expect increased Eu/Eu* if hydrothermal fluids determine the seawater ε_{Nd} composition in intermediate waters, which is not observed (Fig. 2.7c). Thus, the hydrothermal influence from Loihi seamount is an unlikely candidate to explain the positive ε_{Nd}.

We further exclude the possibility of boundary exchange at the Hawaiian margin (bulk sediment ε_{Nd} = +5.6; Vance et al., 2004) due to the lack of basaltic REE signals, especially positive Eu anomalies, seen in surface waters at our sites and in subsurface waters influenced by basaltic margins elsewhere (Zhang et al., 2008; Grenier et al., 2013). Moreover, the lack of a radiogenic ε_{Nd} signal in the deepest coastal samples (Figs. 2.3a-d, section 2.4.1) also argues against boundary exchange to explain the positive ε_{Nd} at mid-depth.

The presence of a water mass with positive ε_{Nd} is supported by a slower [Nd] increase at these depths compared to waters above and below (Fig. 2.8b), as previously observed in the North Atlantic at the depth of strong lateral advection (Stichel et al., 2015). The positive ε_{Nd} excursion is centred at a potential density of 27.4 to 27.5 at all sites, hence below NPIW and in the density range of UCDW (~27.7 in the tropical West Pacific; Grenier et al., 2013) and NEqPIW (~27.3; Bostock et al., 2010). Since the hydrography at ALOHA does not allow for a clear classification of the mid-depth water, both NEqPIW and UCDW could influence these depths. For NEqPIW, present at 700-1000 m in the equatorial Pacific (Bostock et al., 2010), there is no information on its Nd isotope signature from the open ocean Pacific north of the equator (cf. compilation of Lacan et al., 2012). Yet, modified Antarctic Intermediate Water (AAIW), one of the precursors of NEqPIW

(Bostock et al., 2010), carries an ε_{Nd} signature of -2.1 to -3.4 in the central Pacific at 140° W close to the equator (Lacan and Jeandel, 2001). Potential further modification of AAIW/NEqPIW in the equatorial East Pacific by radiogenic Nd from the shelf (Grasse et al., 2012) may contribute to a positive ε_{Nd} signature of NEqPIW that reaches the Hawaiian Islands and mixes there with NPIW (Bostock et al., 2010). Upper CDW, centred at ~1000 m in the North Pacific (e.g., Talley et al., 2011), is modified in its ε_{Nd} in the tropical West Pacific through exchange with margin sediments from an original ε_{Nd} = ~-8 near its source (e.g., Basak et al., 2015) to values as radiogenic as -0.7 (Grenier et al., 2013). Modified UCDW is transported towards the central North Pacific, where it mixes with NPDW (Kawabe and Fujio, 2010) (Fig. 2.1a) and is therefore another possible candidate for the positive mid-depth ε_{Nd} in the North Pacific.

2.4.2.2. Deep waters

At Station ALOHA, the average ε_{Nd} of NPDW (1979-4644 m) of -3.3 ± 0.5 is similar to the typical average NPDW value of ε_{Nd} = -3.9 ± 0.7 (-3 to -5) suggested by Amakawa et al. (2009). Using available data from central and northeast Pacific stations between 20° and 30° N (BO-3, Amakawa et al., 2009; TPS24-76-1, Piepgras and Jacobsen, 1988; SAFe, Pahnke et al., 2012; ALOHA, this study: see Fig. 2.1a for locations) from water depths below 1900 m, we calculate a new average ε_{Nd} for NPDW of -3.5 ± 0.5 (n=15) and an average Nd concentration of 44.4 ± 10 pmol/kg (n=16) in this region (we excluded the lowermost sample of BO-3, due to influence from bottom sediments as stated by Amakawa et al., 2009). This new value excludes stations from the Northwest Pacific that lack the contribution of upwelled UCDW/LCDW and therefore do not represent the deep water that ultimately travels to the Southern Ocean to mix with other water masses. Since the central North Pacific is the region from where modified NPDW starts its way to the Southern Ocean (Kawabe and Fujio, 2010), the new ε_{Nd} and [Nd] values seem to be a good approximation of the endmember composition of NPDW in mixing calculations of modern and past Circumpolar Deep Water.

Lower CDW cannot be identified at Station ALOHA based on hydrographic properties (section 2.3.1). Similarly, the ε_{Nd} of the deep water does not indicate the presence of LCDW with a typical signature of ε_{Nd} = -8 near its source (e.g., Basak et al., 2015), as this should shift the isotope signature towards less radiogenic values at ALOHA, as observed at station BO-5 west of Hawaii (Amakawa et al., 2009). The absence of LCDW influence in the bottom samples confirms previous conclusions that LCDW (or Antarctic Bottom Water) is less present in the eastern and central North Pacific (Piepgras and Jacobsen, 1988; Amakawa et al., 2009), in line with the main travel path of LCDW in the West Pacific (Kawabe and Fujio, 2010).

2.4.2.3. Vertical vs. lateral control on deep water REE concentrations

The REE pattern of ALOHA bottom water (4644 m) normalised to the widely used reference NPDW (~2500 m water depth; Alibo and Nozaki, 1999; Ref. NPDW in Figs. 2.1 and 2.10) is highly enriched in LREEs (Fig. 2.10a), representing the typically observed higher proportional increase of LREEs compared to HREEs with increasing depth through preferential LREE regeneration from particles or bottom sediments (e.g., Elderfield and Greaves, 1982; Sholkovitz et al., 1994). The same is illustrated in the increase of Nd/Er ratios towards the bottom at Station ALOHA (Fig. 2.7a). The ε_{Nd} and [REE] of our deepest samples do not point towards REE release from bottom sediments at ALOHA, as we do not observe a significant increase in concentrations in the lowermost samples and only a small decrease in ε_{Nd}, which matches typical NPDW values (Fig. 2.8; section 2.4.2.2). We point out, however, that our deepest sample was taken 105 m above the seafloor, where any potential bottom influence may have been mixed away already. The results show that porewater fluxes as observed on the Oregon margin, which influence the [REE] and ε_{Nd} of the water column several hundreds of metres above the seafloor (Abbott et al., 2015a,b), do not contribute to the signals at ALOHA and the Oahu coastal sites of this study (see section 2.4.1).

Based on REE concentrations in the South Pacific, Molina-Kescher et al. (2014a) recently proposed that a pattern of LREE enrichment in deep waters when normalised to the reference NPDW of Alibo and Nozaki (1999) is a characteristic feature of LCDW. However, the deep water at ALOHA (this study) as well as deep water in the North Pacific as far north as 44.67° N (Station DE-4, 177° W, 4500 m, Shimizu et al., 1994) and in the eastern North Pacific (Station TPS24-76-1, 24.3° N, 142° W, 4621 m, Piepgras and Jacobsen, 1992), which are not or only very slightly influenced by LCDW, show a similar LREE enrichment as the stations of Molina-Kescher et al. (2014a) in the South Pacific when normalised to the reference NPDW (Fig. 2.10a). Furthermore, the REE patterns from the deep North Pacific show no attenuation of the LREE enrichment relative to the site in the South Pacific (Fig. 2.10b), which would be expected as a result of increasing mixing with NPDW towards the north. The similarity of REE patterns from the North Pacific to those of LCDW in the South Pacific is further visualised by normalisation of the North Pacific deep water REE to LCDW (Station 66, 5155 m depth of Molina-Kescher et al., 2014a) (Fig. 2.10b). The patterns of all deep stations are flat, except for a positive Eu anomaly. We thus suggest that the LREE enrichment in our bottom sample is a typical feature of deep waters from the North and South Pacific and is a function of depth and water mass age (overall REE concentrations are highest in the North Pacific, Fig. 2.10b) rather than related to the presence of LCDW. This observation indicates that deep water REE patterns are largely controlled by vertical processes and thus are a function of water depth and water mass age rather than of specific water masses (see also Osborne et al., 2015), suggesting they cannot be used to trace water masses in the deep North Pacific. This is in contrast to the suggestion of Alibo and Nozaki (2004) that characteristic LREE- and Gd-depleted NPDW-normalised REE patterns in the deep eastern Indian Ocean can be used to trace the southward flow of deep waters. In the North Pacific, a vertical control is further supported by distinct positive Eu anomalies in the LCDW-normalised patterns and reflect REE release from particles at depth.

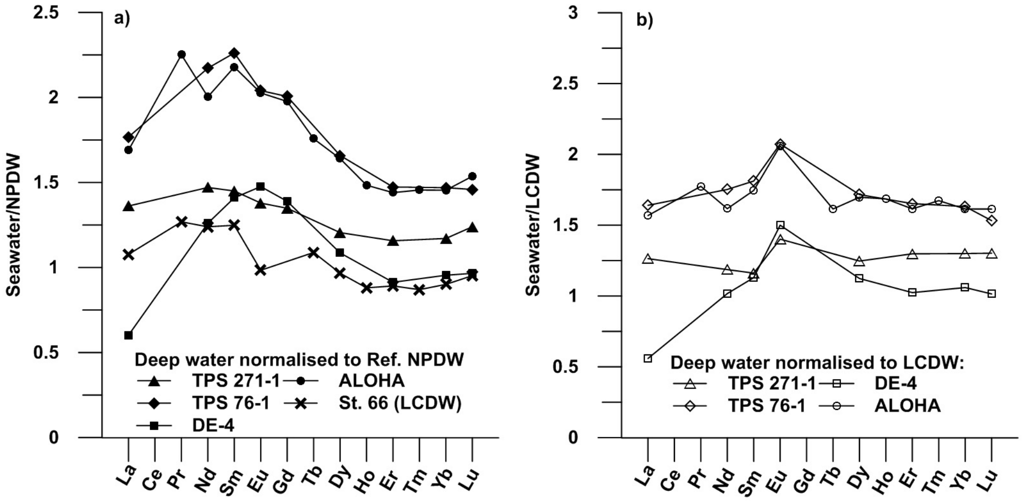

Figure 2.10: REE patterns of North Pacific stations normalised to a) NPDW from site Ref. NPDW (34.4˚ N, 2500 m, Alibo and Nozaki, 1999) and b) LCDW (Station 66, 45˚ S, 5155 m, Molina-Kescher et al., 2014a). Ce data excluded for better visualisation. North Pacific sites: ALOHA (this study), DE-4 (44.4˚ N, 4500 m, Shimizu et al., 1994), TPS24 271-1 (24.2˚ N, 5073 m, Piepgras and Jacobsen, 1992) TPS24 76-1 (24.2˚ N, 4621 m, Piepgras and Jacobsen, 1992) (for locations see Fig. 2.1a).

2.4.3. *Seasonal variability at Station ALOHA*

As discussed in section 2.4.1, contributions from the Hawaiian Islands clearly determine the surface ε_{Nd} and REE signatures at ALOHA during February 2011. Comparison of ε_{Nd} and Nd concentrations from water column profiles sampled at ALOHA during June, July, and August suggest seasonal changes within the upper 400 m (Fig. 2.4). There are two possible explanations for the observed seasonality of ε_{Nd} in surface waters at ALOHA: 1) variable dust input from Asia to the central North Pacific (ε_{Nd} = -10.3; Taylor et al., 1983; Goldstein et al., 1984; Nakai et al., 1993; Liu et al., 1994) with highest deposition during dust outbreak events in spring-early summer (e.g., Duce et al., 1980;

Parrington et al., 1983; Uematsu et al., 1985; Prospero et al., 1989) and 2) variable contributions from Hawaii that are subject to seasonal variations in precipitation and runoff (higher in winter, Oki, 2003; Giambelluca et al., 2013).

Variable Fe and Th isotope concentrations measured at ALOHA are highest during spring and have been attributed to the seasonal deposition of Asian dust (Johnson et al., 2003; Boyle et al., 2005; Fitzsimmons et al., 2015; Hayes et al., 2015). The less radiogenic ε_{Nd} signature and absent Eu anomaly in surface waters at ALOHA during summer (July and August, ε_{Nd} = -1.4 to -0.6) compared to February (ε_{Nd} = +0.8, Eu/Eu* = 1.3), may suggest increased dust influence in summer or reduced Hawaiian influence due to reduced freshwater discharge (Figs. 2.4a, 2.7c, 2.9). Rare earth element concentrations are relatively constant in the upper 200 m with a slight LREE minimum observed during all months within and below the deep chlorophyll maximum (DCM, at ~130 m), potentially due to enhanced scavenging of REEs by organic particles there (Fig. 2.6; see also Stichel et al., 2015). During the summer months, we observe a maximum at subsurface depth (25 - 75 m), which is also seen in Th concentrations and has been attributed to particle cycling (Hayes et al., 2015). Below ~200 m, the REE concentrations increase gradually and are similar throughout the investigated months.

With a simple calculation we can test if dust dissolution could influence [Nd] and ε_{Nd} at ALOHA. We assume an average Nd concentration of approximately 30 ppm for Chinese loess (Taylor et al., 1983; Goldstein et al., 1984; Liu et al., 1993; Nakai et al., 1993) and a measured annual dust deposition rate of 0.43 g/m^2yr^1 at Oahu (Uematsu et al., 1985) of which 80% is deposited during the dust season between February and June (Parrington et al., 1983). Given the wide range of the estimated REE dissolution fraction from dust of 1-20% (Greaves et al., 1994; Tachikawa et al., 1999) we use a fraction of 10% Nd dissolved from dust. This implies a release of 7155 pmol Nd/m^2yr^1 during the dust season to the sea surface. We apply this rate to the upper 5 m of the water column (i.e., the depth of our surface water sample) instead of the mixed layer depth (~30 m; Tab. 2.1), since our data and those of Stichel et al. (2015) show that ε_{Nd} and [Nd] strongly vary within the mixed layer, suggesting a dust influence mainly on the surface layer. This leads to an estimated addition of 1.43 pmol Nd/kg to seawater, which is ~35% of the [Nd] signal at the DCM concentration minimum (~4 pmol/kg; used as background concentration). A mass balance calculation for this dust addition results in a surface water value of ε_{Nd} = -2.7 (endmembers: ALOHA surface water: ε_{Nd} = 0 and [Nd] = 4 pmol/kg; Asian dust: ε_{Nd} = -10.3 and [Nd] = 1.43). For this approach, we assume that the surface water ε_{Nd} signature accumulates in the water column, which is supported by our data, while Nd is rapidly removed through scavenging. These calculations do not allow for a quantification of the dust impact at ALOHA due to uncertainties in the parameters, but they clearly show that dust has the potential to lower the isotope composition of surface waters at ALOHA during times of high input towards values that we observe during summer. The highest uncertainties in our calculation include the dissolution fraction of 1-20%, the uncertainty in the depth used for the inventory calculation, and the unknown background surface water ε_{Nd} and [Nd] at ALOHA, which may be subject to variable contributions from Hawaii.

If dust has an effect on the ε_{Nd} signature in the upper water column, why do we not see increased concentrations? From previous studies, it is known that Nd is released from dust particles, which significantly enhances the surface water concentration (e.g., Greaves et al., 1999; Stichel et al., 2015). Given the proposed impact of dust on surface iron and thorium concentrations at ALOHA (Johnson et al., 2003; Boyle et al., 2005; Fitzsimmons et al., 2015; Hayes et al., 2015), and the above shown influence on the isotope composition, the lack of any changes in REE concentrations suggests that REEs are most likely too rapidly scavenged to be visible in our data. Since none of our samples were taken during a dust event, we are not able to quantify the effect of dust dissolution on REE concentrations. However, the results demonstrate that while the REEs are scavenged from the surface waters, the modified ε_{Nd} signal is still visible in summer i.e., a few months after the highest dust deposition rates.

The second hypothesis for variable surface ε_{Nd} values at ALOHA is that Hawaiian input more significantly overprints the surface water ε_{Nd} and REE signatures during times of higher rainfall (winter). In this case, the ε_{Nd} signatures would be more open ocean-like during the summer months with only little influence from Hawaii (ε_{Nd} = -2.0 to -0.6 compared to ε_{Nd} = -4.5 at the nearest open ocean station BO-3; Amakawa et al., 2009). We observe that the most radiogenic surface ε_{Nd} values in February are accompanied by slightly higher Nd concentrations than in June-August (Fig. 2.4), indicating increased input from Hawaii. The coastal waters were only sampled during cruise KM1107 in February 2011, precluding the direct monitoring of seasonal variability in Hawaiian input.

Our data clearly show that Station ALOHA has a more radiogenic ε_{Nd} signature throughout the year than open ocean stations remote from any Hawaiian influence (e.g., station BO-3 of Amakawa et al., 2009; station SAFe of Pahnke et al., 2012). This clearly demonstrates the dominance of Hawaiian influence on surface waters around Oahu and at station ALOHA. Given the clear impact of Asian dust on surface water Fe concentrations and thorium isotopes, a seasonal modification of the ε_{Nd} and REE by Asian dust is very likely. More detailed time-series of dissolved and, ideally, particulate ε_{Nd} and [REE] at ALOHA and in coastal waters would be required to better characterise these sources and their seasonal variability. Our data demonstrate that the seasonality observed in the upper water column is limited to the surface and subsurface waters. At 750 m depth, the nearly identical ε_{Nd} values of -2.4 to -2.8 throughout the year demonstrate the rapid loss of the seasonal differences with depth.

2.4.4. Colloidal vs. truly dissolved REE concentrations

Colloids are a dominant fraction of REE physicochemical speciation in river water (e.g., Goldstein and Jacobsen, 1988; Elderfield et al., 1990; Sholkovitz, 1992; 1995; Andersson et al., 2001; Rousseau et al., 2015). It has been shown that the colloidal REE fraction is largely removed from water during estuarine mixing and that the resulting colloidal-poor water shows a REE distribution similar to seawater (Sholkovitz and Elderfield, 1988; Elderfield et al., 1990; Sholkovitz, 1992; 1995; Rousseau et al., 2015). Bertine and VernonClark (1996) reported colloidal REE concentrations that make up 0.6-2% of coastal waters in Buzzards Bay, Massachusetts, and up to 6-22% if they consider the loss of 10% through retention by the membrane during filtration. Further, Rousseau et al. (2015) showed that colloidal REE make up less than 10% of the REE at seawater salinity in the Amazon estuary. To our knowledge, there are no studies available in the literature that address the presence or absence of colloidal REEs in open ocean seawater.

Neglecting our measurement uncertainty (see section 2.3.4), REE colloidal fractions of 0-4% (La = 0-8%) are on the same order of magnitude as those reported by Bertine and VernonClark (1996). However, the fact that our measurements of the $REE_{dissolved}$, $REE_{retentate}$ and $REE_{permeate}$ fractions are identical within error is a first indication for the absence of colloidal REEs in these waters. This is in contrast to Fe and Th, which have more significant (>40% and 8-25%, respectively) colloidal fractions within the same samples from Station ALOHA (Fitzsimmons et al., 2015; Hayes et al., 2015). The potential absence of colloidal REEs in September 2013, however, does not exclude the presence of colloidal REEs during the other seasons sampled for this study or during times of maximum dust input.

From the results obtained here, we have to assume that we are monitoring only the truly soluble fraction of REEs in our samples. If this is true during the other seasons, this implies that the dissolved REE concentrations in open ocean surface waters can be attributed entirely to REE cycling in the water column and the interaction between the truly dissolved and particulate phases.

2.5. Conclusions

We showed that Hawaiian coastal waters carry distinct Nd and Ra isotope and REE signals that clearly indicate a prominent lithogenic influence from the Hawaiian Islands. Increased REE surface concentrations in combinations with elevated LREE/HREE ratios and MREE anomalies reflect lithogenic input. This lithogenic influence is clearly sourced by the Hawaiian Islands as shown by radiogenic ε_{Nd} signatures of -1.7 to +1.4 and positive Eu anomalies in surface and subsurface waters, as well as by the presence of relatively short-lived ^{228}Ra in all surface water samples.

Dissolved Nd isotope ratios of ε_{Nd} = -2 to +0.8 in surface waters at ALOHA, significantly more radiogenic than other open ocean surface waters in the central North Pacific, demonstrate that the Hawaiian Islands not only influence the surrounding coastal waters, but also Station ALOHA, located 100 km north of Oahu. The most prominent Hawaiian influence is observed in February, when Eu and MREE anomalies are similar to those in coastal waters and ε_{Nd} = +0.8. In June, July, and August, on the other hand, Eu and MREE anomalies at ALOHA are absent, and ε_{Nd} is more negative (ε_{Nd} = -2, -0.6, -1.4, respectively). Mixing calculations support the assumption that this is either due to reduced Hawaiian influence as a result of lower precipitation and runoff in summer and/or to an overprint from dust (loess) transported to ALOHA from Asia, which is marked by negative ε_{Nd} and no Eu and MREE anomalies. The fact that seasonally variable ε_{Nd} and Eu/Eu* signatures are accompanied by low absolute REE concentrations without pronounced surface maxima suggests a very rapid cycling of REEs in the upper water column.

Our deep water column ε_{Nd} and [REE] profiles at Station ALOHA (0-4644 m) contribute to the sparse coverage of complete water column profiles in the North Pacific. The ε_{Nd} of the upper intermediate (~180-500 m) and deepest layer (> 2000 m) resemble published ε_{Nd} signatures and Nd concentrations of NPIW and NPDW. Radiogenic ε_{Nd} signatures in waters at 1000-2000 m (ε_{Nd} = -2.3 to -2.8) most likely result from influence of a radiogenic water mass, the most probable candidates being modified UCDW or NEqPIW. Using new and existing data for NPDW, we further narrow the ε_{Nd} and [Nd] of NPDW to ε_{Nd} = -3.5 ± 0.5 and [Nd] = 44.4 ± 10 pmol/kg.

Results of the analysis of the colloidal and truly dissolved fractions at ALOHA indicate that there was no significant amount of colloidal REEs at 15 m (in the mixed layer), 130 m (at the DCM), and 1000 m water depth in September 2013. This does not exclude the presence of colloidal REEs during dust input events and needs further investigation. Potential future investigations should include higher-resolution time-series measurements of surface waters at ALOHA, a transect from Oahu to ALOHA, and ground- and river water analyses to better characterise the dust and Hawaiian influence on the isotope and REE compositions at ALOHA.

2.6. Acknowledgements

We thank the scientific parties, captains and crews of *R/V Kilo Moana* cruises KM1107, KM1215 (C-MORE HOE-DYLAN V), KM1219 (C-MORE HOE-DYLAN IX), KM1309 (C-MORE HOE-PhoR I), and KM1316 (C-MORE HOE-PhoR II). We specifically thank C. Hayes, E. Boyle, and G. Carrasco (MIT) for taking seawater samples during C-MORE cruises and for on-board sample processing. The hydrographic data of cruises KM1215, KM1219, KM1309 and KM1316 used in this publication came from the Center for Microbial Oceanography: Research and Education (C-MORE), an NSF Science and Technology Center (EF-0424599). Participation of J.N.F. in the HOE-DYLAN field program was provided by support from the Center for Microbial Oceanograhy: Research & Education, funded by the National Science Foundation (NSF-OIA Award #EF-0424599). Gideon Henderson (University of Oxford) is acknowledged for providing the Coral Sea standard. We further thank all members of the MPI-Marine Isotope Geochemistry Group at the University of Oldenburg, in particular M. Schulz, R. Paffrath, S. Haas and P. Böning for their help in the lab and with mass spectrometric measurements, as well as T. Badewien (ICBM) for help with processing CTD data of cruise KM1107. We also thank the associate editor Thomas M. Marchitto, Myriam Lambelet, Catherine Jeandel, and one anonymous reviewer for their very constructive reviews that significantly improved this manuscript. Financial support for this study came from the Institute for Chemistry and Biology of the Marine Environment (ICBM) and the Max Planck Institute for Marine Microbiology.

2.7. Supplementary data tables

Table A2.1: Site information, hydrographic data, dissolved neodymium isotope ratios, and Ra data for all seawater profiles of this study.

Cast[a]	**Water depth**[a] **(db)**	**θ**[a] **(˚C)**	**σ_θ**[a] **(kg/m^3)**	**Salinity**[a]	**^{143}Nd/^{144}Nd normalised**	**ε_{Nd}**	**Internal error (2σ)**	**External error (2σ)**	**Reported error (2σ)**[b]	**Data quality**[c]	**^{226}Ra (dpm/m^3)**	**Error (1σ)**[e]	**^{228}Ra (dpm/m^3)**	**Error (1σ)**[e]	**^{228}Ra/^{226}Ra**	**Error**[e]	**^{228}Ra inventory (dpm/m^2)**
Station Name/Cruise ID: Pearl Harbor (KM1107-2), Location: 21˚17.087' N; 157˚57.596' W, Sampling Date: 02/25/2011, Bottom Depth: 226 m, MLD: 17 m																	
10	10	24.49	23.64	35.19	0.512664	0.5	0.4	0.4	0.6	1	72.5	3.8	13.5	2.0	0.19	0.16	
10	29	24.28	23.72	35.21	0.512589	-1.0	0.4	0.4	0.6	1							
10	50	24.18	23.75	35.22	0.512637	0.0	0.3	0.4	0.5	1							
10	99	22.41	24.28	35.23	0.512560	-1.5	0.4	0.4	0.6	1							
10	179	18.49	25.10	34.94	0.512486	-3.0	0.4	0.4	0.5	1							
Station Name/Cruise ID: Makaha (KM1107-4), Location: 21˚27.93' N; 158˚14.466' W, Sampling Date: 02/23/2011, Bottom Depth: 367 m, MLD: 62 m																	
1	10	24.53	23.66	35.23	0.512662	0.5	0.3	0.4	0.5	1	80.7	3.3	8.0	1.1	0.10	0.14	
1	31	24.48	23.68	35.24	0.512609	-0.6	0.3	0.4	0.5	1							
1	49	24.30	23.75	35.27	0.512662	0.5	0.3	0.4	0.5	1							
1	100	23.56	23.96	35.24	0.512496	-2.8	0.3	0.4	0.5	1							
1	150	20.88	24.66	35.17	0.512542	-1.9	0.3	0.4	0.5	1							
1	249	15.32	25.58	34.58	0.512470	-3.3	0.3	0.4	0.5	1							
1	344	10.08	26.28	34.15	0.512477	-3.1	0.2	0.4	0.4	1							
Station Name/Cruise ID: Waimea (KM1107-6), Location: 21˚39.453' N; 158˚5.508' W, Sampling Date: 02/23/2011, Bottom Depth: 72 m, MLD: 21 m																	
2	10	24.55	23.61	35.18	0.512712	1.4	0.3	0.4	0.5	1	95.9	4.4	15.8	2.2	0.16	0.14	
2	29	24.10	23.77	35.20	0.512643	0.1	0.3	0.4	0.5	1							
2	50	23.91	23.82	35.21	0.512684	0.9	0.3	0.4	0.5	1							
Station Name/Cruise ID: Kahuku Point (KM1107-7), Location: 21˚45.042' N; 157˚59.123' W, Sampling Date: 02/23/2011, Bottom Depth: 124 m, MLD: 55 m																	
3	11	24.33	23.70	35.20	0.512704	1.3	0.2	0.4	0.5	1	89.4	4.0	18.5	1.8	0.21	0.11	
3	30	24.32	23.70	35.21	0.512658	0.4	0.3	0.4	0.5	1							
3	51	24.25	23.73	35.21	0.512360	-5.4	0.3	0.2	0.4	3							
3	100	23.38	24.00	35.23	0.512606	-0.6	0.3	0.4	0.5	1							
3	108	23.25	24.04	35.23	0.512612	-0.5	1.5	0.4	1.5	1							
Station Name/Cruise ID: Transect #1 (KM1107-8), Location: 21˚50.679' N; 157˚58.973' W, Sampling Date: 02/23/2011, Bottom Depth: 1389 m, MLD: 41 m																	
6	11	24.41	23.66	35.18	0.512600	-0.7	0.4	0.4	0.6	1	98.2	4.2	17.2	2.0	0.17	0.13	258
6	49	24.06	23.79	35.22	0.512593	-0.9	0.4	0.4	0.6	1	80.7	3.2	14.4	1.4	0.18	0.11	862
6	100	23.17	24.08	35.26	0.512553	-1.7	0.3	0.4	0.5	1	97.6	3.3	26.4	2.8	0.27	0.11	2643
6	251	15.31	25.51	34.49	0.512472	-3.2	0.3	0.4	0.5	1	87.1	5.0	15.7	1.7	0.18	0.12	3142
6	347	9.90	26.27	34.10	0.512469	-3.3	0.4	0.4	0.6	1							
6	496	6.94	26.75	34.14	0.512517	-2.4	0.3	0.2	0.3	1	119.5	4.6	20.4	3.0	0.17	0.15	2545
6	743	4.88	27.18	34.35	0.512530	-2.1	0.2	0.2	0.3	1							
6	993	4.00	27.36	34.46	0.512532	-2.1	0.1	0.2	0.3	1							
6	1188	3.54	27.43	34.50	0.512524	-2.2	0.1	0.2	0.2	1							
6	1189	3.54	27.43	34.50	0.512522	-2.3	0.1	0.2	0.3	1							
6	1345	3.13	27.50	34.53	0.512530	-2.1	0.2	0.2	0.3	1							

Table A2.1: continued.

Cast[a]	**Water depth**[a] **(db)**	**θ**[a] **(˚C)**	**σ_θ**[a] **(kg/m^3)**	**Salinity**[a]	**^{143}Nd/^{144}Nd normalised**	**ε_{Nd}**	**Internal error (2σ)**	**External error (2σ)**	**Reported error (2σ)**[b]	**Data quality**[c]	**^{226}Ra (dpm/m^3)**	**Error (1σ)**[e]	**^{228}Ra (dpm/m^3)**	**Error (1σ)**[e]	**^{228}Ra/ ^{226}Ra**	**Error**[e]	**^{228}Ra inventory (dpm/m^2)**
Station Name/Cruise ID: ALOHA (KM1107-11), Location: 22˚45.022' N; 157˚59.995' W, Sampling Date: 02/24/2011, Bottom Depth: 4749 m, MLD: 66 m																	
9	9	24.20	23.74	35.21	0.512678	0.8	0.3	0.3	0.4	1	86.9	4.6	22.1	1.9	0.25	0.10	331
9	49	24.05	23.78	35.21	0.512653	0.3	0.3	0.3	0.5	1	91.0	3.9	18.5	1.8	0.20	0.11	1109
9	102	23.35	24.10	35.35	0.512568	-1.4	0.3	0.3	0.5	1	79.0	2.1	13.8	3.6	0.17	0.26	1381
9	248	17.03	25.32	34.76	0.512443	-3.8	0.3	0.4	0.5	1	77.1	2.7	16.5	2.0	0.21	0.12	3304
9	351	11.88	26.02	34.23	0.512469	-3.3	0.4	0.2	0.4	1							
9	496	7.44	26.59	34.03	0.512460	-3.5	0.2	0.2	0.3	1	131.9	5.0	11.7	1.4	0.09	0.13	1464
9	745	4.62	27.14	34.27	0.512503	-2.6	0.2	0.2	0.3	1							
9	746	4.62	27.14	34.27	0.512496	-2.8	0.4	0.2	0.5	1							
9	991	3.90	27.36	34.45	0.512522	-2.3	0.2	0.2	0.3	1							
9	1489	2.66	27.56	34.56	0.512515	-2.4	0.2	0.2	0.3	1							
9	1979	1.98	27.66	34.61	0.512501	-2.7	0.05	0.2	0.2	1							
9	2960	1.36	27.74	34.65	0.512483	-3.0	0.3	0.2	0.4	1							
9	3938	1.14	27.77	34.67	0.512457	-3.5	0.1	0.2	0.3	1							
9	4644	1.10	27.78	34.67	0.512437	-3.9	0.2	0.2	0.3	1							
9	4644	1.10	27.78	34.67	0.512454	-3.6	0.2	0.2	0.3	1							
Station Name/Cruise ID: ALOHA (KM1215/Hoe-Dylan V), Location: 22˚48.54' N; 158˚1.92' W, Sampling Date: 07/21/2012, Bottom Depth: 4742 m, MLD/DCM[a]**: 37 m / 137 m**																	
74	4	25.10	23.53	35.29	0.512607	-0.6	0.3	0.3	0.5	1							
74	24	24.74	23.65	35.30	0.512341	-5.8	0.3	0.3	0.4	3							
74	75	23.95	23.90	35.31	0.512595	-0.8	0.3	0.3	0.4	1							
74	136	22.02	24.49	35.36	0.512519	-2.3	0.3	0.3	0.4	1							
74	175	20.37	24.83	35.22	0.512451	-3.7	0.4	0.4	0.5	1							
74	250	14.77	25.57	34.41	0.512483	-3.0	0.3	0.3	0.5	1							
74	500	6.94	26.70	34.07	0.512486	-3.0	1.7	0.1	1.7	1							
74	749	4.80	27.14	34.30	0.512514	-2.4	0.2	0.2	0.3	1							
Station Name/Cruise ID: ALOHA (KM1219/Hoe-Dylan IX), Location: 22˚48.48' N; 158˚3' W, Sampling Date: 08/27/2012 and 08/28/2012, Bottom Depth: 4739 m, MLD/DCM[a]**: 33 m / 132 m**																	
34	5	25.68	23.32	35.24	0.512567	-1.4	0.1	0.2	0.2	1							
34	25	25.66	23.33	35.25	0.512615	-0.4	0.2	0.2	0.3	1							
34	75	23.65	23.95	35.27	0.512589	-0.9	0.6	0.2	0.6	1							
34	126	22.23	24.42	35.35	0.512576	-1.2	0.5	0.2	0.5	1							
34	174	19.77	24.88	35.07	0.512511	-2.5	0.2	0.2	0.3	1							
34	248	15.28	25.50	34.46	0.512483	-3.0	0.3	0.2	0.3	1							
40	496	7.66	26.60	34.08	0.512471	-3.3	0.2	0.2	0.3	1							
40	744	4.79	27.12	34.26	0.512501	-2.7	0.2	0.2	0.3	1							

Table A2.1: continued.

Cast [a]	**Water depth** [a] **(db)**	**θ** [a] **(˚C)**	**σ_θ** [a] **(kg/m^3)**	**Salinity** [a]	**^{143}Nd/^{144}Nd normalised**	**ε_{Nd}**	**Internal error (2σ)**	**External error (2σ)**	**Reported error (2σ)** [b]	**Data quality** [c]	**^{226}Ra (dpm/m^3)**	**Error (1σ)** [e]	**^{228}Ra (dpm/m^3)**	**Error (1σ)** [e]	**^{228}Ra/ ^{226}Ra**	**Error** [e]	**^{228}Ra inventory (dpm/m^2)**
Station Name/Cruise ID: ALOHA (KM1309/Hoe-Phor I), Location: 22˚44.986' N; 157˚59.994' W, Sampling Date: 06/01/2013 and 06/02/2013, Bottom Depth: ~4800 m, MLD/DCM [a]:34 m/147m																	
48	5	25.53	23.13	34.93	0.512374	-5.2	0.6	0.1	0.6	3							
48	25	25.43	23.17	34.94	0.512536	-2.0	0.4	0.3	0.5	1							
48	75	23.62	23.94	35.24	0.512547	-1.8	0.5	0.3	0.6	1							
48	120	22.42	24.42	35.42	0.512484	-3.0	0.3	0.3	0.4	1							
48	175	21.02	24.71	35.29	0.512436	-3.9	0.4	0.3	0.5	1							
48	250	17.51	25.21	34.76	0.512422	-4.2	0.7	0.3	0.7	1							
44	500	7.82	26.69	34.22	0.512494	-2.8	0.3	0.1	0.3	1							
44	750	4.81	27.14	34.29	0.512511	-2.5	0.2	0.2	0.3	1							
Station Name/Cruise ID: ALOHA (KM1316/Hoe-Phor II), Location: ~22˚45' N; 158˚ W, Sampling Date: 09/18-19-20/2013, Bottom Depth: ~4800 m, MLD/DCM [a]: 57 m / 130 m																	
	15	26.89	23.15	35.52													
11	130	21.33	24.62	35.29													
16	1000	3.88	27.37	34.46													
Station Name: Wailupe Spring, Location: 21˚16.54' N; 157˚45.73' W, Sampling Date: 05/30/2010																	
	0.8 [d]			5.68	0.512668	0.6	0.2		0.2	1	39.7	3.1	18.9	3.3	0.48	0.19	
	1.4 [d]			1.81	0.512705	1.3	0.2		0.2	1	47.3	4.1	52.9	8.1	1.12	0.18	

MLD: Mixed layer depth; DCM: Deep chlorophyll maximum.

Mixed layer depth corresponds to 0.125 kg/m^3 density offset from surface value (Miller, 1976). DCM not determinable during cruise KM1107.

[a] The hydrographic data (potential temperature, potential density, salinity, MLD, DCM) of cruises KM1215, KM1219, KM1309 and KM1316 used in this publication came from the Center for Microbial Oceanography: Research and Education (C-MORE), an NSF Science and Technology Center (EF-0424599); http://hahana.soest.hawaii.edu/cmoreDS/interface.html.

[b] Calculated propagated error combined from internal and external error, with external errors representing session-based repeated analysis of JNdi-1.

[c] IODE quality flag scheme: 1 = good data, 3 = questionable/suspect data; http://www.iode.org/.

[d] Sediment depth.

[e] 226-Ra and 228-Ra errors are propagated errors combined from errors of peak area and blank peak area; ^{226}Ra/^{228}Ra errors are propagated errors from individual 226-Ra and 228-Ra errors.

Table A2.2: Dissolved rare earth element concentrations (in pmol/kg), calculated anomalies, and elemental ratios for all seawater samples of this study, and REE concentrations of standards and procedural blanks (in pmol/kg).

Cast	Water depth [db]	La	2σ[a]	Ce	2σ[a]	Pr	2σ[a]	Nd	2σ[a]	Sm	2σ[a]	Eu	2σ[a]	Gd	2σ[a]	Tb	2σ[a]	Dy	2σ[a]	Ho	2σ[a]	Er	2σ[a]	Tm	2σ[a]	Yb	2σ[a]	Lu	2σ[a]	Ce/ Ce*[b]	Eu/ Eu*[c]	Gd/ Gd*[d]	(Nd/ Er)$_N$[e]	(Er/ Lu)$_N$[e]	MREE/ MREE*[f]	DQ[g]
Station Name/Cruise ID: Pearl Harbor (KM1107-2), Location: 21˚17.087' N; 157˚57.596' W, Sampling Date: 02/25/2011, Bottom Depth: 226 m, MLD: 17 m																																				
10	10	4.35	0.30	4.74	3.12	1.09	0.04	5.21	0.35	1.13	0.07	0.38	0.02	2.04	0.22	0.27	0.01	2.07	0.13	0.50	0.03	1.62	0.09	0.21	0.01	1.11	0.09	0.18	0.01	0.5	1.37	1.4	0.23	1.3	1.40	1
10	29	5.16	0.36	4.45	2.93	1.25	0.04	5.55	0.38	1.19	0.07	0.39	0.02	2.15	0.23	0.28	0.01	2.04	0.12	0.51	0.03	1.67	0.09	0.21	0.01	1.18	0.10	0.19	0.01	0.4	1.34	1.5	0.24	1.3	1.35	1
10	50	5.45	0.38	4.81	3.17	1.38	0.05	5.74	0.39	1.33	0.08	0.39	0.02	2.32	0.25	0.30	0.01	2.20	0.13	0.55	0.04	1.80	0.10	0.23	0.01	1.26	0.10	0.20	0.01	0.4	1.24	1.5	0.23	1.3	1.37	1
10	99	5.08	0.36	3.59	2.37	1.07	0.04	4.97	0.34	0.98	0.06	0.28	0.01	1.66	0.18	0.23	0.01	1.87	0.11	0.48	0.03	1.56	0.08	0.19	0.01	1.04	0.08	0.16	0.01	0.4	1.18	1.4	0.23	1.4	1.27	1
10	179	5.61	0.39	3.14	2.07	1.05	0.04	4.80	0.33	0.90	0.05	0.26	0.01	1.58	0.17	0.24	0.01	1.91	0.12	0.50	0.03	1.64	0.09	0.21	0.01	1.17	0.10	0.19	0.01	0.3	1.13	1.3	0.21	1.2	1.14	1
Station Name/Cruise ID: Makaha (KM1107-4), Location: 21˚27.93' N; 158˚14.466' W, Sampling Date: 02/23/2011, Bottom Depth: 367 m, MLD: 62 m																																				
1	10	5.36	0.38	4.92	3.24	1.12	0.04	5.26	0.36	1.07	0.06	0.34	0.01	1.76	0.19	0.26	0.01	2.06	0.13	0.49	0.03	1.57	0.08	0.20	0.01	1.07	0.09	0.16	0.01	0.5	1.30	1.3	0.24	1.4	1.36	1
1	31	4.82	0.34	4.03	2.65	1.09	0.04	4.96	0.34	1.03	0.06	0.31	0.01	1.70	0.18	0.25	0.01	1.87	0.11	0.48	0.03	1.48	0.08	0.19	0.01	1.01	0.08	0.16	0.01	0.4	1.24	1.3	0.24	1.4	1.33	1
1	49	5.52	0.39	5.37	3.54	1.35	0.05	5.70	0.39	1.22	0.07	0.36	0.01	1.82	0.20	0.28	0.01	2.06	0.13	0.52	0.03	1.65	0.09	0.21	0.01	1.10	0.09	0.17	0.01	0.5	1.24	1.2	0.25	1.4	1.32	1
1	100	4.32	0.30	3.65	2.41	1.04	0.04	4.45	0.30	0.97	0.06	0.27	0.01	1.59	0.17	0.24	0.01	1.87	0.11	0.48	0.03	1.55	0.08	0.20	0.01	1.19	0.10	0.17	0.01	0.4	1.14	1.3	0.21	1.4	1.23	1
1	150	4.76	0.33	3.22	2.12	0.98	0.03	4.35	0.29	0.85	0.05	0.25	0.01	1.46	0.16	0.23	0.01	1.90	0.12	0.48	0.03	1.68	0.09	0.20	0.01	1.12	0.09	0.18	0.01	0.3	1.12	1.3	0.19	1.4	1.18	1
1	249	7.17	0.50	2.74	1.80	1.20	0.04	5.63	0.38	1.04	0.06	0.31	0.01	1.91	0.21	0.29	0.01	2.41	0.15	0.62	0.04	2.13	0.11	0.28	0.02	1.66	0.14	0.29	0.02	0.2	1.13	1.3	0.19	1.1	1.03	1
1	344	14.0	0.98	4.21	2.77	2.42	0.08	9.46	0.64	1.96	0.12	0.49	0.02	3.10	0.33	0.48	0.02	3.63	0.22	1.00	0.06	3.47	0.19	0.51	0.03	3.14	0.26	0.54	0.03	0.2	1.02	1.3	0.20	0.9	0.87	1
Station Name/Cruise ID: Waimea (KM1107-6), Location: 21˚39.453' N; 158˚5.508' W, Sampling Date: 02/23/2011, Bottom Depth: 72 m, MLD: 21 m																																				
2	10	6.20	0.43	8.21	5.40	1.64	0.06	7.76	0.53	1.75	0.10	0.61	0.02	2.56	0.28	0.39	0.01	2.92	0.18	0.63	0.04	2.05	0.11	0.25	0.01	1.38	0.11	0.21	0.01	0.6	1.48	1.2	0.27	1.4	1.52	1
2	29	5.16	0.36	5.42	3.57	1.32	0.04	5.83	0.39	1.32	0.08	0.42	0.02	2.19	0.24	0.30	0.01	2.12	0.13	0.55	0.04	1.69	0.09	0.22	0.01	1.15	0.09	0.18	0.01	0.5	1.32	1.4	0.25	1.4	1.40	1
2	50	5.24	0.37	5.88	3.87	1.40	0.05	6.03	0.41	1.42	0.08	0.45	0.02	2.12	0.23	0.32	0.01	2.35	0.14	0.57	0.04	1.81	0.10	0.23	0.01	1.23	0.10	0.19	0.01	0.5	1.31	1.2	0.24	1.4	1.40	1
Station Name/Cruise ID: Kahuku Point (KM1107-7), Location: 21˚45.042' N; 157˚59.123' W, Sampling Date: 02/23/2011, Bottom Depth: 124 m, MLD: 55 m																																				
3	11	5.41	0.38	6.77	4.46	1.40	0.05	6.49	0.44	1.45	0.09	0.48	0.02	2.19	0.24	0.32	0.01	2.46	0.15	0.56	0.04	1.79	0.10	0.22	0.01	1.21	0.10	0.19	0.01	0.6	1.40	1.3	0.26	1.4	1.45	1
3	30	5.46	0.38	6.39	4.20	1.33	0.04	6.39	0.43	1.35	0.08	0.45	0.02	2.06	0.22	0.30	0.01	2.30	0.14	0.52	0.03	1.71	0.09	0.21	0.01	1.17	0.09	0.18	0.01	0.5	1.42	1.3	0.27	1.4	1.41	1
3	51	4.70	0.33	4.53	2.98	1.18	0.04	5.10	0.35	1.20	0.07	0.37	0.01	1.83	0.20	0.28	0.01	2.03	0.12	0.53	0.03	1.60	0.09	0.21	0.01	1.05	0.09	0.16	0.01	0.4	1.26	1.3	0.23	1.4	1.38	1
3	100	4.75	0.33	4.33	2.85	1.20	0.04	4.99	0.34	1.14	0.07	0.34	0.01	1.81	0.19	0.27	0.01	1.97	0.12	0.51	0.03	1.62	0.09	0.21	0.01	1.08	0.09	0.17	0.01	0.4	1.22	1.3	0.22	1.4	1.33	1
3	108	4.83	0.34	4.26	2.80	1.14	0.04	5.09	0.34	1.08	0.06	0.34	0.01	1.81	0.19	0.26	0.01	1.94	0.12	0.49	0.03	1.53	0.08	0.20	0.01	1.06	0.09	0.17	0.01	0.4	1.30	1.4	0.24	1.3	1.34	1
Station Name/Cruise ID: Transect #1 (KM1107-8), Location: 21˚50.679' N; 157˚58.973' W, Sampling Date: 02/23/2011, Bottom Depth: 1389 m, MLD: 41 m																																				
6	11	5.00	0.35	4.13	2.72	1.16	0.04	5.06	0.34	1.07	0.06	0.33	0.01	1.74	0.19	0.26	0.01	2.02	0.12	0.50	0.03	1.65	0.09	0.20	0.01	1.06	0.09	0.16	0.01	0.4	1.25	1.3	0.22	1.5	1.36	1
6	49	5.11	0.36	3.62	2.39	1.06	0.04	4.78	0.32	0.97	0.06	0.28	0.01	1.56	0.17	0.23	0.01	1.84	0.11	0.47	0.03	1.60	0.09	0.19	0.01	1.00	0.08	0.15	0.01	0.4	1.17	1.3	0.22	1.5	1.28	1
6	100	7.67	0.54	8.06	5.30	1.73	0.06	7.05	0.48	1.27	0.07	0.35	0.01	1.71	0.18	0.27	0.01	2.01	0.12	0.49	0.03	1.70	0.09	0.21	0.01	1.09	0.09	0.18	0.01	0.5	1.20	1.2	0.30	1.4	1.18	3
6	251	6.44	0.45	2.98	1.96	1.15	0.04	5.24	0.35	0.99	0.06	0.29	0.01	1.78	0.19	0.28	0.01	2.27	0.14	0.57	0.04	2.01	0.11	0.25	0.01	1.46	0.12	0.25	0.01	0.3	1.08	1.3	0.19	1.2	1.10	1
6	347	13.8	0.97	2.49	1.64	2.17	0.07	9.31	0.63	1.80	0.11	0.51	0.02	2.98	0.32	0.48	0.02	3.94	0.24	0.97	0.06	3.57	0.19	0.50	0.03	3.26	0.26	0.56	0.03	0.1	1.09	1.2	0.19	0.9	0.89	1
6	496	22.6	1.58	2.87	1.89	3.41	0.11	13.9	0.94	2.71	0.16	0.75	0.03	4.55	0.49	0.69	0.03	5.26	0.32	1.41	0.09	4.85	0.26	0.74	0.04	4.69	0.38	0.85	0.05	0.1	1.09	1.3	0.21	0.8	0.85	1
6	743	26.0	1.82	3.49	2.29	3.62	0.12	16.1	1.09	2.99	0.18	0.84	0.03	4.67	0.50	0.72	0.03	5.99	0.37	1.55	0.10	5.77	0.31	0.84	0.05	5.86	0.48	1.06	0.06	0.1	1.14	1.2	0.20	0.8	0.76	1
6	993	27.8	1.95	3.62	2.39	3.80	0.13	16.7	1.13	3.10	0.18	0.84	0.03	5.00	0.54	0.79	0.03	6.38	0.39	1.69	0.11	6.36	0.34	0.96	0.05	6.68	0.54	1.23	0.07	0.1	1.07	1.2	0.19	0.7	0.72	1
6	1188	27.7	1.94	3.33	2.19	4.07	0.14	16.3	1.10	3.28	0.19	0.87	0.04	5.39	0.58	0.84	0.03	6.56	0.40	1.87	0.12	6.85	0.37	1.07	0.06	7.36	0.60	1.33	0.07	0.1	1.05	1.3	0.17	0.7	0.70	1
6	1189	29.9	2.09	2.37	1.56	3.61	0.12	17.3	1.17	2.95	0.17	0.86	0.03	5.29	0.57	0.78	0.03	6.49	0.40	1.78	0.12	6.27	0.34	0.98	0.05	6.80	0.55	1.33	0.07	0.1	1.14	1.3	0.20	0.7	0.71	1
6	1345	27.0	1.89	2.87	1.89	3.54	0.12	16.5	1.12	2.90	0.17	0.84	0.03	4.83	0.52	0.75	0.03	6.39	0.39	1.66	0.11	6.19	0.33	0.94	0.05	6.45	0.52	1.21	0.07	0.1	1.13	1.3	0.19	0.7	0.72	1

Table A2.2: continued.

Cast	Water depth [db]	La	$2\sigma^{a}$	Ce	$2\sigma^{a}$	Pr	$2\sigma^{a}$	Nd	$2\sigma^{a}$	Sm	$2\sigma^{a}$	Eu	$2\sigma^{a}$	Gd	$2\sigma^{a}$	Tb	$2\sigma^{a}$	Dy	$2\sigma^{a}$	Ho	$2\sigma^{a}$	Er	$2\sigma^{a}$	Tm	$2\sigma^{a}$	Yb	$2\sigma^{a}$	Lu	$2\sigma^{a}$	Ce/ Ce*^{b}	Eu/ Eu*^{c}	Gd/ Gd*^{d}	(Nd/ Er)$_{N}$ ^{e}	(Er/ Lu)$_{N}$ ^{e}	MREE/ MREE*$_{f}$	DQ^{g}
Station Name/Cruise ID: ALOHA (KM1107-11), Location: 22°45.022' N; 157°59.995' W, Sampling Date: 02/24/2011, Bottom Depth: 4749 m, MLD: 66 m																																				
9	9	5.33	0.37	4.31	2.84	1.19	0.04	5.56	0.38	1.14	0.07	0.37	0.01	1.80	0.19	0.27	0.01	2.00	0.12	0.51	0.03	1.59	0.09	0.20	0.01	1.03	0.08	0.16	0.01	0.4	1.31	1.3	0.25	1.5	1.37	1
9	49	4.97	0.35	4.02	2.64	1.12	0.04	5.09	0.34	1.06	0.06	0.32	0.01	1.70	0.18	0.25	0.01	2.00	0.12	0.49	0.03	1.65	0.09	0.19	0.01	1.04	0.08	0.16	0.01	0.4	1.23	1.3	0.22	1.5	1.35	1
9	102	4.82	0.34	3.25	2.14	1.06	0.04	4.63	0.31	0.93	0.05	0.28	0.01	1.62	0.17	0.24	0.01	1.83	0.11	0.48	0.03	1.49	0.08	0.19	0.01	1.00	0.08	0.16	0.01	0.3	1.17	1.3	0.22	1.3	1.27	1
9	248	6.52	0.46	2.75	1.81	1.17	0.04	5.15	0.35	1.04	0.06	0.30	0.01	1.95	0.21	0.28	0.01	2.31	0.14	0.60	0.04	2.01	0.11	0.27	0.01	1.58	0.13	0.26	0.01	0.2	1.10	1.4	0.19	1.1	1.07	1
9	351	12.3	0.86	3.44	2.27	1.97	0.07	8.93	0.60	1.74	0.10	0.48	0.02	2.95	0.32	0.45	0.02	3.76	0.23	0.92	0.06	3.16	0.17	0.44	0.02	2.84	0.23	0.48	0.03	0.2	1.09	1.3	0.21	0.9	0.97	1
9	496	18.1	1.27	1.74	1.15	2.55	0.09	11.0	0.75	2.10	0.12	0.59	0.02	3.72	0.40	0.53	0.02	4.07	0.25	1.15	0.07	3.69	0.20	0.58	0.03	3.59	0.29	0.66	0.04	0.1	1.10	1.4	0.22	0.8	0.85	1
9	745	30.2	2.11	2.76	1.82	3.87	0.13	18.0	1.22	3.10	0.18	0.87	0.04	5.29	0.57	0.76	0.03	6.26	0.38	1.56	0.10	5.69	0.30	0.83	0.04	5.72	0.47	1.04	0.06	0.1	1.13	1.3	0.23	0.8	0.81	1
9	746	30.7	2.15	2.91	1.92	3.93	0.13	17.9	1.21	3.14	0.18	0.87	0.04	5.39	0.58	0.77	0.03	5.93	0.36	1.64	0.11	5.56	0.30	0.86	0.05	5.54	0.45	1.05	0.06	0.1	1.12	1.4	0.23	0.8	0.80	1
9	991	29.5	2.07	2.74	1.80	3.71	0.12	17.7	1.20	2.98	0.18	0.88	0.04	5.14	0.55	0.78	0.03	6.43	0.39	1.69	0.11	6.34	0.34	0.96	0.05	6.46	0.53	1.22	0.07	0.1	1.15	1.3	0.20	0.7	0.73	1
9	1489	37.9	2.66	3.56	2.34	4.69	0.16	22.1	1.50	3.81	0.22	1.10	0.04	6.54	0.70	0.94	0.04	8.05	0.49	2.13	0.14	7.66	0.41	1.19	0.06	8.31	0.68	1.58	0.08	0.1	1.16	1.3	0.21	0.7	0.71	1
9	1979	42.1	2.95	4.19	2.76	6.31	0.21	27.5	1.86	5.19	0.31	1.40	0.06	8.01	0.86	1.25	0.05	10.3	0.63	2.67	0.17	9.98	0.53	1.50	0.08	10.9	0.89	1.95	0.10	0.1	1.10	1.2	0.20	0.7	0.72	1
9	2960	58.3	4.08	4.89	3.22	9.35	0.31	40.8	2.76	7.89	0.46	2.11	0.09	11.2	1.21	1.81	0.07	13.8	0.84	3.38	0.22	12.3	0.66	1.82	0.10	13.1	1.07	2.32	0.12	0.0	1.11	1.2	0.24	0.8	0.81	1
9	3938	69.2	4.84	4.35	2.86	10.8	0.36	51.4	3.48	9.16	0.54	2.56	0.10	12.7	1.36	1.93	0.07	14.7	0.90	3.39	0.22	11.6	0.62	1.73	0.09	12.1	0.99	2.19	0.12	0.0	1.21	1.2	0.32	0.8	0.89	1
9	4644	69.3	4.85	4.52	2.98	11.2	0.38	50.0	3.39	9.57	0.56	2.60	0.11	13.5	1.45	1.92	0.07	13.9	0.84	3.38	0.22	11.0	0.59	1.73	0.09	11.5	0.94	2.23	0.12	0.0	1.20	1.3	0.33	0.7	0.90	1
9	4644	61.5	4.31	4.54	2.99	11.7	0.39	45.4	3.07	10.1	0.59	2.43	0.10	13.5	1.45	2.05	0.08	13.6	0.83	3.56	0.23	11.9	0.63	1.85	0.10	12.8	1.04	2.26	0.12	0.0	1.06	1.2	0.28	0.8	0.88	1
Station Name/Cruise ID: ALOHA (KM1215/Hoe-Dylan V), Location: 22°48.54' N; 158°1.92' W, Sampling Date: 07/21/2012, Bottom Depth: 4742 m, MLD/DCM ^{a}: 37 m / 137 m																																				
74	4	4.70	0.33	3.64	2.40	1.07	0.04	4.58	0.31	0.93	0.05	0.26	0.01	1.47	0.16	0.23	0.01	1.76	0.11	0.45	0.03	1.46	0.08	0.18	0.01	0.92	0.08	0.14	0.01	0.4	1.13	1.3	0.23	1.5	1.31	1
74	24	5.28	0.37	3.59	2.36	1.53	0.05	6.58	0.45	0.91	0.05	0.28	0.01	1.72	0.18	0.23	0.01	1.81	0.11	0.45	0.03	1.51	0.08	0.18	0.01	0.96	0.08	0.14	0.01	0.3	1.22	1.4	0.32	1.5	1.28	3
74	75	5.41	0.38	3.89	2.56	1.12	0.04	4.96	0.34	0.94	0.06	0.26	0.01	1.62	0.17	0.23	0.01	1.79	0.11	0.46	0.03	1.48	0.08	0.18	0.01	0.95	0.08	0.15	0.01	0.4	1.12	1.4	0.24	1.4	1.30	1
74	136	4.67	0.33	3.13	2.06	1.00	0.03	4.51	0.31	0.86	0.05	0.25	0.01	1.50	0.16	0.22	0.01	1.70	0.10	0.45	0.03	1.46	0.08	0.19	0.01	0.99	0.08	0.16	0.01	0.3	1.13	1.3	0.22	1.3	1.21	1
74	175	4.34	0.30	2.93	1.93	1.00	0.03	4.04	0.27	0.90	0.05	0.24	0.01	1.51	0.16	0.23	0.01	1.81	0.11	0.49	0.03	1.58	0.08	0.21	0.01	1.14	0.09	0.18	0.01	0.3	1.06	1.3	0.19	1.3	1.17	1
74	250	6.63	0.46	2.75	1.81	1.15	0.04	5.09	0.34	0.96	0.06	0.29	0.01	1.82	0.20	0.27	0.01	2.26	0.14	0.58	0.04	1.98	0.11	0.26	0.01	1.56	0.13	0.26	0.01	0.2	1.13	1.4	0.19	1.1	1.05	1
74	500	22.7	1.59	1.95	1.28	3.04	0.10	14.0	0.94	2.44	0.14	0.64	0.03	4.33	0.47	0.62	0.02	4.87	0.30	1.28	0.08	4.45	0.24	0.66	0.04	4.25	0.35	0.77	0.04	0.1	1.05	1.4	0.23	0.8	0.86	1
74	749	27.7	1.94	2.37	1.56	3.99	0.13	16.1	1.09	3.15	0.19	0.81	0.03	5.23	0.56	0.76	0.03	5.64	0.34	1.62	0.11	5.41	0.29	0.87	0.05	5.90	0.48	1.08	0.06	0.1	1.05	1.3	0.22	0.7	0.76	1
Station Name/Cruise ID: ALOHA (KM1219/Hoe-Dylan IX), Location: 22°48.48' N; 158°3' W, Sampling Date: 08/27/2012 and 08/28/2012, Bottom Depth: 4739 m, MLD/DCM ^{a}: 33 m / 132 m																																				
34	5	5.05	0.35	3.57	2.35	1.11	0.04	4.90	0.33	0.95	0.06	0.26	0.01	1.55	0.17	0.23	0.01	1.79	0.11	0.47	0.03	1.48	0.08	0.18	0.01	0.94	0.08	0.14	0.01	0.3	1.12	1.3	0.24	1.5	1.31	1
34	25	7.20	0.50	4.94	3.25	1.47	0.05	6.90	0.47	1.24	0.07	0.38	0.02	2.02	0.22	0.31	0.01	2.46	0.15	0.61	0.04	2.01	0.11	0.24	0.01	1.26	0.10	0.20	0.01	0.4	1.22	1.3	0.25	1.5	1.29	1
34	75	5.99	0.42	4.14	2.73	1.31	0.04	5.53	0.37	1.12	0.07	0.30	0.01	1.76	0.19	0.27	0.01	2.15	0.13	0.53	0.03	1.84	0.10	0.21	0.01	1.14	0.09	0.17	0.01	0.3	1.09	1.2	0.22	1.5	1.29	1
34	126	4.39	0.31	3.23	2.12	1.03	0.03	4.22	0.29	0.85	0.05	0.25	0.01	1.40	0.15	0.22	0.01	1.68	0.10	0.44	0.03	1.51	0.08	0.18	0.01	0.99	0.08	0.15	0.01	0.4	1.14	1.3	0.20	1.4	1.21	1
34	174	4.32	0.30	2.97	1.96	0.93	0.03	4.12	0.28	0.78	0.05	0.23	0.01	1.40	0.15	0.22	0.01	1.79	0.11	0.46	0.03	1.60	0.09	0.19	0.01	1.03	0.08	0.16	0.01	0.3	1.11	1.3	0.19	1.4	1.21	1
34	248	6.07	0.43	2.60	1.71	1.12	0.04	4.64	0.31	0.95	0.06	0.27	0.01	1.70	0.18	0.27	0.01	2.18	0.13	0.57	0.04	1.99	0.11	0.26	0.01	1.49	0.12	0.25	0.01	0.2	1.08	1.3	0.17	1.1	1.04	1
40	496	20.0	1.40	2.94	1.94	3.05	0.10	12.2	0.83	2.49	0.15	0.63	0.03	3.98	0.43	0.61	0.02	4.62	0.28	1.28	0.08	4.28	0.23	0.65	0.04	4.04	0.33	0.73	0.04	0.1	1.02	1.3	0.21	0.8	0.85	1
40	744	28.6	2.00	3.82	2.51	3.87	0.13	19.8	1.34	3.05	0.18	0.80	0.03	4.63	0.50	0.75	0.03	6.21	0.38	1.50	0.10	5.80	0.31	0.80	0.04	5.53	0.45	0.96	0.05	0.1	1.06	1.2	0.25	0.9	0.81	1
Station Name/Cruise ID: ALOHA (KM1309/Hoe-Phor I), Location: 22°44.986' N; 157°59.994' W, Sampling Date: 06/01/2013 and 06/02/2013, Bottom Depth: ~4800 m, MLD/DCM ^{a}: 34 m / 147 m																																				
48	5	6.10	0.43	4.48	2.95	2.12	0.07	8.36	0.57	0.98	0.06	0.30	0.01	1.60	0.17	0.23	0.01	2.29	0.14	0.46	0.03	1.46	0.08	0.18	0.01	0.89	0.07	0.14	0.01	0.3	1.28	1.3	0.42	1.5	1.32	3
48	25	5.06	0.35	2.77	1.83	1.04	0.03	4.64	0.31	0.86	0.05	0.24	0.01	1.46	0.16	0.21	0.01	1.69	0.10	0.42	0.03	1.40	0.08	0.17	0.01	0.89	0.07	0.13	0.01	0.3	1.15	1.4	0.24	1.5	1.30	1
48	75	6.10	0.43	4.98	3.28	1.21	0.04	5.52	0.37	0.99	0.06	0.28	0.01	1.50	0.16	0.23	0.01	1.84	0.11	0.45	0.03	1.50	0.08	0.17	0.01	0.97	0.08	0.15	0.01	0.4	1.17	1.3	0.27	1.4	1.25	1
48	120	4.77	0.33	3.29	2.16	1.08	0.04	4.70	0.32	0.87	0.05	0.25	0.01	1.52	0.16	0.22	0.01	1.72	0.11	0.46	0.03	1.50	0.08	0.19	0.01	1.02	0.08	0.16	0.01	0.3	1.12	1.3	0.23	1.4	1.21	1
48	175	4.61	0.32	3.80	2.50	1.01	0.03	4.43	0.30	0.85	0.05	0.25	0.01	1.43	0.15	0.22	0.01	1.85	0.11	0.44	0.03	1.59	0.09	0.19	0.01	1.07	0.09	0.16	0.01	0.4	1.14	1.3	0.20	1.4	1.21	1
48	250	5.48	0.38	2.63	1.73	1.09	0.04	4.44	0.30	0.90	0.05	0.26	0.01	1.60	0.17	0.24	0.01	2.02	0.12	0.53	0.03	1.74	0.09	0.23	0.01	1.33	0.11	0.23	0.01	0.2	1.09	1.3	0.19	1.1	1.07	1
44	500	20.6	1.44	2.22	1.46	2.77	0.09	12.8	0.86	2.20	0.13	0.60	0.02	3.38	0.36	0.54	0.02	4.60	0.28	1.11	0.07	4.17	0.22	0.58	0.03	3.86	0.31	0.70	0.04	0.1	1.10	1.2	0.22	0.9	0.83	1
44	750	30.8	2.16	4.23	2.78	4.03	0.14	18.1	1.23	3.03	0.18	0.89	0.04	5.11	0.55	0.73	0.03	5.89	0.36	1.52	0.10	5.53	0.30	0.81	0.04	5.43	0.44	1.02	0.06	0.1	1.19	1.4	0.24	0.8	0.79	1
Station Name/Cruise ID: ALOHA (KM1316/Hoe-Phor II), Location: ~22°45' N; 158° W, Sampling Date: 09/18-19-20/2013, Bottom Depth: ~4800 m, MLD/DCM ^{a}: 57 m / 130 m																																				
	15	4.25	0.30	3.14	2.07	0.92	0.03	4.26	0.29	0.79	0.05	0.23	0.01	1.34	0.14	0.20	0.01	1.58	0.10	0.41	0.03	1.36	0.07	0.16	0.01	0.85	0.07	0.13	0.01	0.4	1.18	1.3	0.23	1.5	1.28	1
5	130	4.63	0.32	2.72	1.79	0.99	0.03	4.17	0.28	0.86	0.05	0.24	0.01	1.51	0.16	0.23	0.01	1.80	0.11	0.49	0.03	1.56	0.08	0.20	0.01	1.12	0.09	0.18	0.01	0.3	1.10	1.3	0.19	1.3	1.16	1
10	1000	27.9	1.96	2.19	1.44	4.00	0.13	16.1	1.09	3.21	0.19	0.85	0.03	5.44	0.59	0.82	0.03	6.42	0.39	1.85	0.12	6.45	0.35	1.02	0.06	7.05	0.57	1.33	0.07	0.0	1.04	1.3	0.18	0.7	0.71	1

Table A2.2: continued.

Cast	Water depth [db]	La	2σ [a]	Ce	2σ [a]	Pr	2σ [a]	Nd	2σ [a]	Sm	2σ [a]	Eu	2σ [a]	Gd	2σ [a]	Tb	2σ [a]	Dy	2σ [a]	Ho	2σ [a]	Er	2σ [a]	Tm	2σ [a]	Yb	2σ [a]	Lu	2σ [a]	Ce/Ce*[b]	Eu/Eu*[c]	Gd/Gd*[d]	$(Nd/Er)_N$ [e]	$(Er/Lu)_N$ [e]	MREE/MREE* [f]	DQ[g]
Standards and Blanks																																				
SAFe, 3000m (n = 10 [h])																																				
		65.6		5.96		11.2		46.8		9.35		2.43		14.0		2.05		15.0		3.80		12.8		2.02		14.0		2.58								
2σ SD		4.59		3.92		0.38		3.17		0.55		0.10		1.51		0.08		0.91		0.25		0.69		0.11		1.14		0.14								
2σ RSD (%)		7.0		65.8		3.4		6.8		5.9		4.0		10.8		3.8		6.1		6.5		5.4		5.4		8.1		5.4								
BATS, 15m (n = 4)																																				
		14.1		11.9		3.16		14.6		3.15		0.87		4.68		0.80		6.08		1.42		4.96		0.68		4.26		0.70								
2σ SD		1.03		0.95		0.27		0.77		0.22		0.03		0.32		0.06		0.49		0.08		0.35		0.04		0.37		0.04								
2σ RSD (%)		7.3		8.0		8.7		5.3		7.1		3.9		6.8		7.1		8.1		5.6		7.1		6.3		8.8		5.2								
Procedural Blank (n = 9)																																				
		0.35		0.53		0.05		0.18		0.03		0.01		0.05		0.01		0.02		0.00		0.01		0.00		0.02		0.01								

[a] Error is based on external reproducibility of SAFe measurements, all errors in pmol/kg.

[b] Ce anomaly calculated from PAAS normalised values as($Ce/Ce^*)_N = 3*Ce_N/(2*La_N+Nd_N)$ (e.g., Elderfield and Greaves, 1982).

[c] Eu anomaly calculated from PAAS normalised values as $(Eu/Eu^*)_N = 3*Eu_N/(2*Sm_N+Tb_N)$ (e.g., Zhang et al., 2008).

[d] Gd anomaly calculated from PAAS normalised values as $(Gd/Gd^*)_N = Gd_N/(0.33*Sm_N+0.67*Tb_N)$ according to Bau and Dulski (1996).

[e] elemental ratios calculated using PAAS normalised REE values. PAAS from Taylor and McLennan (1985).

[f] MREE anomaly calculated from PAAS normalised values as $(MREE/MREE^*)_N = 2*(Gd+Tb+Dy)_N/(La+Pr+Nd+Tm+Yb+Lu)_N$ according to Martin et al., (2010).

[g] DQ: Data Quality; IODE quality flag scheme: 1 = good data, 3 = questionable/suspect data; http://www.iode.org/.

[h] SAFe measurements consist of 9 true replicates and one double measurement.

Table A2.3: Rare earth element concentrations in the dissolved, retentate and permeate fractions (in pmol/kg) of samples from cruise KM1316 (Hoe-Phor II) and calculated colloidal REE concentrations.

Fraction [a]	**La**	**2σ** [b]	**Ce**	**2σ** [b]	**Pr**	**2σ** [b]	**Nd**	**2σ** [b]	**Sm**	**2σ** [b]	**Eu**	**2σ** [b]	**Gd**	**2σ** [b]	**Tb**	**2σ** [b]	**Dy**	**2σ** [b]	**Ho**	**2σ** [b]	**Er**	**2σ** [b]	**Tm**	**2σ** [b]	**Yb**	**2σ** [b]	**Lu**	**2σ** [b]	**DQ** [c]
Sample: 15 m, CF = 2																													
Dissolved	4.25	0.30	3.14	2.07	0.92	0.03	4.26	0.29	0.79	0.05	0.23	0.01	1.34	0.14	0.20	0.01	1.58	0.10	0.41	0.03	1.36	0.07	0.16	0.01	0.85	0.07	0.13	0.01	1
Retentate	4.63	0.32	2.95	1.94	0.93	0.03	4.18	0.28	0.83	0.05	0.24	0.01	1.45	0.16	0.21	0.01	1.64	0.10	0.44	0.03	1.38	0.07	0.18	0.01	0.89	0.07	0.14	0.01	1
Permeate	4.13	0.29	2.84	1.87	0.93	0.03	3.98	0.27	0.81	0.05	0.23	0.01	1.41	0.15	0.21	0.01	1.62	0.10	0.43	0.03	1.37	0.07	0.18	0.01	0.87	0.07	0.14	0.01	1
Colloidal (calc.)	0.25		0.05		0.00		0.10		0.01		0.01		0.02		0.00		0.01		0.00		0.00		0.00		0.01		0.00		
Colloidal (%)	5.8		1.7		0.3		2.3		1.5		2.6		1.3		0.5		0.5		1.1		0.3		0.1		1.2		-0.1		
Recovery (%)	103		92		101		96		104		100		107		106		103		107		101		108		103		108		
Sample: 130 m, CF = 2																													
Dissolved	4.63	0.32	2.72	1.79	0.99	0.03	4.17	0.28	0.86	0.05	0.24	0.01	1.51	0.16	0.23	0.01	1.80	0.11	0.49	0.03	1.56	0.08	0.20	0.01	1.12	0.09	0.18	0.01	1
Retentate	4.88	0.34	2.70	1.78	0.94	0.03	4.36	0.30	0.84	0.05	0.25	0.01	1.49	0.16	0.23	0.01	1.79	0.11	0.48	0.03	1.55	0.08	0.20	0.01	1.09	0.09	0.18	0.01	1
Permeate	4.19	0.29	2.70	1.78	0.93	0.03	4.06	0.27	0.82	0.05	0.24	0.01	1.43	0.15	0.23	0.01	1.82	0.11	0.47	0.03	1.64	0.09	0.20	0.01	1.09	0.09	0.17	0.01	1
Colloidal (calc.)	0.35		0.00		0.00		0.15		0.01		0.00		0.03		0.00		-0.02		0.01		-0.04		0.00		0.00		0.00		
Colloidal (%)	7.5		0.1		0.5		3.6		1.1		1.5		2.0		0.9		-0.9		1.6		-2.7		-0.8		0.2		2.2		
Recovery (%)	98		99		95		101		96		100		96		102		101		98		102		99		97		97		
Sample: 1000 m, CF = 2																													
Dissolved	27.9	1.96	2.19	1.44	4.00	0.13	16.1	1.09	3.21	0.19	0.85	0.03	5.44	0.59	0.82	0.03	6.42	0.39	1.85	0.12	6.45	0.35	1.02	0.06	7.05	0.57	1.33	0.07	1
Retentate	29.5	2.07	2.19	1.44	3.56	0.12	17.1	1.16	2.95	0.17	0.85	0.03	5.15	0.55	0.77	0.03	6.31	0.38	1.68	0.11	6.16	0.33	0.93	0.05	6.50	0.53	1.22	0.07	1
Permeate	29.4	2.06	2.20	1.45	3.51	0.12	16.8	1.13	2.77	0.16	0.83	0.03	4.90	0.53	0.73	0.03	5.97	0.36	1.62	0.11	6.03	0.32	0.90	0.05	6.05	0.49	1.16	0.06	1
Colloidal (calc.)	0.09		0.00		0.02		0.19		0.09		0.01		0.12		0.02		0.17		0.03		0.06		0.02		0.22		0.03		
Colloidal (%)	0.3		-0.1		0.6		1.2		2.8		1.0		2.3		2.3		2.7		1.7		0.9		1.5		3.1		2.2		
Recovery (%)	105		100		89		105		89		99		92		91		96		89		95		90		89		89		

[a] colloidal REE concentration calculated by $(REE_{retentate}-REE_{permeate})/CF$ with CF = 2 (Fitzsimmons and Boyle, 2014); Recovery = $(s_{REE}+c_{REE})/d_{REE}*100\%$; % Colloidal = (Colloidal calculated/Dissolved)*100%.

[b] Error is based on external reproducibility of SAFe measurements (see Tab. A2.2), all errors in pmol/kg.

[c] DQ: Data Quality; IODE quality flag scheme: 1 = good data; http://www.iode.org/.

3. Break-up of last glacial deep stratification in the South Pacific

Chandranath Basak[1, †, ‡], Henning Fröllje[1, ‡], Frank Lamy[2], Rainer Gersonde[2], Verena Benz[2], Robert F. Anderson[3], Katharina Pahnke[1]

This chapter corresponds to a full manuscript that is in preparation for submission to the journal *Science*.

‡ These authors contributed equally to this work.

[1] Max Planck Research Group for Marine Isotope Geochemistry, Institute for Chemistry and Biology of the Marine Environment (ICBM), University of Oldenburg, Carl-von-Ossietzky-Str. 9-11, 26129 Oldenburg, Germany.

[2] Alfred Wegener Institute, Helmholtz Centre for Polar and Marine Research, Am Alten Hafen 26, 27568 Bremerhaven, Germany.

[3] Lamont-Doherty Earth Observatory of Columbia University, 61 Route 9W, Palisades, NY 10964, USA.

† Now at: Lamont-Doherty Earth Observatory of Columbia University, 61 Route 9W, Palisades, NY 10964, USA.

Abstract

Stratification of the deep Southern Ocean (SO) during the Last Glacial Maximum (LGM) is thought to have facilitated carbon storage, which was subsequently released during the deglaciation as stratification broke down, thereby contributing to the atmospheric CO_2 rise. Here, we present neodymium isotope evidence in favor of this hypothesis from deep (3000-4000 m) to abyssal (>4000 m) water depths in the Pacific sector of the SO. We show that the LGM deep SO was stratified and Ross Sea Bottom Water expanded northward, highlighting the important role of abyssal waters in sustaining a deep glacial carbon reservoir. The deglacial breakdown of deep stratification was driven by Southern Hemisphere climate and was a prerequisite for the deglacial release of sequestered CO_2 through upwelling.

One sentence summary

Neodymium isotope evidence for last glacial deep stratification in the South Pacific and its Southern Hemisphere-driven deglacial break-up

3.1. Main Text

The Southern Ocean (SO) has long been recognized as a key player in regulating atmospheric CO_2 variations and hence global climate based on the tight coupling between Southern Hemisphere (SH) temperatures and atmospheric CO_2 concentrations (e.g., Genthon et al., 1987). Yet, the mechanisms involved in regulating past CO_2 variations are not yet fully understood. The most promising explanation includes marine biogeochemistry and its interaction with ocean circulation changes in the SO, where CO_2 sequestration and release due to the production of new and upwelling of old deep waters occurs (e.g., Sigman and Boyle, 2000). The SO therefore acts as a window through which ocean and atmosphere interact, and this atmosphere-ocean gas exchange is sensitive to changes in SO climate and the stability of the water column. During the Last Glacial Maximum (LGM), there is evidence that the deep SO was stratified, leading to slower gas exchange in the SO and the presence of an old, radiocarbon depleted water mass in the deep South Pacific (Ronge et al., 2016), overlying better ventilated bottom waters (McCave et al., 2008; Sikes et al., 2016). By the time of late Heinrich Stadial 1 (HS1), the SO water column became destratified and well mixed, releasing sequestered CO_2 to the atmosphere and contributing to the deglacial atmospheric CO_2 rise (Anderson et al., 2009; Burke and Robinson, 2012; Ronge et al., 2016). The proposed destratification mechanisms include southward shifting westerlies and enhanced upwelling (Anderson et al., 2009) as well as sea ice retreat, associated buoyancy flux changes, and increased mixing of northern- and southern-sourced waters (Ferrari et al., 2014). Here we show that deep stratification in the SO also affected the abyssal water column. The break-up of this deep stratification occurred with the onset of SH warming, setting the stage for upwelling and release of sequestered carbon to the atmosphere.

We use neodymium (Nd) isotopes ($^{143}Nd/^{144}Nd$, expressed as ε_{Nd}) measured on fossil fish teeth/debris (FT) and foraminifera from deep (3000-4000 m) to abyssal (>4000 m) water depths in the South Pacific to reconstruct the history of the deep water column structure over the past 30 ka (see Supplementary Online Material (SOM)) (Fig. 3.1). The Nd isotope composition of modern Circumpolar Deep Water (CDW) (ε_{Nd} ~ -8 to -9; Stichel et al., 2012b; Basak et al., 2015) is largely determined by mixing between North Atlantic Deep Water (NADW) with ε_{Nd} = -13.5 near its source (Lacan and Jeandel, 2005b) and North Pacific Deep Water (NPDW) with ε_{Nd} = ~ -3.9 (Amakawa et al., 2009). Previous studies in the South Atlantic have suggested that glacial-interglacial and shorter-term changes in SO deep water ε_{Nd} were controlled by changes in NADW southward export (Piotrowski et al., 2004; Skinner et al., 2013; Lippold et al., 2016). We present evidence from South Pacific deep (E11-2, PS75/073, PS75/056, PS75/059, 3109-3613 m water depth, w.d.) and abyssal (PS75/054, 4085 m w.d.; Fig. 3.1, Table S3.1, SOM) cores that demonstrates instead a strong SH climate control on changes in the SO deep water structure and ε_{Nd} composition over the last 30 ka.

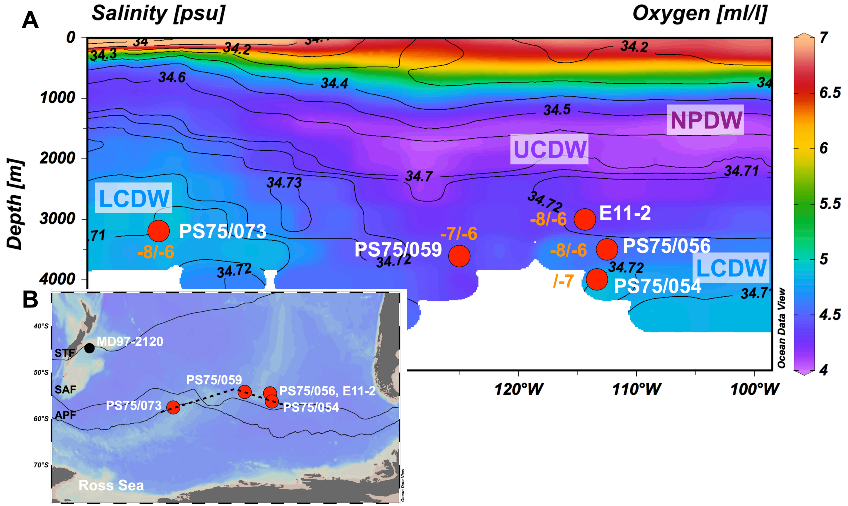

Figure 3.1: Modern hydrography and core locations in the South Pacific. (A) Zonal section (along red stippled line in B) of dissolved oxygen (color; Garcia et al., 2010a) and salinity (contours; Antonov et al., 2010) with depth locations of studied cores. Major deep water masses are marked (NPDW, UCDW, LCDW). (B) Map showing locations of studied sediment cores (red symbols), reference core MD97-2120 (black circle), and major circum-Antarctic fronts (solid lines, after Orsi et al., 1995).

The cores have independent age models based on tuning benthic or planktonic stable isotopes to well-dated core MD97-2120 (Pahnke et al., 2003; Pahnke and Zahn, 2005), except for PS75/054, which is tied to PS75/056 (SOM). The cores cover the entire depth range of modern lower CDW and are therefore ideal for monitoring the evolution of the deep water column structure in the South Pacific over the last deglaciation (Fig. 3.1A, B, SOM). Neodymium isotopes, measured on FT and planktonic foraminifera, show Late Holocene core-top values of -8.3 (PS75/073) and -7.2 to -7.7 (PS75/059, PS75/056, E11-2), consistent with CDW influence with slightly different contributions from NPDW and NADW that are due to the depth and latitudinal positions of the cores (Figs. 3.1A, B, S3.3) (Basak et al., 2015). The deepest core (PS75/054) lacks the Late Holocene, but hydrographic data indicate the presence of LCDW close to the boundary to RSBW (Fig. 3.1, SOM). During the LGM, the average ε_{Nd} at the deep sites was consistently at ~-6 (Figs. 3.1A, 3.2E-H), suggesting one homogenous water mass occupied the deep South Pacific. At abyssal depth (PS75/054), in contrast, a more negative ε_{Nd} of ~-7.5 prevailed throughout the LGM and early deglaciation, suggesting reduced mixing in the deep glacial South Pacific (Figs. 3.1A, 3.2D). The deglaciation in the deep southern cores PS75/056 and PS75/073 was marked by an ε_{Nd} decrease that started with the first SH warming (W1,

~17.5 ka B.P.) recorded in Antarctic ice cores (e.g., Jouzel et al., 2007; Fig. 3.3), and which coincided with HS1 in the Northern Hemisphere (Siani et al., 2013, Figs. 3.2, 3.4). A brief halt in the ε_{Nd} decrease occurred during the ACR, and a second ε_{Nd} decrease was synchronous with the second SH warming at ~12.8 ka (W2). The ε_{Nd} decrease in core E11-2 (56° S, 3109 m w.d.) started at mid-W1, with some delay to the deeper cores. In the northernmost deep core PS75/059 (55° S, 3613 m w.d.), LGM ε_{Nd} values of ~ -6 were maintained until ≤13.5 ka, followed by an ε_{Nd} decrease during W2.

The homogenous glacial South Pacific deep water ε_{Nd} of -6 coincided with a reduced southward export of unradiogenic NADW (Curry and Oppo, 2005; Roberts et al., 2010). The slightly more radiogenic glacial ε_{Nd} in the Pacific relative to the Atlantic (ε_{Nd} = -6.5 to -7.3; Piotrowski et al., 2004; Lippold et al., 2016) results from the higher influence of radiogenic Pacific deep water and/or less direct influence of NADW in the Pacific. The ε_{Nd} of -7.5 at abyssal depth in the South Pacific and the strong ε_{Nd} contrast to overlying deep waters (ε_{Nd} = -6) indicates strong stratification of the deep to bottom layer and a glacial northward expansion of RSBW (Fig. 3.4), in line with a previous suggestion of increased glacial presence of RSBW in the southwest Pacific (McCave et al., 2008). In the glacial Atlantic, AABW is known to have occupied the deep to abyssal basin far into the North Atlantic (Curry and Oppo, 2005; Roberts et al., 2010). Yet, due to the shoaling of NADW and the dependent interplay between the upper and lower circulation cells, evidence for active changes in AABW advection were so far limited. Outside the direct influence of NADW fluctuations and without, or very small (e.g., Rae et al., 2014), interfering changes in NPDW formation, our (carbon-independent) proxy data show for the first time direct evidence for increased RSBW expansion during the LGM. Enhanced brine rejection during sea ice formation has been invoked previously to account for increased formation and higher density of AABW during the last glacial (Adkins et al., 2002; Adkins, 2013). The strong glacial deep stratification inferred from different ε_{Nd} above and below ~3500-4000 m w.d. is consistent with coral-based ^{14}C in Drake Passage (Burke and Robinson, 2012) and with salinity and density reconstructions that show a clear separation between very high-density bottom water at 3600 m w.d. and lower-density water at 3200 m w.d. in the SO (Adkins et al., 2002; Adkins, 2013). This high density of LGM SO bottom water together with a reduced flow speed of the Antarctic Circumpolar Current (ACC; Lamy et al., 2015) would have reduced diapycnal mixing at depth that occurs today through interaction of abyssal current flow with bottom topography (Nikurashin and Ferrari, 2013). Increased formation of high-density RSBW, as suggested by its enhanced glacial northward expansion, and isolation from overlying deep water, would have led to increased carbon transfer to depth and stabilization of the deep water column.

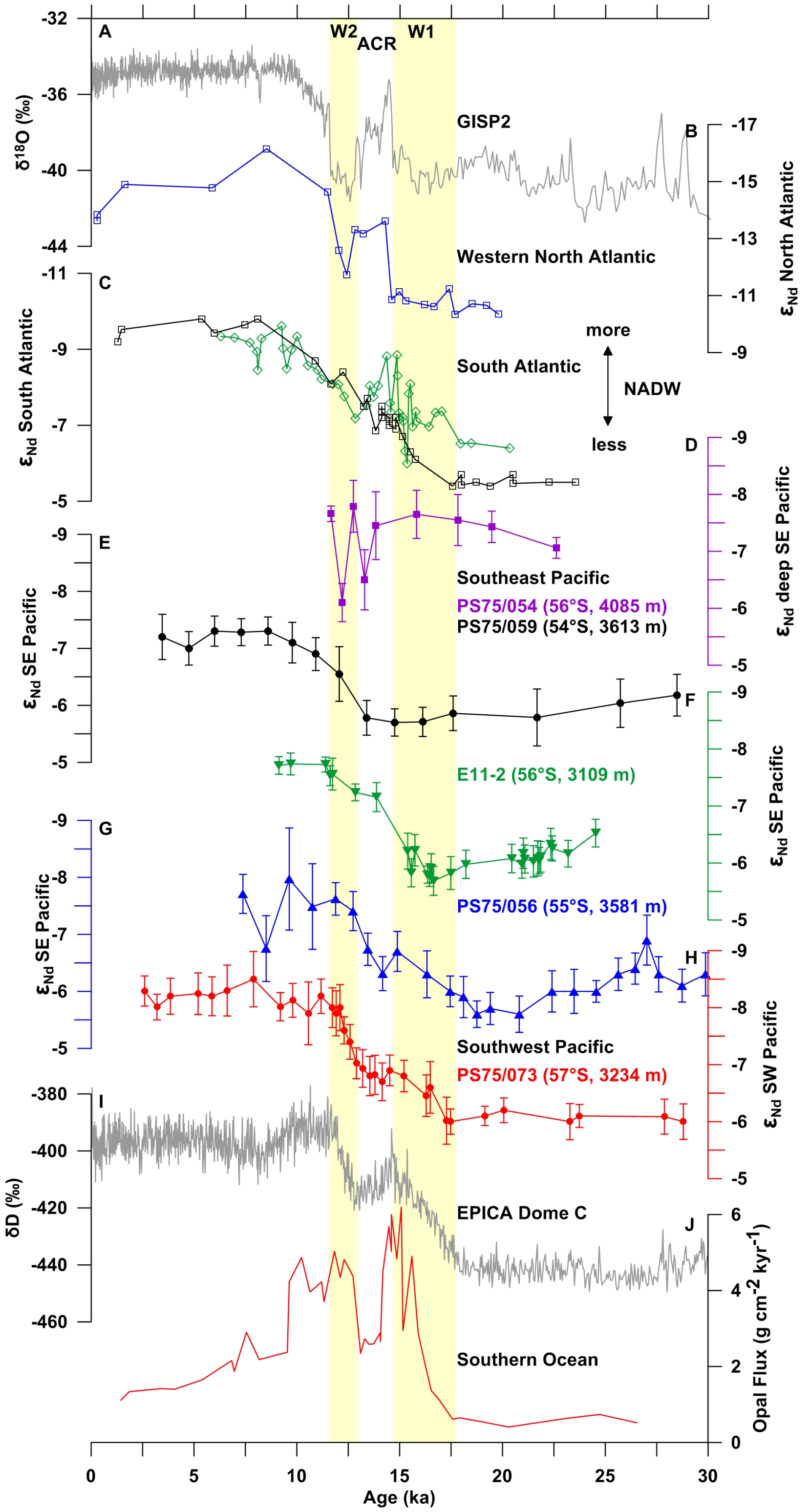

Figure 3.2: Evolution of the SO water column structure, NADW formation, and climate over the last 30 ka. (A) Greenland ice core $\delta^{18}O$ record (Grootes and Stuiver, 1997). (B) ε_{Nd} record of western North Atlantic core GGC6 (Roberts et al., 2010). (C) ε_{Nd} records from South Atlantic cores RC11-83 (Piotrowski et al., 2004) and MD07-3076 (Skinner et al., 2013). (D-H) Fossil fish teeth and planktonic foraminifera ε_{Nd} data from the South Pacific (this study) reflecting water mass evolution during the last glacial-interglacial transition. Vertical error bars are propagated errors (SOM). (I) Deuterium temperature record of EPICA Dome C ice core on the AICC2012 timescale (Jouzel et al., 2007; Veres et al., 2013). (J) Opal fluxes from the APF (core TNO57-13PC) representing SO upwelling (Anderson et al., 2009). W1 and W2 (after Siani et al., 2013) represent warming episodes in the SH and roughly correspond to NH cold phases HS1 and Younger Dryas.

The deglacial deep water ε_{Nd} decrease during W1 (HS1) is a pervasive feature of SO deep waters (Fig. 3.2C, G, H) and has so far been associated with the resumption of NADW formation and incorporation of its unradiogenic ε_{Nd} into CDW (Piotrowski et al., 2004; Skinner et al., 2013; Lippold et al., 2016). Yet, this initial ε_{Nd} decrease in all but one available record from the SO occurred during W1/HS1 and hence predated NADW reinvigoration in the North Atlantic (e.g., Roberts et al., 2010) (Fig. 3.2B). A break-up of deep stratification and hence upward mixing of RSBW with an ε_{Nd} of -7 (Basak et al., 2015) into CDW can explain the ε_{Nd} change in the South Pacific. Core E11-2 exhibits a delayed response to W1. The effect of upward mixing of RSBW must have left the shallower depth of 3109 m at the core site unaffected and only once vertical mixing intensified later during W1, did the ε_{Nd} at this site decrease. Similarly, upward mixing of Weddell Sea Bottom Water (WSBW, ε_{Nd} = -9; Stichel et al., 2012) can account for the ε_{Nd} decrease to -6.5 to -7.5 in the deep South Atlantic (e.g., Piotrowski et al., 2004; Skinner et al., 2013). The ε_{Nd} decrease by 0.6 (1.1) in the South Pacific (South Atlantic) suggests a contribution of 45-50% (30-50%) RSBW (WSBW) to CDW (SOM). With the onset of SH warming, the decline of sea ice coverage (Gersonde et al., 2005), reduction in brine rejection (Adkins et al., 2002), and increase in meltwater input around Antarctica must have led to a decrease in salinity and density of RSBW and other AABW varieties. These property changes of RSBW are akin to modern observations of an AABW freshening and contraction over the recent decades, likely due to a reduction in sea ice formation, higher precipitation, and increased meltwater supply from the West Antarctic Ice Sheet (e.g., Shimada et al., 2012; Purkey and Johnson, 2013). A weakened density contrast between the deep and abyssal layers would have been conducive to vertical mixing and hence destratification at depth. Increasing ACC flow speed during the early deglacial (W1) (Lamy et al., 2015) would have enhanced the interaction with bottom topography, thereby further boosting deep vertical mixing (Nikurashin and Ferrari, 2013).

The halt in the deglacial ε_{Nd} decrease in the deep South Pacific during the ACR, that coincided with the time of NADW resumption (Fig. 3.2, 3.3), confirms the strong SH climate control on the deep water structure and ε_{Nd} signature. Ferrari et al. (2014) argued that Antarctic sea ice expansion and associated buoyancy fluxes during the LGM led to a shoaling of the boundary between the upper (northern-sourced water) and lower (southern-sourced water) overturning cells to <2000 m and hence above the depth of rough topography, resulting in reduced vertical mixing between the cells (Adkins, 2013; Ferrari et al., 2014). Similar, yet diminished, conditions would have marked the ACR, preventing NADW incorporation into the SO. With the onset of W2, mixing between the cells would have increased due to SH warming and sea ice retreat (Ferrari et al., 2014), leading to the final incorporation of NADW into CDW despite reduced NADW formation at this time (the Younger Dryas stadial; Roberts et al., 2010). That is, SH processes initialized the establishment of modern conditions with NADW being mixed into CDW, explaining the second ε_{Nd} decrease in the deep South Pacific.

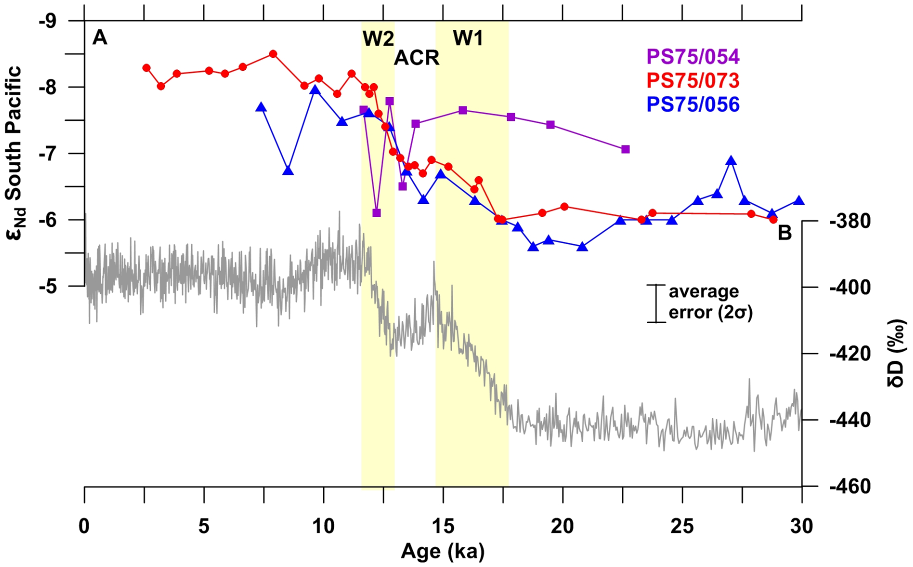

Figure 3.3: Comparison of Southern Ocean ε_{Nd} time series and Antarctic ice core record for the last 30 ka. (A) Downcore ε_{Nd} records from deep cores in the South Pacific. (B) Deuterium temperature record of EPICA Dome C ice core on the AICC2012 timescale (Jouzel et al., 2007; Veres et al., 2013).

In the modern South Pacific, the RSBW northward advection is restricted by the Pacific Antarctic ridge system. The delayed ε_{Nd} decrease in core PS75/059 is due to its northerly location along the western flank of the Pacific-Antarctic Ridge, which left it outside the influence of RSBW during the early deglaciation through bathymetric isolation (Figs. 3.1, 3.4). Alternative plausible mechanisms could be 1) increased non-radiogenic NPDW convection during HS1 (Rae et al., 2014), offsetting the increased radiogenic influence from RSBW, or 2) a southward shift of the Antarctic Polar Front (APF) (Gersonde et al., 2005) and the Subantarctic Front (SAF) in the Southeast Pacific (Ho et al., 2012; Lamy et al., 2015), leading to the observed isolation of this core from the early deglacial RSBW admixture (Fig. 3.4). As deglaciation progressed, NADW was incorporated into the SO and modified the ε_{Nd} of CDW, eventually reflected as decreasing ε_{Nd} at PS75/059. Similarly, recent evidence from a South Atlantic core also exhibits a delayed change in deep water Nd isotopes during the late ACR (Lippold et al., 2016) that was also interpreted in terms of a late NADW incorporation into SO deep waters, as discussed above for our other records.

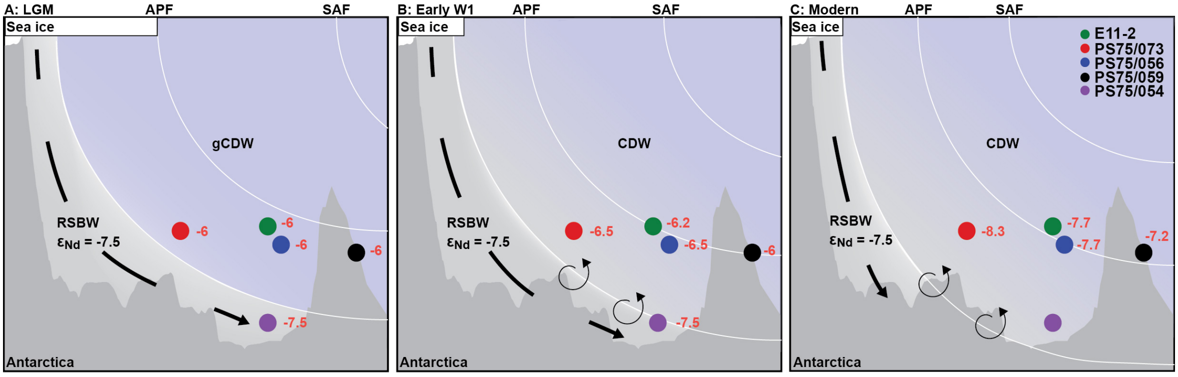

Figure 3.4: Schematic illustration of the South Pacific water column structure for the LGM, deglaciation, and Holocene. (A) LGM: NADW input to SO strongly reduced/absent. RSBW (ε_{Nd} = -7.5) extends further north than today and is isolated from overlying deep water (ε_{Nd} = -6). (B) Early deglacial: SO warming during W1 leads to destratification at depth and increased mixing of RSBW into CDW, changing the CDW ε_{Nd} to ~ -6.5; Atlantic contribution is still attenuated. Core PS75/059 is isolated from early deglacial SO processes. (C) Holocene and modern: AMOC strengthening and SO warming lead to incorporation of NADW into CDW (Ferrari et al., 2014), changing its ε_{Nd} signature to -8. All cores influenced by CDW, RSBW does not extend to deepest site (PS75/054).

Although a high density contrast between deep and abyssal waters has been suggested based on porewater chloride measurements (Adkins et al., 2002), clear evidence of deep stratification in the SO has been elusive. Our results show that RSBW expanded during the LGM, occupying the abyssal South Pacific to at least ~4000 m water depth, and was sharply separated from overlying deep water. This suggests increased formation of very high-density bottom water, most likely through enhanced brine rejection during glacial climates. This facilitated enhanced carbon sequestration and worked towards stabilizing the glacial stratification. Following deglaciation, timing of the first pulse of SH warming is well synchronized with the timing of deep-abyssal destratification and wind driven upwelling in the SO (Anderson et al., 2009) (Fig. 3.2). However, wind forcing only leads to upwelling of deep water from <2000 m w.d. (Toggweiler and Samuels, 1998; Ferrari, 2014), thus, vertical mixing at depth is warranted to break the deep-abyssal stratification in the deglacial SO. The abyssal and deep SO waters, which are considered to be the treasure trove of sequestered carbon during the glacial, mixed into upper deep layers via vertical mixing through mechanisms discussed above (Fig. 3.4), and were eventually pulled to intermediate and surface depths by wind action (Anderson et al., 2009). That is, two mechanisms (deep vertical mixing and wind-driven upwelling), both driven by climate changes in the SH, were instrumental in the release of accumulated carbon from the deep and abyssal SO to the atmosphere during termination 1.

3.2. Acknowledgements

Data presented in this study are available in the SOM and on Pangaea (www.pangaea.de) under DOI: http://doi.pangaea.de/10.1594/PANGAEA.858969. We thank the scientific party, captain, and crew of R/V Polarstern cruise ANT-XXVI/2 and the German Ministry for Education and Research (BMBF) for financially supporting the cruise. We thank M. Schulz and P. Böning from the Max Planck Research Group for Marine Isotope Geochemistry for help with labwork. We are grateful to J. Ullermann (Alfred Wegener Institute) for measuring benthic $\delta^{18}O$ data that we used for age model construction of cores PS75/059 and PS75/056. Financial support for this study came from the National Science Foundation (NSF) under grant OCE-09-35115 to KP, the Institute for Chemistry and Biology of the Marine Environment (ICBM) and the Max Planck Institute for Marine Microbiology.

3.3. Supplementary Material

3.3.1. Material and Methods

3.3.1.1. Sample material and processing

The majority of the cores (PS75/073-2, PS75/059-2, PS75/056-1, PS75/054-1) used in this study were recovered during *RV Polarstern* cruise ANT-XXVI/2 in the South Pacific Ocean in November 2009-January 2010 (Gersonde, 2011). Bulk sediment samples from core E11-2 were obtained from a pre-sampled archive at Lamont Doherty Earth Observatory of Columbia University. Polarstern samples were washed and size-fractionated at the Alfred Wegener Institute Bremerhaven. All following sample processing was done at the University of Oldenburg. Sediment samples were freeze dried and wet sieved to obtain the >63 µm fraction. From the >125 µm and >250 µm fractions, fish teeth and broken fish bones (hereafter called ‘fish debris’) and foraminifera, respectively, were picked for Nd isotope analyses.

Fish debris were picked from cores PS75/054-1, PS75/056-1, PS75/059-2 and PS75/073-2 and were cleaned in multiple steps, involving ultrasonication in optima grade methanol and MilliQ water (Millipore, 18 MΩ). The samples were then treated with a 1:1 solution of H_2O_2 (30%) and MilliQ, followed by dissolution in a 1:1 mixture of HNO_3 and HCl and drydown under a laminar flow hood. The samples were finally re-dissolved in 0.5 mL of 1 N HNO_3 in preparation for column chemistry.

Mixed species of planktonic foraminifera (>250 µm fraction) were picked from cores PS75/054-1, PS75/059-2, PS75/073-2 and E11-2. Foraminifera picked from cores PS75/054-1 and E11-2 were subjected to physical cleaning only, according to published protocols for ‘unclean foraminifera’ (e.g., Roberts et al., 2010; Tachikawa et al., 2014). Cleaning comprised multiple rinses and sonication in optima grade methanol, followed by multiple rinses in deionized water. Following this step, foraminifera were crushed with glass slides to break open the inner chamber before repeating the sonication and rinse steps. The cleaned broken foraminifera fragments were examined under a microscope to ensure that no clay fragments were left in the sample. Cleaned crushed foraminifera were dried and dissolved in <10% acetic acid for 5-10 min. The dissolved solution was centrifuged and the supernatant was dried down and re-dissolved in 1 N HNO_3. Cores PS75/059-2 and PS75/073-2 contained highly fragile foraminifera tests, which were cleaned using a slightly modified cleaning and dissolution protocol of that published by Tachikawa et al. (2014). About 30 mg of uncrushed foraminifera were transferred to a 15 mL centrifuge tube containing 500 µL of ultrapure water and 800-1000 µL of 1 M acetic acid was added at 100-200 µL increments to slowly dissolve the foraminifera. The dissolution process was stopped before the entire sample went into solution in order to minimize the potential of attacking lithogenic particles. This resulted in a residue consisting of chamber fragments and lithogenic particles. The solution-particle mixture was centrifuged at 5000 rpm for 10 min, the supernatant transferred to a 1.5 mL centrifuge tube and centrifuged again at 1000 rpm for 10 min. The final supernatant was transferred to a clean Teflon beaker, dried and transferred to nitric form by drying in concentrated HNO_3 followed by 1 N HNO_3.

We digested the lithogenic particles in order to monitor the Nd isotope signature of these potential contaminating phases that might be attacked during dissolution of foraminiferal calcite. The particle residue was transferred to a clean Teflon beaker and digested using HNO_3, HCl and HF at 100-150˚C. The final solution was dried and transferred to nitric form by drying in 1 N HNO_3.

3.3.1.2. Column chemistry and isotope measurements

In preparation for isotope measurements, Nd from all archives was isolated and purified by two-step column chemistry following established methods (Pin and Zaduegui, 1997). Briefly, rare earth elements (REE) were separated from major cations using Eichrom TRU-Spec resin (particle size 100-150 µm) and Nd was purified from other REE using Eichrom or TrisKem LN-Spec resin (particle size 50-100 µm) and 0.23-0.25 N HCl as eluent. The Nd fraction was completely dried and treated with a 1:1 mixture of H_2O_2 (30%) and concentrated HNO_3 to ensure breakdown of any organic compounds that may have leaked during column chemistry. The samples were finally brought up in 2% HNO_3

for isotope analysis using a ThermoScientific *Neptune Plus* multi-collector inductively coupled plasma mass-spectrometer (MC-ICP-MS) at the University of Oldenburg.

All samples were aspirated into the MC-ICP-MS using a 100 µl nebulizer via a Cetac *Aridus II* desolvating unit. Nitrogen was used in the desolvating unit in order to stabilize the signal and minimize oxide formation. Preamplifier gains were performed at the beginning of each measurement session. Nd isotope data were acquired in static mode with 4 sec integration time over 4 blocks of 12 cycles each. All measured ^{143}Nd/^{144}Nd ratios were corrected for mass bias using an exponential law and a ^{146}Nd/^{144}Nd natural ratio of 0.7219 (O'Nions et al., 1977). In general, the international standard JNdi-1 was analyzed every 3 samples and all reported ^{143}Nd/^{144}Nd ratios were normalized to a JNdi-1 value of 0.512115 (Tanaka et al., 2000) using the mean ^{143}Nd/^{144}Nd of the JNdi-1 measurements of each analytical session. Standards analyzed in the course of the study were always concentration-matched with the samples. The external reproducibility was separately calculated for each session using the analyses of JNdi-1 and was generally better than ±0.3 ε_{Nd} units (2σ). Propagated errors are reported from combined external reproducibility of the measuring session and individual sample error (internal run error, 2σ) (Tab. S3.1). The procedural blank was ≤13 pg Nd (n=22).

3.3.1.3. Age models

The age models of our cores were established by tuning their benthic or planktonic δ^{18}O records to those of high-resolution core MD97-2120 from Chatham Rise in the Southwest Pacific (Pahnke et al., 2003; Pahnke and Zahn, 2005). In order to account for updated ^{14}C-calendar age calibrations (Reimer et al., 2013), reservoir ages (560 ± 40 years (Holocene), 1970 ± 390 years (late glacial, ~28.7 ka), Sikes et al., 2000; Rose et al., 2010), the age of the Kawakawa ash (Vandergoes et al., 2013), and additional ^{14}C ages (Rose et al., 2010), we revised the age scale of core MD97-2120 (Tab. S3.4, Fig. S3.1). Age models of the investigated cores (except PS75/054-1) were created by graphical correlation of benthic δ^{18}O (PS75/056-1, PS75/059-2, E11-2) and planktonic δ^{18}O (PS75/073-2) to reference core MD97-2120 on its updated age scale using the software AnalySeries 2.0.8 (Paillard et al., 1996). The resulting age models of our cores and the updated age model of reference core MD97-2120 are summarized in Table S3.4 and Figure S3.1 and are described in detail in the following.

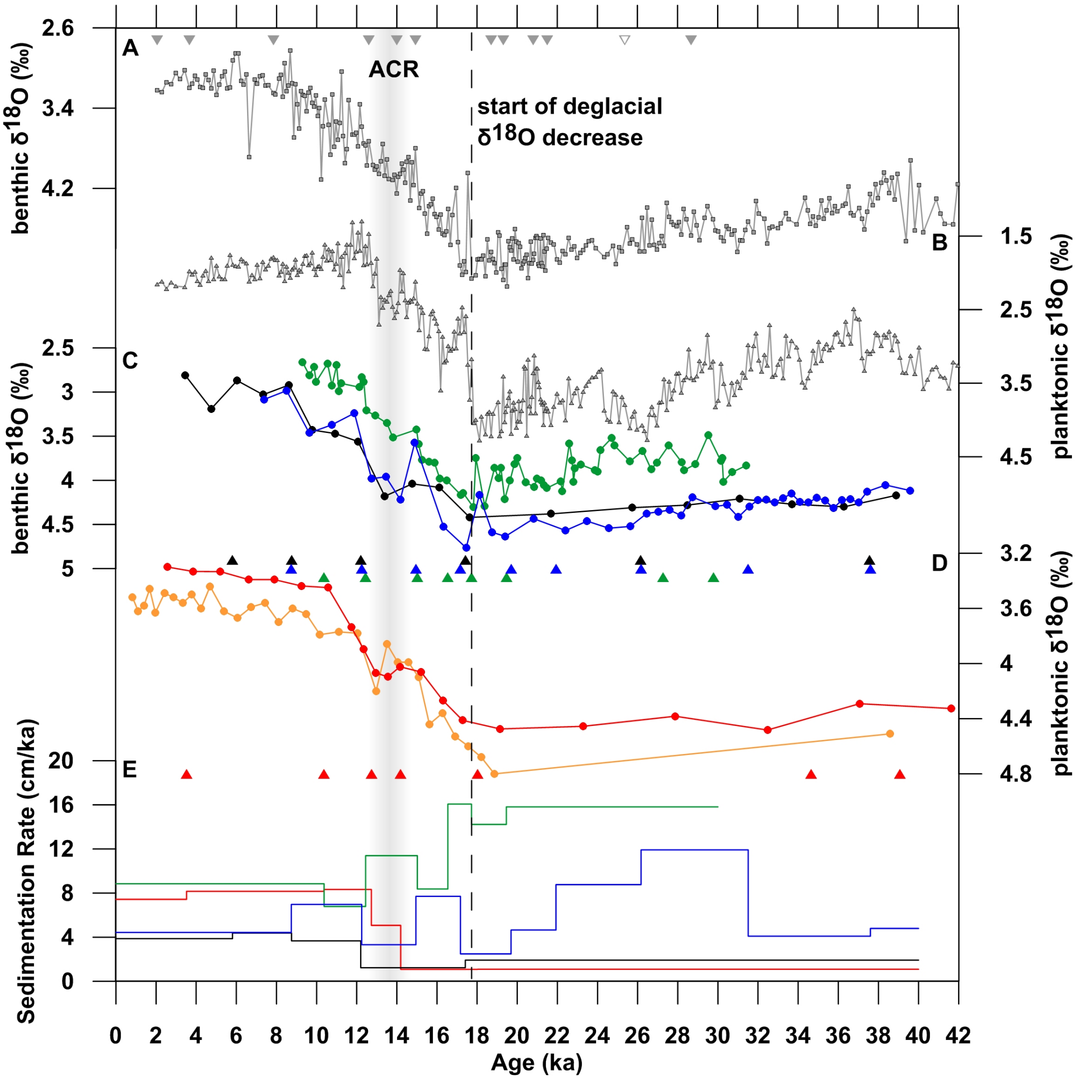

Figure S3.1: Age model of investigated cores and reference core MD97-2120. A) Benthic $\delta^{18}O$ (Pahnke and Zahn, 2005) and B) planktonic $\delta^{18}O$ (Pahnke et al., 2003) of core MD97-2120 on the updated age scale. Grey filled triangles indicate ^{14}C based tie points, open triangle indicates the Kawakawa Tephra tie point. C) Benthic $\delta^{18}O$ of cores PS75/056-1 (blue), PS75/059-2 (black) and E11-2 (green) aligned to MD97-2120. Benthic $\delta^{18}O$ of cores PS75/056-1 and PS75/059-2 have been previously published in Lamy et al. (2014). Data from E11-2 are from Ninnemann and Charles (2002). Triangles mark age tie points. D) Planktonic $\delta^{18}O$ of core PS75/073-2 (red; Benz, 2016) aligned to MD97-2120 together with planktonic $\delta^{18}O$ of nearby core PS75/072-4 (orange; Studer et al., 2015). Red triangles are age tie points. E) Resulting sedimentation rates (colors as in C and D).

The age model of core PS75/056-1 is based on the correlation of the benthic $\delta^{18}O$ isotope record (measured on *Cibicidoices kullenbergi*, published in Lamy et al. (2014)) to benthic $\delta^{18}O$ of core MD97-2120 (Pahnke and Zahn, 2005). The age model is based on seven age tie points within the upper 100 cm, which corresponds to ages of <30 ka. Resulting sedimentation rates range from 2 to 12 cm/ka.

The age model for core PS75/059-2 was created by correlation of benthic $\delta^{18}O$ (measured on *C. kullenbergi,* published in Lamy et al. (2014)) to those of MD97-2120 (Pahnke and Zahn, 2005). This age model is based on six age tie points and results in sedimentation rates of 1 to 4 cm/ka. The deglacial decrease in δ^{18}O is in good agreement with that of PS75/056-1. Good correlation of XRF Sr and Fe data from PS75/059-2 with those of MD97-2120 suggest that the age model is robust. Further, our age model is in good agreement with a recently published age model that is based on XRF tuning (Ronge et al., 2016).

The age model of core PS75/073-2 is based on correlation of planktonic δ^{18}O (measured on *N. pachyderma* sin. (Benz, 2016)) to planktonic (*G. bulloides)* δ^{18}O of core MD97-2120 (Pahnke et al., 2003). The resulting sedimentation rates range between 1 and 8 cm/ka. This age model is in good agreement with that of a recently published age model of nearby core (PS75/072-4), that is based on radiocarbon ages and correlation of planktonic δ^{18}O to the EDC ice core deuterium record (Studer et al., 2015). Further, these authors report similar sedimentations rates (~0.2 to 9.5 cm/ka) as we observe for core PS75/073-2 for the studied interval.

In order to maintain consistency, a new age model for core E11-2 was created based on correlation of the benthic δ^{18}O record (Ninnemann and Charles, 2002) to that of core MD97-2120 (Pahnke and Zahn, 2005). Sedimentation rates derived from this age model range between 6 and 16 cm/ka. The age model shows good agreement with the age model of nearby core PS75/056-1. When compared to the published age model by Ninnemann and Charles (2002), all intervals exhibit age differences of <1 ka, which has no bearing on the overall conclusions of this study.

The age model of core PS75/054-1 is directly linked to that of core PS75/056-1 through correlation of XRF core scanner Sr and Fe data. It is created using four Fe-based age tie points accompanied by two Sr-based age tie points, which results in sedimentation rates of 4 to 9 cm/ka (Fig. S3.2). We chose to correlate Sr and Fe data of core PS75/054-1 to PS75/056-1 instead of MD97-2120 to account for potential differences in dust supply to the Southeast and Southwest Pacific, which is known to affect these elements.

Overall, the age models for the cores (except PS75/054-1) are independently derived. The age models of cores PS75/059-2, PS75/073-2, and E11-2 match those of previously published age models of cores PS75/059-2 (Ronge et al., 2016), PS75/074-2 (Studer et al., 2015) and E11-2 (Ninnemann and Charles, 2002). Thus, the age scales provide accurate relative ages between cores and the best achievable absolute ages.

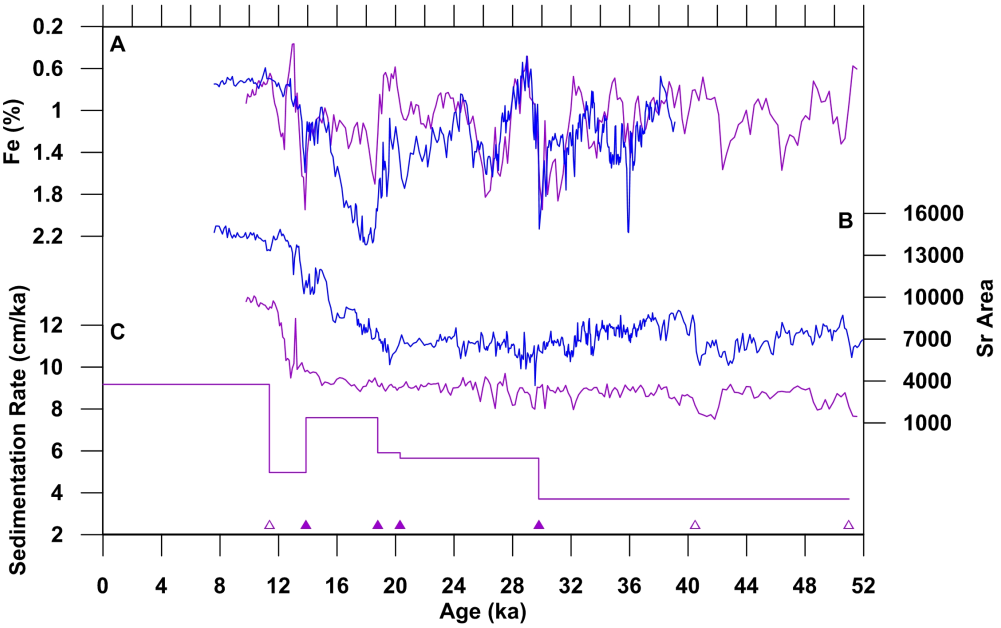

Figure S3.2: Age model of core PS75/054-1 (purple) aligned to core PS75/056-1 (blue). A) Fe data and B) Sr data from XRF core scanner (Alfred Wegener Institute, Bremerhaven). C) Resulting sedimentation rate. Age tie points indicated by filled (Fe) and open (Sr) triangles.

3.3.2. Supplementary text

3.3.2.1. Hydrography and core locations

The Southern Ocean is dominated by the eastward flowing Antarctic Circumpolar Current (ACC) and the circum-Antarctic frontal system with the Subantarctic Front (SAF) to the north, the Southern AAC Front to the south, and the Antarctic Polar Front (APF) in between (e.g., Orsi, 1995). Deep water that upwells south of the APF feeds both Antarctic Bottom Water (AABW) close the Antarctic continent and Antarctic Intermediate and Mode Water formation north of the APF (e.g., Sloyan and Rintoul, 2001a; Talley et al., 2013). In the South Pacific, the overall location of the SAF and the APF varies by ~ 5°, with a more northward position in the west and southward in the east (Orsi, 1995; Fig. 3.1). The Southern Ocean's major water mass, the Circumpolar Deep Water (CDW), is subdivided into an upper and lower branch. Lower CDW (LCDW) is identified by a salinity maximum that is inherited from North Atlantic Deep Water (NADW) (Reid and Lynn, 1971; Orsi, 1995). Upper CDW (UCDW) is typically identified as an oxygen minimum layer, which is derived from oxygen-depleted, nutrient-rich Indian Deep Water (IDW) and North Pacific Deep Water (NPDW) (Callahan, 1972). Lower CDW and UCDW are transported into the North Pacific, where they are transformed to NPDW and return to the Southern Ocean in the East Pacific along the South American continent at 1500-3500 m water depth (Kawabe and Fujio, 2010). North of the SAF, UCDW is centered at approximately 1500 m depth and LCDW covers depths below 2000 m.

Core PS75/073 (3234 m) from the central/southwest Pacific is bathed today by LCDW and located below the modern APF. By virtue of its location in the center of the ACC (Fig. 3.1), this core offers the ideal opportunity to study the evolution of pure CDW over the last deglaciation. Southeast Pacific cores PS75/056-1, PS75/059-2, E11-2, and PS75/054-1 are all located north of the modern SAF i.e., north of the ACC core. Currently, cores PS75/056-1 (3581 m) and E11-2 (3109) are bathed by LCDW, but are located close to the LCDW/UCDW boundary with some influence of low-oxygen UCDW (Fig. 3.1). Thus, these two cores are best fitted to monitor past changes in the mixing proportions between LCDW and UCDW. Based on salinity values, core PS75/059-2 (3613 m) also represents LCDW, but it is separated from the other cores by the East-Pacific Rise (EPR) and has significant influence of low-oxygen NPDW (Fig. 3.1). Below LCDW, northward spreading dense AABW that is formed in the Weddell Sea, Ross Sea, and along the Adélie Coast, covers the abyss around Antarctica. In the South Pacific, the expansion of Ross Sea Bottom Water (RSBW), the coldest and saltiest variety of AABW, is restricted by bottom topography to areas south of the Pacific-Antarctic Ridge system (Orsi, 1999). Mixture of RSWB with overlying LCDW leads to erosion of the typical hydrographic properties along its flowpath towards the southeast Pacific (Orsi, 1999), which is also seen in the ε_{Nd} signatures (e.g., Basak et al., 2015). Core PS75/054-1 (4085 m) is located at the deeper limit of LCDW, close to the LCDW/RSBW boundary (Fig. 3.1). Its proximity to the LCDW/RSBW boundary is ideal to investigate past changes in RSBW. Together, the southeast Pacific cores (E11-2, PS75/056-1, PS75/054-1) define an approximate meridional depth transect that can track the evolution of the water mass structure in the Southern Ocean during the last deglaciation.

3.3.2.2. Neodymium isotopes as a water mass tracer

The neodymium isotope composition ($^{143}Nd/^{144}Nd$) is expressed in the ε_{Nd} notation and defined as $\varepsilon_{Nd} = [(^{143}Nd/^{144}Nd)_{sample}/(^{143}Nd/^{144}Nd)_{CHUR} -1]*10{,}000$ where CHUR is the Chondritic Uniform Reservoir with $^{143}Nd/^{144}Nd = 0.512638$ (Jacobsen and Wasserburg, 1980). The heterogeneous distribution of ε_{Nd} on the continents (e.g., Jeandel et al., 2007) is imprinted to seawater by transport of Nd from the continents to the ocean through rivers, dust and interaction with margin sediments known as ‘boundary exchange’. Together with the short residence time of Nd in the ocean of 300-1000 years (Tachikawa et al., 2003; Arsouze et al., 2009; Rempfer et al., 2011), seawater ε_{Nd} allows the tracing of water masses back to their source region (Frank, 2002; Goldstein and Hemming, 2003; Lacan and Jeandel, 2001; 2005a).

In the modern ocean, NADW has an ε_{Nd} signature of -13.5 (Piepgras and Wasserburg, 1987: Lacan and Jeandel, 2005b), whereas NPDW is more radiogenic with an ε_{Nd} signature of -3 to -5 (Piepgras and Jacobsen, 1988; Amakawa et al., 2009). Circumpolar Deep Water as a mixture of NADW and NPDW has intermediate values (ε_{Nd} = -8 to -9; Carter et al., 2012; Basak et al., 2015; Stichel et al., 2012b). Deep waters formed around Antarctica carry a distinct ε_{Nd} signal depending on the formation region, ranging from ε_{Nd} = -7 in the Pacific sector (RSBW; Carter et al., 2012; Rickli et al., 2014; Basak et al., 2015) to -9 in the Atlantic of the Southern Ocean (Stichel et al., 2012b). In the South Pacific, the main water masses carry distinct seawater ε_{Nd} signatures (e.g., NPDW, CDW, RSBW; Carter et al., 2012; Molina-Kescher et al., 2014a; Rickli et al., 2014; Basak et al., 2015). Thus, Nd isotopes are an ideal proxy to study the paleo-water column structure in the South Pacific.

Fish teeth and Fe-Mn oxide coatings on foraminifera and sediment particles capture the bottom water ε_{Nd} signature at the sediment water interface and do not lose that signal during subsequent burial in the sediment column (e.g., Martin and Haley, 2000; Martin et al., 2010; Roberts et al., 2010). These archives have been effectively used to extract pristine paleo bottom water signatures and used as a proxy to trace water masses in past oceans (e.g., Piotrowski et al., 2004; Roberts et al., 2010; Pahnke et al., 2008).

3.3.2.3. Testing fidelity of sedimentary archives and Nd isotope proxy in the South Pacific

One pre-requisite to interpret ε_{Nd} changes in relation to water mass mixing and ocean circulation changes is to establish the fidelity of sedimentary archive-derived core-top ε_{Nd} values in reflecting overlying bottom waters. The ε_{Nd} values from the core-tops in the South Pacific region show excellent agreement with those of overlying and/or nearby published bottom water (Fig. S3.3). Recent studies using dissolved Nd isotopes indicate potential influence of NPDW to the isotope composition of deep waters in the southeast Pacific (Basak et al., 2015; Molina-Kescher et al., 2014a). Thus, we interpret paleo ε_{Nd} signatures of the southeast Pacific (cores PS75/056, PS75/059, E11-2) in the context of admixture of NPDW and South Pacific CDW. Core PS75/073-2 is situated along the western flank of the Pacific-Antarctic Ridge. The core-top ε_{Nd} signature of -8.3 matches the nearest deep water representing CDW (Fig. S3.3; Basak et al., 2015). We thus consider this core as a representative of pure CDW composition in the South Pacific, removed from direct influence of NPDW.

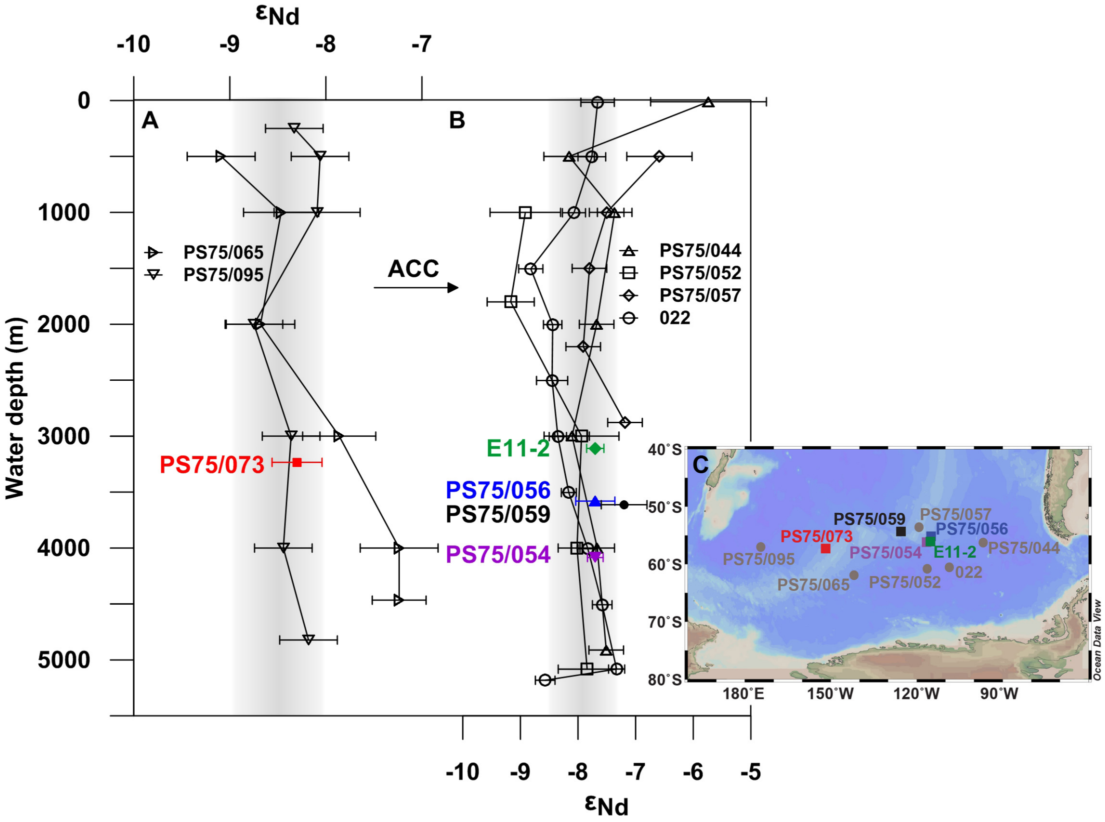

Figure S3.3: Comparison of sedimentary core-top ε_{Nd} signatures with water column profiles (black open symbols, Basak et al., 2015; Carter et al., 2012) from A) the Western/Central and B) the Eastern Pacific sector of the Southern Ocean. Grey bars indicate range of ε_{Nd} for CDW. Bottom waters at site PS75/065 are influenced by RSBW (Basak et al., 2015). Arrow indicates general flow direction of the ACC, which becomes progressively more radiogenic from west to east, as expressed by increasing ε_{Nd} values of CDW. Seawater ε_{Nd} profiles from stations PS75/044, PS75/052, PS75/057, PS75/065, and PS75/095 from Basak et al. (2015), data of station 022 from Carter et al. (2012). C) Locations of sediment cores (colored) and seawater stations (grey) used in A) and B). Map created with Ocean Data View (Schlitzer, 2014).

Neodymium isotope values of contemporaneous fossil fish teeth and debris have been demonstrated to be identical (Thomas and Via, 2007; Martin et al., 2010). Here, separate analyses of contemporaneous fossil fish teeth and fish debris from one interval in core PS75/073-2 show that these two archives record the same ε_{Nd} values within analytical uncertainty, confirming the previous results (Tab. S3.2). In order to check the reproducibility between fossil fish teeth within a single sample, two samples with abundant teeth material were divided into sub-samples and consequently analyzed for Nd isotopes. The Nd isotope results of the subsamples are in agreement within analytical uncertainty (Tab. S3.2).

Mixed species of planktonic foraminifera were analyzed in samples and/or cores where fish debris was absent or revealed high measurement errors as a result of low availability and subsequent low Nd concentrations. To establish reliability of our foraminifera based ε_{Nd} results, a few of these analyses have been underpinned by fossil fish debris values during the course of this study (Tab. S3.1). Foraminifera ε_{Nd} vs. fish teeth/debris ε_{Nd} from the same sample show agreement within analytical error and closely follow a 1:1 line independent of the applied cleaning protocol (Tab. S3.2, Fig. S3.4A). Further, true replicates of uncleaned foraminifera reveal ε_{Nd} values within error, demonstrating the reproducibility of the analysis (Tab. S3.2). Based on our results, it is reasonable to assume that ε_{Nd} derived from fossil fish debris and Fe-Mn oxide coatings on foraminifera both record past bottom water ε_{Nd} in the South Pacific.

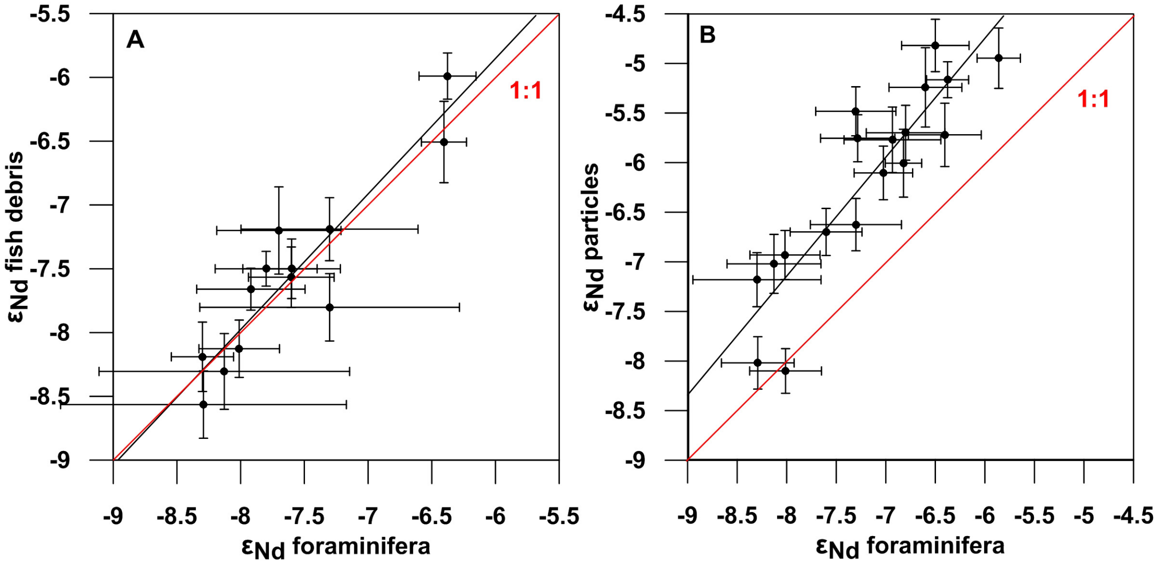

Figure S3.4: ε_{Nd} values derived from foraminifera, fossil fish debris, and total digested silicate particles plotted in ε_{Nd}-ε_{Nd} space. A) Fish debris ε_{Nd} vs. foraminifera ε_{Nd} fall close to the ideal 1:1 line indicating fish debris and foraminifera archives can be used interchangeably. B) Total digested silicate particle ε_{Nd} vs. foraminifera ε_{Nd} exhibit a systematic offset of 1-2 epsilon units towards more radiogenic values in particles. The silicate particles used in these analyses were collected from inside the foraminifera tests collected during crushing and cleaning procedures. Detailed data presented in Tables S3.2 and S3.3.

Leftover clay and/or lithogenic particles in foraminifera chambers are considered as one of the main sources of contamination when using a foraminiferal archive for ε_{Nd} studies (e.g., Elmore et al., 2011). To test the extent of contamination from these clay particles in samples that were not physically cleaned, we measured the ε_{Nd} composition of the residual particles following dissolution of the samples (Tab. S3.3). Compositionally, these residual particles are a mixture of lithogenic particles and some undissolved foraminiferal calcite. The ε_{Nd} signatures in these residual particles are in general more radiogenic and constantly offset by ~1-2 ε_{Nd} units compared to the corresponding foraminifera and fish teeth (Fig. S3.4B, Tabs. S3.2, S3.3). Given this constant offset and the consistency between fish teeth and foraminifera ε_{Nd} we rule out contaminating influence of lithogenic material on uncleaned foraminifera for the study area in the South

Pacific. Based on our results and on what has been previously reported for directly dissolved foraminifera (Charbonnier et al., 2012), we suggest that physical cleaning of foraminifera can be avoided when incremental dissolution of foraminifera is applied; this is at least true for our study region in the South Pacific, however, this approach should be tested on a regional basis.

3.3.2.4. Mixing calculations

We performed simple mixing calculations of glacial CDW and glacial AABW for cores PS75/056-1 and PS75/073-2. The results show that it is possible to explain the ~0.6 ε_{Nd} decrease during the early deglacial warming phase in the Southern Ocean (W1) by mixing of RSBW with overlying CDW. Applying our calculation to South Atlantic cores support this observation. The mixed ε_{Nd} and [Nd] signals (εNd_{mix} and $[Nd]_{mix}$) are calculated as given in equations 3.1 and 3.2 with $\varepsilon Nd_{CDW,AABW}$ and $[Nd]_{CDW,AABW}$ being the isotope signatures and concentrations in the two water masses and *f* being the fraction of water mass 1. A detailed description is given in the following.

$$\varepsilon \mathrm{Nd}_{\mathrm{mix}} = \frac{(\varepsilon \mathrm{Nd}_{CDW} \cdot [\mathrm{Nd}]_{CDW} \cdot f) + (\varepsilon \mathrm{Nd}_{AABW} \cdot [\mathrm{Nd}]_{AABW} \cdot (f-1))}{([Nd]_{CDW} \cdot f) + ([Nd]_{AABW} \cdot (f-1))} \tag{3.1}$$

$$[\mathrm{Nd}]_{\mathrm{mix}} = ([\mathrm{Nd}]_{\mathrm{CDW}} \cdot f) + ([\mathrm{Nd}]_{\mathrm{AABW}} \cdot (f-1)) \tag{3.2}$$

First, the ε_{Nd} composition and Nd concentration of glacial CDW are calculated based on conservative mixing of the endmembers of NADW and NPDW using their modern ε_{Nd} and [Nd] given as $\varepsilon Nd_{NADW} = -13.5$, $[Nd]_{NADW} = 17.5$ pmol/kg (Piepgras and Wasserburg, 1987) and $\varepsilon Nd_{NPDW} = -3.8$, $[Nd]_{NPDW} = 51.7$ (Piepgras and Jacobsen, 1988), respectively. Based on Nd isotope data presented in this study, we calculated a 25% lower NADW contribution to CDW during the LGM compared to today, in line with previous calculations from the South Atlantic and the Drake Passage (Piotrowski et al., 2004; Robinson and van de Flierdt, 2009). We assume stable endmember ε_{Nd} of NADW and NPDW based on studies by Foster et al. (2007), van de Flierdt et al. (2006), and Marchitto et al. (2005), although a changing NADW endmember during climate change events has also been reported (Wilson et al., 2014; Böhm et al., 2015; Roberts and Piotrowski, 2015). Further, we assume no change in the Nd concentration based on a model study from the North Atlantic (Foster and Vance, 2006). These authors concluded that decreased chemical weathering from the surrounding continental crust during the glacials is balanced by the exposure of more continental crust due to lower sea level, keeping the oceanic cation inventory constant between glacials and interglacials.

Second, we calculate the admixture of AABW (which for the South Pacific equals RSBW) into CDW for which we use the modern endmember concentration of RSBW (28 pmol/kg; Basak et al., 2015) and the average glacial CDW (gCDW) isotope signature and concentration from the mixing calculation above (εNd_{gCDW} = -6, $[Nd]_{gCDW}$ = 36 pmol/kg). The isotope composition of glacial AABW (RSBW in the Pacific) is represented by ε_{Nd} = -7.4 derived from core PS75/054-1 and is similar to the modern RSBW signature (Basak et al., 2015). In cores PS75/073-2 and PS75/056-1, ε_{Nd} decreases by 0.6 units from the average glacial to early deglacial values. Based on individual calculations for the two cores we observe that an increase of 40-50% in the volume of AABW in CDW is needed to produce the isotope shift during early W1. Less radiogenic values in the late deglaciation and the Holocene are governed by intensified NADW admixture to CDW. When calculating the mixing of glacial WSBW (Weddell Sea Bottom Water) (using modern values of ε_{Nd} = -9 and [Nd] = 26 pmol/kg, Stichel et al., 2012b) into CDW for South Atlantic core MD07-3076 (Skinner et al., 2013) and Cape Basin core RC11-83 (Piotrowski et al., 2004; 2012), a similar admixture of 30-50% WSBW into CDW can account for the observed early deglacial ε_{Nd} shift of ~-1.1. This confirms that the admixture of AABW into CDW has the potential to produce the observed early deglacial ε_{Nd} shift in both the South Pacific and the South Atlantic.

To test the sensitivity of the mass balance calculation, we varied the concentration by decreasing or increasing [Nd] in AABW and CDW by 10%. We decided to test the sensitivity with respect to changing Nd concentration, because we have the least constraint on the Nd concentration of different water masses in the past. The amount of AABW needed to produce a change of 0.6 ε_{Nd} units (given by the average change in ε_{Nd} between 19-14 ka) in Southeast Pacific CDW varies between ~45% and ~55%. The highest amount of AABW (55%) is needed when the concentration in glacial AABW is lowered by 10% compared to modern values while the concentration in glacial CDW is enhanced by 10%. On the other hand, a 10% higher concentration in AABW compared to modern and corresponding 10% lower CDW concentration gives the lowest amount of AABW needed (45%). Since concentration changes have only minor influence on the resulting calculations, we used the conservative mixture derived values for the calculation of the AABW fraction in our cores.

3.3.3. Supplementary data tables

Table S3.1: Core information and composite ε_{Nd} records of all cores from this study.

Sample interval (cm)	Age (ka)	Material	Normalized $^{143}Nd/^{144}Nd$ [a]	ε_{Nd}	± Internal ε_{Nd} error (2σ SE)	± External ε_{Nd} error (2σ SD)	± Propagated error
E11-2-1, 56˚S, 115˚W, 3109 m							
21-22	9.13	foraminifera	0.512243	-7.7	0.08	0.13	0.15
26-27	9.70	foraminifera	0.512241	-7.7	0.14	0.13	0.19
41-42	11.39	foraminifera	0.512242	-7.7	0.02	0.13	0.13
43-44	11.62	foraminifera	0.512252	-7.5	0.12	0.13	0.18
44-45	11.73	foraminifera	0.512250	-7.6	0.17	0.22	0.28
53-54	12.84	foraminifera	0.512267	-7.2	0.07	0.13	0.15
60-61	13.88	foraminifera	0.512271	-7.2	0.22	0.13	0.26
72-73	15.39	foraminifera	0.512320	-6.2	0.20	0.24	0.31
74-75	15.57	foraminifera	0.512339	-5.8	0.09	0.23	0.25
76-77	15.74	foraminifera	0.512319	-6.2	0.16	0.23	0.28
83-84	16.36	foraminifera	0.512341	-5.8	0.08	0.13	0.15
84-85	16.45	foraminifera	0.512341	-5.8	0.15	0.13	0.20
85-86	16.53	foraminifera	0.512335	-5.9	0.22	0.13	0.26
86-87	16.65	foraminifera	0.512347	-5.7	0.12	0.22	0.25
93-94	17.49	foraminifera	0.512339	-5.8	0.19	0.22	0.29
103-104	18.22	foraminifera	0.512332	-6.0	0.11	0.22	0.25
137-138	20.45	foraminifera	0.512326	-6.1	0.12	0.22	0.25
144-145	20.94	foraminifera	0.512332	-6.0	0.11	0.22	0.25
145-146	21.01	foraminifera	0.512322	-6.2	0.15	0.22	0.27
146-147	21.08	foraminifera	0.512327	-6.1	0.11	0.22	0.25
152-153	21.51	foraminifera	0.512329	-6.0	0.17	0.22	0.28
155-156	21.72	foraminifera	0.512326	-6.1	0.21	0.22	0.30
156-157	21.79	foraminifera	0.512328	-6.0	0.07	0.22	0.23
157-158	21.86	foraminifera	0.512325	-6.1	0.16	0.22	0.27
164-165	22.35	foraminifera	0.512313	-6.3	0.16	0.22	0.27
165-166	22.42	foraminifera	0.512317	-6.3	0.02	0.22	0.22
176-177	23.19	foraminifera	0.512322	-6.2	0.08	0.22	0.23
195-196	24.53	foraminifera	0.512304	-6.5	0.10	0.22	0.24
PS75/073-2, 57˚12.27’S, 151˚36.63’W, 3234 m							
3-4	2.58	foraminifera	0.512213	-8.3	0.16	0.21	0.26
7.5-8.5	3.18	foraminifera	0.512227	-8.0	0.08	0.21	0.22
12.5-13.5	3.86	fish teeth/debris	0.512215	-8.3	0.06	0.31	0.32
22.5-23.5	5.20	fish debris/foram. [b]		-8.3	0.26	0.26	0.37
27.5-28.5	5.87	fish debris	0.512217	-8.2	0.18	0.29	0.34
33-34	6.61	fish debris	0.512211	-8.3	0.33	0.30	0.45
42.5-43.5	7.89	fish debris	0.512205	-8.4	0.39	0.29	0.49
52.5-53.5	9.24	foraminifera	0.512227	-8.0	0.13	0.21	0.25
57-58	9.84	foraminifera	0.512221	-8.1	0.21	0.21	0.30
62.5-63.5	10.56	fish teeth/debris	0.512234	-7.9	0.48	0.27	0.55
67.5-68.5	11.18	fish debris	0.512220	-8.2	0.08	0.29	0.30
72-73	11.73	fish teeth/debris	0.512226	-8.0	0.16	0.31	0.35
73-75	11.91	fish debris	0.512231	-7.9	0.32	0.23	0.39
75-76	12.10	fish debris	0.512230	-8.0	0.11	0.39	0.41
77-78	12.34	foraminifera	0.512248	-7.6	0.11	0.21	0.24
79-80	12.59	fish debris	0.512258	-7.4	0.20	0.23	0.30
82-83	12.95	foraminifera	0.512278	-7.0	0.17	0.21	0.27
84-85	13.19	foraminifera	0.512283	-6.9	0.19	0.27	0.33
87-88	13.55	fish teeth/debris	0.512291	-6.8	0.15	0.31	0.34
89-90	13.79	foraminifera	0.512288	-6.8	0.21	0.27	0.34
92-93	14.15	fish teeth/debris	0.512297	-6.7	0.16	0.29	0.33
94-95	14.52	fish debris	0.512285	-6.9	0.14	0.23	0.27
97.5-98.5	15.21	foraminifera	0.512296	-6.7	0.18	0.21	0.28
103-104	16.29	fish debris/foram. [b]		-6.5	0.27	0.24	0.36
104-105	16.49	fish teeth	0.512298	-6.6	0.31	0.33	0.45
108-109	17.28	fish debris/foram. [b]		-6.0	0.18	0.37	0.41
109-110	17.48	fish teeth/debris	0.512330	-6.0	0.13	0.18	0.22
113-114	19.14	fish teeth/debris	0.512326	-6.1	0.12	0.12	0.17
114-115	20.06	fish teeth	0.512320	-6.2	0.05	0.21	0.22
117.5-118.5	23.28	fish teeth	0.512328	-6.0	0.07	0.31	0.32
118-119	23.74	fish teeth	0.512325	-6.1	0.09	0.18	0.20
122.5-123.5	27.88	fish teeth [b]		-6.1	0.25	0.18	0.31

Table S3.1: continued.

Sample interval (cm)	Age (ka)	Material	Normalized $^{143}Nd/^{144}Nd$ [a]	ε_{Nd}	± Internal ε_{Nd} error (2σ SE)	± External ε_{Nd} error (2σ SD)	± Propagated error
123.5-124.5	28.79	fish teeth	0.512328	-6.0	0.23	0.21	0.31
PS75/056-1, 55°09.74'S, 114°47.31'W, 3581 m							
0-1.5	7.38	fish debris	0.512243	-7.7	0.12	0.32	0.34
4.5-6	8.51	fish debris	0.512292	-6.7	0.48	0.32	0.58
9.5-11	9.63	fish debris	0.512229	-8.0	0.86	0.25	0.90
14.5-16	10.76	fish debris	0.512254	-7.5	0.67	0.34	0.75
19.5-21	11.89	fish debris	0.512247	-7.6	0.14	0.25	0.29
24.5-26	12.74	fish debris	0.512258	-7.4	0.24	0.25	0.35
29.5-31	13.45	fish debris	0.512293	-6.7	0.13	0.25	0.28
34.5-36	14.17	fish debris	0.512314	-6.3	0.16	0.25	0.30
39.5-41	14.89	fish debris	0.512294	-6.7	0.25	0.25	0.35
44.4-46 [c]	16.33	fish debris	0.512315	-6.3	0.36	0.20	0.41
49.5-51	17.46	fish debris	0.512329	-6.0	0.10	0.25	0.27
54.5-56	18.11	fish debris	0.512335	-5.9	0.26	0.25	0.36
59.5-61	18.76	fish debris	0.512353	-5.6	0.03	0.23	0.23
64.5-66	19.41	fish debris	0.512347	-5.7	0.16	0.23	0.28
69.5-71	20.82	fish debris	0.512351	-5.6	0.22	0.23	0.32
74.5-76	22.41	fish debris	0.512331	-6.0	0.28	0.23	0.36
79.5-81	23.48	fish debris	0.512328	-6.0	0.31	0.23	0.39
84.5-86	24.56	fish debris	0.512330	-6.0	0.14	0.13	0.19
89.5-91	25.63	fish debris	0.512314	-6.3	0.22	0.18	0.28
94.5-96	26.45	fish debris	0.512311	-6.4	0.11	0.25	0.27
99.5-101	27.02	fish debris	0.512286	-6.9	0.36	0.25	0.44
104.5-106	27.59	fish debris	0.512313	-6.3	0.15	0.27	0.31
114.5-116	28.73	fish debris	0.512325	-6.1	0.10	0.27	0.29
124.5-126	29.87	fish debris	0.512315	-6.3	0.30	0.23	0.38
PS75/059-2, 54°12.80'S, 125°25.53'W, 3613 m							
2-3	3.46	fish debris	0.512270	-7.2	0.26	0.30	0.40
7-8	4.75	fish debris	0.512282	-6.9	0.09	0.28	0.29
12-13	6.04	foraminifera	0.512264	-7.3	0.16	0.21	0.26
17-18	7.33	foraminifera	0.512265	-7.3	0.11	0.21	0.24
22-23	8.62	foraminifera	0.512264	-7.3	0.13	0.21	0.25
27-28	9.78	fish debris	0.512276	-7.1	0.22	0.28	0.36
32-33	10.92	fish debris	0.512284	-6.9	0.07	0.28	0.29
37-38	12.06	foraminifera [b]		-6.6	0.38	0.30	0.48
42-43	13.40	fish teeth/debris	0.512342	-5.8	0.14	0.27	0.30
47-48	14.76	fish teeth/debris	0.512346	-5.7	0.13	0.20	0.24
52-53	16.12	fish teeth/debris	0.512345	-5.7	0.16	0.20	0.26
57-58	17.63	foraminifera	0.512338	-5.9	0.22	0.21	0.30
62-63	21.68	fish teeth/debris	0.512341	-5.8	0.42	0.27	0.50
67-68	25.73	fish teeth	0.512329	-6.0	0.30	0.30	0.42
72-73	28.48	fish teeth/debris	0.512321	-6.2	0.21	0.30	0.37
PS75/054-1, 56°9.105'S, 115°7.982'W, 4085 m							
17.5-19	11.66	foraminifera	0.512245	-7.7	0.04	0.13	0.14
22.5-24	12.21	fish debris	0.512325	-6.1	0.10	0.32	0.34
27.5-29	12.75	fish debris/foram. [b]		-7.8	0.30	0.35	0.46
32.5-34	13.30	fish debris	0.512304	-6.5	0.42	0.32	0.53
37.5-39	13.84	fish debris/foram. [b]		-7.5	0.49	0.35	0.60
47.5-49	15.82	fish debris/foram. [b]		-7.7	0.32	0.27	0.42
57.5-59	17.83	fish debris/foram. [b]		-7.6	0.21	0.39	0.45
67.5-69	19.48	foraminifera	0.512257	-7.4	0.15	0.23	0.27
87.5-89	22.62	foraminifera	0.512276	-7.1	0.13	0.13	0.18

[a] Sample $^{143}Nd/^{144}Nd$ ratios measured by MC-ICP-MS were normalized to the mean of JNdi-1 of the particular analytical session, relative to a JNdi-1 value of 0.512115 (Tanaka et al., 2000).

[b] average of two individual measurements (fish teeth, fish debris, foraminifera) from the same sample. Individual results in Table S3.2.

[c] Sample analyzed at Helmholtz Institute for Marine Research, Geomar, Kiel (Germany).

Table S3.2: Data of individual analyses of fish teeth/debris and foraminifera.

Sample interval (cm)	Age (ka)	Material	Normalized ^{143}Nd/^{144}Nd	ε_{Nd}	± Internal ε_{Nd} error (2σ SE)	± External ε_{Nd} error (2σ SD)	± Propagated error
PS75/073-2, 57°12.27'S, 151°36.63'W, 3234 m							
3-4	2.58	fish teeth/debris	0.512199	-8.6	0.86	0.72	1.12
3-4	2.58	foraminifera	0.512213	-8.3	0.16	0.21	0.26
7.5-8.5	3.18	fish debris	0.512221	-8.1	0.10	0.30	0.32
7.5-8.5	3.18	foraminifera	0.512227	-8.0	0.08	0.21	0.22
22.5-23.5	5.20	fish debris	0.512218	-8.2	0.14	0.20	0.24
22.5-23.5	5.20	foraminifera	0.512211	-8.3	0.22	0.16	0.27
52.5-53.5	9.24	fish debris [a]	0.512335	-5.9	0.98	0.27	1.02
52.5-53.5	9.24	foraminifera	0.512227	-8.0	0.13	0.21	0.25
57-58	9.84	fish debris [a]	0.512212	-8.3	0.67	0.72	0.98
57-58	9.84	foraminifera	0.512221	-8.1	0.21	0.21	0.30
77-78	12.34	fish debris [a]	0.512250	-7.6	0.17	0.29	0.34
77-78	12.34	foraminifera	0.512248	-7.6	0.11	0.21	0.24
89-90	13.79	fish teeth/debris [a]	0.512261	-7.4	0.41	0.33	0.53
89-90	13.79	foraminifera	0.512288	-6.8	0.21	0.27	0.34
103-104	16.29	fish debris	0.512304	-6.5	0.13	0.12	0.18
103-104	16.29	foraminifera	0.512310	-6.4	0.24	0.21	0.32
108-109	17.28	fish debris	0.512324	-6.1	0.07	0.20	0.21
108-109	17.28	fish teeth	0.512335	-5.9	0.17	0.31	0.35
122.5-123.5	27.88	fish teeth	0.512328	-6.0	0.22	0.12	0.25
122.5-123.5	27.88	fish teeth	0.512324	-6.1	0.12	0.13	0.18
127.5-128.5	32.47	fish teeth [b]	0.512314	-6.3	0.19	0.12	0.22
127.5-128.5	32.47	fish teeth [b]	0.512335	-5.9	0.17	0.12	0.21
PS75/059-2, 54°12.80'S, 125°25.53'W, 3613 m							
12-13	6.04	fish debris [a]	0.512238	-7.8	0.98	0.28	1.02
12-13	6.04	foraminifera	0.512264	-7.3	0.16	0.21	0.26
22-23	8.62	fish debris [a]	0.512269	-7.2	0.64	0.27	0.69
22-23	8.62	foraminifera	0.512264	-7.3	0.13	0.21	0.25
37-38	12.06	foraminifera	0.512298	-6.6	0.34	0.21	0.40
37-38	12.06	foraminifera	0.512303	-6.5	0.16	0.21	0.26
77-78	31.08	fish debris [b]	0.512331	-6.0	0.10	0.20	0.22
77-78	31.08	foraminifera [b]	0.512311	-6.4	0.02	0.18	0.18
PS75/054-1, 56°9.105'S, 115°7.982'W, 4085 m							
27.5-29	12.75	fish debris	0.512246	-7.6	0.28	0.32	0.43
27.5-29	12.75	foraminifera	0.512232	-7.9	0.10	0.13	0.16
37.5-39	13.84	fish debris	0.512269	-7.2	0.47	0.13	0.49
37.5-39	13.84	foraminifera	0.512241	-7.7	0.12	0.32	0.34
47.5-49	15.82	fish debris	0.512253	-7.5	0.32	0.24	0.40
47.5-49	15.82	foraminifera	0.512238	-7.8	0.04	0.13	0.14
57.5-59	17.83	fish debris	0.512253	-7.5	0.21	0.32	0.38
57.5-59	17.83	foraminifera	0.512247	-7.6	0.04	0.23	0.23

[a] values used in supplementary figures for archive- or replicate-comparison but not included in the composite records (Tab. S3.1). These values are excluded from the composite record due to higher error or low voltage during measurement.

[b] values used in supplementary figures for archive- or replicate-comparison but not included in the composite records due to ages >30 ka (Tab. S3.1).

Table S3.3: Data of individual analyses of lithogenic particles from inside foraminifera shells.

Sample interval (cm)	Age (ka)	Normalized $^{143}Nd/^{144}Nd$	ε_{Nd}	± Internal ε_{Nd} error (2σ SE)	± External ε_{Nd} error (2σ SD)	± Propagated error
PS75/073-2, 57˚12.27’S, 151˚36.63’W, 3234 m						
3-4	2.58	0.512229	-8.0	0.16	0.33	0.37
7.5-8.5	3.18	0.512221	-8.1	0.15	0.33	0.36
22.5-23.5	5.20	0.512270	-7.2	0.34	0.55	0.65
52.5-53.5	9.24	0.512283	-6.9	0.24	0.26	0.35
57-58	9.84	0.512280	-7.0	0.34	0.33	0.47
77-78	12.34	0.512297	-6.7	0.15	0.33	0.36
82-83	12.95	0.512325	-6.1	0.14	0.26	0.30
84-85	13.19	0.512342	-5.8	0.33	0.36	0.49
89-90	13.79	0.512332	-6.0	0.09	0.16	0.18
97.5-98.5	15.21	0.512346	-5.7	0.30	0.26	0.40
103-104	16.29	0.512345	-5.7	0.26	0.26	0.37
PS75/059-2, 54˚12.80’S, 125˚25.53’W, 3613 m						
12-13	6.04	0.512301	-6.6	0.32	0.33	0.46
17-18	7.33	0.512343	-5.8	0.27	0.26	0.37
22-23	8.62	0.512357	-5.5	0.31	0.26	0.40
37-38	12.06	0.512369	-5.2	0.26	0.26	0.37
37-38	12.06	0.512391	-4.8	0.22	0.26	0.34
57-58	17.63	0.512384	-5.0	0.06	0.21	0.22
77-78	31.08	0.512373	-5.2	0.03	0.21	0.21

Table S3.4: Updated age model tie points of reference core MD97-2120 and tie points of the investigated cores.

Core	Sample interval (cm)	Age (ka)	Type	Sed. Rate (cm/ka)	Data Reference
MD97-2120	22.5	2.06	^{14}C	8.8	Pahnke et al. (2003)
	36.5	3.66	^{14}C	14.8	Pahnke et al. (2003)
	98.5	7.86	^{14}C	21.9	Pahnke et al. (2003)
	202.5	12.61	^{14}C	20.3	Pahnke et al. (2003)
	230.5	13.99	^{14}C	23.7	Pahnke et al. (2003)
	252.5	14.92	^{14}C	20.6	Pahnke et al. (2003)
	330.5	18.7	^{14}C	23.3	Rose et al. (2010)
	344.5	19.3	^{14}C	30.7	Rose et al. (2010)
	390.5	20.8	^{14}C	39.3	Rose et al. (2010)
	418	21.5	^{14}C	13.7	Rose et al. (2010)
	471	25.36	Kawakawa Tephra	16.3	Vandergoes et al. (2013)
	525	28.67	^{14}C	14.8	Pahnke et al. (2003)
PS75/056-1	6.6	8.74	Benthic $\delta^{18}O$	4.4	Lamy et al. (2014)
	22.1	12.25	Benthic $\delta^{18}O$	7.0	Lamy et al. (2014)
	40.9	14.95	Benthic $\delta^{18}O$	3.3	Lamy et al. (2014)
	48.3	17.17	Benthic $\delta^{18}O$	7.7	Lamy et al. (2014)
	67.7	19.69	Benthic $\delta^{18}O$	2.5	Lamy et al. (2014)
	73.3	21.93	Benthic $\delta^{18}O$	4.7	Lamy et al. (2014)
	93.0	26.17	Benthic $\delta^{18}O$	8.8	Lamy et al. (2014)
	139.8	31.51	Benthic $\delta^{18}O$	11.9	Lamy et al. (2014)
	212.4	37.60	Benthic $\delta^{18}O$	4.1	Lamy et al. (2014)
PS75/059-2	11.6	5.81	Benthic $\delta^{18}O$	3.9	Lamy et al. (2014)
	23.0	8.75	Benthic $\delta^{18}O$	4.4	Lamy et al. (2014)
	38.1	12.20	Benthic $\delta^{18}O$	3.7	Lamy et al. (2014)
	57.2	17.41	Benthic $\delta^{18}O$	1.2	Lamy et al. (2014)
	68.0	26.16	Benthic $\delta^{18}O$	1.9	Lamy et al. (2014)
	89.9	37.55	Benthic $\delta^{18}O$	1.9	Lamy et al. (2014)

Table S3.4: continued.

Core	Sample interval (cm)	Age (ka)	Type	Sed. Rate (cm/ka)	Data Reference
E11-2	32.5	10.37	Benthic $\delta^{18}O$	8.8	Ninnemann and Charles (2002)
	50.8	12.44	Benthic $\delta^{18}O$	6.8	Ninnemann and Charles (2002)
	68.3	15.02	Benthic $\delta^{18}O$	11.4	Ninnemann and Charles (2002)
	85.6	16.54	Benthic $\delta^{18}O$	8.4	Ninnemann and Charles (2002)
	95.5	17.72	Benthic $\delta^{18}O$	16.1	Ninnemann and Charles (2002)
	123.4	19.46	Benthic $\delta^{18}O$	14.2	Ninnemann and Charles (2002)
	234.5	27.27	Benthic $\delta^{18}O$	15.8	Ninnemann and Charles (2002)
	274.2	29.78	Benthic $\delta^{18}O$	15.8	Ninnemann and Charles (2002)
PS75/073-2	10.5	3.52	Planktonic $\delta^{18}O$	7.4	Benz (2016)
	61.4	10.37	Planktonic $\delta^{18}O$	8.2	Benz (2016)
	80.7	12.73	Planktonic $\delta^{18}O$	8.3	Benz (2016)
	92.8	14.19	Planktonic $\delta^{18}O$	5.1	Benz (2016)
	112.3	18.02	Planktonic $\delta^{18}O$	1.1	Benz (2016)
	130.4	34.64	Planktonic $\delta^{18}O$	1.1	Benz (2016)
	135.2	39.06	Planktonic $\delta^{18}O$	1.1	Benz (2016)
PS75/054-1	15.6	11.37	XRF Sr	9.2	
	38.6	13.88	XRF Fe	5.0	
	62.9	18.78	XRF Fe	7.6	
	74.6	20.31	XRF Fe	5.9	
	130.6	29.79	XRF Fe	5.7	
	191.0	40.48	XRF Sr	3.7	
	230.0	50.98	XRF Sr	3.7	

4. Neodymium isotope evidence for variable glacial-interglacial deep-water mixing in the Southern Ocean over the last 140 ka

Henning Fröllje[1], Katharina Pahnke[1], Chandranath Basak[1,†],
Frank Lamy[2], Rainer Gersonde[2]

This chapter corresponds to a full manuscript that was prepared
for submission to the journal *Paleoceanography*.

[1] Max Planck Research Group for Marine Isotope Geochemistry, Institute for Chemistry and Biology of the Marine Environment (ICBM), University of Oldenburg, Carl-von-Ossietzky-Str. 9-11, 26129 Oldenburg, Germany.

[2] Alfred Wegener Institute, Helmholtz Centre for Polar and Marine Research, Am Alten Hafen 26, 27568 Bremerhaven, Germany.

[†] Now at: Lamont-Doherty Earth Observatory of Columbia University, 61 Route 9W, Palisades, NY 10964, USA.

Key Points

- Similar composition of CDW during the last two glacials in the Southeast Pacific due to reduced contribution of NADW
- Similar deep water ε_{Nd} decrease at T1 and T2, in line with Atlantic and Southern Ocean control on CDW composition
- Higher proportion of NADW in Pacific CDW during MIS 4 compared to MIS 2 and 6 is consistent with a North Atlantic control

Abstract

Circumpolar Deep Water (CDW) in the Southern Ocean is a mixture of North Atlantic Deep Water (NADW) and North Pacific Deep Water. Variations in the relative contributions of Atlantic- and Pacific-derived waters to CDW during past climates can be traced by neodymium (Nd) isotopes extracted from sedimentary archives. A new Nd isotope record from the Pacific sector of the Southern Ocean from the depth of modern CDW shows climate-related variations in the North Atlantic contribution to CDW, but no complete cessation during at least the past 140 ka. We observe a comparable contribution of NADW to CDW during Marine Isotope Stage (MIS) 5 and late Holocene and modern times. During the penultimate glaciation of MIS 6, Nd isotopes indicate a reduced North Atlantic component in CDW similar to that observed during the last glacial. The last two glacial terminations (T1, T2) show the same but attenuated variations compared to the deep South Atlantic and Indian Oceans due to the lack of direct NADW influence in the Southeast Pacific. We therefore suggest that our record ideally monitors endmember changes in Southern Ocean CDW and hence constrains the strength of the meridional overturning circulation. The Nd isotope decrease in CDW prior to NADW re-strengthening, previously described for T1, is also seen during T2, suggesting the same Southern Ocean control. A notable feature of our Nd isotope record are less radiogenic Nd isotope ratios during MIS 4 compared to MIS 2 and 6, indicating higher NADW input consistent with a North Atlantic control.

4.1. Introduction

The Southern Ocean plays a major role in the global overturning circulation through the formation of intermediate and bottom waters and through mixing and redistribution of deep water masses from the Atlantic, Pacific and Indian Oceans. In the modern climate, it is this region, where the upper and lower meridional overturning cells are connected through upwelling of deep waters, thereby facilitating ocean-atmosphere heat and gas-exchange (e.g., Marshall and Speer, 2012; Talley, 2013). During the Last Glacial Maximum (LGM), when North Atlantic Deep Water (NADW) advection was replaced by the formation of Glacial North Atlantic Intermediate Water, nutrient and circulation proxies show that the deep North Atlantic was filled with southern-sourced waters (e.g., Duplessy et al., 1988; Curry and Oppo, 2005; Lynch-Stieglitz et al., 2007; Gutjahr et al., 2008; Roberts et al., 2010; Lippold et al., 2016). At this time, expansion of Antarctic sea ice, buoyancy flux changes, equatorward shifted westerlies, and changing deep water properties have been suggested to have caused enhanced polar stratification and reduced vertical mixing of northern and southern-sourced waters (Adkins et al., 2002; Toggweiler et al., 2006; Adkins, 2013; Ferrari et al., 2014). At glacial terminations, several processes in the Southern Ocean, such as southward migration of westerlies, sea-ice retreat, decreasing nutrient utilization, breakdown of polar stratification and reorganizations of the global circulation have been suggested to have impacted global climate through the release of carbon from previously isolated, CO_2-rich deep waters (e.g., Sigman and Boyle, 2000; Anderson et al., 2009; Sigman et al., 2010; Skinner et al., 2010; Burke and Robinson, 2012; Abelmann et al., 2015). It is therefore crucial to understand water mass circulation changes in the Southern Ocean in the course of past climate variations as one of these mechanisms. Neodymium isotope ratios have the potential to shed light on changes in deep water mixing and can hence contribute to our understanding of the dynamics of the Southern Ocean.

Neodymium isotopes ($^{143}Nd/^{144}Nd$) have been established as a tracer for water mass origin and can hence be used to investigate past ocean circulation changes (e.g., Frank, 2002; Goldstein and Hemming, 2003). Particularly, Nd isotopes have been used to study changes in the presence of northern- *versus* southern-sourced waters during the last deglaciation (e.g., Piotrowski et al., 2004; Pahnke et al., 2008; Roberts et al., 2010; Lippold et al., 2016) and throughout the last glacial-interglacial cycle (Piotrowski et al., 2005; 2009; Böhm et al., 2015; Jonkers et al., 2015; Wilson et al., 2015; Molina-Kescher et al., 2016). The neodymium isotope composition is typically expressed in ε_{Nd} notation, which is defined as $\varepsilon_{Nd} = [(^{143}Nd/^{144}Nd)_{sample}/(^{143}Nd/^{144}Nd)_{CHUR} -1]*10{,}000$ where CHUR is the Chondritic Uniform Reservoir with $^{143}Nd/^{144}Nd = 0.512638$ (Jacobsen and Wasserburg, 1980). The heterogenic distribution of ε_{Nd} on the continents is imprinted on surface seawater by transport of dissolved and particulate material (e.g., Frank, 2002; Goldstein and Hemming, 2003), as well as through boundary exchange processes at continental margins (Lacan and Jeandel, 2001; 2005a). In the deep and open ocean, neodymium isotopes are considered a robust, quasi-conservative water mass tracer with a comparably short residence time of 300-1000 years (Tachikawa et al., 2003; Arsouze et al., 2009; Rempfer et al., 2011) compared to the whole ocean mixing time of ~1500 years (Broecker and Peng, 1982). Different water masses therefore carry a distinct isotope composition that is set in their formation regions: NADW has an ε_{Nd} of -13.5 (Piepgras and Wasserburg, 1987; Lacan and Jeandel, 2005b), whereas the deep North Pacific has a more radiogenic (i.e., more positive) composition of ~-3.5 (e.g., Fröllje et al., 2016; Fröllje et al., 2016, corresponds to chapter 2 of this thesis. Hereafter just referred to as Fröllje et al., 2016). Circumpolar Deep Water (CDW) is a mixture of NADW and North Pacific Deep Water (NPDW), with intermediate values of -8 to -9 (Piepgras and Wasserburg, 1982; Stichel et al., 2012b; Carter et al., 2012; Basak et al., 2015). Deep waters formed around Antarctica carry a distinct ε_{Nd} signal depending on the formation region. In the Pacific sector of the Southern Ocean, Ross Sea Bottom Water (RSBW) carries a typical ε_{Nd} signature of -7 (Carter et al., 2012; Rickli et al., 2014; Basak et al., 2015), whereas bottom water originating from the Weddell Sea is less radiogenic with an ε_{Nd} signature of -9 (Stichel et al., 2012b). The use of Nd isotopes as a paleo-water mass tracer is based on the transmission of the bottom water signal to sedimentary archives such as fish teeth/debris (e.g., Martin and Haley, 2000; Thomas et al., 2003; Martin and Scher, 2004), foraminifera (e.g., Roberts et al., 2010), or iron manganese oxide coatings on sediment particles (e.g., Rutberg et al., 2000; Piotrowski et al., 2004; Gutjahr et al., 2008; Pahnke et al., 2008), from which the pristine bottom water ε_{Nd} signature can be extracted.

Here we present a ~140 ka long ε_{Nd} record, analysed on fossil fish teeth and debris, from Southeast Pacific gravity core PS75/056-1. The core was retrieved from 3581 m water depth and is bathed today by Lower Circumpolar Deep Water (LCDW) with some influence of overlying Upper Circumpolar Deep Water (UCDW) and NPDW (section 4.3.1 and Fig. 4.1).

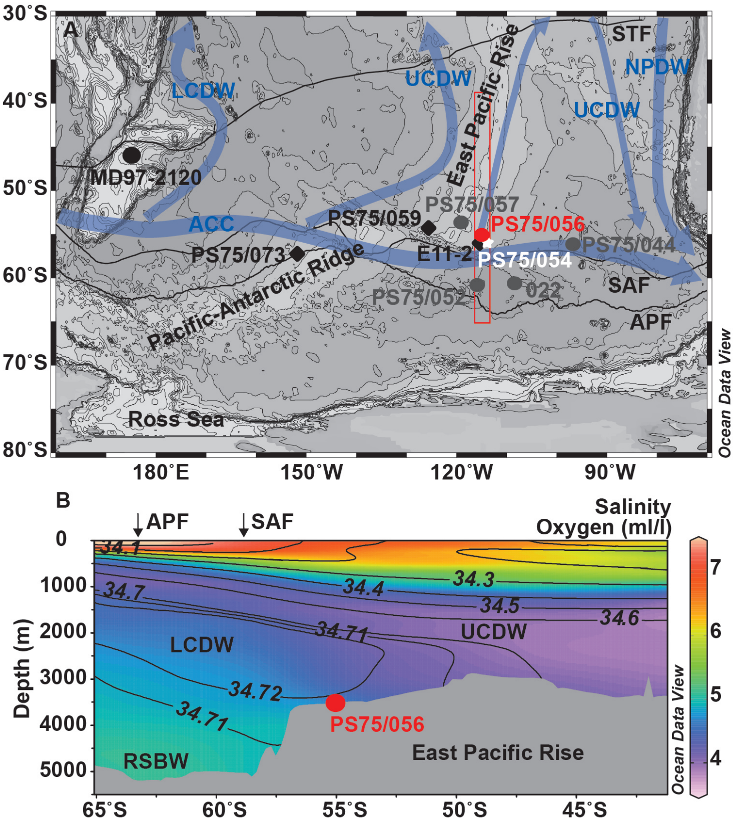

Figure 4.1: A) Location of sediment core PS75/056-1 (red circle) in the Southeast Pacific Ocean and locations of CTD station PS75/054 (Gersonde, 2011; white star), and sites of seawater ε_{Nd} profiles (Carter et al., 2012; Basak et al., 2015; gray circles). Sediment cores PS75/073-2 and PS75/059-2 (Basak et al., in prep.) and E11-2 (Ninnemann and Charles, 2002) discussed in the text, are indicated by black diamonds, age model reference core MD97-2120 by black circle. STF = Subtropical Front, SAF = Subantarctic Front, APF = Antarctic Polar Front. Frontal positions after Orsi et al. (1995). Schematic circulation after Kawabe and Fujio (2010). B) Meridional section along ~115°W (red box in A). Colors: oxygen concentration (ml/l) (Garcia et al., 2010a), contours: salinity (Antonov et al., 2010). Arrows indicate approximate positions of APF and SAF. Figures created with Ocean Data View (Schlitzer, 2014).

The core location in the Southeast Pacific represents the far end of the active NADW flow path. This core has been previously investigated for its Nd isotope composition throughout the last deglaciation (Basak et al., in prep.; Basak et al., in prep., corresponds to chapter 3 of this thesis. Hereafter just referred to as Basak et al., in prep.), its benthic foraminiferal δ^{13}C variation over the last 260 ka (Ullermann et al., 2016), and for varying dust deposition during the last ~250 ka (Lamy et al., 2014). The ε_{Nd} record of core PS75/056-1 covering the past 30 ka in combination with a deeper record, indicates deep stratification in the Southern Ocean during the LGM and an early deglacial breakup of this stratification in response to Southern Ocean warming (Basak et al., in prep.). For the first time, deep water ε_{Nd} in the Southern Ocean could be clearly shown to partly respond to changes in the Southern Hemisphere climate rather than being entirely controlled by varying southward export of NADW (Basak et al., in prep.). During the last 30 ka, the

Heinrich Stadial 1 (HS1) marks the time window when paleo proxy evidence suggests interruption of NADW formation in the North Atlantic (e.g., McManus et al., 2004). Changes in accordance with the state of NADW formation during the HS1 are not reflected in the Southeast Pacific, and only after HS1 did the increased influence of NADW in CDW become discernible (Basak et al., in prep.). We build upon this work by extending the existing ε_{Nd} record back to the penultimate glacial period (Marine Isotope Stage (MIS) 6). Our study location allows us to investigate the changes in deep water mixing in the Southern Ocean outside the direct influence of NADW throughout the last glacial-interglacial cycle and to compare the last two glacial maxima and glacial terminations. The data therefore provide an ε_{Nd} endmember record for Southern Ocean CDW over the past 140 ka.

Variations in NADW contribution to southeast Pacific CDW over the last ~100 ka and ~260 ka, respectively, have previously been shown based on stable carbon isotopes from core PS75/056-1 (Ullermann et al., 2016) and core E11-2 (56° S; 3109 m water depth) (Ninnemann and Charles, 2002), the latter being located only ~1° south of core PS75/056-1 (Fig. 4.1A), giving us the opportunity to compare the new ε_{Nd} dataset to the existing carbon isotope results and allowing to test if processes other than ocean circulation influenced the carbon isotope changes.

Using Nd isotopes, previous studies demonstrated that the penultimate deglaciation is characterized by an increase in northern-sourced deep water contribution to South Atlantic CDW (Piotrowski et al., 2005; Jonkers et al., 2015). This is similar to what has been observed in the deep Atlantic and Pacific Southern Ocean for the last deglaciation (e.g., Piotrowski et al., 2004; Robinson and van de Flierdt, 2009; Noble et al., 2013; Skinner et al., 2013; Lippold et al., 2016; Basak et al., in prep.), with an observed additional contribution from Southern Ocean bottom waters to the early deglacial ε_{Nd} decrease in the South Pacific (Basak et al., in prep.). In a recent study, Molina-Kescher et al. (2016) presented two downcore records from the South Pacific (44-46° S) covering the last ~250 ka that show glacial-interglacial variations in deep water ε_{Nd} signatures with reduced NADW contributions to the South Pacific during glacials. However, their records show very subtle glacial-interglacial changes of ~1 ε_{Nd} unit and are clearly influenced by Pacific water masses throughout the whole record as indicated by ε_{Nd} values between -5 and -6, being significantly more radiogenic than South Pacific CDW (Molina-Kescher et al., 2016). Wilson et al. (2015) proposed that the glacial Nd isotope signature in the deep Indian Ocean may have resulted from the isolation of the deep Southern Ocean from NADW influence, in line with a suggested glacial two-cell overturning structure that reduced the mixing of northern-sourced intermediate and southern-sourced deep waters

(Lund et al., 2011; Adkins, 2013; Ferrari et al., 2014). Moreover, varying amounts of northern- *versus* southern-sourced water have been suggested for observed millennial-scale ε_{Nd} variations in the North and South Atlantic during MIS 3 (Piotrowski et al., 2008; Gutjahr et al., 2010; Gutjahr and Lippold, 2011; Böhm et al., 2015). Thus, by being located within CDW in the Southeast Pacific and hence outside the active flowpath of NADW, core PS75/056-1 is ideally suited to study the evolution of CDW composition throughout the last glacial-interglacial cycle and inter-basin differences in past Southern Ocean water mass mixing.

4.2. Modern hydrography in the Southeast Pacific

The most prominent water mass in the Southern Ocean is CDW that is generally divided into LCDW and UCDW. Lower CDW is identified by its salinity maximum, which is a remnant of high-salinity NADW (Reid and Lynn, 1971; Orsi et al., 1995). Deep waters from the Pacific and Indian Oceans imprint their low oxygen, high nutrient signature onto UCDW (Callahan, 1972). Beside the eastward flowing Antarctic Circumpolar Current (ACC), the circulation in the Southeast Pacific is characterized by the southward flow of modified NPDW along the Chilean Coast and the northward flow of UCDW along the East Pacific Rise (EPR) in the upper deep layer at ~1500-3500 m (Kawabe and Fujio, 2010; Fig. 4.1). Antarctic Bottom Water (AABW), supplied from its formation regions in the Weddell Sea, the Ross Sea, and Adélie Coast-Wilkes Land, is the densest water mass in the Southern Ocean and is underlying LCDW (Orsi, 1999). Ross Sea Bottom Water covers the abyss of the Southeast Pacific basin, being formed on the Ross Sea shelf by mixing of upwelled CDW with cool and saline surface waters and inhibited from northward expansion by the Pacific-Antarctic ridge system (e.g., Jacobs, 1970; Orsi, 1999). The southward shoaling isopycnals divide the Southern Ocean into frontal zones (e.g., Orsi, 1995). Upwelling of CDW south of the Antarctic Polar Front (APF) supplies the deep and shallow overturning branches, feeding AABW formed on the Antarctic shelves, and Antarctic Intermediate Water and Subantarctic Mode Water formed north of the ACC (e.g., Marshall and Speer 2012; Talley 2013). In the Southeast Pacific, the APF is located at 60-65° S (Orsi et al., 1995; Fig. 4.1A). The second major front, the Subantarctic Front (SAF), located between 55° and 60° S in this region, separates the Polar Frontal Zone from the Subantarctic Zone and marks the northern boundary of the ACC (Orsi, 1995; Talley et al., 2011). North of the SAF, UCDW is centered at a typical potential density of 27.6 kg/m^3, located at approximately 1500 m depth, whereas LCDW occupies the depth below 2000 m, characterized by a typical potential density of 27.8 kg/m^3 and salinity of >34.7. South of the SAF, UCDW and LCDW shoal along the isopycnals (Fig. 4.1B; Talley et al., 2011).

4.3. Material and Methods

4.3.1. Core locations and sample material

The gravity core PS75/056-1 (55˚09.74' S, 114˚47.31' W, 3581 m water depth) was recovered during *R/V Polarstern* cruise ANT-XXVI/2 in the Southeast Pacific Ocean (Gersonde, 2011). The coring site is located southeast of the EPR in the Subantarctic Zone just north of the modern SAF (Fig. 4.1A) and is bathed today by LCDW with some potential influence from overlying UCDW and modified NPDW as indicated by lower oxygen concentrations (Fig. 4.1B). Lower CDW can be identified below 2000 m depth at the nearby CTD station PS75/054 by its typical salinity maximum (Gersonde, 2011; Fig. 4.1B). In agreement with this, Basak et al. (2015) suggested the presence of LCDW at stations PS75/044, PS75/052 and PS75/057 between ~2000 and ~4000 m water depth based on neutral density ranges (cf. Fig. 4.1A for locations). Upper CDW at these sites was found at 1000-2000 m water depth (Basak et al., 2015). Sediments investigated in this study were sampled from 130 to 720 cm core depth within core PS75/056-1, extending the previously studied most recent interval (0-125 cm depth; Basak et al., in prep.) beyond ~30 ka BP back to the penultimate glacial stage of MIS 6. The sediments are mainly composed of nannofossil and diatom oozes with varying amounts of foraminifera (Gersonde et al., 2010).

4.3.2. Sample processing

The washed sediment >125 µm fraction was used to pick fossil fish teeth and debris. Previous results show that fish teeth and debris from the same sample have identical ε_{Nd} values (Thomas and Via, 2007; Martin et al., 2010; Basak et al., in prep.), allowing us to combine them for analytical purposes whenever necessary. Martin et al. (2010) showed that an extensive chemical cleaning is not necessary to obtain pristine bottom water Nd isotope signals. Thus, the teeth/debris were physically cleaned by ultrasonication in optima-grade methanol and MilliQ water (18 MΩ, Millipore) followed by treatment with a 1:1 mixture of H_2O_2 (30%) and MilliQ water. Finally, the teeth/debris were dissolved in a 1:1 mixture of HNO_3 and HCl. All reagents used were of ultra-clean quality (<1ppt Nd).

4.3.3. Column chemistry and isotope measurements

We isolated Nd from the fish teeth/debris samples by two-step column chemistry (modified from Pin and Zalduegui, 1997). In the first step, rare earth elements (REE) were isolated using 100 µl of Eichrom TRU-Spec resin (particle size of 100-150 µm). In a second step, Nd was separated from interfering REEs using pre-calibrated Teflon columns loaded with 250 µl of TrisKem Ln-Spec resin (particle size of 50-100 µm) and 0.23 N HCl as eluent. The collected Nd fraction was evaporated until dry, following which it was treated with a 1:1 mixture of H_2O_2 (30%) and concentrated HNO_3 to oxidize any resin-derived organic compounds, and dried again. The samples were re-dissolved in 2% HNO_3 and concentration-matched with standards (typically 5ppb, 10ppb, 20ppb Nd) prior to Nd isotope analyses. The Nd isotope compositions were analyzed using a ThermoScientific *Neptune Plus* multi-collector inductively coupled plasma mass spectrometer (MC-ICP-MS) at the University of Oldenburg. We used a Cetac *Aridus II* desolvating nebulizer system for sample introduction. All samples were measured in 1 ml sample solution and typical analytical routine constituted 4x12 cycles and peak centering at the beginning of each sample. Samples and standards were corrected for instrumental mass bias with $^{146}Nd/^{144}Nd = 0.7219$ using an exponential law (O'Nions et al., 1977). Each measurement session was accompanied by multiple analyses of Nd standard JNdi-1 (generally every three samples). The $^{143}Nd/^{144}Nd$ ratios of all samples were normalized to the reported JNdi-1 value of $^{143}Nd/^{144}Nd = 0.512115$ (Tanaka et al., 2000). We used the JNdi-1 measurements for the calculation of the external reproducibility of each session, which generally ranged between ±0.1 and ±0.4 ε_{Nd} units (2σ SD, n = 4-16 per session). Errors of the samples are reported as propagated errors, combined from internal and external reproducibility (Tab. S4.1). Mass bias corrected and JNdi-1 normalized $^{143}Nd/^{144}Nd$ ratio for Nd standard La Jolla was 0.511858 ± 0.000017 (n = 4) and was thus identical to the reported value of 0.511858 (Lugmair et al., 1983). The procedural blank was ≤8 pg Nd (n = 7).

4.3.4. Age model

The age model for core PS75/056-1 is based on graphical correlation of the benthic $\delta^{18}O$ record (measured on monospecific samples of *Cibicidoices kullenbergi*; Lamy et al., 2014), to the Southwest Pacific reference core MD97-2120 from Chatham Rise (Pahnke and Zahn, 2005). For this purpose, we updated the original age model for core MD97-2120 using re-calibrated planktonic ^{14}C ages of Pahnke et al. (2003) and Rose et al. (2010) (using the new radiocarbon calibration curve of Reimer et al., 2013) and the updated age of the Kawakawa Tephra (Vandergoes et al., 2013) for the interval 0-30 ka (Basak et al., in prep.), and tuning of the sea surface temperature (SST) record (Pahnke et al., 2003) to the Antarctic EPICA Dome C δD record on the AICC2012 timescale (Jouzel et al., 2007; Veres et al., 2013; Bazin et al., 2013) for the interval >30 ka (this study; Fig. 4.2; Tab. S4.2). The resulting age model of core PS75/056-1 for the past 150 ka results in sedimentation rates of 2-12 cm/ka (Tab. S4.2; Fig. 4.2) and shows good agreement with the benthic δ^{18}O LR04 stack (Lisiecki and Raymo, 2005) and a recently published age model of this core (Ullermann et al., 2016). The age model for the interval 0-30 ka was previously reported in Basak et al. (in prep.).

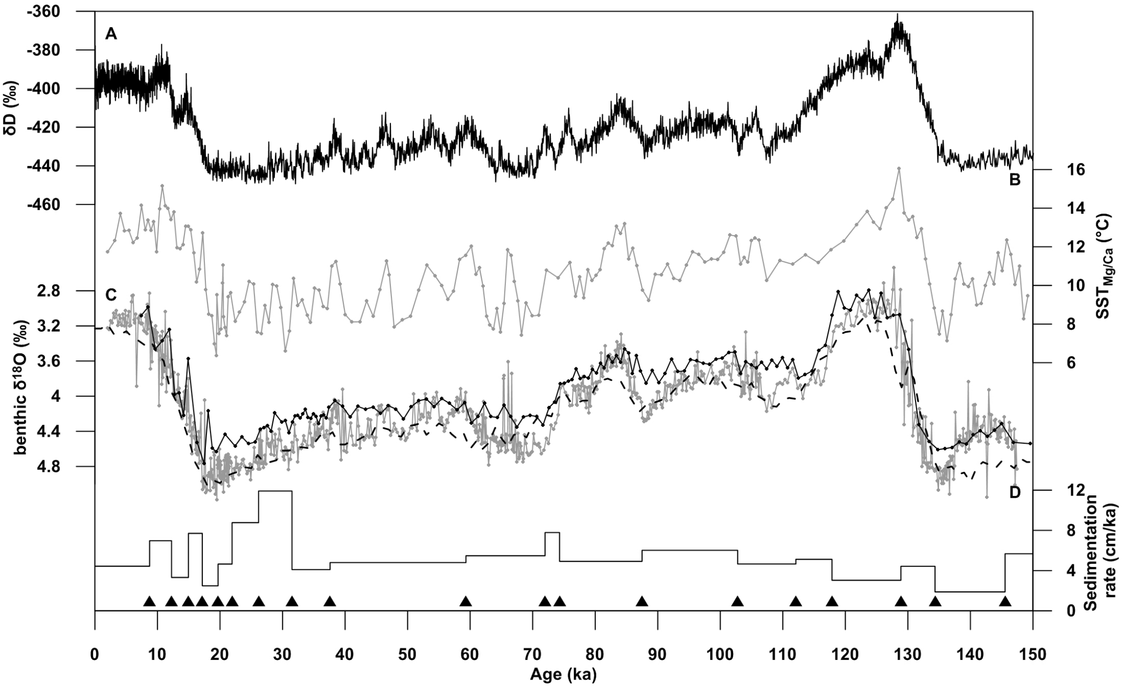

Figure 4.2: Age model of core PS75/056-1. A) Antarctic EPICA Dome C ice core δD record on the AICC2012 timescale (Jouzel et al., 2007; Veres et al., 2013; Bazin et al., 2013). B) Mg/Ca-derived SST record of reference core MD97-2120 (Pahnke et al., 2003) on its updated age scale (for details see text). C) Benthic δ^{18}O of core PS75/056-1 (back line; Lamy et al., 2014) with benthic δ^{18}O of reference core MD97-2120 (grey line; Pahnke and Zahn, 2005) on its updated age scale, and benthic δ^{18}O of LR04 stack (black dashed line; Lisiecki and Raymo, 2005). D) Sedimentation rate of core PS75/056-1. Age tie points are illustrated by triangles. Age model of PS75/056-1 for the interval 0-30 ka from Basak et al. (in prep.).

4.4. Results

Here we report Nd isotope data obtained during this study together with those from the most recent interval (~0-30 ka) originally reported in Basak et al. (in prep.). The compiled results are listed in Table S4.1 and are presented in Figures 4.4-4.6. Data obtained in the course of this study are available on PANGAEA (www.pangaea.de) under doi: /10.1594/PANGAEA.858876. The exclusive use of fish teeth and debris, analogous sample processing, and measuring methodologies under same laboratory setup ensures data comparability between this study and that of Basak et al. (in prep.). Thus we are confident that combining results from both studies do not affect the quality of the overall record presented here.

The core-top value of -7.7 ± 0.3 (3581 m water depth; Basak et al., in prep) is consistent with the deep water Nd isotope composition of nearby stations (Fig. 4.3; Carter et al., 2012; Basak et al., 2015).

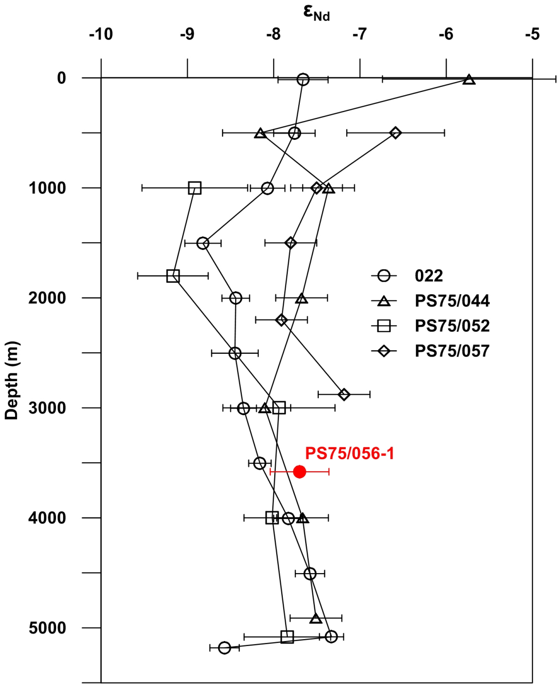

Figure 4.3: Coretop ε_{Nd} of fossil fish debris of core PS75/056-1 (red circle, from Basak et al., in prep.) in comparison to Southeast Pacific ε_{Nd} seawater profiles (for locations see Fig. 4.1A). Seawater data of PS75/044, PS75/052, and PS75/057 from Basak et al. (2015), station 022 from Carter et al. (2012).

The downcore ε_{Nd} signatures of core PS75/056-1 range from -5.6 to -7.7 over the last ~140 ka, with the general pattern of more radiogenic signatures during glacials and less radiogenic signatures during interglacials (Fig. 4.4). Full glacial stages are characterized by the most radiogenic ε_{Nd} values of -5.8 ± 0.2 during the LGM (18-22 ka) and MIS 6 (132-138 ka) (Fig. 4.4). We observe a rapid decrease by 1.5 to 2 ε_{Nd} units during the transitions from glacial to interglacial conditions starting at approximately 132 ka and 18 ka (Fig. 4.5). During MIS 5, ε_{Nd} varies between -7.7 and -6.6 and has an average ε_{Nd} signature of -7.2 ± 0.3. There are three significant excursions towards more radiogenic ε_{Nd} values during this stage centered at approximately 80 ka, 87 ka, and 101 ka (Fig. 4.4). Starting at ~77 ka, ε_{Nd} increases to more radiogenic signatures of -6.6 ± 0.1 during MIS 4, without reaching the full glacial values of MIS 2 and MIS 6. This is followed by gradually decreasing ε_{Nd} values that reach ε_{Nd} = -7.4 at ~46 ka, being similar to the signature during the interglacials of MIS 5 and the Holocene. From there on, ε_{Nd} gradually increases throughout MIS 3 and the early MIS 2 towards the full glacial values of the LGM (Fig. 4.4).

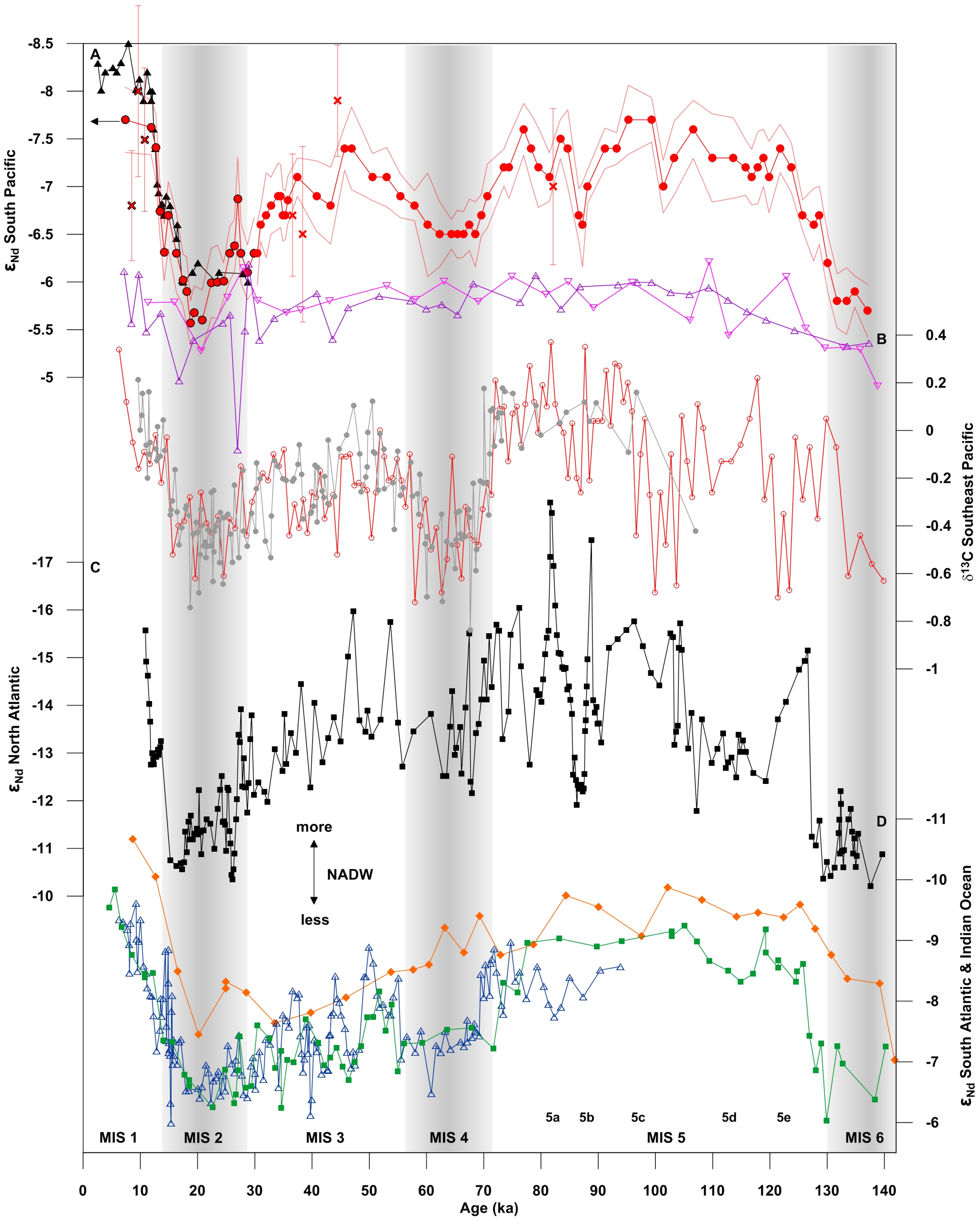

Figure 4.4: Proxy records over the last 140 ka. A) Neodymium isotope signatures of Southeast Pacific core PS75/056-1 (Basak et al., in prep. (black-lined red circles), this study (red circles)), Southwest Pacific core PS75/073-2 (57˚S, Basak et al., in prep.; black triangles) and South Pacific cores SO213-59-2 (purple triangles) and SO213-60-1 (pink triangles) (Molina-Kescher et al., 2016). Arrow marks average ε_{Nd} signature of modern deep water in the Southeast Pacific (2800-4000 m, see Figs. 4.1 and 4.3 for details). Crosses indicate ε_{Nd} values of core PS75/056-1 with internal errors >0.45 (Tab. S4.1). Thin red lines mark the range of analytical uncertainty (propagated errors). B) Benthic $\delta^{13}C$ of Southeast Pacific cores PS75/056-1 (Ullermann et al., 2016; red circles) and E11-2 (56˚S, Ninnemann and Charles, 2002; grey circles). C) ε_{Nd} of North Atlantic core ODP1063 from the Bermuda Rise (33˚N, Böhm et al., 2015). D) ε_{Nd} of South Atlantic cores RC11-83/TNO57-21 (Cape Basin, 40/41˚S, Piotrowski et al., 2005; blue triangles) and GeoB 3808-6 (Central Atlantic, 31˚S, Jonkers et al., 2015; orange diamonds), and equatorial Indian Ocean core SK129-CR2 (3˚N, Piotrowski et al., 2009; green squares). Note different ε_{Nd} scales in A, C, and D. Grey bars indicate glacial stages.

4.5. Discussion

4.5.1. Does the ε_{Nd} record document past deep water signatures?

Agreement of the core-top fossil fish teeth/debris Nd isotopes with that of dissolved Nd isotopes in the Southeast Pacific CDW has been previously demonstrated (Basak et al., in prep.) and is also illustrated in Figure 4.3. Physically cleaned fossil fish teeth and debris have been demonstrated to reliably record the bottom water ε_{Nd} signature (Martin and Haley, 2000; Thomas et al., 2003; Martin and Scher, 2004) even in areas with potential influence of easily leachable basaltic material and hydrothermal input such as in the vicinity of the EPR (Molina-Kescher et al., 2014b). Given our record is entirely based on thorough physical cleaning of fossilized bio-phosphate (section 4.3.2), we exclude systematic contamination from particles, which could potentially modify the measured isotope signature. Therefore we interpret our record as the bottom water ε_{Nd} signature of CDW in the Southeast Pacific.

However, the isotope signature of the bottom water itself may be influenced by external Nd contributions that do not result from water mass mixing. The core location in the central Southeast Pacific, remote from any landmasses, precludes significant influence from rivers (Fig. 4.1A), and atmospheric deposition of particles has been shown not to influence the deep water ε_{Nd} signature even in areas of high dust deposition (e.g., Jones et al., 1994; Stichel et al., 2015). Moreover, using a mass balance calculation, Carter et al. (2012) showed that dust input is too little to explain surface water ε_{Nd} differences in the Southeast Pacific ACC. Since surface ocean ε_{Nd} signatures experience limited contribution from dust, the deep ocean is least likely to be affected. Hence, although dust deposition varied between glacial and interglacial periods at our core site (Lamy et al., 2014), this is not expected to have affected the bottom water ε_{Nd} signature. A process that may contribute to the isotope composition of deep water is boundary exchange (Lacan and Jeandel, 2001; 2005a), which has recently been suggested to occur at the Antarctic margin (Carter et al., 2012; Rickli et al., 2014) and the Deep Western Boundary Currents at Chatham Rise and the Madagascan margin (Wilson et al., 2012; Noble et al., 2013). A possible candidate for boundary exchange in deep waters in the open Southeast Pacific is the EPR (Jeandel et al., 2013; Basak et al., 2015). Further, exchange with the seafloor or re-suspended sediments as well as contributions from pore water fluids may influence bottom water ε_{Nd} signatures (Carter et al., 2012; Abbott et al., 2015b). Core PS75/056-1 is located in the open ocean far from continental margins and not close to oceanic ridges (Fig. 4.1). Modern ocean dissolved Nd isotope signatures in this area have been interpreted to reflect water mass mixing rather than boundary exchange (Basak et al., 2015), and radiogenic modification of the seawater ε_{Nd} signature by boundary exchange is only observed for one site located directly above the ridge (Basak et al., 2015) and for one location were bottom waters were sampled very close to the seafloor (Carter et al., 2012). Thus, the variability observed in the ε_{Nd} record at site PS75/056-1 over the last 140 ka most likely results from water mass mixing, which is also supported by co-variability of ε_{Nd} with $\delta^{13}C$ from cores PS75/056-1 and E11-2 (Ninnemann and Charles, 2002; Ullermann et al., 2016) (Fig. 4.4). Basak et al. (2015) concluded that admixture of NPDW into circumpolar waters influences the isotope composition north of the SAF. Therefore, we interpret the more positive core-top ε_{Nd} signatures in core PS75/056-1 (ε_{Nd} = -7.7) relative to CDW in the Southwest Pacific (ε_{Nd} = -8.3, Basak et al., in prep.) and other Southern Ocean sectors (e.g., Piotrowski et al., 2004) as increased influence of NPDW to the eastern and central South Pacific CDW, in line with previous studies (Molina-Kescher et al., 2014a; 2016; Basak et al., 2015; Basak et al., in prep.).

4.5.2. Glacial-interglacial variability of Southeast Pacific deep water ε_{Nd}

Modern CDW, as a mixture of NADW and NPDW, has an ε_{Nd} signature of -8 to -9 (Piepgras and Wasserburg, 1982; Stichel et al., 2012b; Basak et al., 2015). By simple mixing calculations using Nd isotopes and concentrations of the North Atlantic and North Pacific endmembers, Stichel et al. (2012b) showed that modern CDW from the South Atlantic is composed of approximately 70-75% NADW. During the LGM, the fraction of NADW in CDW was significantly lower, as indicated by more positive ε_{Nd} and more negative benthic $\delta^{13}C$ in the deep Southern Ocean (e.g., Ninnemann and Charles, 2002; Hodell et al., 2003; Piotrowski et al., 2004; McCave et al., 2008; Noble et al., 2013; Skinner et al., 2013; Lippold et al., 2016; Basak et al., in prep.).

Our new results show that the Nd isotope composition of CDW in the Southeast Pacific was similar to that of the Holocene during most parts of MIS 5 (ε_{Nd} = -7.2 ± 0.3). This implies a comparable contribution of NADW to the composition of CDW during both intervals (Fig. 4.4). Similarly, during the mid of MIS 3 (~46 ka), ε_{Nd} values of -7.4 ± 0.4 suggest a comparable composition of CDW as during the interglacials (Fig. 4.4). Neodymium isotope ratios of ε_{Nd} = -5.8 ± 0.2 during both MIS 6 and the LGM suggest a similar CDW composition during these periods. That is, relative contributions of NADW and NPDW to CDW and hence the circulation dynamics during these glacial periods must have been similar. Following Basak et al. (in prep.) who suggested deep stratification in the Southeast Pacific during the LGM, we interpret the MIS 6 ε_{Nd} record at core PS75/056-1 to reflect a water mass, isolated from significant AABW influence. A deep stratification during the LGM is also in line with $\delta^{13}C$ and radiocarbon records from the Southwest

Pacific that show a better ventilation of deep waters of Ross Sea origin below ~3500-4000 m than in overlying waters (McCave et al., 2008; Sikes et al., 2016).

Assuming simple conservative mixing of NADW and NPDW, we can estimate their relative contributions to CDW in the Southeast Pacific. We use the following endmembers: ε_{Nd} = -13.5 and [Nd] = 17.5 pmol/kg (Piepgras and Wasserburg, 1987) for the NADW and ε_{Nd} = -3.5 and [Nd] = 44.4 pmol/kg (Fröllje et al., 2016) for the NPDW. We assume temporal stability of the endmember compositions of Atlantic and Pacific-derived waters over the last 140 ka based on studies by van de Flierdt et al. (2006) and Foster et al. (2007) for the Atlantic and Abouchami et al. (1997) and Marchitto et al. (2005) for the Pacific. We also assume no change in the Nd concentration based on the study of Foster and Vance (2006). From model results and Pb isotope variations in North Atlantic ferromanganese crusts, these authors concluded that the higher exposure of continental shelves during glacials due to the lower sea level was compensated by decreased chemical weathering, thereby balancing the total cation flux to the oceans over glacial-interglacial timescales. Our calculations show that during the interglacials the Southeast Pacific was represented by ~65% NADW in comparison to the modern values of 70-75% NADW in the Atlantic sector of the Southern Ocean (Stichel et al., 2012b) and the Southwest Pacific (Holocene sediments of core PS75/073-2, Basak et al., in prep.). This reflects the location of the Southeast Pacific at the far end of the NADW flow path (see also Molina-Kescher et al., 2016). In addition, the Southeast Pacific also experiences higher influence of NPDW (section 4.5.1). The Atlantic-derived fraction in CDW was ~40% during the LGM and MIS 6, thus reduced by 25% compared to the modern and MIS 5. During MIS 4, the Atlantic component was ~50% and thus only reduced by 15% compared to interglacial conditions.

Analogous to the last deglaciation (Basak et al., in prep.), the transition from the penultimate glacial (MIS 6) into MIS 5e is represented by a decrease in ε_{Nd} values by 1.5 to 2 units in core PS75/056-1 (Fig. 4.5), suggesting a re-strengthening of NADW advection (Piotrowski et al., 2004; 2009; Noble et al., 2013; Skinner et al., 2013; Jonkers et al., 2015; Lippold et al., 2016; Basak et al., in prep.). Basak et al. (in prep.) suggested that additionally, the Southern Ocean had significant influence on the CDW ε_{Nd} signature at the start of the last glacial termination (T1) through increased mixing of AABW formed in the Ross Sea (ε_{Nd} = -7; e.g., Basak et al., 2015). They showed that the isotope composition of CDW decreased before NADW advection re-strengthened, precluding an exclusive NADW control on CDW ε_{Nd} changes. Our age model and the sedimentation rates of PS75/056-1 during the penultimate deglaciation do not allow for such detailed interpretation of the factors contributing to the ε_{Nd} decrease across termination 2 (T2). Yet, the early decrease in ε_{Nd} relative to North Atlantic ε_{Nd} records (e.g., Böhm et al., 2015) also at T2 and a pattern similar to T1 with a brief halt in the ε_{Nd} decrease, makes it likely that the Southern Ocean processes also contributed to the ε_{Nd} decrease during the penultimate deglaciation (Figs. 4.4, 4.5). Future studies will be necessary to increase the resolution and age control across T2 to test this assumption.

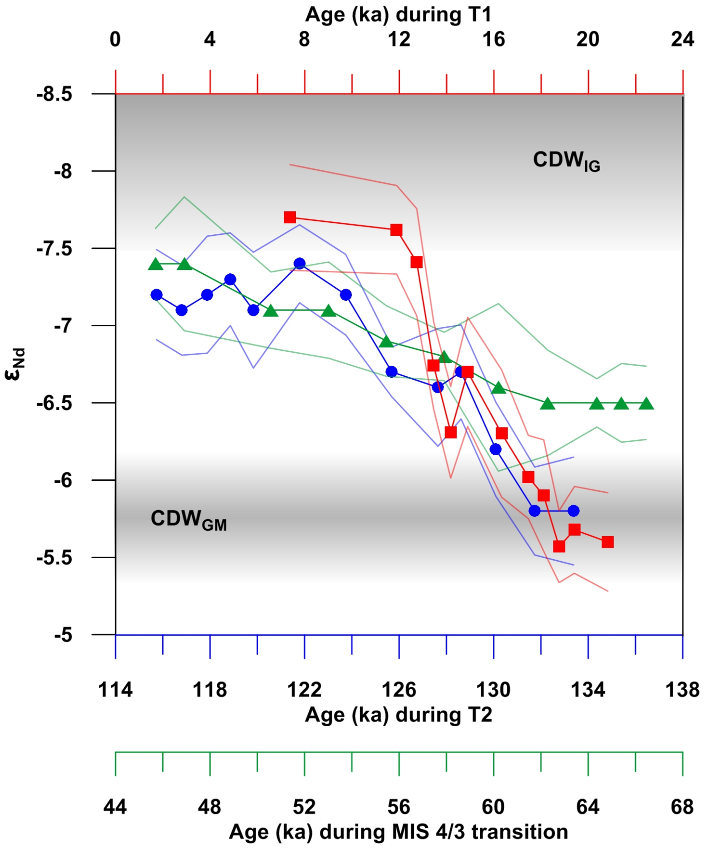

Figure 4.5: ε_{Nd} of core PS75/056-1 from three time-intervals of T1 (red squares; Basak et al., in prep.), T2 (blue circles; this study) and the MIS 4/3 transition (green triangles; this study). Grey areas mark interglacial (IG) and glacial maximum (GM) compositions of CDW in the Southeast Pacific. Thin colored lines show analytical uncertainty (propagated errors).

4.5.3. Inter-basin differences in CDW ε_{Nd} composition

Despite the similar glacial-interglacial ε_{Nd} variability between ocean basins, there are considerable differences in absolute ε_{Nd} values between the Southeast Pacific site and its counterparts in the Indian and Atlantic Oceans (Figs. 4.4, 4.6). Core GeoB3808-6 from the central South Atlantic (31° S, 15° W, 3213 m), is located at the boundary between NADW and southern-sourced deep waters (Jonkers et al., 2015), whereas cores SO213-59-2 (45° S, 116° W, 3161 m) and SO213-60-1 (44°S, 119° W, 3471 m) contain a significant portion of Pacific waters throughout the records (Molina-Kescher et al., 2016). In contrast, core PS75/056-1 (55° S, 114° W, 3581 m) and those from the equatorial Indian Ocean

(SK129-CR2, 3° N, 76° E, 3800 m; Piotrowski et al., 2009) and Cape Basin (RC11-83/TNO57-21, 40-41° S, 7-9° E, 4718-4981 m; Piotrowski et al., 2005), reflect the modern composition and past evolution of CDW (see section 4.5.1 and Piotrowski et al., 2005; 2009). As discussed in section 4.5.1, core PS75/056-1 is subject to a small direct contribution from modified NPDW. South Atlantic and Indian Ocean cores, on the other hand, exhibit a higher proportion and/or some direct influence of NADW. Piotrowski et al. (2009) suggested that the identical glacial ε_{Nd} signature of -6.5 at the Indian and South Atlantic sites indicates the presence of the same southern-sourced deep water mass. The CDW ε_{Nd} in the Southeast Pacific was in average more radiogenic by ~1.2 to 1.4 ε_{Nd} units during MIS 5 and the Holocene (ε_{Nd} = -7.2 to -7.7), and by ~0.8 units during MIS 6 and the LGM (ε_{Nd} = -5.8 ± 0.2) compared to the South Atlantic and Indian Ocean records (Fig. 4.6). Therefore, the Southeast Pacific, being located at the end of the NADW advection route, receives CDW whose ε_{Nd} has been modified due to gradual mixing with deep and bottom waters along its flowpath around Antarctica during both glacials and interglacials. The spatial ε_{Nd} difference between basins (expressed as $\Delta\varepsilon_{Nd}$ in Fig. 4.6) can thus be best explained by a varying contribution of direct NADW in the Atlantic and Indian Oceans and its negligible contribution in the South Pacific, that in turn receives a higher proportion of NPDW.

Moreover, different bottom water masses in the Atlantic/Indian and Pacific sectors of the Southern Ocean with their distinct ε_{Nd} signatures (Weddell Sea Bottom Water ε_{Nd} = -9 (Stichel et al., 2012b) and RSBW ε_{Nd} = -7 (Rickli et al., 2014; Basak et al., 2015)) were potentially isolated from overlying CDW (McCave et al., 2008; Basak et al., in prep.). Thus, a glacial dominance of these waters is unlikely to explain the different absolute glacial values of ε_{Nd} = -6.5 in the Atlantic and Indian Oceans and ε_{Nd} = -5.8 in the Pacific. Instead, the different glacial ε_{Nd} signatures in CDW in the Southern Ocean sectors are best explained by different proportions of NADW and NPDW in glacial CDW.

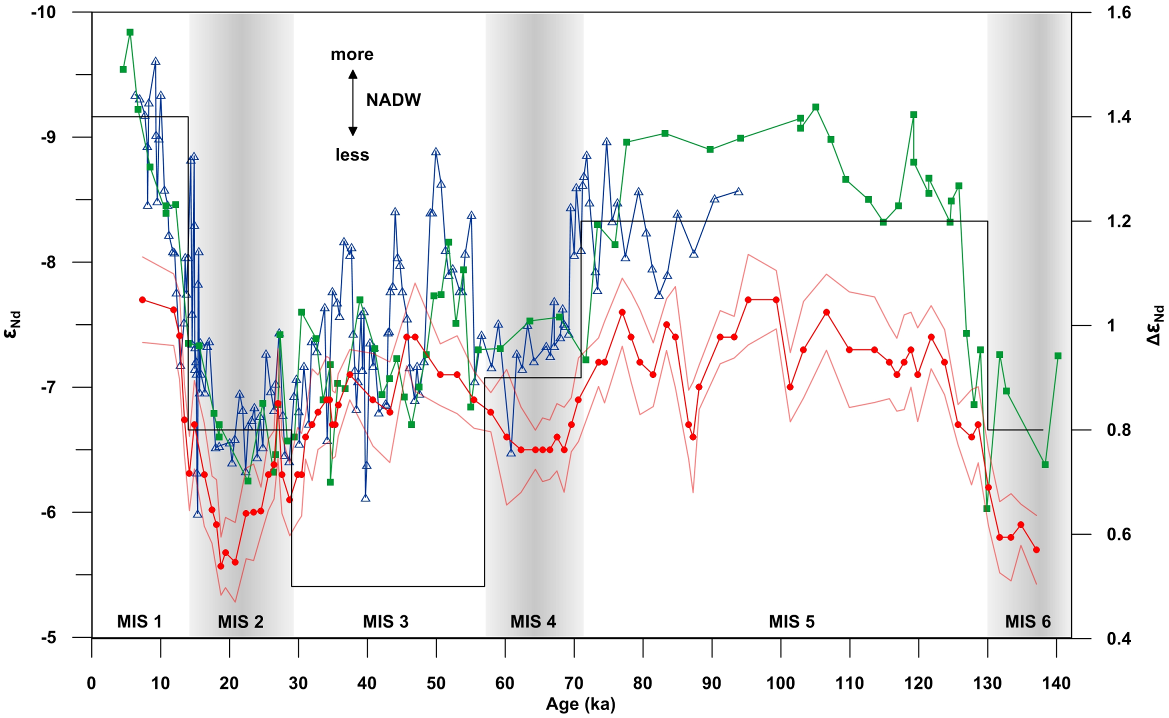

Figure 4.6: Comparison of ε_{Nd} records of cores bathed today by CDW. PS75/056-1 (Basak et al., in prep. and this study; red circles), RC11-83/TNO57-21 (Southeast Atlantic, Piotrowski et al., 2005; blue triangles) and SK129-CR2 (tropical Indian Ocean, Piotrowski et al., 2009; green squares) on the same ε_{Nd} scale. Thin red lines show analytical uncertainty (propagated errors) of core PS75/056-1. Black line indicates the average calculated ε_{Nd} difference ($\Delta\varepsilon_{Nd}$) between the Southeast Pacific and the averaged South Atlantic/Indian sites for MIS 1-6 (0-138 ka). Low $\Delta\varepsilon_{Nd}$ during MIS 3 is due to highly variable ε_{Nd} signatures in the Atlantic and Indian Ocean records.

Consistent with the above observation, the ε_{Nd} difference between the Southeast Pacific and the two sites in the South Atlantic and Indian Oceans was enhanced during interglacials, when NADW advection was stronger. South Atlantic and Indian Oceans ε_{Nd} decreased at the glacial terminations by 2.5-3 ε_{Nd} units to values of ε_{Nd} = -9 to -10 during the interglacials, while ε_{Nd} in the Southeast Pacific decreased by ~2 units to ε_{Nd} = -7.5 to -7.7 in the Holocene and MIS 5 (Fig. 4.6). This is in line with a higher magnitude of $\delta^{13}C$ changes in the South Atlantic than in the South Pacific at glacial-interglacial transitions (Ninnemann and Charles, 2002) and reflects the stronger influence of NADW in the South Atlantic and the transmission of this signal into the Indian Ocean. The basic difference of the South Pacific ε_{Nd} record compared to those from the South Atlantic/Indian Oceans is the missing or muted influence of fluctuations in active NADW flow and/or depth variation due to its location at the end of the NADW route. We do not expect that variability in NPDW contributions i.e., through glacial deepening of NPDW (Matsumoto et al., 2002), are responsible for the lower magnitude of variability in the Pacific record (see also Molina-Kescher et al., 2016). Although downcore ε_{Nd} records for the last 30 ka (PS75/073-2, PS75/056-1, PS75/059-2; for locations see Fig. 4.1A) suggest locally different degrees of NPDW influence in the Southwest and Southeast Pacific (Basak et al., in prep.), this does not significantly affect the absolute glacial-interglacial ε_{Nd} change. That is, core PS75/073-2, located south of the APF and bathed by pure LCDW without any active influence of NPDW, shows a similar magnitude of change in deglacial ε_{Nd} as PS75/056-1 (~2 ε_{Nd} units; Fig. 4.4 and Basak et al., in prep.). We therefore suggest that the observed glacial-interglacial changes in PS75/056-1 reliably record endmember changes of CDW. Hence, the additional 0.5-1.4 changes in ε_{Nd} in the Atlantic potentially result from direct NADW contributions.

4.5.4. Evolution of the ε_{Nd} signature in Southeast Pacific CDW during Marine Isotope Stages 3 and 4

A notable feature of our ε_{Nd} record is the different isotope composition of CDW during MIS 4 (ε_{Nd} = -6.6 ± 0.2) compared to the full glacial stages of MIS 2 and MIS 6 (ε_{Nd} = -5.8). More radiogenic ε_{Nd} signatures during MIS 4 than during MIS 2 and 6 also prevailed in the deep South Atlantic and equatorial Indian Oceans (Piotrowski et al., 2005; 2009; Fig. 4.6). The relative difference in ε_{Nd} values between full glacials and MIS 4 is nearly the same in all of the three cores (~1 ε_{Nd} unit), although the absolute values are less radiogenic at the Atlantic and Indian Ocean sites by ~0.9 ε_{Nd} units (Fig. 4.6), again suggesting a higher NADW component at the latter sites and a higher NPDW influence in the Southeast Pacific. Given the similarity in the ε_{Nd} increase during the MIS 5a/4 transition in all available Southern Ocean records (Piotrowski et al., 2005; 2009; this study) suggests that although the absolute amount of NADW in the Southeast Pacific was lower than in the other basins (as expressed by more radiogenic ε_{Nd} values), the reduction of NADW contribution influenced CDW at all sites.

Less radiogenic ε_{Nd} values during MIS 4 compared to MIS 2/6 suggest that the NADW fraction in CDW was higher during MIS 4, in line with deep North Atlantic ε_{Nd} signatures that were intermediate between glacial and interglacial signatures (Fig. 4.4; Böhm et al., 2015). Sortable silt, $^{231}Pa/^{230}Th$, and $\delta^{13}C$ data from the North Atlantic indicate a shoaled and weakened deep overturning during MIS 4 similar to the LGM (Guihou et al., 2011; Thornalley et al., 2013), which has recently been suggested to coincide with enhanced carbon storage in the deep Atlantic (Yu et al., 2016). By combining $^{231}Pa/^{230}Th$ and Nd isotope data from Bermuda Rise core ODP 1063, Böhm et al. (2015) showed that the North Atlantic circulation gradually changed from MIS 5 to MIS 2 and was in an intermediate state between full glacial and interglacial conditions during MIS 4. In contrast, full glacial conditions prevailed in the Southern Ocean during MIS 4, implying a water mass geometry akin to the LGM (Schaefer et al., 2015). These authors showed that New

Zealand glacier accumulation was similar during the LGM and MIS 4 and so were sea-ice extent, surface and deep temperatures, dust flux, and ocean stratification in the Southern Ocean (Schaefer et al., 2015 and references therein). With comparable boundary conditions between the LGM and MIS 4 it is only reasonable to assume that MIS 4 also had similar deep Nd and carbon divide in the South Pacific as observed during the LGM (McCave et al., 2008; Basak et al., in prep.). Thus, in accordance with the LGM conditions, we do not expect significant AABW contribution to Southeast Pacific CDW during MIS 4. Consequently, the different ε_{Nd} compositions of CDW during MIS 2/6 and MIS 4 under similar, i.e., full glacial, Southern Ocean climatic conditions (Schaefer et al., 2015) indicate that different amounts of NADW determined the CDW composition in the Southeast Pacific.

The following transition from MIS 4 into MIS 3 is characterized by a gradual ε_{Nd} decrease (from ε_{Nd} = -6.5 to -7.4) in the Southeast Pacific (Fig. 4.4), suggesting an increase in the contribution of NADW to CDW. This is potentially accompanied by upward mixing of AABW similar to T1 and T2. Comparable ε_{Nd} signatures during mid-MIS 3 and the interglacials (ε_{Nd} > -7.2) in our record hint towards a similar water mass geometry during these intervals. The long-term gradual increase in the ε_{Nd} values in core PS75/056-1 throughout MIS 3 towards the LGM suggests a gradual decrease of the NADW fraction in CDW with lowest proportion reached at the LGM (Fig. 4.4). The occurrence of negative ε_{Nd} signatures during mid-MIS 3 (peak values at ~46 ka) was delayed compared to Atlantic and Indian Ocean peak values (Fig. 4.6). Despite some uncertainties in the age model in this part of our record (Fig. 4.2), age model uncertainties are not large enough to produce the observed delay by 8-9 ka, which is supported by peak $\delta^{13}C$ values in core E11-2 at the same time (Ninnemann and Charles, 2002; Fig. 4.4). Rather, we speculate that the early pulses of NADW contribution to the South Atlantic and Indian Ocean sites at the MIS 4/3 transition i.e., during Dansgaard-Oeschger interstadial 14 (Böhm et al., 2015; Piotrowski et al., 2008), are not recorded in the Southeast Pacific. This is similar to what is observed during the last deglacial: while a ‘false start’ of NADW production is recorded in the Southeast Atlantic during the last deglaciation prior to the Bølling warming (Piotrowski et al., 2004), this NADW pulse is neither recorded in core PS75/056-1, nor in a higher resolved core form the Southwest Pacific (Basak et al., in prep.; Fig. 4.4) and the Indian Ocean (Piotrowski et al., 2009). Variability observed in the South Atlantic and Indian Oceans during MIS 3 have been attributed to short-term variations in NADW formation (Piotrowski et al., 2008; 2009; Gutjahr et al., 2010; Gutjahr and Lippold, 2011). We suggest, that the lack of small-scale variations in the Southeast Pacific during MIS 3 and early MIS 2 is due to the isolation of the South Pacific from short-term NADW pulses rather than to inadequate temporal resolution of our record., This observation is consistent with that of Piotrowski et al. (2009), who showed slightly attenuated ε_{Nd} variability during MIS 3 in the equatorial Indian Ocean compared to the South Atlantic.

4.5.5. Decoupling of ε_{Nd} and carbon isotope signals

Benthic foraminiferal $\delta^{13}C$ is widely used as a paleoceanographic proxy for water mass circulation (e.g., Duplessy et al., 1988; Ninnemann and Charles, 2002; Curry and Oppo, 2005). Yet, benthic $\delta^{13}C$ is additionally influenced by processes other than ocean circulation such as air-sea gas exchange and/or enhanced organic matter degradation at the seafloor (e.g., Broecker and Maier-Reimer, 1992; Mackensen et al., 1993). It has been demonstrated that both Nd isotopes and $\delta^{13}C$ signals from the same core generally co-vary, suggesting they are predominantly recording glacial-interglacial water mass variations in the South Atlantic and Indian Oceans (Piotrowski et al., 2005; 2009; Jonkers et al., 2015; Wilson et al., 2015). However, differences in the proxies were used to infer that carbon and neodymium isotope signals were decoupled during some parts of the last glacial-interglacial cycle in particular at glacial inceptions and climate transitions in the Atlantic and Indian Oceans in that benthic $\delta^{13}C$ was additionally influenced by changing global mean $\delta^{13}C$, nutrient cycling, and/or air-sea gas exchange (Piotrowski et al., 2005; 2009; Wilson et al., 2015). A lead of carbon isotope over ε_{Nd} changes at glacial-interglacial transitions and decoupling of both proxies in glacial climates in the Atlantic and Indian Oceans was suggested to reflect a Southern Ocean control on $\delta^{13}C$, whereas Nd isotopes were suggested to reflect the North Atlantic-controlled water mass signal (Piotrowski et al., 2005; Wilson et al., 2015). High consistency in the long-term pattern of $\delta^{13}C$ (cores PS75/056-1, E11-2) and ε_{Nd} in PS75/056-1 suggests that the same process influenced both proxies for most of the time recorded (Fig. 4.4). Thus, our Nd isotope record confirms the interpretation of Ninnemann and Charles (2002) that $\delta^{13}C$ in core E11-2 records glacial-interglacial variability in NADW advection to the Southeast Pacific.

However, Nd isotope signatures are not identical during MIS 2 and MIS 4 (see section 4.5.4), while $\delta^{13}C$ shows the same values in both stages (Fig. 4.4). Our ε_{Nd} record clearly suggests a higher NADW component during MIS 4 than during MIS 2 and 6, whereas $\delta^{13}C$ values suggest the same amount of NADW during MIS 2 and MIS 4. Further, Ninnemann and Charles (2002) observed that the glacial $\delta^{13}C$ values in core E11-2 are similar to those of NPDW, suggesting an isolation of the South Pacific from NADW supply. In contrast, the ε_{Nd} record of core PS75/056-1 shows that the glacial Southeast Pacific did not reach the modern day NPDW endmember composition of ε_{Nd} = -3.5 (e.g., Fröllje et al.,

2016) but was less radiogenic than NPDW by 2 and 3 ε_{Nd} units during the LGM and MIS 4, respectively, implying a significant contribution of Atlantic-derived waters (Fig. 4.4).

Our results from the Southeast Pacific thus confirm previous observations of a decoupling of Nd and carbon isotope signals during glacial inceptions (Wilson et al., 2015), but do not allow interpreting lead-lag relationships as observed in the South Atlantic (Piotrowski et al., 2005) due to the lower sampling resolution in our core. Similar $\delta^{13}C$ values during MIS 2 and 4 in core E11-2 are in line with prevailing full glacial conditions in the Southern Hemisphere during both periods as reflected by equal Southern Ocean sea surface and deep temperatures, sea-ice extent, ocean stratification, dust fluxes and New Zealand glacier accumulation (Schaefer et al., 2015 and references therein). In contrast, the ε_{Nd} record of core PS75/056-1 in combination with that from the Bermuda Rise (Böhm et al., 2015) suggests a North Atlantic water mass control on the composition of Southeast Pacific CDW (Fig. 4.4). On the basis of differences in absolute ε_{Nd} between NPDW and CDW during all glacials and deviations in ε_{Nd} between MIS 2/6 and MIS 4, the similarities in $\delta^{13}C$ values can only be explained when considering additional processes apart from water mass mixing that lowered the $\delta^{13}C$ in CDW in the Southeast Pacific (and in other sectors of the Southern Ocean). This highlights the use of Nd isotopes for disentangling circulation-related changes in carbon isotopes from those governed by biogeochemical processes.

4.6. Conclusions

By extending the existing Nd isotope record of core PS75/056-1 (Basak et al., in prep.) throughout the last glacial-interglacial cycle to about 140 ka, we demonstrate that the amount of NADW in Southeast Pacific CDW was similar during the two most recent interglacial periods. Further, full glacials of MIS 2 and 6 were characterized by the same amount of NADW reduction, whereas MIS 4 experienced a 10% higher NADW component. This is consistent with stronger NADW formation during MIS 4 than during MIS 2 and 6 in the North Atlantic, but in contrast to the full-glacial conditions characterizing MIS 4 in the Southern Hemisphere, clearly demonstrating the NADW control on the glacial-interglacial composition of CDW. The penultimate glacial termination shows an early ε_{Nd} decrease at the time of Southern Hemisphere warming but prior to the re-strengthening of NADW in the North Atlantic, similar to the situation in the Southeast Pacific during T1 described previously (Basak et al., in prep.). This obvious Southern Ocean control on ε_{Nd} has been explained by the breakup of deep stratification in the Southern Ocean and an increased admixture of RSBW into CDW. Our new data now indicate that this was also a feature of T2. The MIS 4/3 transition, on the other hand, was more gradual, but resulted in ε_{Nd} signatures similar to interglacials during mid-MIS 3, indicating a similar water mass geometry as during interglacials.

Differences in the ε_{Nd} signature of CDW between the Pacific, Atlantic, and Indian Oceans reflect the higher active influence of NADW in the Atlantic and Indian Oceans. We consider the ε_{Nd} record of PS75/056-1 a reliable record of the CDW endmember composition and suggest that it can be used to disentangle active influence of NADW at the Atlantic and Indian Ocean core sites from water mass mixing within CDW. Moreover, it demonstrates that Atlantic component water also entered the Southern Ocean during full glacial conditions. The lack of millennial-scale fluctuations in the Southeast Pacific during MIS 3 and the MIS 5/4 transition, that mark the records from the South Atlantic and tropical Indian Oceans, suggests isolation of the Pacific sector of the Southern Ocean from small scale NADW pulses.

We further showed that deep Southeast Pacific $\delta^{13}C$ changes are decoupled from ε_{Nd} variations during glacials, suggesting additional influence of biogeochemical processes in the Southern Ocean on benthic $\delta^{13}C$, in line with previous studies (Piotrowski et al., 2005; 2009; Wilson et al., 2015).

4.7. Acknowledgements

Data presented in this article are provided in Tables S4.1-S4.2 in the supporting information and on Pangaea (www.pangaea.de) under doi: 10.1594/PANGAEA.858876. We thank the entire scientific party, captain, and crew of *R/V Polarstern* cruise ANT-XXVI/2 and the German Ministry for Education and Research (BMBF) for financially supporting the cruise. We are grateful to the members of the Max Planck Research Group for Marine Isotope Geochemistry in particular M. Schulz for help with daily laboratory work and P. Böning for help with isotope measurements. Financial support for this study came from the Institute for Chemistry and Biology of the Marine Environment (ICBM) and the Max Planck Institute for Marine Microbiology.

4.8. Supplementary data tables

Table S4.1: Neodymium isotope record of core PS75/056-1 over the last 140 ka (30-140 ka: this study, 0-30 ka: Basak et al., in prep.).

Sample interval (cm)	Age (ka)	Normalized $^{143}Nd/^{144}Nd$ [b]	ε_{Nd}	± Internal ε_{Nd} error (2σ SE)	± External ε_{Nd} error (2σ SD)	± Propagated ε_{Nd} error [c]
0-1 [a]	7.38	0.512243	-7.7	0.12	0.32	0.34
4.5-6 [a, d]	8.51	0.512292	-6.8	0.48	0.32	0.58
9.5-11 [a, d]	9.63	0.512229	-8.0	0.86	0.25	0.90
14.5-16 [a, d]	10.76	0.512254	-7.5	0.67	0.34	0.75
19.5-21 [a]	11.89	0.512247	-7.6	0.14	0.25	0.29
24.5-26 [a]	12.74	0.512258	-7.4	0.24	0.25	0.35
29.5-31 [a]	13.45	0.512293	-6.7	0.13	0.25	0.28
34.5-36 [a]	14.17	0.512314	-6.3	0.16	0.25	0.30
39.5-41 [a]	14.89	0.512294	-6.7	0.25	0.25	0.35
44.5-46 [a]	16.33	0.512315	-6.3	0.36	0.20	0.41
49.5-51 [a]	17.46	0.512329	-6.0	0.10	0.25	0.27
54.5-56 [a]	18.11	0.512335	-5.9	0.26	0.25	0.36
59.5-61 [a]	18.76	0.512353	-5.6	0.03	0.23	0.23
64.5-66 [a]	19.41	0.512347	-5.7	0.16	0.23	0.28
69.5-71 [a]	20.82	0.512351	-5.6	0.22	0.23	0.32
74.5-76 [a]	22.41	0.512331	-6.0	0.28	0.23	0.36
79.5-81 [a]	23.45	0.512328	-6.0	0.31	0.23	0.39
84.5-86 [a]	24.56	0.512330	-6.0	0.14	0.13	0.19
89.5-91 [a]	25.63	0.512314	-6.3	0.22	0.18	0.28
94.5-96 [a]	26.45	0.512311	-6.4	0.11	0.25	0.27
99.5-101 [a]	27.02	0.512286	-6.9	0.36	0.25	0.44
104.5-106 [a]	27.59	0.512313	-6.3	0.15	0.27	0.31
114.5-116 [a]	28.73	0.512325	-6.1	0.10	0.27	0.29
124.5-126 [a]	29.87	0.512315	-6.3	0.30	0.23	0.38
129.5-131	30.44	0.512317	-6.3	0.19	0.27	0.33
134.5-136	31.01	0.512302	-6.6	0.15	0.09	0.17
144.5-146	31.98	0.512293	-6.7	0.30	0.33	0.45
154.5-156	32.82	0.512290	-6.8	0.19	0.23	0.30
169.5-171	34.08	0.512286	-6.9	0.26	0.23	0.35
174.5-176	34.50	0.512285	-6.9	0.29	0.16	0.33
179.5-181	34.92	0.512295	-6.7	0.22	0.16	0.27
184.5-186	35.34	0.512293	-6.7	0.18	0.18	0.25
189.5-191	35.76	0.512287	-6.9	0.10	0.23	0.25
199.5-201 [d]	36.60	0.512297	-6.7	0.55	0.33	0.64
209.5-211	37.44	0.512276	-7.1	0.09	0.18	0.20
214.5-216 [d]	38.36	0.512305	-6.5	0.88	0.27	0.92
224.5-226	40.80	0.512287	-6.9	0.29	0.23	0.37
234.5-236	43.25	0.512290	-6.8	0.33	0.23	0.40
239.5-241 [d]	44.47	0.512234	-7.9	0.46	0.36	0.58
244.5-246	45.69	0.512259	-7.4	0.21	0.09	0.23
250-251	46.91	0.512257	-7.4	0.28	0.33	0.43
265-266	50.57	0.512273	-7.1	0.09	0.23	0.25
275-276	53.02	0.512275	-7.1	0.21	0.23	0.31
285-286	55.46	0.512286	-6.9	0.18	0.14	0.23
295-296	57.90	0.512287	-6.8	0.07	0.14	0.16
305-306	60.20	0.512300	-6.6	0.43	0.33	0.54
315-316	62.28	0.512306	-6.5	0.29	0.18	0.34
325-326	64.37	0.512307	-6.5	0.07	0.14	0.16
330-331	65.41	0.512302	-6.5	0.18	0.18	0.25
335-336	66.45	0.512303	-6.5	0.11	0.21	0.24
340-341	67.49	0.512299	-6.6	0.20	0.18	0.27
345-346	68.53	0.512304	-6.5	0.25	0.23	0.34
350-351	69.58	0.512294	-6.7	0.12	0.18	0.22
355-356	70.62	0.512284	-6.9	0.26	0.21	0.33

Table S4.1: continued.

Sample interval (cm)	**Age (ka)**	**Normalized ^{143}Nd/^{144}Nd [b]**	**ε_{Nd}**	**± Internal ε_{Nd} error (2σ SE)**	**± External ε_{Nd} error (2σ SD)**	**± Propagated ε_{Nd} error [c]**
375-376	74.40	0.512271	-7.2	0.23	0.23	0.33
395-396	76.97	0.512246	-7.6	0.22	0.16	0.27
405-406	78.25	0.512260	-7.4	0.33	0.14	0.36
415-416	79.54	0.512270	-7.2	0.35	0.23	0.42
430-431	81.47	0.512272	-7.1	0.18	0.18	0.25
435-436 [d]	82.11	0.512278	-7.0	0.75	0.33	0.82
445-446	83.40	0.512254	-7.5	0.13	0.16	0.21
455-456	84.68	0.512260	-7.4	0.31	0.26	0.40
470-471	86.61	0.512292	-6.7	0.21	0.18	0.28
475-476	87.25	0.512300	-6.6	0.21	0.39	0.44
480-481	88.13	0.512279	-7.0	0.11	0.14	0.18
495-496	91.18	0.512259	-7.4	0.14	0.16	0.21
505-506	93.21	0.512257	-7.4	0.09	0.14	0.17
515-516	95.25	0.512244	-7.7	0.04	0.36	0.36
535-536	99.31	0.512242	-7.7	0.17	0.16	0.23
545-546	101.35	0.512278	-7.0	0.21	0.18	0.28
555-556	103.27	0.512262	-7.3	0.11	0.37	0.39
575-576	106.59	0.512249	-7.6	0.27	0.14	0.30
595-596	109.92	0.512266	-7.3	0.29	0.36	0.46
615-616	113.58	0.512266	-7.3	0.22	0.36	0.42
625-626	115.73	0.512266	-7.2	0.11	0.27	0.29
630-631	116.81	0.512273	-7.1	0.11	0.27	0.29
635-636	117.88	0.512268	-7.2	0.08	0.37	0.38
640-641	118.86	0.512262	-7.3	0.13	0.27	0.30
645-646	119.83	0.512274	-7.1	0.06	0.37	0.37
655-656	121.79	0.512259	-7.4	0.21	0.14	0.25
665-666	123.74	0.512269	-7.2	0.22	0.14	0.26
675-676	125.69	0.512292	-6.7	0.08	0.14	0.16
685-686	127.64	0.512299	-6.6	0.09	0.37	0.38
690-691	128.62	0.512294	-6.7	0.27	0.14	0.30
695-696	130.09	0.512318	-6.2	0.12	0.28	0.30
700-701	131.74	0.512341	-5.8	0.09	0.27	0.28
705-706	133.38	0.512340	-5.8	0.31	0.16	0.35
710-711	134.81	0.512334	-5.9	0.04	0.16	0.16
720-721	137.07	0.512347	-5.7	0.05	0.27	0.27

[a] Data originally reported in Basak et al. (in prep.).

[b] Reported ^{143}Nd/^{144}Nd ratios were normalized to the session-average JNdi-1 value relative to the reported JNdi-1 value of 0.512115 (Tanaka et al., 2000).

[c] Propagated error combined from internal and external reproducibility.

[d] ε_{Nd} values with internal errors ≥0.45 excluded from figures due to bad measurement.

Table S4.2: Updated age model for reference core MD97-2120 using ^{14}C ages, the Kawakawa Tephra (cf. Basak et al., in prep.), and tuning of SST record (Pahnke et al., 2003) to EPICA Dome C δD record on AICC2012 age scale (Jouzel et al., 2007; Veres et al., 2013; Bazin et al., 2013) (this study), and age model for core PS75/056-1 based on tuning the benthic δ^{18}O record (Lamy et al., 2014) to that of MD97-2120 (Pahnke and Zahn, 2005) (Basak et al., in prep. (<30 ka); this study (>30 ka)).

Core	Depth (cm)	Age (ka)	Type	Sed. rate (cm/ka)	Data reference
MD97-2120	22.5	2.06	^{14}C	8.8	Pahnke et al. (2003)
	36.5	3.66	^{14}C	14.8	Pahnke et al. (2003)
	98.5	7.86	^{14}C	21.9	Pahnke et al. (2003)
	202.5	12.61	^{14}C	20.3	Pahnke et al. (2003)
	230.5	13.99	^{14}C	23.7	Pahnke et al. (2003)
	252.5	14.92	^{14}C	20.6	Pahnke et al. (2003)
	330.5	18.7	^{14}C	23.3	Rose et al. (2010)
	344.5	19.3	^{14}C	30.7	Rose et al. (2010)
	390.5	20.8	^{14}C	39.3	Rose et al. (2010)
	418	21.5	^{14}C	13.7	Rose et al. (2010)
	471	25.36	Kawakawa Tephra	16.3	Vandergoes et al. (2013)
	525	28.67	^{14}C	14.8	Pahnke et al. (2003)
	682.4	39.29	SST tuning to EDC δD	9.4	Pahnke et al. (2003)
	756.3	47.19	SST tuning to EDC δD	7.6	Pahnke et al. (2003)
	815.2	54.91	SST tuning to EDC δD	10.6	Pahnke et al. (2003)
	875.5	60.61	SST tuning to EDC δD	17.8	Pahnke et al. (2003)
	1017.8	68.58	SST tuning to EDC δD	9.9	Pahnke et al. (2003)
	1048.6	71.69	SST tuning to EDC δD	5.3	Pahnke et al. (2003)
	1073.6	76.38	SST tuning to EDC δD	15.4	Pahnke et al. (2003)
	1233.0	86.75	SST tuning to EDC δD	10.0	Pahnke et al. (2003)
	1393.7	102.80	SST tuning to EDC δD	17.1	Pahnke et al. (2003)
	1456.4	106.46	SST tuning to EDC δD	4.9	Pahnke et al. (2003)
	1537.8	123.14	SST tuning to EDC δD	9.8	Pahnke et al. (2003)
	1594.9	128.99	SST tuning to EDC δD	14.7	Pahnke et al. (2003)
	1696.4	135.91	SST tuning to EDC δD	14.7	Pahnke et al. (2003)
PS75/056-1	6.6	8.74	benthic δ^{18}O tuning to MD97-2120	4.4	Lamy et al. (2014)
	22.1	12.25	benthic δ^{18}O tuning to MD97-2120	7.0	Lamy et al. (2014)
	40.9	14.95	benthic δ^{18}O tuning to MD97-2120	3.3	Lamy et al. (2014)
	48.3	17.17	benthic δ^{18}O tuning to MD97-2120	7.7	Lamy et al. (2014)
	67.7	19.69	benthic δ^{18}O tuning to MD97-2120	2.5	Lamy et al. (2014)
	73.3	21.93	benthic δ^{18}O tuning to MD97-2120	4.7	Lamy et al. (2014)
	93.0	26.17	benthic δ^{18}O tuning to MD97-2120	8.8	Lamy et al. (2014)
	139.8	31.51	benthic δ^{18}O tuning to MD97-2120	11.9	Lamy et al. (2014)
	212.4	37.60	benthic δ^{18}O tuning to MD97-2120	4.1	Lamy et al. (2014)
	301.4	59.33	benthic δ^{18}O tuning to MD97-2120	4.8	Lamy et al. (2014)
	362.0	71.98	benthic δ^{18}O tuning to MD97-2120	5.5	Lamy et al. (2014)
	374.7	74.30	benthic δ^{18}O tuning to MD97-2120	7.8	Lamy et al. (2014)
	477.3	87.49	benthic δ^{18}O tuning to MD97-2120	4.9	Lamy et al. (2014)
	552.6	102.78	benthic δ^{18}O tuning to MD97-2120	6.0	Lamy et al. (2014)
	608.5	112.08	benthic δ^{18}O tuning to MD97-2120	4.7	Lamy et al. (2014)
	635.4	117.86	benthic δ^{18}O tuning to MD97-2120	5.1	Lamy et al. (2014)
	691.8	128.88	benthic δ^{18}O tuning to MD97-2120	3.0	Lamy et al. (2014)
	708.4	134.34	benthic δ^{18}O tuning to MD97-2120	4.4	Lamy et al. (2014)
	758.0	145.54	benthic δ^{18}O tuning to MD97-2120	1.9	Lamy et al. (2014)

5. Leaching of sedimentary Fe-Mn oxides fails to produce reliable Nd isotope records in the deep South Pacific

Abstract

Neodymium isotopes extracted from fossil fish teeth and/or foraminifera are considered as reliable proxy to trace water mass distribution in the past ocean. Inadequate presence of fish teeth or foraminifera within the sediments is one of the limitations that often complicate paleoceanographic studies. This has been particularly true in the deep South Pacific. Authigenic Fe-Mn oxide coatings of marine sediment particles are also considered a potential archive of bottom water Nd isotopes, however, reliable extraction of the bottom water Nd signal from these oxide phases is complicated. Establishing the feasibility of Fe-Mn oxides as a potential archive of bottom water Nd isotopes in the deep South Pacific could increase the spatial resolution of cores that record changing ε_{Nd} signatures throughout the last glacial-interglacial transition in this area. In this study, different leaching experiments were undertaken to extract authigenic Fe-Mn oxides from marine sediments in the deep South Pacific. These experiments were designed to develop a gentle leaching procedure that does not attack sedimentary phases other than Fe-Mn oxides.

Best agreement between Nd isotopes derived from the leached solutions from a particular sediment interval and that of the few existing contemporaneous fish teeth were achieved when i) the coarse fraction of sediments (>63 µm) was used, ii) the leaching procedure was performed with low concentrated acetic acid (2%), and iii) a carbonate removal step was omitted at the beginning of the experiment. However, measured ε_{Nd} signatures from none of the leaching solutions could fully reproduce fish teeth and modern bottom water ε_{Nd} signatures in the deep Pacific cores. Results from these experiments suggest that leaching methods should be carefully tested against more robust archives, such as fish teeth or foraminifera, for a given location before interpreting potential paleo-seawater variability. This is especially true for low carbonate environments, given the observed effect of initial carbonate removal, which increases the offset in ε_{Nd} signatures measured in leaching solutions and contemporaneous fish teeth.

5.1. Introduction

Neodymium isotope ratios ($^{143}Nd/^{144}Nd$, expressed as ε_{Nd}; for details see chapter 1) are widely used as tracer for paleoceanographic investigations (e.g., Frank, 2002; Goldstein and Hemming, 2003). Fossil fish teeth/debris and foraminifera are the most reliable sedimentary archives for the extraction of paleo seawater ε_{Nd} signatures (e.g., Martin and Haley, 2000; Martin and Scher, 2004; Thomas et al., 2003; Thomas, 2004; Thomas and Via, 2007; Martin et al., 2010; Roberts et al., 2010; 2012; Piotrowski et al., 2012; Kraft et al., 2013; Molina-Kescher et al., 2014b; Huck et al., 2016). However, the lack of availability of these archives often becomes the major limitation, which hinders its application in sediments collected from great water depths. In the deep South Pacific, most deep sea samples studied here (>4500 m water depth) are characterised by an absence of fossil fish remains and low carbonate preservation is potentially responsible for low foraminiferal abundance. This is in contrast to deep sites of ~3000-4100 m water depth from the South Pacific, where ε_{Nd} records are entirely based on the analysis of fossil fish teeth/debris and foraminifera (cf. chapters 3 and 4 of this thesis). Many previous studies have shown that Nd isotopes measured in leached solutions of sedimentary Fe-Mn oxide coatings represent reliable past bottom water ε_{Nd} signatures (e.g., Rutberg et al., 2000; Bayon et al., 2002; Piotrowski et al., 2004; 2012; Pahnke et al., 2008; Gutjahr et al., 2008; Martin et al., 2010; Böhm et al., 2015; Jonkers et al., 2015; Wei et al., 2016). Unlike Nd isotope signatures derived from fossil fish remains and foraminifera, the leachate-derived Nd isotope values are more easily affected by the local lithology of the sample or the presence of pre-formed riverine Fe-Mn oxides (Bayon et al., 2004; Elmore et al., 2011; Charbonnier et al., 2012; Kraft et al., 2013; Noble et al., 2013; Wilson et al., 2013; 2015; Molina-Kescher et al., 2014b; Osborne et al., 2014; Wu et al., 2015). Any attempt to use ferromanganese oxides in a particular oceanic setting is often preceded by sets of leaching experiments and comparison to more robust archives aiming to achieve the 1:1 relationship between the Nd isotope signatures of leachings and that of ambient seawater (Gutjahr et al., 2007; Martin et al., 2010; Charbonnier et al., 2012; Wilson et al., 2012; 2013; 2015; Molina-Kescher et al., 2014b; Osborne et al., 2014; Wu et al., 2015; Wei et al., 2016). Thus, in the absence of conventional archives, and in order to increase the spatial coverage of last deglacial deep sea ε_{Nd} records in the South Pacific, a series of leaching experiments were undertaken to test the applicability of using Fe-Mn oxides as an archive for past bottom water ε_{Nd}.

The primary objective of this study was to develop a gentle leaching method for Fe-Mn oxides that reliably extracts the ε_{Nd} signature from deep sediments in the South Pacific. The investigated cores are from the western and central South Pacific Ocean collected at water depth >4500 m (Tab. 5.1). Materials from *USNS Eltanin* cores E14-6 and E17-9 were provided by the core repository of the Antarctic Marine Geology Research Facility at Florida State University. Sediment samples from core PS75/095-5 and its associated multicore PS75/095-6 were provided by the Alfred Wegener Institute for Polar and Marine Research at Bremerhaven and collected on board *RV Polarstern* during expedition ANT-XXVI/2 (Gersonde, 2011). The following sections provide a description of the experiments and their results together with implications for future studies that use Fe-Mn oxide leachings.

Table 5.1: Core locations in the South Pacific Ocean. PS75/095-6 is the associated multicore of piston core PS75/095-5.

Core	Latitude	Longitude	Water depth (m)
PS75/095-5	57°01.18' S	174˚25.80' W	4853
PS75/095-6	57°01.18' S	174˚25.87' W	4857
E14-6	57°0.6' S	160˚9.0' W	4517
E17-9	63°4.8' S	135˚4.8' W	4849

5.2. Methods

5.2.1. Sample processing and fish teeth preparation

All sediments were freeze-dried, wet-sieved to separate the >63 µm fraction, and dried in an oven at 50˚ C. The >63 µm fraction was used for isolating fish teeth under a binocular microscope. Fish teeth were found in two sampling intervals in core E14-6 and in one sample interval in core PS75/095 and E17-9 each. Fish teeth were cleaned and prepared for measurement using the standard protocol described in chapters 3 and 4. Briefly, the fish teeth were sonicated in methanol and MilliQ water (18 MΩ, Millipore), treated with a 1:1 mixture of MilliQ water and 30% H_2O_2, dissolved in a mixture of concentrated HNO_3 and HCl (1:1), and re-dissolved in 1 N HNO_3. Two-step column chemistry was performed for isolation of Nd (modified from Pin and Zalduegui, 1997). First, Eichrom TRU-Spec resin (particle size of 100-150 µm) was used for isolation of REEs, followed by separation of Nd from interfering REEs by TrisKem Ln-Spec resin (particle size of 50-100 µm) with 0.23 N HCl as eluent. The samples were treated with a mixture of HNO_3:H_2O_2 (1:1) and dissolved in 2% HNO_3 for analysis. All used acids were of optima grade quality.

5.2.2. Leaching experiments

To test the effect of lithogenic particle contamination on Nd isotope signatures in sediment-derived Fe-Mn oxide leachates, the two sampling intervals in core E14-6 were chosen, where i) adequate fish teeth were present for chemical analyses and ii) sufficient amount of detrital materials could be retrieved in the fine (<63 µm) and coarse (>63 µm) fraction (Tab. 5.2). First, following previous studies (Wilson et al., 2013; 2015; Molina-Kescher et al., 2014b; Wu et al., 2015), the prior removal of carbonates from the sediments, usually done with buffered acetic acid, was tested against no carbonate removal. Second, based on previous internal results from another South Pacific core (C. Basak, 2012, pers. comm.), the conventional leaching protocol, which uses 0.02 M hydroxylamine hydrochloride (HH) in 25% (v/v) acetic acid (e.g., Chester and Hughes, 1967; Rutberg et al., 2000; Piotrowski et al., 2004), was modified by decreasing the strength of the acetic acid to 10%, 2%, and 1% (v/v). Additionally, both fine and coarse size fractions were tested.

The general leaching protocol started with decarbonation of the samples with Na-acetate buffered acetic acid with a pH of 5 (made from mixture of optima grade glacial acetic acid and MilliQ water) for approximately 12 h (optional, see above). After all CO_2 has gassed out, samples were washed repeatedly with MilliQ water and subsequently leached with the corresponding leaching solution (1%, 2%, 10% (v/v)) for 1-1.5 h in a rotating shaker. Afterwards, the samples were centrifuged twice for 5 min at 4000 rpm, the supernatant transferred to a clean Teflon beaker, dried at 140 ˚C and re-dissolved in 1 N HNO_3 in preparation for column chemistry.

In detail, in the first experiment, the fine fraction of two samples was split into five subsamples and leached with 0.02 M HH in 2% (v/v) and 10% (v/v) acetic acid, each with and without an initial decarbonation step. A leaching solution of 0.02 M HH in 1% (v/v) was only used without prior carbonate removal due to limited amount of material. Based on the results from these tests, the coarse fraction of both samples, which had very limited amount of material, was leached with the 2% leaching solution, without previously removing the carbonate fraction. An overview of the conducted leaching experiments is given in Figure 5.1 and Table 5.2.

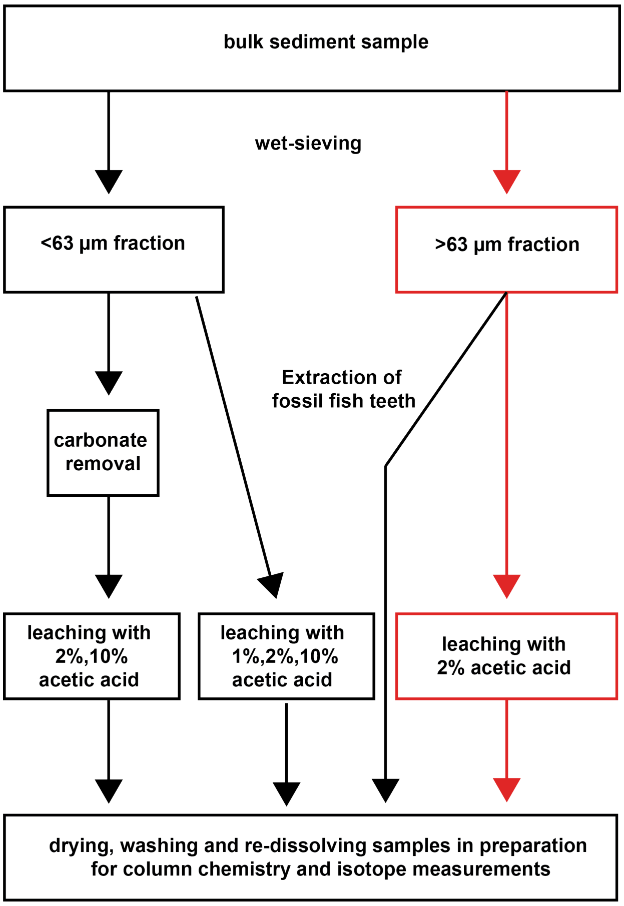

Figure 5.1: Flowchart of procedures conducted to extract Fe-Mn oxides from deep-sea sediments. Red-bordered path indicates the method that was used for creating the downcore record of core E14-6 (Fig. 5.3). All leaching solutions had 0.02 M HH. Carbonate removal was done using Na-acetate buffered acetic acid with a pH of 5.

Based on the results from the above described experiments the ultimate protocol used for the creation of a downcore record of core E14-6 and for leaching additional samples from the others cores included leaching of the >63 µm fraction of dry sediment samples with 0.02 M HH in 2% (v/v) acetic acid for 1 h in a rotating shaker followed by centrifuging and decanting twice to remove any remaining particles. The prior removal of carbonates was avoided. Column chemistry was done as described in section 5.2.1 and in more detail in chapters 3 and 4.

5.2.3. Isotope measurements

All samples were measured for their Nd isotope composition on a ThermoScientific *Neptune Plus* multi-collector inductively coupled plasma mass spectrometer (MC-ICP-MS) at the University of Oldenburg. A more detailed description of the measurement setup is given in chapters 3 and 4. All samples were corrected for instrumental mass bias with $^{146}Nd/^{144}Nd = 0.7219$ using an exponential law (O'Nions et al., 1977). The Nd standard

JNdi-1 was measured at the same concentrations as the samples in each session and all samples were normalised to the reported JNdi-1 value of $^{143}Nd/^{144}Nd = 0.512115$ (Tanaka et al., 2000). External reproducibility of the measurements was calculated for each session from JNdi-1 values, and was generally better ±0.3 ε_{Nd} units (2σ SD). The errors for the individual measurements are reported as propagated errors, gained from the combination of external reproducibility of the measurement session and individual internal errors (Tab. 5.2 and 5.3). The procedural blank included the leaching step and column chemistry and was <11 pg Nd (n=4).

5.3. Results and discussion

5.3.1. Leaching protocol tested on samples from core E14-6

The results of the leaching experiments conducted on samples from two intervals of core E14-6 show that the leaching procedure using 0.02 M HH in 2% acetic acid on the coarse fraction without initial decarbonation yields the best results when compared to the corresponding fish teeth ε_{Nd} data (Fig. 5.2). Fish teeth and leachates in these samples reveal slightly different ε_{Nd} values, with the leachates being more positive by 0.3-0.4 ε_{Nd} units. Yet, this observation is only based on two samples and thus cannot be considered a systematic offset. Further, the two fish teeth used in this record were particularly hard to clean. During dissolution of the teeth, both had observable adhered particles, which could not be further cleaned off with standard procedures and are thus potentially compromised by contamination. Martin et al. (2010) previously reported that leaching of the >63 µm fraction leads to less contamination from clays, which is in agreement with the results obtained here. The lack of sufficient material in the coarse fraction precluded further splitting of the samples, and thus a systematic study of the effects of acid strength, sample to solution ratio and decarbonation on this size fraction was not possible.

All other leaching procedures tested on these samples reveal more radiogenic ε_{Nd} values, suggesting enhanced contamination from lithogenic sediments that are in general more radiogenic than seawater in the South Pacific (e.g., Noble et al., 2013; Molina-Kescher et al., 2014b). The results least similar to fish teeth are achieved when a carbonate removal step is performed before the leaching of the Fe-Mn oxides from the <63 µm fraction (Fig. 5.2). Similar results regarding the removal of carbonate were recently published for leaching experiments conducted on sediments from the South Pacific north of 50° S (Molina-Kescher et al., 2014b), the Indian Ocean (Wilson et al., 2013; 2015) and the South China Sea (Wu et al., 2015). These studies showed that decarbonation of samples prior to the HH leaching leads to dissolution of non-authigenic phases during the HH leaching, thereby shifting ε_{Nd} signatures towards the bulk sediment composition. Direct leaching (i.e., no prior removal of carbonates) of the <63 µm fraction with 0.02 M HH in 1%, 2%, and 10% acetic acid lead to results closer to the 1:1 line in Figure 5.2, but still are too radiogenic. Comparison of the results using 1%, 2%, and 10% acetic acid shows that simple lowering of the acid strength in the HH-leaching solution does not necessarily lead to better agreement between leachate and fish teeth ε_{Nd}. This raises the questions if the acid strength is an important variable in the leaching process.

Table 5.2: Results of leaching experiments conducted on two samples of core E14-6 together with those of additional cores and fish teeth measurements. Bottom water at site PS75/095 has an ε_{Nd} signature of -8.2 ± 0.3 (4822 m water depth; Basak et al., 2015).

Core	**Interval (cm)**	**Material**	**Carbonate removal**	**Acetic acid strength**	**ε_{Nd}**	**± Propagated error**
E14-6	47-49 cm	Fish teeth			-6.3	0.26
E14-6	47-49 cm	<63µm	yes	2%	-3.7	0.18
E14-6	47-49 cm	<63µm	no	2%	-5.5	0.23
E14-6	47-49 cm	<63µm	yes	10%	-3.9	0.18
E14-6	47-49 cm	<63µm	no	10%	-5.4	0.20
E14-6	47-49 cm	<63µm	no	1%	-4.6	0.48
E14-6	47-49 cm	>63µm	no	2%	-5.9	0.14
E14-6	77-79 cm	Fish teeth			-6.6	0.17
E14-6	77-79 cm	<63µm	yes	2%	-3.9	0.27
E14-6	77-79 cm	<63µm	no	2%	-5.9	0.25
E14-6	77-79 cm	<63µm	yes	10%	-3.9	0.19
E14-6	77-79 cm	<63µm	no	10%	-5.4	0.18
E14-6	77-79 cm	<63µm	no	1%	-5.5	0.20
E14-6	77-79 cm	>63µm	no	2%	-6.3	0.30
E17-9	44-46 cm	Fish teeth			-5.3	0.21
E17-9	44-46 cm	<63 µm	no	2%	-3.1	0.21
E17-9	44-46 cm	>63µm	no	2%	-4.0	0.29
PS75/095-5	48.5-50 cm	Fish teeth			-6.7	0.34
PS75/095-5	48.5-50 cm	>63µm	no	2%	-5.6	0.22
PS75/095-6	0-1 cm	>63µm	no	2%	-7.1	0.16

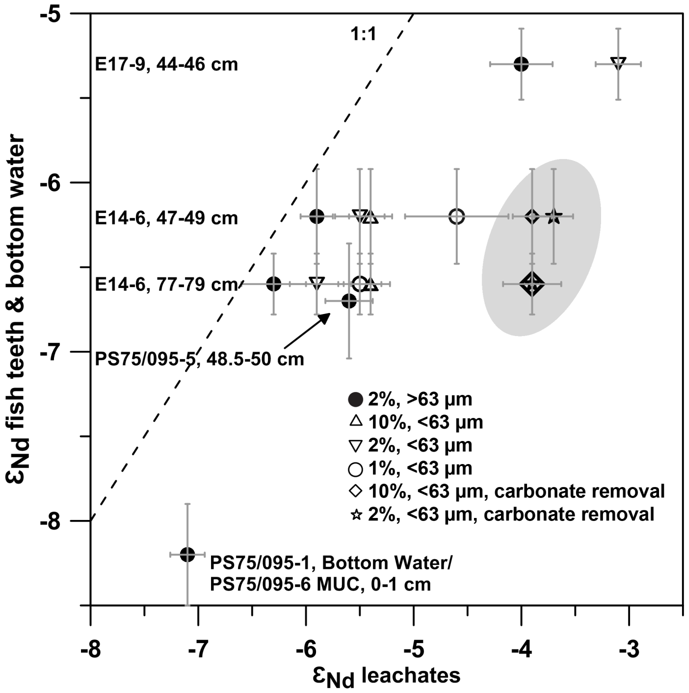

Figure 5.2: Comparison of leaching results to fish teeth and bottom water measurements. Black circles indicate >63 µm fraction of samples leached with 0.02 M HH in 2% acetic acid without prior carbonate removal. Results on the same horizontal level are from the same sample interval. Grey area marks the samples, which have undergone carbonate removal. Note that the two rightmost data points of sample 77-79 cm from core E14-6 lie on top of each other. Leachate data of MUC PS75/095-6 is compared to bottom water data of the same site (PS75/095 in Basak et al., 2015).

The results obtained here suggest that the critical step is the decarbonation, rather than the strength of the acetic acid of the HH solution (Fig. 5.2). However, carbonate contents in the two studied sample intervals are very low (≤0.1% $CaCO_3$; Chase et al., 2003), thus, attacking of sedimentary phases other than carbonates by the decarbonation acid obviously also influences the ε_{Nd} signature of the ultimately used HH-leaching solution. From the available data it is not clear which phases were attacked, but Fe-Mn oxides are potential candidates. This would explain the higher deviation of the HH-leaching solution from fish teeth in these samples, but clearly needs more detailed and systematic investigations, for example by additionally measuring the ε_{Nd} signatures in the decarbonation acid and/or lithogenic element concentrations in the HH-leaching solution. Another difficulty is the unknown ideal sample to solution ratio and the very low amount of material in the coarse fraction of ~0.15 g (see section 5.3.3). Hence, from the results gained in this study, it can only be concluded that from the conducted experiments, leaching of the >63 µm fraction with 2% acetic acid and omission of initial decarbonation yields the best results. Despite the discussed ambiguities, this protocol was used to create an ε_{Nd} record of core E14-6 (section 5.3.2; Fig. 5.3, Tab. 5.3), although the consistency of the data is highly questionable due to scarce reliable reference values from fossil fish teeth and the observed fish teeth-leachate offset. Additionally, results from the other cores show that the developed procedure is not robust in similar environments at nearby sites (see section 5.3.3 and Fig. 5.2).

5.3.2. Downcore record of core E14-6

On first glance, the observed trend in ε_{Nd} of core E14-6 looks similar to those reported for other South Pacific cores (Noble et al., 2013; chapter 3). The most pronounced change in ε_{Nd} signatures is observed between the uppermost two samples representing the Holocene and late deglaciation, and the deeper samples originating from the early glacial termination and the last glacial period (Fig. 5.3). Higher carbonate contents in the upper ~30 cm of this core (12-23% $CaCO_3$; Chase et al., 2003; comprising the uppermost two samples; Tab 5.3) might have buffered the lithogenic fraction of the sediments from being attacked by the acetic acid. Results presented here and in previous studies (Wilson et al., 2013; 2015; Molina-Kescher et al., 2014b; Wu et al., 2015) showed that application of initial decarbonation can affect leaching results. Based on these observations the sediments carbonate content is a critical variable in the leaching process. It is therefore reasonable to speculate that the glacial sediments in core E14-6 with less then 0.1% carbonate were significantly attacked by the leaching solution even when the decarbonation step is omitted. The different carbonate content thus has the potential to significantly contribute to the observed Holocene-glacial offset.

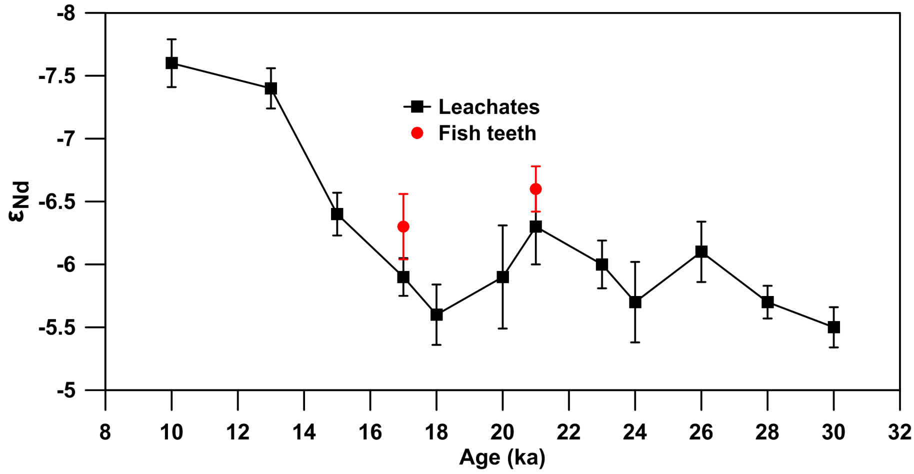

Figure 5.3: Leachate record of core E14-6 supplemented by two fish teeth measurements. Leaching of the sediments coarse fraction (>63 µm) was done using 0.02 M HH in 2% acetic acid. Ages interpolated from age model published in Chase et al. (2003).

The two uppermost samples of this core (ε_{Nd} = -7.5 ± 0.1) deviate by 0.6-0.8 ε_{Nd} units from modern bottom waters at the nearest site (ε_{Nd} = -8.2 at PS75/095; Basak et al., 2015), suggesting a higher (i.e., double) offset than observed by comparison of leachates to fish teeth (Fig. 5.3). This agrees with the high deviation of leachates of nearby cores PS75/095-5/6 and E17-9 from fish teeth and bottom waters at these sites (0.7-1.3 ε_{Nd} units; Fig. 5.2 and section 5.3.3). In this case, contaminating particles that could not be cleaned off from fish teeth samples of core E14-6 (see section 5.3.1), may have compromised the ε_{Nd} signatures of these, that is they are shifted in the direction of the more radiogenic sediment composition. Thus, the measured offset of 0.3-0.4 ε_{Nd} units between leachates and contemporaneous fish teeth does probably not reflect the real offset.

In summary, ε_{Nd} signatures in core E14-6 cannot be considered representative of contemporaneous bottom waters in the Southwest Pacific. Given the indicated lithological control on the extraction of ε_{Nd} signals by HH-leaching solutions, a higher chronological resolution of more reliable reference values from fish debris or foraminifera is needed for the verification and interpretation of the downcore record.

Table 5.3: Combined results of sediment core E14-6.

Core	Interval (cm)	Age (ka)[a]	Material	^{143}Nd/^{144}Nd	ε_{Nd}	± Internal error (2σ)	± External error (2σ)	± Propagated error
E14-6	7-9.5	10	leachate	0.512249	-7.6	0.14	0.12	0.18
E14-6	25-27	13	leachate	0.512261	-7.4	0.10	0.12	0.16
E14-6	35-37	15	leachate	0.512310	-6.4	0.11	0.12	0.16
E14-6	47-49	17	leachate	0.512336	-5.9	0.08	0.12	0.14
E14-6	47-49	17	fish teeth	0.512317	-6.3	0.12	0.23	0.26
E14-6	57-59	18	leachate	0.512351	-5.6	0.20	0.12	0.23
E14-6	67-69	20	leachate	0.512334	-5.9	0.29	0.29	0.41
E14-6	77-79	21	leachate	0.512314	-6.3	0.27	0.12	0.30
E14-6	77-79	21	fish teeth	0.512301	-6.6	0.04	0.17	0.17
E14-6	87-89	23	leachate	0.512329	-6.0	0.15	0.12	0.19
E14-6	97-99	24	leachate	0.512346	-5.7	0.17	0.27	0.32
E14-6	107-109	26	leachate	0.512325	-6.1	0.20	0.12	0.23
E14-6	117-119	28	leachate	0.512346	-5.7	0.02	0.12	0.12
E14-6	128-130	30	leachate	0.512354	-5.5	0.10	0.12	0.16

[a] Ages interpolated from age model published in Chase et al. (2003). For details see text.

Further, the low sample (1 sample per 10 cm) and age model resolution do not allow for a clear attribution of the ε_{Nd} shift observed in core E14-6 to a specific time of the last deglaciation. The ages used in Figure 5.3 were interpolated based on a published age model, which depends on abundance stratigraphy of *Eucampia antarctica* (L. Burckle, unpublished data) and *Cycladophora davisiana* (J. Hays, unpublished data) and one glacial radiocarbon date (Y. Zheng, unpublished data) (Chase et al., 2003). According to this age model, the position of the Last Glacial Maximum (LGM; ~18 ka B.P.) is at ~50-60 cm depth. In another study, the LGM depth for this core was set to 112-113 cm (Crosta et al., 1998), which yields a discrepancy of approximately 50-60 cm for the position of the LGM between the age models. From the above discussion it became clear that it is neither possible to come up with a reliable ε_{Nd} value for glacial bottom waters in core E14-6 nor a precise timing of the ε_{Nd} excursion can be determined. Overall, the lack of consistency in ε_{Nd} between different archives prevents the use of Fe-Mn leachates in this core for paleo-circulation reconstructions.

5.3.3. Leaching protocol tested at other South Pacific sites

When tested on additional samples from cores E17-9, PS75/095-5 and PS75/095-6 the established leaching procedure (2% acetic acid, >63µm) failed to produce results that are within error of the corresponding fish teeth or bottom water (Tab. 5.2; Fig. 5.2). The ε_{Nd} signature of the leachates is significantly more radiogenic by more than 1 ε_{Nd} unit. One possible problem might be the even lower amount of material available in the >63 µm fraction in these cores compared to E14-6. In core E14-6 it was possible to leach ~0.15 g of sediment, whereas in the other cores the sample volume was <0.1 g. Due to the lack of material to test the right amount of leaching solution only 3 mL was used for leaching the coarse fractions, instead of 12 mL used to leach ~0.5 g of the fine fraction. It was shown before that the sample to solution ratio has an effect on the leaching results (Piotrowski et al., 2012; Wilson et al., 2013; Wu et al., 2015). Thus, it can very well be, that the amount of material was too low in all samples, including those of core E14-6, and that sufficient amount of sediment or the further reduction of acid volume would have lead to results closer to the fish teeth values. Overall, the results support the conclusion drawn above, that leaching of Fe-Mn oxides fail to reliably reproduce past ε_{Nd} seawater signatures.

Based on previous studies by Elmore et al. (2011) and Roberts et al. (2010), Piotrowski et al. (2012) concluded that leachings of marine sediments do not necessarily record reliable past seawater ε_{Nd} signals in all marine settings. The results presented here confirm this conclusion and suggest that leaching methods should be crosschecked with ε_{Nd} of other paleo-seawater archives e.g., fossil fish debris or foraminifera, before interpreting the records. Establishing a reliable leaching protocol for the Southeast Pacific would require more systematic testing of variables during the leaching process (cf. Wilson et al., 2013).

5.4. Acknowledgements

The Antarctic Marine Geology Research Facility at Florida State University and F. Lamy and R. Gersonde (both AWI) are acknowledged for providing material of Eltanin and Polarstern cores, respectively. C. Basak, C. Ehlert and K. Pahnke contributed to the discussion and interpretations of the results. P. Böning helped with isotope measurements and M. Schulz is acknowledged for help with daily labwork. Financial support for this study came from the Institute for Chemistry and Biology of the Marine Environment (ICBM) and the Max Planck Institute for Marine Microbiology.

6. Conclusions and perspectives

6.1. Main conclusions

The major research objectives of this thesis as outlined in the introduction were to (1) investigate the input of REEs and Nd isotopes to coastal and open ocean waters near the Hawaiian Islands to contribute to a better understanding of trace element and isotope sources and cycling in seawater, particularly in the North Pacific (chapter 2) and (2) to study last deglacial and glacial-interglacial ocean circulation and water mass mixing in the South Pacific, a highly relevant area for global ocean and climate change in the past (chapters 3, 4 and 5). Hence, Nd isotopes were used to study processes in present-day seawater as well as in the past ocean. These two applications are intrinsically linked, since understanding the mechanisms that control budgets and cycling of rare earth elements (and therefore Nd isotopes) in the modern ocean is of paramount importance for their application in paleoceanographic studies. During the past years, additional geochemical processes have been observed that influence the Nd isotope composition of seawater, thereby compromising the generally conservative behaviour of Nd isotopes. These include boundary exchange at continental margins and potentially oceanic ridges and the seafloor (Lacan and Jeandel, 2001, 2005a; Jeandel et al., 2007; 2013; Carter et al., 2012), and benthic flux of REEs from the sediments into bottom waters (Haley and Klinkhammer, 2003; Abbott et al., 2015a,b). Here, the connection between modern Nd budgets and cycling and the paleoceanographic application of Nd isotopes as water mass tracer becomes notably obvious in the determination of the ε_{Nd} signature of NPDW in the North Pacific and the use of NPDW as a mixing component in glacial CDW. Although the adjustment of the Nd concentration and Nd isotope signature of NPDW presented in chapter 2 ([Nd] = 44.4 pmol/kg, ε_{Nd} = -3.5) has only a small effect on mixing calculations when compared to what has often been used as endmember composition ([Nd] = 51.7 pmol/kg, ε_{Nd} = -3.8; Piepgras and Jacobsen, 1988), it reflects the necessity to constantly improve our knowledge of modern processes and budgets to more confidently interpret Nd isotope records for paleoceanographic studies and to better understand their limits.

In the following, the main conclusions and implications of this thesis are summarised with respect to what has been outlined as goals in the introduction section.

(1) Neodymium isotopes and rare earth elements monitor Hawaiian contributions to the coastal and open ocean, and seasonal variations in the Nd isotope signature are ascribed to the variable influence of local *versus* distal sources in the open ocean North Pacific.

The use of Nd isotopes and rare earth elements to trace lithogenic element input to the ocean was investigated in the North Pacific Ocean near the Hawaiian Island of Oahu, with particular emphasis on the surface and subsurface waters (chapter 2). One goal of this study was to evaluate the influence of the Hawaiian Islands to the Nd isotope signature, REE concentrations, and REE patterns in coastal waters and the open ocean North Pacific. It was shown that the coastal waters around Oahu carry a lithogenic REE signal, expressed in relatively flat shale-normalised REE patterns and Gd, Eu, and MREE anomalies together with elevated Ra isotope activities. The radiogenic surface water ε_{Nd} signature (ε_{Nd} = -0.7 to +1.4) clearly hints towards a strong Hawaiian input to these waters. This Hawaiian signal was also observed in the offshore North Pacific, 100 km off Oahu at Hawaii Ocean Time-series Station ALOHA. The combined use of REEs, and Nd and Ra isotopes allowed ascribing this signal to surface and subsurface input from the Hawaiian Islands, showing that volcanic islands cannot be ignored in the REE and Nd isotope budget in the North Pacific. Furthermore, this study aimed to disentangle the influence of local Hawaiian *versus* distal sources that are imprinted to the surface waters by deposition of Asian dust. It was shown that seasonal variability at ALOHA is potentially imprinted to the surface waters by varying contributions from the Hawaiian Islands and Asian dust. Influence of dust deposition to the surface water ε_{Nd} signature is supported by mixing calculations, whereas the low variability and low concentrations of REEs in surface waters was suggested to result from rapid REE cycling in the upper water column. Finally, this study presented new results on colloidal *versus* truly dissolved fractions of REEs in the open ocean. No colloidal associated REEs were found in samples taken from three depths (mixed layer, deep chlorophyll maximum, deep water) at station ALOHA in September 2013. These results, as a first approach, suggest the lack of REE association to colloidal material in the open ocean, which is in contrast to what has been observed in river water (e.g., Goldstein and Jacobsen, 1988; Elderfield et al., 1990; Sholkovitz, 1992; 1995; Andersson et al., 2001; Rousseau et al., 2015). This topic still comprises open research questions, specifically on the dependence of colloidal-associated REEs to lithogenic input events (i.e., dust events) and the general validity of this approach on a wider spatial and temporal scale.

(2) Neodymium isotopes trace intermediate and deep waters in the modern central North Pacific at Station ALOHA and in combination with REE concentrations contribute to a better characterisation of Pacific deep water.

The central North Pacific has a rather sparse coverage of full water column profiles that allow characterisation of deep water masses with respect to their Nd isotope composition and REE pattern (cf. Lacan et al., 2012). Using analyses of Nd isotopes and REE concentrations at Station ALOHA, this study contributes to a higher resolution of complete water column profiles in this area of the world ocean. In particular, by presenting an updated ε_{Nd} signature for NPDW, the study contributes to the better characterisation of this water mass, one of the two endmembers in the meridional overturning circulation that are often used in mixing calculations in modern and paleo seawater studies (e.g., Piotrowski et al., 2004; Robinson and van de Flierdt, 2009; Stichel et al., 2012b; chapters 3 and 4) (see above). Moreover, one important outcome is the overprint of the deep water REE concentration by vertical processes and the resulting impracticality of the use of REE patterns to trace water masses in the deep Pacific.

<u>(3) Southern Ocean processes contributed to the observed changes in water mass structure and mixing in the deep South Pacific during glacial terminations in addition to the general variability of North Atlantic and North Pacific deep water fractions in CDW during the last deglaciation and the last glacial-interglacial cycle.</u>

Neodymium isotopes extracted from fish teeth/debris and foraminifera, were used to reconstruct past variations in ocean circulation and water mass mixing in the deep South Pacific sector of the Southern Ocean (chapters 3 and 4). In chapter 3, the major findings were (1) a prevailing deep stratification in this area during the LGM, expressed in different ε_{Nd} signatures in deep cores (ε_{Nd} = -6 at ~3000-3700 m and ε_{Nd} = -7.5 at >4000 m depth), confirming stable carbon isotope and radiocarbon results (McCave et al., 2008; Sikes et al., 2016; Ronge et al., 2016), which suggests an isolation of bottom waters from CDW in this region, (2) a breakdown of this deep-stratification accompanied by decreasing ε_{Nd} signatures in waters <3700 m with the onset of Southern Hemisphere warming, and (3) a bathymetric and meridional control on deep water mixing processes in the South Pacific. From the observed results it was concluded that de-stratification in the Southern Ocean and mixing of bottom waters into CDW occurred prior to the re-strengthening of NADW formation in the North Atlantic and must have been driven by processes related to climate change in the Southern Hemisphere. Mixing calculations simulating the admixture of glacial RSBW into CDW showed the general feasibility of this process. The results from this study imply that ε_{Nd} records from the last glacial termination should not be interpreted solely in terms of variable NADW advection but should consider the prominent role of Southern Hemisphere climate in deep water mass mixing. Moreover, the results provide evidence for a change in the deep water chemistry due to the de-stratification of the deep Southern Ocean and the role of abyssal waters in sustaining the deep glacial carbon reservoir. Significant NADW influence was demonstrated to control the late deglacial ε_{Nd}

decrease in the South Pacific, and was responsible for the majority of the observed Nd isotope shift in South Pacific CDW.

In chapter 4, the Nd isotope record of core PS75/056-1 was extended into the penultimate glacial period of MIS 6. This 140,000 years long Nd isotope record was used to study the evolution of Nd isotope signatures in the Southeast Pacific over the last glacial-interglacial cycle and is the first record of this timescale and from the high latitude Southern Ocean that is entirely based on fossil fish teeth and debris and therefore can be considered highly reliable. Major findings of this study include attenuated magnitudes of deglacial ε_{Nd} changes in the Southeast Pacific compared to the Atlantic and Indian Ocean due to lower or complete lack of direct NADW influence. The glacial-interglacial variability was similar between the basins and glacial ε_{Nd} signatures that do not reach the NPDW endmember argue against a complete cessation of NADW contribution to the Southern Ocean during the last 140,000 years. Comparison of the last two glacials (MIS 2 and 6) suggested a similar water mass structure during glacial periods, which was significantly different from interglacials (Holocene, MIS 5) and also had less NADW contribution than the glacial MIS 4. It was further concluded that glacial-interglacial changes in water mass mixing and circulation are mainly governed by changes in NADW advection. Yet, an early deglacial Southern Ocean influence on the CDW ε_{Nd} signature similar to that during termination 1 (chapter 3) was also observed for termination 2. Another finding was a decoupling of Nd and carbon isotope signals, in particular during glacial periods, which is in agreement with previous studies (Piotrowski et al., 2005; Wilson et al., 2015). These results imply that carbon isotope records in the South Pacific cannot be interpreted as exclusively governed by water mass circulation. Instead, changes in Southern Ocean primary productivity likely contribute to the benthic carbon isotope signal. Finally, absent millennial-scale variability of Nd isotopes in the Southeast Pacific was observed and suggested to arise from the missing translation of Northern Hemisphere-induced small-scale changes to South Pacific CDW.

(4) Leaching solutions of ferromanganese oxides from deep South Pacific sediments do not confidently record paleo seawater Nd signatures and leaching protocols need to be extensively tested before applying them in paleoceanographic investigations.

Chapter 5 focused on the reliability of Nd isotope signatures extracted from sedimentary ferromanganese oxides in the deep South Pacific. The major conclusion drawn from this study was that the used leaching protocols are not able to reproduce ambient bottom water ε_{Nd} signatures in this area of the world ocean. Lowering the acid strength did not solve this problem and the findings suggest a particularly critical role of the decarbonation step that is occasionally performed prior to the leaching procedure. Leaching records have been successfully used at other locations to study past water mass circulation (e.g., Piotrowski et al., 2004; Pahnke et al., 2008), but limitations of this method have already been pointed out in many studies (e.g., Bayon et al., 2004; Elmore et al., 2011; Molina-Kescher et al., 2014b; Wilson et al., 2013; 2015). Here, it was shown that even when omitting decarbonation of the samples and lowering the acid strength of the leaching solution, leaching protocols do not reproduce seawater ε_{Nd} signatures in the South Pacific. Further, the results suggest a critical role of the used size fraction of sediments in the leaching process. Thus, this study has shown that the use of ferromanganese leaching solutions to reconstruct past seawater ε_{Nd} signatures needs to be tested against more robust archives on a core-to-core basis before interpreting the results in a paleoceanographic context.

6.2. Perspectives

A couple of open research questions and some ideas for future methodological improvements arise from the results presented in this thesis.

From an analytical point of view, the most obvious question to further investigate is if and how leaching procedures can be improved to produce reliable results of paleo-seawater ε_{Nd} signals in sediments from the deep South Pacific. Previous results (Wilson et al., 2013; 2015; Molina-Kescher et al., 2014b; Wu et al., 2015) and observations from this study suggest that the primary point to address in this context is the influence of the sediments carbon content and the performed initial decarbonation step. Another important variable in improving the success of leaching procedures may be the right choice of the size fraction of sediments (chapter 5; Martin et al., 2010) as well as the ratio between volume of leach solution and amount of sediment material (Piotrowski et al., 2012; Wilson et al., 2013; Wu et al., 2015). Using sedimentary ferromanganese oxide leachates to investigate Nd isotope variations in South Pacific sediments therefore requires systematic studies on the different variables in leaching protocols, similar to what has been done previously for Indian Ocean sediments (Wilson et al., 2013). A reliable leaching protocol for deep South Pacific sediments would be of great benefit for studying past water mass mixing and circulation changes in this area, since the rare presence of foraminifera and fossil bio-phosphates especially in deep to abyssal sediments restrict the availability of deep records and call for different archives to extract Nd isotopes.

In chapter 3 it was demonstrated that foraminifera that are neither chemically nor physically cleaned reliably record past seawater ε_{Nd} signatures. While the omission of chemical cleaning has been previously demonstrated to confidently record past seawater

ε_{Nd} signatures (e.g., Roberts et al., 2010; 2012; Tachikawa et al., 2014), most studies conducted a physical cleaning of foraminifera before dissolution. Direct dissolution of physically (and chemically) uncleaned foraminifera samples has been previously demonstrated to agree with fish teeth values for Cretaceous samples (Charbonnier et al., 2012). Another potential methodological approach is therefore to systematically test the analyses of fully uncleaned foraminifera in combination with a gentle dissolution protocol in other oceanic areas. This ideally includes analyses of trace element concentrations and REE patterns in the calcite fraction (e.g., Charbonnier et al., 2012; Tachikawa et al., 2013; Molina-Kescher et al., 2014b) in combination with the presented approach of measuring the isotope signal in the residual particles to faithfully monitor the detrital contamination in the leaching solutions. This may further allow simplifying cleaning and dissolution protocols of foraminifera for Nd isotope studies.

From the results obtained in chapter 2 it is obvious that the association of REEs and colloidal material in seawater needs to be investigated in more detail. As a first approach, it has been shown in this study, that the open ocean at Station ALOHA does not have colloidal-bound REEs. Yet, it remains unclear, if this observation is temporally limited to times of low dust input, and therefore calls for a systematic time series study. Further, this investigation needs to be extended to a wider area, and may also include the measurement of colloidal and truly dissolved REEs in coastal waters and ideally within a transect from the coastal waters to Station ALOHA. Such a horizontal transect would also allow to further investigate the role of the Hawaiian Islands to the trace metal content at station ALOHA, which so far has been considered negligible (e.g., Karl and Lukas, 1996; Boyle et al., 2005; Fitzsimmons et al., 2015). Another point to address within this topic is a more detailed study of seasonal variations at Station ALOHA on a monthly base. This ideally includes measurements of dissolved and particulate REEs and Nd isotopes in seawater in combination with analyses of Nd and REEs in Hawaiian groundwater, river water and Asian dust collected at the same time to better characterise these sources and their contribution of trace elements to surface waters.

In the paleoceanographic context, there is clearly a need for more isotope records from the deep South Pacific sector of the Southern Ocean. This is especially true for the southwestern and central parts of this area and for locations north of the Pacific-Antarctic Ridge system to further investigate the extension of glacial RSBW in the South Pacific. One important question to address in future studies may be the evolution of the Nd isotope signature of RSBW (and other varieties of AABW) throughout the last deglaciation and the last glacial-interglacial cycle, to gain control on the endmember stability of this water mass.

The 140,000 years record presented in chapter 4 shows that it might be of interest to increase not only the spatial resolution of deep-sea records, but more importantly that a higher time-resolved record is needed to investigate if small-sale variability, as observed in the Atlantic Ocean especially during MIS 3 and MIS 5, can also be found in the South Pacific. This would also allow investigating if the interoceanic difference in ε_{Nd} disappears at times of decreased NADW advection during Northern Hemisphere cold stadials. Finally, a higher sampling resolution in termination 2 is necessary for a more detailed comparison of the last two glacial terminations in order to verify the suggested Southern Ocean contribution to the initial deglacial ε_{Nd} change during termination 2 equivalent to the last glacial termination.

7. References

Abbott, A. N., Haley, B. A., McManus, J., and Reimers, C. E. (2015a). The sedimentary flux of dissolved rare earth elements to the ocean. *Geochimica et Cosmochimica Acta*, *154*, 186-200, doi:10.1016/j.gca.2015.01.010.

Abbott, A. N., Haley, B. A., and McManus, J. (2015b). Bottoms up: Sedimentary control of the deep North Pacific Ocean's epsilon(Nd) signature. *Geology*, *43*(11), 1035-1038, doi:10.1130/G37114.1.

Abelmann, A., Gersonde, R., Knorr, G., Zhang, X., Chapligin, B., Maier, E., Esper, O., Friedrichsen, H., Lohmann, G., Meyer, H., and Tiedemann, R. (2015). The seasonal sea-ice zone in the glacial Southern Ocean as a carbon sink. *Nature Communications*, *6*, Artn 8136, doi:10.1038/Ncomms9136.

Abouchami, W., Goldstein, S. L., Galer, S. J. G., Eisenhauer, A., and Mangini, A. (1997). Secular changes of lead and neodymium in central Pacific seawater recorded by a Fe-Mn crust. *Geochimica et Cosmochimica Acta*, *61*(18), 3957-3974, doi:10.1016/S0016-7037(97)00218-4.

Adkins, J. F. (2013). The role of deep ocean circulation in setting glacial climates. *Paleoceanography*, *28*(3), 539-561, doi:10.1002/palo.20046.

Adkins, J. F., McIntyre, K., and Schrag, D. P. (2002). The salinity, temperature, and delta O-18 of the glacial deep ocean. *Science*, *298*(5599), 1769-1773, doi:10.1126/Science.1076252.

Albarede, F., Goldstein, S. L., and Dautel, D. (1997). The neodymium isotopic composition of manganese nodules from the Southern and Indian oceans, the global oceanic neodymium budget, and their bearing on deep ocean circulation. *Geochimica et Cosmochimica Acta*, *61*(6), 1277-1291, doi:10.1016/S0016-7037(96)00404-8.

Alibo, D. S., and Nozaki, Y. (1999). Rare earth elements in seawater: Particle association, shale-normalization, and Ce oxidation. *Geochimica et Cosmochimica Acta*, *63*(3-4), 363-372, doi:10.1016/S0016-7037(98)00279-8.

Alibo, D. S., and Nozaki, Y. (2004). Dissolved rare earth elements in the eastern Indian Ocean: chemical tracers of the water masses. *Deep-Sea Research Part I-Oceanographic Research Papers*, *51*(4), 559-576, doi:10.1016/j.dsr.2003.11.004.

Amakawa, H., Nozaki, Y., Alibo, D. S., Zhang, J., Fukugawa, K., and Nagai, H. (2004). Neodymium isotopic variations in Northwest Pacific waters. *Geochimica et Cosmochimica Acta*, *68*(4), 715-727, doi:10.1016/S0016-7037(03)00501-5.

Amakawa, H., Sasaki, K., and Ebihara, M. (2009). Nd isotopic composition in the central North Pacific. *Geochimica et Cosmochimica Acta*, *73*(16), 4705-4719, doi:10.1016/J.Gca.2009.05.058.

Anderson, R. F., Ali, S., Bradtmiller, L. I., Nielsen, S. H. H., Fleisher, M. Q., Anderson, B. E., and Burckle, L. H. (2009). Wind-Driven Upwelling in the Southern Ocean and the Deglacial Rise in Atmospheric CO2. *Science*, *323*(5920), 1443-1448, doi:10.1126/science.1167441.

Andersson, P. S., Dahlqvist, R., Ingri, J., and Gustafsson, O. (2001). The isotopic composition of Nd in a boreal river: A reflection of selective weathering and colloidal transport. *Geochimica et Cosmochimica Acta*, *65*(4), 521-527, doi:10.1016/S0016-7037(00)00535-4.

Antonov, J. I., Seidov, D., Boyer, T. P., Locarnini, R. A., Mishonov, A. V., Garcia, H. E., Baranova, O. K., Zweng, M. M., and Johnson, D. R. (2010). World Ocean Atlas 2009, Volume 2: Salinity. In *S. Levitus, Ed. NOAA Atlas NESDIS 69*, p. 184, U.S. Government Printing Office, Washington, D.C.

Arsouze, T., Dutay, J. C., Lacan, F., and Jeandel, C. (2009). Reconstructing the Nd oceanic cycle using a coupled dynamical - biogeochemical model. *Biogeosciences*, *6*(12), 2829-2846, doi:10.5194/bg-6-2829-2009.

Asahara, Y., Tanaka, T., Kamioka, H., and Nishimura, A. (1995). Asian Continental Nature of Sr-87/Sr-86 Ratios in North Central Pacific Sediments. *Earth and Planetary Science Letters*, *133*(1-2), 105-116, doi:10.1016/0012-821x(95)00048-H.

Basak, C., Pahnke, K., Frank, M., Lamy, F., and Gersonde, R. (2015). Neodymium isotopic characterization of Ross Sea Bottom Water and its advection through the southern South Pacific. *Earth and Planetary Science Letters*, *419*, 211-221, doi:10.1016/J.Eps1.2015.03.011.

Bau, M. (1991). Rare-Earth Element Mobility during Hydrothermal and Metamorphic Fluid Rock Interaction and the Significance of the Oxidation-State of Europium. *Chemical Geology*, *93*(3-4), 219-230, doi:10.1016/0009-2541(91)90115-8.

Bau, M., and Dulski, P. (1996). Anthropogenic origin of positive gadolinium anomalies in river waters. *Earth and Planetary Science Letters*, *143*(1-4), 245-255, doi:10.1016/0012-821x(96)00127-6.

Bayon, G., German, C. R., Boella, R. M., Milton, J. A., Taylor, R. N., and Nesbitt, R. W. (2002). An improved method for extracting marine sediment fractions and its application to Sr and Nd isotopic analysis. *Chemical Geology*, *187*(3-4), 179-199, doi:10.1016/S0009-2541(01)00416-8.

Bayon, G., German, C. R., Burton, K. W., Nesbitt, R. W., and Rogers, N. (2004). Sedimentary Fe-Mn oxyhydroxides as paleoceanographic archives and the role of aeolian flux in regulating oceanic dissolved REE. *Earth and Planetary Science Letters*, *224*(3-4), 477-492, doi:10.1016/j.epsl.2004.05.033.

Bazin, L., Landais, A., Lemieux-Dudon, B., Kele, H. T. M., Veres, D., Parrenin, F., Martinerie, P., Ritz, C., Capron, E., Lipenkov, V., Loutre, M. F., Raynaud, D., Vinther, B., Svensson, A., Rasmussen, S. O., Severi, M., Blunier, T., Leuenberger, M., Fischer, H., Masson-Delmotte, V., Chappellaz, J., and Wolff, E. (2013). An optimized multi-proxy, multi-site Antarctic ice and gas orbital chronology (AICC2012): 120-800 ka. *Climate of the Past*, *9*(4), 1715-1731, doi:10.5194/cp-9-1715-2013.

Benz, V. (2016). Late Quaternary paleoceanographic history of the Pacific sector of the Southern Ocean based on diatom evidence, 183 pp, Universität Bremen, Bremen.

Bertine, K. K., and VernonClark, R. (1996). Elemental composition of the colloidal phase isolated by cross-flow filtration from coastal seawater samples. *Marine Chemistry*, *55*(1-2), 189-204, doi:10.1016/S0304-4203(96)00056-4.

Bertram, C. J., and Elderfield, H. (1993). The Geochemical Balance of the Rare-Earth Elements and Neodymium Isotopes in the Oceans. *Geochimica et Cosmochimica Acta*, *57*(9), 1957-1986, doi:10.1016/0016-7037(93)90087-D.

Björkman, K., and Fontanez, K. (2013). CMORE HOE-PhoR 1: Chief Scientist Report, Univ. of Hawaii, http://hahana.soest.hawaii.edu/hoephor/documents/documents.html.

Böhm, E., Lippold, J., Gutjahr, M., Frank, M., Blaser, P., Antz, B., Fohlmeister, J., Frank, N., Andersen, M. B., and Deininger, M. (2015). Strong and deep Atlantic meridional overturning circulation during the last glacial cycle. *Nature*, *517*, 73-76, doi:10.1038/nature14059.

Bostock, H. C., Opdyke, B. N., and Williams, M. J. M. (2010). Characterising the intermediate depth waters of the Pacific Ocean using delta C-13 and other geochemical tracers. *Deep-Sea Research Part I-Oceanographic Research Papers*, *57*(7), 847-859, doi:10.1016/J.Dsr.2010.04.005.

Boyle, E. A., Bergquist, B. A., Kayser, R. A., and Mahowald, N. (2005). Iron, manganese, and lead at Hawaii Ocean Time-series station ALOHA: Temporal variability and an intermediate water hydrothermal plume. *Geochimica et Cosmochimica Acta*, *69*(4), 933-952, doi:10.1016/J.Gca.2004.07.034.

Broecker, W. S. (1991). The great ocean conveyor. *Oceanography*, *4*(2), 79-89, doi:10.5670/oceanog.1991.07.

Broecker, W. S., and Peng, T. H. (1982). Tracers in the Sea, Lamont-Doherty Geological Observatory, Columbia University, Palisades, NY.

Broecker, W. S., and Denton, G. H. (1989). The Role of Ocean-Atmosphere Reorganizations in Glacial Cycles. *Geochimica et Cosmochimica Acta*, *53*(10), 2465-2501, doi:10.1016/0016-7037(89)90123-3.

Broecker, W. S., and Maier-Reimer, E. (1992). The influence of air and sea exchange on the carbon isotope distribution in the sea. *Global Biogeochemical Cycles*, *6*(3), 315-320, doi:10.1029/92GB01672.

Broecker, W. S., Li, Y. H., and Cromwell, J. (1967). Radium-226 and Radon-222: Concentration in Atlantic and Pacific Oceans. *Science*, *158*, 1307-1310, doi:10.1126/science.158.3806.1307

Broecker, W. S., Kaufman, A., Ku, T. L., Chung, Y. C., and Craig, H. (1970). Radium 226 measurements from the 1969 North Pacific Geosecs sation. *Journal of Geophysical Research*, *75*, 7682-7685, doi:10.1029/JC075i036p07682.

Buesseler, K. O., Bauer, J. E., Chen, R. F., Eglinton, T. I., Gustafsson, O., Landing, W., Mopper, K., Moran, S. B., Santschi, P. H., VernonClark, R., and Wells, M. L. (1996). An intercomparison of cross-flow filtration techniques used for sampling marine colloids: Overview and organic carbon results. *Marine Chemistry*, *55*(1-2), 1-31, doi:10.1016/S0304-4203(96)00046-1.

Burke, A., and Robinson, L. F. (2012). The Southern Ocean's Role in Carbon Exchange During the Last Deglaciation. *Science*, *335*(6068), 557-561, doi:10.1126/science.1208163.

Burton, K. W., and Vance, D. (2000). Glacial-interglacial variations in the neodymium isotope composition of seawater in the Bay of Bengal recorded by planktonic foraminifera. *Earth and Planetary Science Letters*, *176*(3-4), 425-441, doi:10.1016/S0012-821x(00)00011-X.

Byrne, R. H., and Kim, K. H. (1990). Rare-Earth Element Scavenging in Seawater. *Geochimica et Cosmochimica Acta*, *54*(10), 2645-2656, doi:10.1016/0016-7037(90)90002-3.

Callahan, J. E. (1972). Structure and Circulation of Deep-Water in Antarctic. *Deep-Sea Research*, *19*(8), 563-&, doi:10.1016/0011-7471(72)90040-X.

Cannon, G. A. (1966). Tropical waters in the western Pacific Ocean, August-September 1957. *Deep-Sea Research*, *13*, 1139-1148, doi:10.1016/0011-7471(66)90705-4.

Cantrell, K. J., and Byrne, R. H. (1987). Rare-Earth Element Complexation by Carbonate and Oxalate Ions. *Geochimica et Cosmochimica Acta*, *51*(3), 597-605, doi:10.1016/0016-7037(87)90072-X.

Carter, P., Vance, D., Hillenbrand, C. D., Smith, J. A., and Shoosmith, D. R. (2012). The neodymium isotopic composition of waters masses in the eastern Pacific sector of the Southern Ocean. *Geochimica et Cosmochimica Acta*, *79*, 41-59, doi:10.1016/j.gca.2011.11.034.

Charbonnier, G., Puceat, E., Bayon, G., Desmares, D., Dera, G., Durlet, C., Deconinck, J. F., Amedro, F., Gourlan, A. T., Pellenard, P., and Bomou, B. (2012). Reconstruction of the Nd isotope composition of seawater on epicontinental seas: Testing the potential of Fe-Mn oxyhydroxide coatings on foraminifera tests for deep-time investigations. *Geochimica et Cosmochimica Acta*, *99*, 39-56, doi:10.1016/j.gca.2012.09.012.

Charles, C. D., and Fairbanks, R. G. (1992). Evidence from Southern-Ocean Sediments for the Effect of North-Atlantic Deep-Water Flux on Climate. *Nature*, *355*(6359), 416-419, doi:10.1038/355416a0.

Chase, Z., Anderson, R. F., Fleisher, M. Q., and Kubik, P. W. (2003). Accumulation of biogenic and lithogenic material in the Pacific sector of the Southern Ocean during the past 40,000 years. *Deep-Sea Research Part Ii-Topical Studies in Oceanography*, *50*(3-4), 799-832, doi:10.1016/S0967-0645(02)00595-7.

Chester, R., and Hughes, M. J. (1967). A chemical technique for the separation of ferro-manganese minerals, carbonate minerals and adsorbed traces elements from pelagic sediments. *Chemical Geology*, *2*, 249-262, doi:10.1016/0009-2541(67)90025-3.

Clemente, T., and Samo, T. (2013). CMORE HOE-PhoR II: Chief Scientist Report, Univ. of Hawaii, http://hahana.soest.hawaii.edu/hoephor/documents/documents.html.

Crosta, X., Pichon, J. J., and Burckle, L. H. (1998). Application of modern analog technique to marine Antarctic diatoms: Reconstruction of maximum sea-ice extent at the Last Glacial Maximum. *Paleoceanography*, *13*(3), 284-297, doi:10.1029/98pa00339.

Curry, W. B., and Oppo, D. W. (2005). Glacial water mass geometry and the distribution of delta C-13 of Sigma CO2 in the western Atlantic Ocean. *Paleoceanography*, *20*(1), Artn Pa1017, doi:10.1029/2004pa001021.

de Baar, H. J. W., Bacon, M. P., Brewer, P. G., and Bruland, K. W. (1985a). Rare-Earth Elements in the Pacific and Atlantic Oceans. *Geochimica et Cosmochimica Acta*, *49*(9), 1943-1959, doi:10.1016/0016-7037(85)90089-4.

de Baar, H. J. W., Brewer, P. G., and Bacon, M. P. (1985b). Anomalies in Rare-Earth Distributions in Seawater - Gd and Tb. *Geochimica et Cosmochimica Acta*, *49*(9), 1961-1969, doi:10.1016/0016-7037(85)90090-0.

Duce, R. A., Unni, C. K., Ray, B. J., Prospero, J. M., and Merrill, J. T. (1980). Long-Range Atmospheric Transport of Soil Dust from Asia to the Tropical North Pacific - Temporal Variability. *Science*, *209*(4464), 1522-1524, doi:10.1126/Science.209.4464.1522.

Dulaiova, H., and Burnett, W. C. (2004). An Efficient Method for Gamma Spectrometric Determination of Radium-226, 228 via Manganese Fibers. *Limnology and Oceanography-Methods*, *2*, 256-261, doi:10.4319/lom.2004.2.256.

Duplessy, J. C., Shackleton, N. J., Fairbanks, R. G., Labeyrie, L., Oppo, D., and Kallel, N. (1988). Deepwater Source Variations during the Last Climatic Cycle and Their Impact on the Global Deepwater Circulation. *Paleoceanography*, *3*(3), 343-360, doi:10.1029/PA003i003p00343.

Elderfield, H. (1988). The Oceanic Chemistry of the Rare-Earth Elements. *Philosophical Transactions of the Royal Society a-Mathematical Physical and Engineering Sciences*, *325*(1583), 105-126, doi:10.1098/Rsta.1988.0046.

Elderfield, H., and Greaves, M. J. (1982). The Rare-Earth Elements in Sea-Water. *Nature*, *296*(5854), 214-219, doi:10.1038/296214a0.

Elderfield, H., and Pagett, R. (1986). Rare-Earth Elements in Ichthyoliths - Variations with Redox Conditions and Depositional Environment. *Science of the Total Environment*, *49*, 175-197, doi:10.1016/0048-9697(86)90239-1.

Elderfield, H., Upstillgoddard, R., and Sholkovitz, E. R. (1990). The Rare-Earth Elements in Rivers, Estuaries, and Coastal Seas and Their Significance to the Composition of Ocean Waters. *Geochimica et Cosmochimica Acta*, *54*(4), 971-991, doi:10.1016/0016-7037(90)90432-K.

Elderfield, H., Ferretti, P., Greaves, M., Crowhurst, S., McCave, I. N., Hodell, D., and Piotrowski, A. M. (2012). Evolution of Ocean Temperature and Ice Volume Through the Mid-Pleistocene Climate Transition. *Science*, *337*(6095), 704-709, doi:10.1126/science.1221294.

Elmore, A. C., Piotrowski, A. M., Wright, J. D., and Scrivner, A. E. (2011). Testing the extraction of past seawater Nd isotopic composition from North Atlantic deep sea sediments and foraminifera. *Geochemistry Geophysics Geosystems*, *12*, Artn Q09008, doi:10.1029/2011gc003741.

Ferrari, R. (2014). Oceanography: What goes down must come up. Nature, 513, 179-180, doi:10.1038/513179a.

Ferrari, R., Jansen, M. F., Adkins, J. F., Burke, A., Stewart, A. L., and Thompson, A. F. (2014). Antarctic sea ice control on ocean circulation in present and glacial climates. *Proceedings of the National Academy of Sciences*, *111*(24), 8753-8758, doi:10.1073/pnas.1323922111.

Fitzsimmons, J. N., and Boyle, E. A. (2014). Assessment and comparison of Anopore and cross flow filtration methods for the determination of dissolved iron size fractionation into soluble and colloidal phases in seawater. *Limnology and Oceanography-Methods*, *12*, 246-263, doi:10.4319/Lom.2014.12.246.

Fitzsimmons, J. N., Hayes, C. T., Al-Subiai, S. N., Zhang, R. F., Morton, P. L., Weisend, R. E., Ascani, F., and Boyle, E. A. (2015). Daily to decadal variability of size-fractionated iron and iron-binding ligands at the Hawaii Ocean Time-series Station ALOHA. *Geochimica et Cosmochimica Acta*, *171*, 303-324, doi:10.1016/j.gca.2015.08.012.

Foster, G. L., and Vance, D. (2006). Negligible glacial-interglacial variation in continental chemical weathering rates. *Nature*, *444*(7121), 918-921, doi:10.1038/nature05365.

Foster, G. L., Vance, D., and Prytulak, J. (2007). No change in the neodymium isotope composition of deep water exported from the North Atlantic on glacial-interglacial time scales. *Geology*, *35*(1), 37-40, doi:10.1130/G23204A.1.

Frank, M. (2002). Radiogenic isotopes: Tracers of past ocean circulation and erosional input. *Reviews of Geophysics*, *40*(1), Artn 1001, doi:10.1029/2000rg000094.

Frank, M., Whiteley, N., Kasten, S., Hein, J. R., and O'Nions, K. (2002). North Atlantic deep water export to the Southern Ocean over the past 14 Myr: Evidence from Nd and Pb isotopes in ferromanganese crusts. *Paleoceanography*, *17*(2), Artn 1022, doi:10.1029/2000pa000606.

Fröllje, H., Pahnke, K., Schnetger, B., Brumsack, H.-J., Dulai, H., and Fitzsimmons, J. N. (2016). Hawaiian imprint on dissolved Nd and Ra isotopes and rare earth elements in the central North Pacific: local survey and seasonal variability. *Geochimica et Cosmochimica Acta, 189*, 110-131, http://dx.doi.org/10.1016/j.gca.2016.06.001.

Garcia, H. E., Locarnini, R. A., Boyer, T. P., Antonov, J. I., Baranova, O. K., Zweng, M. M., and Johnson, D. R. (2010a). World Ocean Atlas 2009, Volume 3: Dissolved Oxygen, Apparent Oxygen Utilization, and Oxygen Saturation. In *S. Levitus, Ed. NOAA Atlas NESDIS 70*, p. 344, U.S. Government Printing Office, Washington, D.C.

Garcia, H. E., Locarnini, R. A., Boyer, T. P., Antonov, J. I., Zweng, M. M., Baranova, O. K., and Johnson, D. R. (2010b). World Ocean Atlas 2009, Volume 4: Nutrients (phosphate, nitrate, silicate). In *S. Levitus, Ed. NOAA Atlas NESDIS 71*, p. 398, U.S. Government Printing Office, Washington, D.C.

Garrison, G. H., Glenn, C. R., and McMurtry, G. M. (2003). Measurement of submarine groundwater discharge in Kahana Bay, O'ahu, Hawai'i. *Limnology and Oceanography*, *48*(2), 920-928, doi:10.4319/lo.2003.48.2.0920.

Genthon, C., Barnola, J. M., Raynaud, D., Lorius, C., Jouzel, J., Barkov, N. I., Korotkevich, Y. S., and Kotlyakov, V. M. (1987). Vostok ice core: climatic response to CO2 and orbital forcing changes over the last climatic cycle. *Nature*, *329*, 414-418, doi:10.1038/329414a0.

German, C. R., Klinkhammer, G. P., Edmond, J. M., Mitra, A., and Elderfield, H. (1990). Hydrothermal Scavenging of Rare-Earth Elements in the Ocean. *Nature*, *345*(6275), 516-518, doi:10.1038/345516a0.

Gersonde, R. (2011). The Expedition of the Research Vessel "Polarstern" to the polar South Pacific in 2009/2010 (ANT-XXVI/2 - BIPOMAC), Berichte zur Polar und Meersforschung, Alfred Wegener Institute Bremerhaven.

Gersonde, R., Crosta, X., Abelmann, A., and Armand, L. (2005). Sea-surface temperature and sea ice distribution of the Southern Ocean at the EPILOG Last Glacial Maximum—a circum-Antarctic view based on siliceous microfossil records. *Quaternary Science Reviews*, *24*(7–9), 869-896, doi:10.1016/j.quascirev.2004.07.015.

Gersonde, R., Lamy, F., Steph, S., and Esper, O. (2010). Documentation of sediment core PS75/056-1, Alfred Wegener Institute - Polarstern core repository, doi:10.1594/PANGAEA.740096.

Giambelluca, T. W., Chen, Q., Frazier, A. G., Price, J. P., Chen, Y. L., Chu, P. S., Eischeid, J. K., and Delparte, D. M. (2013). Online Rainfall Atlas of Hawai'i. *Bulletin of the American Meteorological Society*, *94*(3), 313-316, doi:10.1175/Bams-D-11-00228.

Goldstein, S. J., and Jacobsen, S. B. (1988). Rare-Earth Elements in River Waters. *Earth and Planetary Science Letters*, *89*(1), 35-47, doi:10.1016/0012-821x(88)90031-3.

Goldstein, S. L., and Hemming, S. R. (2003). Long lived isotopic tracers in oceanography, paleoceanography, and ice sheet dynamics. In *Treatise on Geochmistry*, edited by H. Elderfield, pp. 453-489, Elsevier, New York.

Goldstein, S. L., O'Nions, R. K., and Hamilton, P. J. (1984). A Sm-Nd Isotopic Study of Atmospheric Dusts and Particulates from Major River Systems. *Earth and Planetary Science Letters*, *70*(2), 221-236, doi:10.1016/0012-821x(84)90007-4.

Gordon, A. L. (2001). Bottom Water Formation. In *Encyclopedia of Ocean Sciences*, edited by J. H. Steele, K. K. Turekian and S. A. Thorpe, pp. 334-340, Academic Press.

Grasse, P., Stichel, T., Stumpf, R., Stramma, L., and Frank, M. (2012). The distribution of neodymium isotopes and concentrations in the Eastern Equatorial Pacific: Water mass advection versus particle exchange. *Earth and Planetary Science Letters*, *353*, 198-207, doi:10.1016/J.Epsl.2012.07.044.

Greaves, M. J., Statham, P. J., and Elderfield, H. (1994). Rare-Earth Element Mobilization from Marine Atmospheric Dust into Seawater. *Marine Chemistry*, *46*(3), 255-260, doi:10.1016/0304-4203(94)90081-7.

Greaves, M. J., Elderfield, H., and Sholkovitz, E. R. (1999). Aeolian sources of rare earth elements to the Western Pacific Ocean. *Marine Chemistry*, *68*(1-2), 31-38, doi:10.1016/S0304-4203(99)00063-8.

Grenier, M., Jeandel, C., Lacan, F., Vance, D., Venchiarutti, C., Cros, A., and Cravatte, S. (2013). From the subtropics to the central equatorial Pacific Ocean: Neodymium isotopic composition and rare earth element concentration variations. *Journal of Geophysical Research-Oceans*, *118*(2), 592-618, doi:10.1029/2012jc008239.

Grootes, P., and Stuiver, M. (1997). Oxygen 18/16 variability in Greenland snow and ice with 10^{-3} to 10^{5} year time resolution. *Journal of Geophysical Research*, *102*(C12), 26455-26470, doi:10.1029/97JC00880.

Guihou, A., Pichat, S., Govin, A., Nave, S., Michel, E., Duplessy, J. C., Telouk, P., and Labeyrie, L. (2011). Enhanced Atlantic Meridional Overturning Circulation supports the Last Glacial Inception. *Quaternary Science Reviews*, *30*(13-14), 1576-1582, doi:10.1016/j.quascirev.2011.03.017.

Gutjahr, M., and Lippold, J. (2011). Early arrival of Southern Source Water in the deep North Atlantic prior to Heinrich event 2. *Paleoceanography*, *26*, Artn Pa2101, doi:10.1029/2011pa002114.

Gutjahr, M., Frank, M., Stirling, C. H., Klemm, V., van de Flierdt, T., and Halliday, A. N. (2007). Reliable extraction of a deepwater trace metal isotope signal from Fe-Mn oxyhydroxide coatings of marine sediments. *Chemical Geology*, *242*(3-4), 351-370, doi:10.1016/j.chemgeo.2007.03.021.

Gutjahr, M., Frank, M., Stirling, C. H., Keigwin, L. D., and Halliday, A. N. (2008). Tracing the Nd isotope evolution of North Atlantic deep and intermediate waters in the Western

North Atlantic since the Last Glacial Maximum from Blake Ridge sediments. *Earth and Planetary Science Letters*, *266*(1-2), 61-77, doi:10.1016/j.epsl.2007.10.037.

Gutjahr, M., Hoogakker, B. A. A., Frank, M., and McCave, I. N. (2010). Changes in North Atlantic Deep Water strength and bottom water masses during Marine Isotope Stage 3 (45-35 ka BP). *Quaternary Science Reviews*, *29*(19-20), 2451-2461, doi:10.1016/j.quascirev.2010.02.024.

Haley, B. A., and Klinkhammer, G. P. (2003). Complete separation of rare earth elements from small volume seawater samples by automated ion chromatography: method development and application to benthic flux. *Marine Chemistry*, *82*(3-4), 197-220, doi:10.1016/S0304-4203(03)00070-7.

Haley, B. A., Klinkhammer, G. P., and McManus, J. (2004). Rare earth elements in pore waters of marine sediments. *Geochimica et Cosmochimica Acta*, *68*(6), 1265-1279, doi:10.1016/J.Gca.2003.09.012.

Hall, I. R., McCave, I. N., Shackleton, N. J., Weedon, G. P., and Harris, S. E. (2001). Intensified deep Pacfic inflow and ventilation in Pleistocene glacial times. *Nature*, *412*(6849), 809-812, doi:10.1038/35090552.

Halliday, A. N., Davidson, J. P., Holden, P., Owen, R. M., and Olivarez, A. M. (1992). Metalliferous Sediments and the Scavenging Residence Time of Nd near Hydrothermal Vents. *Geophysical Research Letters*, *19*(8), 761-764, doi:10.1029/92gl00393.

Hannigan, R. E., and Sholkovitz, E. R. (2001). The development of middle rare earth element enrichments in freshwaters: weathering of phosphate minerals. *Chemical Geology*, *175*(3-4), 495-508, doi:10.1016/S0009-2541(00)00355-7.

Hathorne, E. C., Haley, B., Stichel, T., Grasse, P., Zieringer, M., and Frank, M. (2012). Online preconcentration ICP-MS analysis of rare earth elements in seawater. *Geochemistry Geophysics Geosystems*, *13*, Artn Q01020, doi:10.1029/2011gc003907.

Hayes, C. T., Fitzsimmons, J. N., Boyle, E. A., McGee, D., Anderson, R. F., Weisend, R., and Morton, P. L. (2015). Thorium isotopes tracing the iron cycle at the Hawaii Ocean Time-series Station ALOHA. *Geochimica et Cosmochimica Acta*, *169*, 1-16, doi:10.1016/j.gca.2015.07.019.

Henderson, G. M., Anderson, R. F., Adkins, J., Andersson, P., Boyle, E. A., Cutter, G., de Baar, H., Eisenhauer, A., Frank, M., Francois, R., Orians, K., Gamo, T., German, C., Jenkins, W., Moffett, J., Jeandel, C., Jickells, T., Krishnaswami, S., Mackey, D., Measures, C. I., Moore, J. K., Oschlies, A., Pollard, R., van der Loeff, M. R. D., Schlitzer, R., Sharma, M., von Damm, K., Zhang, J., Masque, P., and Grp, S. W. (2007). GEOTRACES - An international study of the global marine biogeochemical cycles of trace elements and their isotopes. *Chemie Der Erde-Geochemistry*, *67*(2), 85-131, doi:10.1016/j.chemer.2007.02.001.

Ho, S. L., Mollenhauer, G., Lamy, F., Martinez-Garcia, A., Mohtadi, M., Gersonde, R., Hebbeln, D., Nunez-Ricardo, S., Rosell-Mele, A., and Tiedemann, R. (2012). Sea surface temperature variability in the Pacific sector of the Southern Ocean over the past 700 kyr. *Paleoceanography*, *27*, PA4202, doi:10.1029/2012PA002317.

Hodell, D. A., Charles, C. D., and Ninnemann, U. S. (2000). Comparison of interglacial stages in the South Atlantic sector of the southern ocean for the past 450 kyr: implifications for Marine Isotope Stage (MIS) 11. *Global and Planetary Change*, *24*(1), 7-26, doi:10.1016/S0921-8181(99)00069-7.

Hodell, D. A., Venz, K. A., Charles, C. D., and Ninnemann, U. S. (2003). Pleistocene vertical carbon isotope and carbonate gradients in the South Atlantic sector of the Southern Ocean. *Geochemistry Geophysics Geosystems*, *4*, Artn 1004, doi:10.1029/2002gc000367.

Hongo, Y., Obata, H., Alibo, D. S., and Nozaki, Y. (2006). Spatial variations of rare earth elements in North Pacific surface water. *Journal of Oceanography*, *62*(4), 441-455, doi:10.1007/S10872-006-0067-1.

Huck, C. E., van de Flierdt, T., Jiménez-Espejo, F. J., Bohaty, S. M., Röhl, U., and Hammond, S. J. (2016). Robustness of fossil fish teeth for seawater neodymium isotope reconstructions under variable redox conditions in an ancient shallow marine setting. *Geochemistry Geophysics Geosystems*, *17*, 679-698, doi:10.1002/2015GC006218.

Huh, C. A., and Ku, T. L. (1998). A 2-D section of 228Ra and 226Ra in the Northeast Pacific. *Oceanologica Acta*, *21*, 533-542, doi:10.1016/S0399-1784(98)80036-4.

Jacobs, S. S., Amos, A. F., and Bruchhau.Pm (1970). Ross-Sea Oceanography and Antarctic Bottom Water Formation. *Deep-Sea Research*, *17*(6), 935-&, doi:10.1016/0011-7471(70)90046-X.

Jacobsen, S. B., and Wasserburg, G. J. (1980). Sm-Nd Isotopic Evolution of Chondrites. *Earth and Planetary Science Letters*, *50*(1), 139-155, doi:10.1016/0012-821x(80)90125-9.

Jeandel, C., Thouron, D., and Fieux, M. (1998). Concentrations and isotopic compositions of neodymium in the eastern Indian Ocean and Indonesian straits. *Geochimica et Cosmochimica Acta*, *62*(15), 2597-2607, doi:10.1016/S0016-7037(98)00169-0.

Jeandel, C., Arsouze, T., Lacan, F., Techine, P., and Dutay, J. C. (2007). Isotopic Nd compositions and concentrations of the lithogenic inputs into the ocean: A compilation, with an emphasis on the margins. *Chemical Geology*, *239*(1-2), 156-164, doi:10.1016/J.Chemgeo.2006.11.013.

Jeandel, C., Delattre, H., Grenier, M., Pradoux, C., and Lacan, F. (2013). Rare earth element concentrations and Nd isotopes in the Southeast Pacific Ocean. *Geochemistry Geophysics Geosystems*, *14*(2), 328-341, doi:10.1029/2012gc004309.

Jickells, T. D., An, Z. S., Andersen, K. K., Baker, A. R., Bergametti, G., Brooks, N., Cao, J. J., Boyd, P. W., Duce, R. A., Hunter, K. A., Kawahata, H., Kubilay, N., laRoche, J., Liss, P. S., Mahowald, N., Prospero, J. M., Ridgwell, A. J., Tegen, I., and Torres, R. (2005). Global iron connections between desert dust, ocean biogeochemistry, and climate. *Science*, *308*(5718), 67-71, doi:10.1126/Science.1105959.

Johannesson, K. H., and Burdige, D. J. (2007). Balancing the global oceanic neodymium budget: Evaluating the role of groundwater. *Earth and Planetary Science Letters*, *253*(1-2), 129-142, doi:10.1016/J.Epsl.2006.10.021.

Johannesson, K. H., Chevis, D. A., Burdige, D. J., Cable, J. E., Martin, J. B., and Roy, M. (2011). Submarine groundwater discharge is an important net source of light and middle REEs to coastal waters of the Indian River Lagoon, Florida, USA. *Geochimica et Cosmochimica Acta*, *75*(3), 825-843, doi:10.1016/J.Gca.2010.11.005.

Johnson, K. S., Elrod, V. A., Fitzwater, S. E., Plant, J. N., Chavez, F. P., Tanner, S. J., Gordon, R. M., Westphal, D. L., Perry, K. D., Wu, J. F., and Karl, D. M. (2003). Surface ocean-lower atmosphere interactions in the Northeast Pacific Ocean Gyre: Aerosols, iron, and the ecosystem response. *Global Biogeochemical Cycles*, *17*(2), Artn 1063, doi:10.1029/2002gb002004.

Jones, C. E., Halliday, A. N., Rea, D. K., and Owen, R. M. (1994). Neodymium Isotopic Variations in North Pacific Modern Silicate Sediment and the Insignificance of Detrital Ree Contributions to Seawater. *Earth and Planetary Science Letters*, *127*(1-4), 55-66, doi:10.1016/0012-821x(94)90197-X.

Jones, C. E., Halliday, A. N., Rea, D. K., and Owen, R. M. (2000). Eolian inputs of lead to the North Pacific. *Geochimica et Cosmochimica Acta*, *64*(8), 1405-1416, doi:10.1016/S0016-7037(99)00439-1.

Jones, K. M., Khatiwala, S. P., Goldstein, S. L., Hemming, S. R., and van de Flierdt, T. (2008). Modeling the distribution of Nd isotopes in the oceans using an ocean general circulation model. *Earth and Planetary Science Letters*, *272*(3-4), 610-619, doi:10.1016/j.epsl.2008.05.027.

Jonkers, L., Zahn, R., Thomas, A., Henderson, G., Abouchami, W., Francois, R., Masque, P., Hall, I. R., and Bickert, T. (2015). Deep circulation changes in the central South

Atlantic during the past 145 kyrs reflected in a combined Pa-231/Th-230, Neodymium isotope and benthic delta C-13 record. *Earth and Planetary Science Letters*, *419*, 14-21, doi:10.1016/j.epsl.2015.03.004.

Jouzel, J., Masson-Delmotte, V., Cattani, O., Dreyfus, G., Falourd, S., Hoffmann, G., Minster, B., Nouet, J., Barnola, J. M., Chappellaz, J., Fischer, H., Gallet, J. C., Johnsen, S., Leuenberger, M., Loulergue, L., Luethi, D., Oerter, H., Parrenin, F., Raisbeck, G., Raynaud, D., Schilt, A., Schwander, J., Selmo, E., Souchez, R., Spahni, R., Stauffer, B., Steffensen, J. P., Stenni, B., Stocker, T. F., Tison, J. L., Werner, M., and Wolff, E. W. (2007). Orbital and millennial Antarctic climate variability over the past 800,000 years. *Science*, *317*(5839), 793-796, doi:10.1126/science.1141038.

Karl, D. M., and Lukas, R. (1996). The Hawaii Ocean Time-series (HOT) program: Background, rationale and field implementation. *Deep-Sea Research Part Ii-Topical Studies in Oceanography*, *43*(2-3), 129-156, doi:10.1016/0967-0645(96)00005-7.

Kawabe, M., and Fujio, S. (2010). Pacific Ocean Circulation Based on Observation. *Journal of Oceanography*, *66*(3), 389-403, doi:10.1007/s10872-010-0034-8.

Kelly, J. L., Glenn, C. R., and Lucey, P. G. (2013). High-Resolution Aerial Infrared Mapping of Groundwater Discharge to the Coastal Ocean. *Limnology and Oceanography-Methods*, *11*, 262-277, doi:10.4319/lom.2013.11.262.

Kim, I., and Kim, G. (2011). Large fluxes of rare earth elements through submarine groundwater discharge (SGD) from a volcanic island, Jeju, Korea. *Marine Chemistry*, *127*(1-4), 12-19, doi:10.1016/J.Marchem.2011.07.006.

Kim, I., and Kim, G. (2014). Submarine groundwater discharge as a main source of rare earth elements in coastal waters. *Marine Chemistry*, *160*, 11-17, doi:10.1016/J.Marchem.2014.01.003.

Klevenz, V., Vance, D., Schmidt, D. N., and Mezger, K. (2008). Neodymium isotopes in benthic foraminifera: Core-top systematics and a down-core record from the Neogene south Atlantic. *Earth and Planetary Science Letters*, *265*(3-4), 571-587, doi:10.1016/j.epsl.2007.10.053.

Kraft, S., Frank, M., Hathorne, E. C., and Weldeab, S. (2013). Assessment of seawater Nd isotope signatures extracted from foraminiferal shells and authigenic phases of Gulf of Guinea sediments. *Geochimica et Cosmochimica Acta*, *121*, 414-435, doi:10.1016/j.gca.2013.07.029.

Kulaksiz, S., and Bau, M. (2007). Contrasting behaviour of anthropogenic gadolinium and natural rare earth elements in estuaries and the gadolinium input into the North Sea. *Earth and Planetary Science Letters*, *260*(1-2), 361-371, doi:10.1016/j.epsl.2007.06.016.

Kurtz, A. C., Derry, L. A., and Chadwick, O. A. (2001). Accretion of Asian dust to Hawaiian soils: Isotopic, elemental, and mineral mass balances. *Geochimica et Cosmochimica Acta*, *65*(12), 1971-1983, doi:10.1016/S0016-7037(01)00575-0.

Kwon, E. Y., Kim, G., Primeau, F., Moore, W. S., Cho, H.-M., DeVries, T., Sarmiento, J. L., Charette, M. A., and Cho, Y.-K. (2014). Global Estimate of Submarine Groundwater Discharge Based on an Observationally Constrained Radium Isotope Model. *Geophysical Research Letters*, *41*(8438-8444), doi:10.1002/2014GL061574.

Lacan, F., and Jeandel, C. (2001). Tracing Papua New Guinea imprint on the central Equatorial Pacific Ocean using neodymium isotopic compositions and Rare Earth Element patterns. *Earth and Planetary Science Letters*, *186*(3-4), 497-512, doi:10.1016/S0012-821x(01)00263-1.

Lacan, F., and Jeandel, C. (2005a). Neodymium isotopes as a new tool for quantifying exchange fluxes at the continent-ocean interface. *Earth and Planetary Science Letters*, *232*(3-4), 245-257, doi:10.1016/J.Epsl.2005.01.004.

Lacan, F., and Jeandel, C. (2005b). Acquisition of the neodymium isotopic composition of the North Atlantic Deep Water. *Geochemistry Geophysics Geosystems*, *6*, Artn Q12008, doi:10.1029/2005gc000956.

Lacan, F., Tachikawa, K., and Jeandel, C. (2012). Neodymium isotopic composition of the oceans: A compilation of seawater data. *Chemical Geology*, *300*, 177-184, doi:10.1016/J.Chemgeo.2012.01.019.

Lamy, F., Gersonde, R., Winckler, G., Esper, O., Jaeschke, A., Kuhn, G., Ullermann, J., Martinez-Garcia, A., Lambert, F., and Kilian, R. (2014). Increased Dust Deposition in the Pacific Southern Ocean During Glacial Periods. *Science*, *343*(6169), 403-407, doi:10.1126/science.1245424.

Lamy, F., Arz, H. W., Kilian, R., Lange, C. B., Lembke-Jene, L., Wengler, M., Kaiser, J., Baeza-Urrea, O., Hall, I. R., Harada, N., and Tiedemann, R. (2015). Glacial reduction and millennial-scale variations in Drake Passage throughflow. *Proceedings of the National Academy of Sciences*, *112*(44), 13496-13501, doi:10.1073/pnas.1509203112.

Lippold, J., Gutjahr, M., Blaser, P., Christner, E., de Carvalko Ferreira, M. L., Mulitza, S., Christl, M., Wombacher, F., Böhm, E., Antz, B., Cartapanis, O., Vogel, H., and Jaccard, S. L. (2016). Deep water provenance and dynamics of the (de)glacial Atlantic meridional overturning circulation. *Earth and Planetary Science Letters*, *445*, 68-78, doi:10.1016/j.epsl.2016.04.013.

Lisiecki, L. E., and Raymo, M. E. (2005). A Pliocene-Pleistocene stack of 57 globally distributed benthic delta O-18 records (vol 20, art no PA1003, 2005). *Paleoceanography*, *20*(2), Artn Pa2007, doi:10.1029/2005pa001164.

Liu, C. Q., Masuda, A., Okada, A., Yabuki, S., Zhang, J., and Fan, Z. L. (1993). A Geochemical Study of Loess and Desert Sand in Northern China - Implications for Continental-Crust Weathering and Composition. *Chemical Geology*, *106*(3-4), 359-374, doi:10.1016/0009-2541(93)90037-J.

Liu, C. Q., Masuda, A., Okada, A., Yabuki, S., and Fan, Z. L. (1994). Isotope Geochemistry of Quaternary Deposits from the Arid Lands in Northern China. *Earth and Planetary Science Letters*, *127*(1-4), 25-38, doi:10.1016/0012-821x(94)90195-3.

Lugmair, G. W., Shimamura, T., Lewis, R. S., and Anders, E. (1983). Sm-146 in the Early Solar-System - Evidence from Neodymium in the Allende Meteorite. *Science*, *222*(4627), 1015-1018, doi:10.1126/Science.222.4627.1015.

Lund, D. C., Adkins, J. F., and Ferrari, R. (2011). Abyssal Atlantic circulation during the Last Glacial Maximum: Constraining the ratio between transport and vertical mixing. *Paleoceanography*, *26*, Artn Pa1213, doi:10.1029/2010pa001938.

Lüthi, D., Le Floch, M., Bereiter, B., Blunier, T., Barnola, J. M., Siegenthaler, U., Raynaud, D., Jouzel, J., Fischer, H., Kawamura, K., and Stocker, T. F. (2008). High-resolution carbon dioxide concentration record 650,000-800,000 years before present. *Nature*, *453*(7193), 379-382, doi:10.1038/nature06949.

Lynch-Stieglitz, J., Adkins, J. F., Curry, W. B., Dokken, T., Hall, I. R., Herguera, J. C., Hirschi, J. J. M., Ivanova, E. V., Kissel, C., Marchal, O., Marchitto, T. M., McCave, I. N., McManus, J. F., Mulitza, S., Ninnemann, U., Peeters, F., Yu, E. F., and Zahn, R. (2007). Atlantic meridional overturning circulation during the Last Glacial Maximum. *Science*, *316*(5821), 66-69, doi:10.1126/science.1137127.

Mackensen, A., Hubberten, H. W., Bickert, T., Fischer, G., and Futterer, D. K. (1993). The Delta-C-13 in Benthic Foraminiferal Tests of Fontbotia-Wuellerstorfi (Schwager) Relative to the Delta-C-13 of Dissolved Inorganic Carbon in Southern-Ocean Deep-Water - Implications for Glacial Ocean Circulation Models. *Paleoceanography*, *8*(5), 587-610, doi:10.1029/93pa01291.

Marchitto, T. M., Lynch-Stieglitz, J., and Hemming, S. R. (2005). Deep pacific CaCO3 compensation and glacial-interglacial atmosphericCO(2). *Earth and Planetary Science Letters*, *231*(3-4), 317-336, doi:10.1016/j.epsl.2004.12.024.

Marshall, J., and Speer, K. (2012). Closure of the meridional overturning circulation through Southern Ocean upwelling. *Nature Geoscience*, *5*(3), 171-180, doi:10.1038/NGEO1391.

Martin, E. E., and Haley, B. A. (2000). Fossil fish teeth as proxies for seawater Sr and Nd isotopes. *Geochimica et Cosmochimica Acta*, *64*(5), 835-847, doi:10.1016/S0016-7037(99)00376-2.

Martin, E. E., and Scher, H. D. (2004). Preservation of seawater Sr and Nd isotopes in fossil fish teeth: bad news and good news. *Earth and Planetary Science Letters*, *220*(1-2), 25-39, doi:10.1016/S0012-821X(03)00030-5.

Martin, E. E., Blair, S. W., Kamenov, G. D., Scher, H. D., Bourbon, E., Basak, C., and Newkirk, D. N. (2010). Extraction of Nd isotopes from bulk deep sea sediments for paleoceanographic studies on Cenozoic time scales. *Chemical Geology*, *269*(3-4), 414-431, doi:10.1016/j.chemgeo.2009.10.016.

Martinez-Garcia, A., Sigman, D. M., Ren, H. J., Anderson, R. F., Straub, M., Hodell, D. A., Jaccard, S. L., Eglinton, T. I., and Haug, G. H. (2014). Iron Fertilization of the Subantarctic Ocean During the Last Ice Age. *Science*, *343*(6177), 1347-1350, doi:10.1126/science.1246848.

Martinez-Mendez, G., Molyneux, E. G., Hall, I. R., and Zahn, R. (2009). Variable water column structure of the South Atlantic on glacial-interglacial time scales. *Quaternary Science Reviews*, *28*(27-28), 3379-3387, doi:10.1016/j.quascirev.2009.09.022.

Masuda, A., and Ikeuchi, Y. (1979). Lanthanide Tetrad Effect Observed in Marine-Environment. *Geochemical Journal*, *13*(1), 19-22, doi:10.2343/geochemj.13.19.

Matsumoto, K., and Lynch-Stieglitz, J. (1999). Similar glacial and Holocene deep water circulation inferred from southeast Pacific benthic foraminiferal carbon isotope composition. *Paleoceanography*, *14*(2), 149-163, doi:10.1029/1998pa900028.

Matsumoto, K., Lynch-Stieglitz, J., and Anderson, R. F. (2001). Similar glacial and Holocene Southern Ocean hydrography. *Paleoceanography*, *16*(5), 445-454, doi:10.1029/2000pa000549.

Matsumoto, K., Oba, T., Lynch-Stieglitz, J., and Yamamoto, H. (2002). Interior hydrography and circulation of the glacial Pacific Ocean. *Quaternary Science Reviews*, *21*(14-15), 1693-1704, doi:10.1016/S0277-3791(01)00142-1.

McCartney, M. S. (1977). Subantarctic Mode Water. In *A Voyage of Discovery: George Deacon 70th Anniversary Volume*, edited by M. V. Angel, pp. 103-119, Pergamon.

McCave, I. N., Carter, L., and Hall, I. R. (2008). Glacial-interglacial changes in water mass structure and flow in the SW Pacific Ocean. *Quaternary Science Reviews*, *27*(19-20), 1886-1908, doi:10.1016/j.quascirev.2008.07.010.

McManus, J. F., Francois, R., Gherardi, J. M., Keigwin, L. D., and Brown-Leger, S. (2004). Collapse and rapid resumption of Atlantic meridional circulation linked to deglacial climate changes. *Nature*, *428*(6985), 834-837, doi:10.1038/nature02494.

Menard, H. W., and Smith, S. M. (1966). Hypsometry of Ocean Basin Provinces. *Journal of Geophysical Research*, *71*(18), 4305-&, doi:10.1029/JZ071i018p04305.

Miller, J. R. (1976). Salinity Effect in a Mixed Layer Ocean Model. *Journal of Physical Oceanography*, *6*(1), 29-35, doi:10.1175/1520-0485(1976)006<0029:Tseiam>2.0.Co;2.

Mitra, A., Elderfield, H., and Greaves, M. J. (1994). Rare-Earth Elements in Submarine Hydrothermal Fluids and Plumes from the Mid-Atlantic Ridge. *Marine Chemistry*, *46*(3), 217-235, doi:10.1016/0304-4203(94)90079-5.

Moffett, J. W. (1990). Microbially Mediated Cerium Oxidation in Sea-Water. *Nature*, *345*(6274), 421-423, doi:10.1038/345421a0.

Molina-Kescher, M., Frank, M., and Hathorne, E. (2014a). South Pacific dissolved Nd isotope compositions and rare earth element distributions: Water mass mixing versus biogeochemical cycling. *Geochimica et Cosmochimica Acta*, *127*, 171-189, doi:10.1016/j.gca.2013.11.038.

Molina-Kescher, M., Frank, M., and Hathorne, E. C. (2014b). Nd and Sr isotope compositions of different phases of surface sediments in the South Pacific: Extraction of seawater signatures, boundary exchange, and detrital/dust provenance. *Geochemistry Geophysics Geosystems*, *15*(9), 3502-3520, doi:10.1002/2014GC005443.

Molina-Kescher, M., Frank, M., Tapia, R., Ronge, T. A., Nürnberg, D., and Tiedemann, R. (2016). Reduced admixture of North Atlantic Deep Water to the deep central South Pacific during the last two glacial periods. *Paleoceanography*, doi:10.1002/2015PA002863.

Monnin, E., Indermuhle, A., Dallenbach, A., Fluckiger, J., Stauffer, B., Stocker, T. F., Raynaud, D., and Barnola, J. M. (2001). Atmospheric CO2 concentrations over the last glacial termination. *Science*, *291*(5501), 112-114, doi:10.1126/Science.291.5501.112.

Moore, W. S., Sarmiento, J. L., and Key, R. M. (2008). Submarine groundwater discharge revealed by 228Ra distribution in the upper Atlantic Ocean. *Nature Geoscience*, *1*, 309-311, doi:10.1038/ngeo183.

Moosdorf, N., Stieglitz, T., Waska, H., Durr, H. H., and Hartmann, J. (2015). Submarine groundwater discharge from tropical islands: a review. *Grundwasser*, *20*(1), 53-67, doi:10.1007/S00767-014-0275-3.

Moy, A. D., Howard, W. R., and Gagan, M. K. (2006). Late Quaternary palaeoceanography of the Circumpolar Deep Water from the South Tasman Rise. *Journal of Quaternary Science*, *21*(7), 763-777, doi:10.1002/jqs.1067.

Nakai, S., Halliday, A. N., and Rea, D. K. (1993). Provenance of Dust in the Pacific-Ocean. *Earth and Planetary Science Letters*, *119*(1-2), 143-157, doi:10.1016/0012-821x(93)90012-X.

Nikurashin, M., and Ferrari, R. (2013). Overturning circulation driven by breaking internal waves in the deep ocean. *Geophysical Research Letters*, *40*(12), 3133-3137, doi:10.1002/grl.50542.

Ninnemann, U. S., and Charles, C. D. (2002). Changes in the mode of Southern Ocean circulation over the last glacial cycle revealed by foraminiferal stable isotopic variability. *Earth and Planetary Science Letters*, *201*(2), 383-396, doi:10.1016/S0012-821x(02)00708-2.

Noble, T. L., Piotrowski, A. M., and McCave, I. N. (2013). Neodymium isotopic composition of intermediate and deep waters in the glacial southwest Pacific. *Earth and Planetary Science Letters*, *384*, 27-36, doi:10.1016/j.epsl.2013.10.010.

Nozaki, Y. (2001). Rare Earth Elements and Their Isotopes. In *Encyclopedia of Ocean Sciences*, edited by J. H. Steele, K. K. Turekian and S. A. Thorpe, pp. 840–845, Academic Press.

Nozaki, Y., Lerche, D., Alibo, D. S., and Tsutsumi, M. (2000). Dissolved indium and rare earth elements in three Japanese rivers and Tokyo Bay: Evidence for anthropogenic Gd and In. *Geochimica et Cosmochimica Acta*, *64*(23), 3975-3982, doi:10.1016/S0016-7037(00)00472-5.

O'Nions, R. K., Hamilton, P. J., and Evensen, N. M. (1977). Variations in Nd-143/Nd-144 and Sr-87/Sr-86 Ratios in Oceanic Basalts. *Earth and Planetary Science Letters*, *34*(1), 13-22, doi:10.1016/0012-821x(77)90100-5.

Okazaki, Y., Timmermann, A., Menviel, L., Harada, N., Abe-Ouchi, A., Chikamoto, M. O., Mouchet, A., and Asahi, H. (2010). Deepwater Formation in the North Pacific During the Last Glacial Termination. *Science*, *329*(5988), 200-204, doi:10.1126/science.1190612.

Oki, D. S. (2003). Surface Water in Hawaii: U.S. Geological Survey Fact Sheet 045-03, 6 p.

Orsi, A. H., and Wiederwohl, C. L. (2009). A recount of Ross Sea waters. *Deep-Sea Research Part II-Topical Studies in Oceanography*, *56*(13-14), 778-795, doi:10.1016/j.dsr2.2008.10.033.

Orsi, A. H., Whitworth, T., and Nowlin, W. D. (1995). On the Meridional Extent and Fronts of the Antarctic Circumpolar Current. *Deep-Sea Research Part I-Oceanographic Research Papers*, *42*(5), 641-673, doi:10.1016/0967-0637(95)00021-W.

Orsi, A. H., Johnson, G. C., and Bullister, J. L. (1999). Circulation, mixing, and production of Antarctic Bottom Water. *Progress in Oceanography*, *43*(1), 55-109, doi:10.1016/S0079-6611(99)00004-X.

Osborne, A. H., Newkirk, D. R., Groeneveld, J., Martin, E. E., Tiedemann, R., and Frank, M. (2014). The seawater neodymium and lead isotope record of the final stages of Central American Seaway closure. *Paleoceanography*, *29*(7), 715-729, doi:10.1002/2014PA002676.

Osborne, A. H., Haley, B. A., Hathorne, E. C., Plancherel, Y., and Frank, M. (2015). Rare earth element distribution in Caribbean seawater: Continental inputs versus lateral transport of distinct REE compositions in subsurface water masses. *Marine Chemistry*, *177*, 172-183, doi:10.1016/j.marchem.2015.03.013.

Pahnke, K., and Zahn, R. (2005). Southern hemisphere water mass conversion linked with North Atlantic climate variability. *Science*, *307*(5716), 1741-1746, doi:10.1126/science.1102163.

Pahnke, K., Zahn, R., Elderfield, H., and Schulz, M. (2003). 340,000-year centennial-scale marine record of Southern Hemisphere climatic oscillation. *Science*, *301*(5635), 948-952, doi:10.1126/Science.1084451.

Pahnke, K., Goldstein, S. L., and Hemming, S. R. (2008). Abrupt changes in Antarctic Intermediate Water circulation over the past 25,000 years. *Nature Geoscience*, *1*(12), 870-874, doi:10.1038/Ngeo360.

Pahnke, K., van de Flierdt, T., Jones, K. M., Lambelet, M., Hemming, S. R., and Goldstein, S. L. (2012). GEOTRACES intercalibration of neodymium isotopes and rare earth element concentrations in seawater and suspended particles. Part 2: Systematic tests and baseline profiles. *Limnology and Oceanography-Methods*, *10*, 252-269, doi:10.4319/Lom.2012.10.252.

Paillard, D., Labeyrie, L., and Yiou, P. (1996). Macintosh Program performs time-series analysis. *Eos, Transactions American Geophysical Union*, *77*(39), 379, doi:10.1029/96EO00259.

Palmer, M. R., and Elderfield, H. (1986). Rare-Earth Elements and Neodymium Isotopes in Ferromanganese Oxide Coatings of Cenozoic Foraminifera from the Atlantic-Ocean. *Geochimica et Cosmochimica Acta*, *50*(3), 409-417, doi:10.1016/0016-7037(86)90194-8.

Parrington, J. R., Zoller, W. H., and Aras, N. K. (1983). Asian Dust - Seasonal Transport to the Hawaiian-Islands. *Science*, *220*(4593), 195-197, doi:10.1126/Science.220.4593.195.

Pearce, C. R., Jones, M. T., Oelkers, E. H., Pradoux, C., and Jeandel, C. (2013). The effect of particulate dissolution on the neodymium (Nd) isotope and Rare Earth Element (REE) composition of seawater. *Earth and Planetary Science Letters*, *369*, 138-147, doi:10.1016/J.Epsl.2013.03.023.

Pena, L. D., Goldstein, S. L., Hemming, S. R., Jones, K. M., Calvo, E., Pelejero, C., and Cacho, I. (2013). Rapid changes in meridional advection of Southern Ocean intermediate waters to the tropical Pacific during the last 30 kyr. *Earth and Planetary Science Letters*, *368*, 20-32, doi:10.1016/j.epsl.2013.02.028.

Petit, J. R., Jouzel, J., Raynaud, D., Barkov, N. I., Barnola, J. M., Basile, I., Bender, M., Chappellaz, J., Davis, M., Delaygue, G., Delmotte, M., Kotlyakov, V. M., Legrand, M., Lipenkov, V. Y., Lorius, C., Pepin, L., Ritz, C., Saltzman, E., and Stievenard, M. (1999). Climate and atmospheric history of the past 420,000 years from the Vostok ice core, Antarctica. *Nature*, *399*(6735), 429-436, doi:10.1038/20859.

Piepgras, D. J., and Wasserburg, G. J. (1982). Isotopic Composition of Neodymium in Waters from the Drake Passage. *Science*, *217*(4556), 207-214, doi:10.1126/Science.217.4556.207.

Piepgras, D. J., and Wasserburg, G. J. (1987). Rare-Earth Element Transport in the Western North-Atlantic Inferred from Nd Isotopic Observations. *Geochimica et Cosmochimica Acta*, *51*(5), 1257-1271, doi:10.1016/0016-7037(87)90217-1.

Piepgras, D. J., and Jacobsen, S. B. (1988). The Isotopic Composition of Neodymium in the North Pacific. *Geochimica et Cosmochimica Acta*, *52*(6), 1373-1381, doi:10.1016/0016-7037(88)90208-6.

Piepgras, D. J., and Jacobsen, S. B. (1992). The Behavior of Rare-Earth Elements in Seawater - Precise Determination of Variations in the North Pacific Water Column. *Geochimica et Cosmochimica Acta*, *56*(5), 1851-1862, doi:10.1016/0016-7037(92)90315-A.

Pin, C., and Zalduegui, J. F. S. (1997). Sequential separation of light rare-earth elements, thorium and uranium by miniaturized extraction chromatography: Application to isotopic analyses of silicate rocks. *Analytica Chimica Acta*, *339*(1-2), 79-89, doi:10.1016/S0003-2670(96)00499-0.

Piotrowski, A. M., Goldstein, S. L., Hemming, S. R., and Fairbanks, R. G. (2004). Intensification and variability of ocean thermohaline circulation through the last deglaciation. *Earth and Planetary Science Letters*, *225*(1-2), 205-220, doi:10.1016/J.Epsl.2004.06.002.

Piotrowski, A. M., Goldstein, S. L., Hemming, S. R., and Fairbanks, R. G. (2005). Temporal relationships of carbon cycling and ocean circulation at glacial boundaries. *Science*, *307*(5717), 1933-1938, doi:10.1126/science.1104883.

Piotrowski, A. M., Goldstein, S. L., Hemming, S. R., Fairbanks, R. G., and Zylberberg, D. R. (2008). Oscillating glacial northern and southern deep water formation from combined neodymium and carbon isotopes. *Earth and Planetary Science Letters*, *272*(1-2), 394-405, doi:10.1016/j.epsl.2008.05.011.

Piotrowski, A. M., Banakar, V. K., Scrivner, A. E., Elderfield, H., Galy, A., and Dennis, A. (2009). Indian Ocean circulation and productivity during the last glacial cycle. *Earth and Planetary Science Letters*, *285*(1-2), 179-189, doi:10.1016/j.epsl.2009.06.007.

Piotrowski, A. M., Galy, A., Nicholl, J. A. L., Roberts, N., Wilson, D. J., Clegg, J. A., and Yu, J. (2012). Reconstructing deglacial North and South Atlantic deep water sourcing using foraminiferal Nd isotopes. *Earth and Planetary Science Letters*, *357*, 289-297, doi:10.1016/j.epsl.2012.09.036.

Pomies, C., Davies, G. R., and Conan, S. M. H. (2002). Neodymium in modern foraminifera from the Indian Ocean: implications for the use of foraminiferal Nd isotope compositions in paleo-oceanography. *Earth and Planetary Science Letters*, *203*(3-4), 1031-1045, doi:10.1016/S0012-821x(02)00924-X.

Prospero, J. M., Uematsu, M., and Savoie, D. L. (1989). Mineral aerosol transport to the Pacific Ocean. In *Chemical Oceanography*, edited by J. P. Riley, pp. 87-218, Academic Press, New York.

Purkey, S. G., and Johnson, G. C. (2013). Antarctic Bottom Water Warming and Freshening: Contributions to Sea Level Rise, Ocean Freshwater Budgets, and Global Heat Gain. *Journal of Climate*, *26*, 6105-6122, doi:10.1175/JCLI-D-12-00834.1.

Rae, J. W. B., Sarnthein, M., Foster, G. L., Ridgwell, A., Grootes, P. M., and Elliott, T. (2014). Deep water formation in the North Pacific and deglacial CO2 rise. *Paleoceanography*, *29*(6), 645-667, doi:10.1002/2013PA002570.

Reid, J. L. (1986). On the Total Geostrophic Circulation of the South-Pacific Ocean - Flow Patterns, Tracers and Transports. *Progress in Oceanography*, *16*(1), 1-61, doi:10.1016/0079-6611(86)90036-4.

Reid, J. L. (1997). On the total geostrophic circulation of the Pacific Ocean: flow patterns, tracers, and transports. *Progress in Oceanography*, *39*(4), 263-352, doi:10.1016/S0079-6611(97)00012-8.

Reid, J. L., and Lynn, R. J. (1971). Influence of Norwegian-Greenland and Weddell Seas Upon Bottom Waters of Indian and Pacific Oceans. *Deep-Sea Research*, *18*(11), 1063-&, doi:10.1016/0011-7471(71)90094-5.

Reimer, P. J., Bard, E., Bayliss, A., Beck, J. W., Blackwell, P. G., Ramsey, C. B., Buck, C. E., Cheng, H., Edwards, R. L., Friedrich, M., Grootes, P. M., Guilderson, T. P., Haflidason, H., Hajdas, I., Hatte, C., Heaton, T. J., Hoffmann, D. L., Hogg, A. G., Hughen, K. A., Kaiser, K. F., Kromer, B., Manning, S. W., Niu, M., Reimer, R. W., Richards, D. A., Scott, E. M., Southon, J. R., Staff, R. A., Turney, C. S. M., and van der Plicht, J. (2013). Intcal13 and Marine13 Radiocarbon Age Calibration Curves 0-50,000 Years Cal Bp. *Radiocarbon*, *55*(4), 1869-1887, doi:10.2458/azu_js_rc.55.16947.

Rempfer, J., Stocker, T. F., Joos, F., Dutay, J. C., and Siddall, M. (2011). Modelling Nd-isotopes with a coarse resolution ocean circulation model: Sensitivities to model parameters and source/sink distributions. *Geochimica et Cosmochimica Acta*, *75*(20), 5927-5950, doi:10.1016/J.Gca.2011.07.044.

Ren, Z. Y., Hanyu, T., Miyazaki, T., Chang, Q., Kawabata, H., Takahashi, T., Hirahara, Y., Nichols, A. R. L., and Tatsumi, Y. (2009). Geochemical Differences of the Hawaiian Shield Lavas: Implications for Melting Process in the Heterogeneous Hawaiian Plume. *Journal of Petrology*, *50*(8), 1553-1573, doi:10.1093/Petrology/Egp041.

Rickli, J., Gutjahr, M., Vance, D., Fischer-Goedde, M., Hillenbrand, C. D., and Kuhn, G. (2014). Neodymium and hafnium boundary contributions to seawater along the West Antarctic continental margin. *Earth and Planetary Science Letters*, *394*, 99-110, doi:10.1016/J.Eps1.2014.03.008.

Roberts, N. L., and Piotrowski, A. M. (2015). Radiogenic Nd isotope labeling of the northern NE Atlantic during MIS 2. *Earth and Planetary Science Letters*, *423*, 125-133, doi:10.1016/j.epsl.2015.05.011.

Roberts, N. L., Piotrowski, A. M., McManus, J. F., and Keigwin, L. D. (2010). Synchronous Deglacial Overturning and Water Mass Source Changes. *Science*, *327*(5961), 75-78, doi:10.1126/science.1178068.

Roberts, N. L., Piotrowski, A. M., Elderfield, H., Eglinton, T. I., and Lomas, M. W. (2012). Rare earth element association with foraminifera. *Geochimica et Cosmochimica Acta*, *94*, 57-71, doi:10.1016/j.gca.2012.07.009.

Robinson, L. F., and van de Flierdt, T. (2009). Southern Ocean evidence for reduced export of North Atlantic Deep Water during Heinrich event 1. *Geology*, *37*(3), 195-198, doi:10.1130/G25363A.1.

Ronge, T. A., Steph, S., Tiedemann, R., Prange, M., Merkel, U., Nurnberg, D., and Kuhn, G. (2015). Pushing the boundaries: Glacial/interglacial variability of intermediate and deep waters in the southwest Pacific over the last 350,000 years. *Paleoceanography*, *30*(2), 23-38, doi:10.1002/2014PA002727.

Ronge, T. A., Tiedemann, R., Lamy, F., Köhler, P., Alloway, B. V., De Pol-Holz, R., Pahnke, K., Southon, J., and Wacker, L. (2016). Radiocarbon constraints on the extent and evolution of the South Pacific glacial carbon pool. *Nature Communications*, *7*, 11487, doi:10.1038/ncomms11487.

Rose, K. A., Sikes, E. L., Guilderson, T. P., Shane, P., Hill, T. M., Zahn, R., and Spero, H. J. (2010). Upper-ocean-to-atmosphere radiocarbon offsets imply fast deglacial carbon dioxide release. *Nature*, *466*(7310), 1093-1097, doi:10.1038/nature09288.

Rousseau, T. C. C., Sonke, J. E., Chmeleff, J., van Beek, P., Souhaut, M., Boaventura, G., Seyler, P., and Jeandel, C. (2015). Rapid neodymium release to marine waters from lithogenic sediments in the Amazon estuary. *Nature Communications*, *6*, Artn 7592, doi:10.1038/Ncomms8592.

Rutberg, R. L., Hemming, S. R., and Goldstein, S. L. (2000). Reduced North Atlantic Deep Water flux to the glacial Southern Ocean inferred from neodymium isotope ratios. *Nature*, *405*(6789), 935-938, doi:10.1038/35016049.

Schaefer, J. M., Putnam, A. E., Denton, G. H., Kaplan, M. R., Birkel, S., Doughty, A. M., Kelley, S., Barrell, D. J. A., Finkel, R. C., Winckler, G., Anderson, R. F., Ninneman, U. S., Barker, S., Schwartz, R., Andersen, B. G., and Schluechter, C. (2015). The Southern Glacial Maximum 65,000 years ago and its Unfinished Termination. *Quaternary Science Reviews*, *114*, 52-60, doi:10.1016/j.quascirev.2015.02.009.

Scher, H. D., and Martin, E. E. (2004). Circulation in the Southern Ocean during the Paleogene inferred from neodymium isotopes. *Earth and Planetary Science Letters*, *228*(3-4), 391-405, doi:10.1016/j.epsl.2004.10.016.

Scher, H. D., and Martin, E. E. (2008). Oligocene deep water export from the North Atlantic and the development of the Antarctic Circumpolar Current examined with neodymium isotopes. *Paleoceanography*, *23*(1), Artn Pa1205, doi:10.1029/2006pa001400.

Schlitzer, R. (2014). Ocean Data View, http://odv.awi.de.

Shabani, M. B., Akagi, T., and Masuda, A. (1992). Preconcentration of Trace Rare-Earth Elements in Seawater by Complexation with Bis(2-Ethylhexyl) Hydrogen Phosphate and 2-Ethylhexyl Dihydrogen Phosphate Adsorbed on a C18 Cartridge and Determination by Inductively Coupled Plasma Mass-Spectrometry. *Analytical Chemistry*, *64*(7), 737-743, doi:10.1021/Ac00031a008.

Shaw, H. F., and Wasserburg, G. J. (1985). Sm-Nd in Marine Carbonates and Phosphates - Implications for Nd Isotopes in Seawater and Crustal Ages. *Geochimica et Cosmochimica Acta*, *49*(2), 503-518, doi:10.1016/0016-7037(85)90042-0.

Shimada, K., Aoki, S., Ohshima, K. I., and Rintoul, S. R. (2012). Influence of Ross Sea Bottom Water changes on the warming and freshening of the Antarctic Bottom Water in the Australian-Antarctic Basin. *Ocean Science*, *8*, 419-432, doi:10.5194/os-8-419-2012.

Shimizu, H., Tachikawa, K., Masuda, A., and Nozaki, Y. (1994). Cerium and Neodymium Isotope Ratios and Ree Patterns in Seawater from the North Pacific-Ocean. *Geochimica et Cosmochimica Acta*, *58*(1), 323-333, doi:10.1016/0016-7037(94)90467-7.

Sholkovitz, E. R. (1992). Chemical Evolution of Rare-Earth Elements - Fractionation between Colloidal and Solution Phases of Filtered River Water. *Earth and Planetary Science Letters*, *114*(1), 77-84, doi:10.1016/0012-821x(92)90152-L.

Sholkovitz, E. R. (1995). The Aquatic Chemistry of Rare Earth Elements in Rivers and Estuaries. *Aquatic Geochemistry*, *1*(1), 1-34, doi:10.1007/Bf01025229.

Sholkovitz, E. R., and Elderfield, H. (1988). Cycling of Dissolved Rare Earth Elements in Chesapeake Bay. *Global Biogeochemical Cycles*, *2*(2), 157-176, doi:10.1029/GB002i002p00157.

Sholkovitz, E. R., Landing, W. M., and Lewis, B. L. (1994). Ocean Particle Chemistry - the Fractionation of Rare-Earth Elements between Suspended Particles and Seawater. *Geochimica et Cosmochimica Acta*, *58*(6), 1567-1579, doi:10.1016/0016-7037(94)90559-2.

Sholkovitz, E. R., Elderfield, H., Szymczak, R., and Casey, K. (1999). Island weathering: river sources of rare earth elements to the Western Pacific Ocean. *Marine Chemistry*, *68*(1-2), 39-57, doi:10.1016/S0304-4203(99)00064-X.

Siani, G., Michel, E., De Pol-Holz, R., DeVries, T., Lamy, F., Carel, M., Isguder, G., Dewilde, F., and Lourantou, A. (2013). Carbon isotope records reveal precise timing of enhanced Southern Ocean upwelling during the last deglaciation. *Nature Communications*, *4*, Artn 2758, doi:10.1038/Ncomms3758.

Siddall, M., Khatiwala, S., van de Flierdt, T., Jones, K., Goldstein, S. L., Hemming, S., and Anderson, R. F. (2008). Towards explaining the Nd paradox using reversible scavenging in an ocean general circulation model. *Earth and Planetary Science Letters*, *274*(3-4), 448-461, doi:10.1016/J.Epsl.2008.07.044.

Siegenthaler, U., and Sarmiento, J. L. (1993). Atmospheric Carbon-Dioxide and the Ocean. *Nature*, *365*(6442), 119-125, doi:10.1038/365119a0.

Siegenthaler, U., Stocker, T. F., Monnin, E., Luthi, D., Schwander, J., Stauffer, B., Raynaud, D., Barnola, J. M., Fischer, H., Masson-Delmotte, V., and Jouzel, J. (2005). Stable carbon cycle-climate relationship during the late Pleistocene. *Science*, *310*(5752), 1313-1317, doi:10.1126/science.1120130.

Sigman, D. M., and Boyle, E. A. (2000). Glacial/interglacial variations in atmospheric carbon dioxide. *Nature*, *407*(6806), 859-869, doi:10.1038/35038000.

Sigman, D. M., Hain, M. P., and Haug, G. H. (2010). The polar ocean and glacial cycles in atmospheric CO2 concentration. *Nature*, *466*(7302), 47-55, doi:10.1038/nature09149.

Sikes, E. L., Samson, C. R., Guilderson, T. P., and Howard, W. R. (2000). Old radiocarbon ages in the southwest Pacific Ocean during the last glacial period and deglaciation. *Nature*, *405*(6786), 555-559, doi:10.1038/35014581.

Sikes, E. L., Cook, M. S., and Guilderson, T. P. (2016). Reduced deep ocean ventilation in the Southern Pacific Ocean during the last glaciation persisted into the deglaciation. *Earth and Planetary Science Letters*, *438*, 130-138, doi:10.1016/j.epsl.2015.12.039.

Skinner, L. C., Fallon, S., Waelbroeck, C., Michel, E., and Barker, S. (2010). Ventilation of the Deep Southern Ocean and Deglacial CO2 Rise. *Science*, *328*(5982), 1147-1151, doi:10.1126/science.1183627.

Skinner, L. C., Scrivner, A. E., Vance, D., Barker, S., Fallon, S., and Waelbroeck, C. (2013). North Atlantic versus Southern Ocean contributions to a deglacial surge in deep ocean ventilation. *Geology*, *41*(6), 667-670, doi:10.1130/G34133.1.

Skinner, L. C., McCave, I. N., Carter, L., Fallon, S., Scrivner, A. E., and Primeau, F. (2015). Reduced ventilation and enhanced magnitude of the deep Pacific carbon pool during the last glacial period. *Earth and Planetary Science Letters*, *411*, 45-52, doi:10.1016/j.epsl.2014.11.024.

Sloyan, B. M., and Rintoul, S. R. (2001a). The Southern Ocean limb of the global deep overturning circulation. *Journal of Physical Oceanography*, *31*(1), 143-173, doi:10.1175/1520-0485(2001)031<0143:Tsolot>2.0.Co;2.

Sloyan, B. M., and Rintoul, S. R. (2001b). Circulation, renewal, and modification of Antarctic mode and intermediate water. *Journal of Physical Oceanography*, *31*(4), 1005-1030, doi:10.1175/1520-0485(2001)031<1005:Cramoa>2.0.Co;2.

Staudigel, H., Doyle, P., and Zindler, A. (1985). Sr and Nd Isotope Systematics in Fish Teeth. *Earth and Planetary Science Letters*, *76*(1-2), 45-56, doi:10.1016/0012-821x(85)90147-5.

Stichel, T., Pahnke, K., Goldstein, S. L., Hartman, A. E., and Scher, H. (2012a). The geochemistry of seawater neodymium isotopes in the TAG hydrothermal plume at the Mid Atlantic Ridge. Abstract OS41A-1690 presented at 2012 Fall Meeting, AGU, San Francisco, Calif., 3-7 Dec.

Stichel, T., Frank, M., Rickli, J., and Haley, B. A. (2012b). The hafnium and neodymium isotope composition of seawater in the Atlantic sector of the Southern Ocean. *Earth and Planetary Science Letters*, *317*, 282-294, doi:10.1016/J.Epsl.2011.11.025.

Stichel, T., Hartman, A. E., Duggan, B., Goldstein, S. L., Scher, H., and Pahnke, K. (2015). Separating biogeochemical cycling of neodymium from water mass mixing in the Eastern North Atlantic. *Earth and Planetary Science Letters*, *412*, 245-260, doi:10.1016/J.Epsl.2014.12.008.

Studer, A. S., Sigman, D. M., Martinez-Garcia, A., Benz, V., Winckler, G., Kuhn, G., Esper, O., Lamy, F., Jaccard, S. L., Wacker, L., Oleynik, S., Gersonde, R., and Haug, G.

H. (2015). Antarctic Zone nutrient conditions during the last two glacial cycles. *Paleoceanography*, *30*(7), 845-862, doi:10.1002/2014PA002745.

Suga, T., Hanawa, K., and Toba, Y. (1989). Sub-Tropical Mode Water in the 137-Degrees-E Section. *Journal of Physical Oceanography*, *19*(10), 1605-1618, doi:10.1175/1520-0485(1989)019<1605:Smwits>2.0.Co;2.

Suga, T., Kato, A., and Hanawa, K. (2000). North Pacific Tropical Water: its climatology and temporal changes associated with the climate regime shift in the 1970s. *Progress in Oceanography*, *47*(2-4), 223-256, doi:10.1016/S0079-6611(00)00037-9.

Tachikawa, K., Jeandel, C., and Roy-Barman, M. (1999). A new approach to the Nd residence time in the ocean: the role of atmospheric inputs. *Earth and Planetary Science Letters*, *170*(4), 433-446, doi:10.1016/S0012-821x(99)00127-2.

Tachikawa, K., Athias, V., and Jeandel, C. (2003). Neodymium budget in the modern ocean and paleo-oceanographic implications. *Journal of Geophysical Research-Oceans*, *108*(C8), Artn 3254, doi:10.1029/1999jc000285.

Tachikawa, K., Toyofuku, T., Basile-Doelsch, I., and Delhaye, T. (2013). Microscale neodymium distribution in sedimentary planktonic foraminiferal tests and associated mineral phases. *Geochimica et Cosmochimica Acta*, *100*, 11-23, doi:10.1016/j.gca.2012.10.010.

Tachikawa, K., Piotrowski, A. M., and Bayon, G. (2014). Neodymium associated with foraminiferal carbonate as a recorder of seawater isotopic signatures. *Quaternary Science Reviews*, *88*, 1-13, doi:10.1016/j.quascirev.2013.12.027.

Talley, L. D. (1993). Distribution and Formation of North Pacific Intermediate Water. *Journal of Physical Oceanography*, *23*(3), 517-537, doi:10.1175/1520-0485(1993)023<0517:Dafonp>2.0.Co;2.

Talley, L. D. (1999). Some aspects of ocean heat transport by the shallow, intermediate and deep overturning circulations. In *Mechanisms of Global Climate Change at Millennial Time Scales*, edited by P. U. Clark, R. S. Webb and L. D. Keigwin, pp. 1-22, American Geophysical Union.

Talley, L. D. (2008). Freshwater transport estimates and the global overturning circulation: Shallow, deep and throughflow components. *Progress in Oceanography*, *78*(4), 257-303, doi:10.1016/J.Pocean.2008.05.001.

Talley, L. D. (2013). Closure of the Global Overturning Circulation Through the Indian, Pacific, and Southern Oceans: Schematics and Transports. *Oceanography*, *26*(1), 80-97, doi:10.5670/oceanog.2013.07.

Talley, L. D., Pickard, G. L., Emery, W. J., and Swift, J. H. (2011). Descriptive Physical Oceanography: An Introduction. 6th ed., Academic Press.

Tanaka, R., Makishima, A., and Nakamura, E. (2008). Hawaiian double volcanic chain triggered by an episodic involvement of recycled material: Constraints from temporal Sr-Nd-Hf-Pb isotopic trend of the Loa-type volcanoes. *Earth and Planetary Science Letters*, *265*(3-4), 450-465, doi:10.1016/J.Epsl.2007.10.035.

Tanaka, T., Togashi, S., Kamioka, H., Amakawa, H., Kagami, H., Hamamoto, T., Yuhara, M., Orihashi, Y., Yoneda, S., Shimizu, H., Kunimaru, T., Takahashi, K., Yanagi, T., Nakano, T., Fujimaki, H., Shinjo, R., Asahara, Y., Tanimizu, M., and Dragusanu, C. (2000). JNdi-1: a neodymium isotopic reference in consistency with La Jolla neodymium. *Chemical Geology*, *168*(3-4), 279-281, doi:10.1016/S0009-2541(00)00198-4.

Taylor, S. R., and McLennan, S. M. (1985). The Continental Crust: Its Composition and Evolution. An Examination of the Geochemical Record Preserved in Sedimentary Rocks, Blackwell, Oxford.

Taylor, S. R., Mclennan, S. M., and Mcculloch, M. T. (1983). Geochemistry of Loess, Continental Crustal Composition and Crustal Model Ages. *Geochimica et Cosmochimica Acta*, *47*(11), 1897-1905, doi:10.1016/0016-7037(83)90206-5.

Thomas, D. J. (2004). Evidence for deep-water production in the North Pacific Ocean during the early Cenozoic warm interval. *Nature*, *430*(6995), 65-68, doi:10.1038/nature02639.

Thomas, D. J., and Via, R. K. (2007). Neogene evolution of Atlantic thermohaline circulation: Perspective from Walvis Ridge, southeastern Atlantic Ocean. *Paleoceanography*, *22*(2), Artn Pa2212, doi:10.1029/2006pa001297.

Thomas, D. J., Bralower, T. J., and Jones, C. E. (2003). Neodymium isotopic reconstruction of late Paleocene-early Eocene thermohaline circulation. *Earth and Planetary Science Letters*, *209*(3-4), 309-322, doi:10.1016/S0012-821X(03)00096-7.

Thornalley, D. J. R., Barker, S., Becker, J., Hall, I. R., and Knorr, G. (2013). Abrupt changes in deep Atlantic circulation during the transition to full glacial conditions. *Paleoceanography*, *28*(2), 253-262, doi:10.1002/palo.20025.

Toggweiler, J. R., and Samuels, B. (1998). On the Ocean's Large-Scale Circulation near the Limit of No Vertical Mixing. *Journal of Physical Oceanography*, *28*(9), 1832-1852, doi:10.1175/1520-0485(1998)028<1832:OTOSLS>2.0.CO;2.

Toggweiler, J. R., Russell, J. L., and Carson, S. R. (2006). Midlatitude westerlies, atmospheric CO2, and climate change during the ice ages. *Paleoceanography*, *21*(2), Artn Pa2005, doi:10.1029/2005pa001154.

Tomczak, J. S., and Godfrey, M. (1994). Regional Oceanography: An Introduction, Pergamon Press.

Tsuchiya, M. (1991). Flow Path of the Antarctic Intermediate Water in the Western Equatorial South-Pacific Ocean. *Deep-Sea Research Part a-Oceanographic Research Papers*, *38*, S273-S279, doi:10.1016/S0198-0149(12)80013-6.

Uematsu, M., Duce, R. A., and Prospero, J. M. (1985). Deposition of Atmospheric Mineral Particles in the North Pacific-Ocean. *Journal of Atmospheric Chemistry*, *3*(1), 123-138, doi:10.1007/Bf00049372.

Ullermann, J., Lamy, F., Ninneman, U. S., Lembke-Jene, L., Gersonde, R., and Tiedemann, R. (2016). Pacific-Atlantic Circumpolar Deep Water coupling during the last 500 ka. *Paleoceanography*, doi:10.1002/2016PA002932.

van de Flierdt, T., and Frank, M. (2010). Neodymium isotopes in paleoceanography Introduction. *Quaternary Science Reviews*, *29*(19-20), 2439-2441, doi:10.1016/j.quascirev.2010.07.001.

van de Flierdt, T., Frank, M., Lee, D. C., Halliday, A. N., Reynolds, B. C., and Hein, J. R. (2004). New constraints on the sources and behavior of neodymium and hafnium in seawater from Pacific Ocean ferromanganese crusts. *Geochimica et Cosmochimica Acta*, *68*(19), 3827-3843, doi:10.1016/j.gca.2004.03.009.

van de Flierdt, T., Robinson, L. F., Adkins, J. F., Hemming, S. R., and Goldstein, S. L. (2006). Temporal stability of the neodymium isotope signature of the Holocene to glacial North Atlantic. *Paleoceanography*, *21*(4), Artn Pa4102, doi:10.1029/2006pa001294.

van de Flierdt, T., Robinson, L. F., and Adkins, J. F. (2010). Deep-sea coral aragonite as a recorder for the neodymium isotopic composition of seawater. *Geochimica et Cosmochimica Acta*, *74*(21), 6014-6032, doi:10.1016/j.gca.2010.08.001.

van de Flierdt, T., Pahnke, K., Amakawa, H., Andersson, P., Basak, C., Coles, B., Colin, C., Crocket, K., Frank, M., Frank, N., Goldstein, S. L., Goswami, V., Haley, B. A., Hathorne, E. C., Hemming, S. R., Henderson, G. M., Jeandel, C., Jones, K., Kreissig, K., Lacan, F., Lambelet, M., Martin, E. E., Newkirk, D. R., Obata, H., Pena, L., Piotrowski, A. M., Pradoux, C., Scher, H. D., Schoberg, H., Singh, S. K., Stichel, T., Tazoe, H., Vance, D., Yang, J. J., and Partici, G. I. (2012). GEOTRACES intercalibration of neodymium isotopes and rare earth element concentrations in seawater and suspended particles. Part 1: reproducibility of results for the international intercomparison. *Limnology and Oceanography-Methods*, *10*, 234-251, doi:10.4319/Lom.2012.10.234.

Vance, D., and Burton, K. (1999). Neodymium isotopes in planktonic foraminifera: a record of the response of continental weathering and ocean circulation rates to climate change. *Earth and Planetary Science Letters*, *173*(4), 365-379, doi:10.1016/S0012-821x(99)00244-7.

Vance, D., and Thirlwall, M. (2002). An assessment of mass discrimination in MC-ICPMS using Nd isotopes. *Chemical Geology*, *185*(3-4), 227-240, doi:10.1016/S0009-2541(01)00402-8.

Vance, D., Scrivner, A. E., Beney, P., Staubwasser, M., Henderson, G. M., and Slowey, N. C. (2004). The use of foraminifera as a record of the past neodymium isotope composition of seawater. *Paleoceanography*, *19*(2), Artn Pa2009, doi:10.1029/2003pa000957.

Vandergoes, M. J., Hogg, A. G., Lowe, D. J., Newnham, R. M., Denton, G. H., Southon, J., Barrell, D. J. A., Wilson, C. J. N., McGlone, M. S., Allan, A. S. R., Almond, P. C., Petchey, F., Dabell, K., Dieffenbacher-Krall, A. C., and Blaauw, M. (2013). A revised age for the Kawakawa/Oruanui tephra, a key marker for the Last Glacial Maximum in New Zealand. *Quaternary Science Reviews*, *74*, 195-201, doi:10.1016/j.quascirev.2012.11.006.

Veres, D., Bazin, L., Landais, A., Kele, H. T. M., Lemieux-Dudon, B., Parrenin, F., Martinerie, P., Blayo, E., Blunier, T., Capron, E., Chappellaz, J., Rasmussen, S. O., Severi, M., Svensson, A., Vinther, B., and Wolff, E. W. (2013). The Antarctic ice core chronology (AICC2012): an optimized multi-parameter and multi-site dating approach for the last 120 thousand years. *Climate of the Past*, *9*(4), 1733-1748, doi:10.5194/cp-9-1733-2013.

von Blanckenburg, F. (1999). Perspectives: Paleoceanography - Tracing past ocean circulation? *Science*, *286*(5446), 1862-1863, doi:10.1126/science.286.5446.1862b.

Waddell, L. M., Hendy, I. L., Moore, T. C., and Lyle, M. W. (2009). Ventilation of the abyssal Southern Ocean during the late Neogene: A new perspective from the subantarctic Pacific. *Paleoceanography*, *24*, Artn Pa3206, doi:10.1029/2008pa001661.

Watson, A. J., Vallis, G. K., and Nikurashin, M. (2015). Southern Ocean buoyancy forcing of ocean ventilation and glacial atmospheric CO2. *Nature Geoscience*, *8*, 861-864, doi:10.1038/NGEO2538.

Wei, R., Abouchami, W., Zahn, R., and Masque, P. (2016). Deep circulation changes in the South Atlantic since the Last Glacial Maximum from Nd isotope and multi-proxy records. *Earth and Planetary Science Letters*, *434*, 18–29, doi:10.1016/j.epsl.2015.11.001.

White, W. B., and Walker, A. E. (1985). The Influence of the Hawaiian Archipelago Upon the Wind-Driven Sub-Tropical Gyre in the Western North Pacific. *Journal of Geophysical Research-Oceans*, *90*(Nc4), 7061-7074, doi:10.1029/Jc090ic04p07061.

Wijffels, S. E., Toole, J. M., Bryden, H. L., Fine, R. A., Jenkins, W. J., and Bullister, J. L. (1996). The water masses and circulation at 10 degrees N in the Pacific. *Deep-Sea Research Part I-Oceanographic Research Papers*, *43*(4), 501-544, doi:10.1016/0967-0637(96)00006-4.

Wilson, D. J., Piotrowski, A. M., Galy, A., and McCave, I. N. (2012). A boundary exchange influence on deglacial neodymium isotope records from the deep western Indian Ocean. *Earth and Planetary Science Letters*, *341*, 35-47, doi:10.1016/j.epsl.2012.06.009.

Wilson, D. J., Piotrowski, A. M., Galy, A., and Clegg, J. A. (2013). Reactivity of neodymium carriers in deep sea sediments: Implications for boundary exchange and paleoceanography. *Geochimica et Cosmochimica Acta*, *109*, 197-221, doi:10.1016/j.gca.2013.01.042.

Wilson, D. J., Crocket, K. C., van de Flierdt, T., Robinson, L. F., and Adkins, J. F. (2014). Dynamic intermediate ocean circulation in the North Atlantic during Heinrich Stadial 1: A radiocarbon and neodymium isotope perspective. *Paleoceanography*, *29*(11), 1072-1093, doi:10.1002/2014PA002674.

Wilson, D. J., Piotrowski, A. M., Galy, A., and Banakar, V. K. (2015). Interhemispheric controls on deep ocean circulation and carbon chemistry during the last two glacial cycles. *Paleoceanography*, *30*(6), 621-641, doi:10.1002/2014PA002707.

Wilson, S., and Tozzi, S. (2012). Chief Scientist Report for CMORE HOE DYLAN IV, Univ. of Hawaii, http://hahana.soest.hawaii.edu/hoedylan/documents/documents.html.

Wilson, S., and Fitzsimmons, J. N. (2012). Chief Scientist Report for CMORE HOE DYLAN V, Univ. of Hawaii, http://hahana.soest.hawaii.edu/hoedylan/documents/documents.html.

Wu, Q., Colin, C., Liu, Z., Thil, F., Dubois-Dauphin, Q., Frank, N., Tachikawa, K., Bordier, L., and Douville, E. (2015). Neodymium isotopic composition in foraminifera and authigenic phases of the South China Sea sediments: Implications for the hydrology of the North Pacific Ocean over the past 25 kyr. *Geochemistry Geophysics Geosystems*, *16*, 3883–3904, doi:10.1002/2015GC005871.

Yasuda, I. (2004). North Pacific intermediate water: Progress in SAGE (SubArctic Gyre Experiment) and related projects. *Journal of Oceanography*, *60*(2), 385-395, doi:10.1023/B:Joce.0000038344.25081.42.

You, Y. Z. (2003). The pathway and circulation of North Pacific Intermediate Water. *Geophysical Research Letters*, *30*(24), Artn 2291, doi:10.1029/2003gl018561.

You, Y. Z., Suginohara, N., Fukasawa, M., Yasuda, I., Kaneko, I., Yoritaka, H., and Kawamiya, M. (2000). Roles of the Okhotsk Sea and Gulf of Alaska in forming the North Pacific Intermediate Water. *Journal of Geophysical Research-Oceans*, *105*(C2), 3253-3280, doi:10.1029/1999jc900304.

Yu, J., Menviel, L., Jin, Z. D., Thornalley, D. J. R., Barker, S., Marino, G., Rohling, E. J., Cai, Y., Zhang, F., Wang, X., Dai, Y., Chen, P., and Broecker, W. S. (2016). Sequestration of carbon in the deep Atlantic during the last glaciation. *Nature Geoscience, 9,* 319-324, doi:10.1038/NGEO2657.

Zhang, Y., Lacan, F., and Jeandel, C. (2008). Dissolved rare earth elements tracing lithogenic inputs over the Kerguelen Plateau (Southern Ocean). *Deep-Sea Research Part Ii-Topical Studies in Oceanography*, *55*(5-7), 638-652, doi:10.1016/J.Dsr2.2007.12.029.

Zheng, X.-Y., Plancherel, Y., Saito, M. A., Scott, P. M., and Henderson, G. M. (2016). Rare earth elements (REEs) in the tropical South Atlantic and quantitative deconvolution of their non-conservative behavior. *Geochimica et Cosmochimica Acta*, *177*, 217-237, doi:10.1016/j.gca.2016.01.018.

Zimmermann, B., Porcelli, D., Frank, M., Rickli, J., Lee, D. C., and Halliday, A. N. (2009). The hafnium isotope composition of Pacific Ocean water. *Geochimica et Cosmochimica Acta*, *73*(1), 91-101, doi:10.1016/J.Gca.2008.09.033.

8. Data handling

Data presented in this thesis will be available for download in the PANGAEA database (www.pangaea.de). Data packages will be password protected until the publication of the associated manuscript.

Chapter 2:
Data are available under: http://doi.pangaea.de/10.1594/PANGAEA.855127. Part of these data (GEOTRACES Process Study GPpr05; cruise KM1107) will also be published as part of the GEOTRACES Intermediate Data Product 2017 (IDP2017) and available through the GEOTRACES International Data Assembly Centre (GDAC) (http://www.bodc.ac.uk/geotraces/).

Chapter 3:
Data are available under: http://doi.pangaea.de/10.1594/PANGAEA.858969.

Chapter 4:
Data are available under: http://doi.pangaea.de/10.1594/PANGAEA.858876.

Danksagung

Zunächst geht mein Dank an Dr. Katharina Pahnke, die mir die Möglichkeit gegeben hat, in der Arbeitsgruppe Marine Isotopengeochemie über Nd Isotope und Seltene Erden zu promovieren und die interessanten Fragestellungen zu bearbeiten. Ihre ständige Bereitschaft für Fragen und Diskussionen und die große Unterstützung während der gesamten Zeit haben entscheidend zum Gelingen dieser Arbeit beigetragen. Weiterhin danke ich Dr. Pahnke für die Begutachtung dieser Arbeit. Ebenfalls geht mein Dank an Prof. Dr. Thorsten Dittmar, für die Bereitschaft zur Übernahme der Begutachtung dieser Arbeit, sowie an Prof. Dr. Hans-Jürgen Brumsack, für die hilfreichen Diskussionen und die Bereitschaft Teil des Prüfungskomitees zu sein.

Ein großer Dank geht an Dr. Philipp Böning, Dr. Claudia Ehlert, Melanie Behrens, Ronja Paffrath, Bianca Liguori, Martina Schulz und Dr. Torben Struve, für die ausgesprochen gute Zusammenarbeit, die zahlreichen fachlichen und nicht-fachlichen Diskussionen und die angenehme Arbeitsatmosphäre. Besonders danken möchte ich Martina Schulz für die unschätzbar große Hilfe im Labor, Dr. Philipp Böning für die Unterstützung bei den ICP-MS und MC-ICP-MS Messungen und die Diskussion vieler analytischer Probleme sowie Dr. Claudia Ehlert und Ronja Paffrath für das Korrekturlesen einiger Kapitel dieser Arbeit. Ein großer Dank geht auch an Dr. Chandranath Basak, für die bereichernden Diskussionen, die wertvollen Einblicke in Themen der Paläoozeanographie, die gute Zusammenarbeit während seiner Zeit in Oldenburg, und die überaus produktive und kommunikative Arbeit an unserem Manuskript in der Zeit danach. Außerdem danke ich Susanne Wendeling für die Erledigung einer Reihe von administrativen Angelegenheiten.

Ich danke auch allen Mitgliedern der AG Mikrobiogeochemie, insbesondere Eleonore Gründken für Unterstützung bei Messungen und Dr. Bernhard Schnetger für Hilfe bei analytischen Fragestellungen während der ICP-MS Messungen. Außerdem danke ich Felix Mielke und Kim Arndt für das Picken von zahlreichen Proben und die langen Stunden am Mikroskop sowie Sebastian Haas für die gute Zusammenarbeit während seines Forschungsprojekts.

Weiterhin geht mein Dank an die Kooperationspartner vom AWI Bremerhaven, allen voran Dr. Frank Lamy, für die sehr gute Zusammenarbeit und die hilfreichen Diskussionen, sowie an Dr. Rainer Gersonde, Verena Benz, Dr. Thomas Ronge, Marc Wengler und Dr. Johannes Ullermann für die Informationen und Diskussionen zu Altersmodellen und den unkomplizierten Probenaustausch. Ferner danke ich allen Co-Autoren der in dieser Arbeit enthaltenden Manuskripte für die gute Zusammenarbeit und allen Personen, die an Probenahmen und Probenaufbereitungen mitgewirkt haben und nicht alle namentlich erwähnt werden können.

Ferner danke ich meiner Familie, die mich auf meinem Weg fortwährend unterstützt hat. Zu guter Letzt gilt mein besonderer Dank meiner Frau Linda, für ihre großartige Unterstützung, für Rückhalt und Motivation, ihre unendliche Geduld, und dafür, ständig für mich da gewesen zu sein.

Curriculum vitae

Persönliche Daten

Name:	Henning Fröllje
Geburtsdatum, -ort:	01.07.1984, Oldenburg
Staatsangehörigkeit:	deutsch

Akademischer Werdegang

10/2006 - 10/2009	Bachelor of Science Umweltwissenschaften, Carl von Ossietzky Universität Oldenburg, Bachelorarbeit: Geochemische Charakterisierung eines Sedimentkernes (14-GC-3) aus dem Schwarzen Meer (Meteor-Ausfahrt M72/5)
10/2009 - 06/2012	Master of Science Marine Umweltwissenschaften, Carl von Ossietzky Universität Oldenburg, Masterarbeit: „Trace metals as indicators for depositional conditions in organic-rich sediments off Northern Chile and Peru“
seit 09/2012	Wissenschaftlicher Mitarbeiter am Max Planck Institut für Marine Mikrobiologie Bremen in der AG Marine Isotopengeochemie und Promotionsstudent an der Carl von Ossietzky Universität Oldenburg
seit 09/2013	Promotionsstudent in Environmental Sciences and Biodiversity der Graduiertenschule Naturwissenschaft und Technik der Carl von Ossietzky Universität Oldenburg

Erklärung

Hiermit erkläre ich, dass ich die Arbeit unter Befolgung der Leitlinien guter wissenschaftlicher Praxis der Carl von Ossietzky Universität Oldenburg selbstständig verfasst und nur die angegebenen Hilfsmittel benutzt habe. Ich erkläre, dass die Dissertation weder in ihrer Gesamtheit noch in Teilen einer anderen wissenschaftlichen Hochschule zur Begutachtung in einem Promotionsverfahren vorliegt oder vorgelegen hat. Zusätzlich erkläre ich, dass im Zusammenhang mit dem Promotionsvorhaben keine kommerziellen Vermittlungs- oder Beratungsdienste in Anspruch genommen worden sind. Teile dieser Dissertation sind, wie angegeben, für die Veröffentlichung akzeptiert oder in Vorbereitung für die Veröffentlichung.

Oldenburg, im Juni 2016

Henning Fröllje